POSITIONAL ORDER IN LEAD SCANDIUM TANTALATE (PST) AS A <<TOOL>> FOR THE INVESTIGATION OF RELAXOR FERROELECTRIC BEHAVIOR IN THIN FILMS

THÈSE N^O 3144 (2004)

PRÉSENTÉE À LA FACULTÉ SCIENCES ET TECHNIQUES DE L'INGÉNIEUR

Institut des matériaux

SECTION DES MATÉRIAUX

ÉCOLE POLYTECHNIQUE FÉDÉRALE DE LAUSANNE

POUR L'OBTENTION DU GRADE DE DOCTEUR ÈS SCIENCES TECHNIQUES

PAR

Kyle BRINKMAN

M.sc in Ceramic Engineering, Clemson University, Etats-Unis
et de nationalité américaine

acceptée sur proposition du jury:

Prof. N. Setter, directrice de thèse
Prof. H. Hofmann, rapporteur
Prof. M. Kosec, rapporteur
Prof. J. Petzelt, rapporteur
Dr A. Tagantsev, rapporteur

Lausanne, EPFL
2004

To My Parents

Abstract

Relaxor ferroelectric thin films exhibit a drastic reduction in the dielectric constant and associated properties in the thin film form, even for thicknesses in the micron range, which are essentially infinity for the size effects typically investigated in conventional ferroelectrics. In order to investigate this phenomenon, the material system Lead Scandium Tantalum (PST) was fabricated by a Sol-Gel technique using mixed acetate and alkoxide precursors. The positional order of the "B" site species was tailored through different annealing procedures to produce *ordered* (conventional ferroelectric) and *disordered* (relaxor ferroelectric) PST thin films.

With regards to processing, it was found that the dehydration of scandium acetate by acetic acid anhydride, followed by precursor modification via the solvent 2-Methoxyethanol was necessary for a stable "B" site Sc/Ta complex and subsequent stoichiometric thin films. Excess lead was required in amounts greater than 20% to compensate for lead loss during annealing and avoid the formation of secondary phases. Disordered films with measurable properties were only achieved at *low* annealing temperatures near 700°C. Higher temperatures up to 1000°C resulted in "B" site ordering, and at annealing temperatures above 1000°C significant film degradation was observed. The ordering of PST thin films was limited to low degrees of order (S=0.22) on Pt/Si substrates after annealing at 800°C for 20 minutes. Higher degrees of order were achieved on single crystal substrates by extended time annealing in a controlled atmosphere. An ordering degree of S=0.91 observed for PST films on sapphire substrates annealed at 850°C for 35 hours.

Highly ordered films showed the development of a ferroelectric state, and had dielectric properties comparable with ordered ceramic samples. Disordered films fabricated on numerous substrates and under many processing conditions consistently displayed dielectric constant values reduced by an order of magnitude as compared to ceramic or single crystals. A direct comparison of ordered and disordered PST on a common substrate showed that the dielectric constant *increased* with an *increase* in "B" site order in thin films,

while in ceramics the *opposite* effect was observed (a decrease in the dielectric constant with an increase in order).

In terms of lattice dynamics, ordered PST thin films unexpectedly showed that the transverse optic (TO1) mode softened to the Burns temperature, with the simultaneous appearance of a central mode (CM) attributed to the appearance of polar regions in the paraelectric phase. Higher processing temperatures were seen to increase the dielectric strength of the CM. Ordered and disordered samples displayed drastically different behavior at low frequencies (below 1MHz), while possessing essentially the *same* lattice dynamics.

It was shown by comparing the *"In-Plane"* and *"Out-of-Plane"* dielectric response that the commonly observed low values of dielectric constant in relaxor thin films cannot be explained by a passive layer, at least in nominally thick films near 1 micron in thickness. The changes in the dielectric constant introduced as a result of thermal induced stress were small and relatively insignificant as compared to the order of magnitude reduction in the dielectric constant of thin films as compared to ceramics. A study on the effects of grain size from dielectric measurements showed no detectable change in the value of the dielectric constant by reducing the grain size from 325 to 140 nm. In addition, even epitaxial films fabricated on STO and MgO substrates displayed a reduced dielectric response. Self-polarization was observed in PST thin films and the quantitative impact on the dielectric response was estimated to be near a 10% reduction in the dielectric constant at temperatures close to the dielectric maximum.

A hypothesis was proposed to explain the reduced dielectric response in relaxor thin films emphasizing that the *quantitative* contribution of polar regions may be different. Disordered relaxor PST thin films were annealed at 700°C resulting in a *Low-Temperature* disordered state, while ceramic samples were annealed at temperatures in excess of 1500°C leading to a *High-Temperature* disordered state. *Both* states of disorder evolved to the *same* long range ordered ferroelectric state after annealing at temperatures near 900°C.

Version Abrégée

Les relaxeurs ferroélctriques à base de couches minces possédent des propriètès diélectriques bien inférieures aux propriétés obtenues lorsque ceux-ci sont réalisés à base de matériaux massifs. De plus, la forme et l'épaisseur du film mince auront une grande influence sur les propriétés ferroélectriques obtenues. Afin d'investiguer ce phénoméne, le " Lead Scandium Tantalum" (PST) a été fabriqué par la technique de dépôt Sol-Gel. Nous avons, pour cela, utilisé des précurseurs d'acétate et d'alkoxide. Les films de PST ainsi obtenus peuvent être soit ferroélectrique soit relaxeur. Pour cela, il nous suffit de maîtriser l'ordre positionnel du site B. Celui-ci est contrôler par des méthodes de recuits. Le PST sera ferroélectrique lorsque le site B est ordonné et relaxeur dans le cas contraire (désordonné).

À l'égard du procédé de fabrication, il a été montré que la déshydratation de l'acétate de scandium par l'acide acétique anhydride suivi de la modification précoce via le solvant 2 methoxyethanol est nécessaire pour obtenir un site B stable et une couche mince stœchiométrique. Un excés de plomb supérieur à 20% est nécessaire afin de compenser la perte de plomb durant le recuit et ainsi éviter la formation de phases secondaires. Nous montrons qu'il est nécessaire de travailler à des températures de recuit proche de 700°C pour obtenir des films relaxeur (désordonnés) possédant des propriétés mesurables. Pour des températures voisines de 1000°C , nous obtenons des films ordonnés et des propriétés mesurables. Mais pour des températures supérieures à 1000°C une dégradation significative des films est observée.

Les films fortement ordonnés montrent le développement d'un état ferroélectrique et des propriétés diélectriques comparables à celles des céramiques massives ordonnées. Les films présentant une structure désordonnée (fabriqués sur plusieurs substrats et sous différentes conditions de traitements) montrent des valeurs de constantes diélectriques réduites d'un facteur 10 comparé à la céramique ou au cristal simple. Une comparaison

directe entre des couches de PST ordonnées et désordonnées, déposés sur un même substrat, montre que les constantes diélectriques augmentent avec l'augmentation de l'ordre du site B, tandis que pour la céramique, l'effet inverse est observé (diminution des constantes diélectriques avec l'augmentation de l'ordre).

En terme de "Lattice Dynamics (LD)", les films ordonnés de PST montrent de façon inattendue que la fréquence du mode optique transverse (TO1) décroît jusque la température de Burns. A cette température, nous observons aussi l'apparition d'un mode central attribué à l'apparition des régions polaires à l'intérieur de la phase paraélectrique. De plus, l'augmentation de la température de recuit pendant le procédé semble augmenter la contribution diélectrique du mode central.

Nous montrons, au travers d'une étude comparative de la réponse diélectrique "In-Plane" et "Out-Plane", que les faibles valeurs de constantes diélectriques obtenues dans les deux cas, ne peut pas s'expliquer a l'aide d'une couche de passivation pour des films ayant une épaisseur supérieur à 1 micromètre d'épaisseur. Les changements des constantes diélectriques résultants d'un stress thermique, sont minimes et relativement insignifiants comparé à la réduction d'un facteur 10 dans la constante diélectrique des couches minces, comparé à la céramique. Une étude concernant l'influence de la taille des grains sur la valeur de la constante diélectrique montre qu'il n'y a aucun changement détectable de celle-ci pour des tailles de grains comprises entre 325 à 140 nm. L'auto-polarisation est observée à l'intérieur des couches minces de PST et celle-ci a pour effet de diminuer la constante diélectrique de 10% environ pour des températures proches de la valeur de la constante diélectrique maximale.

Une nouvelle hypothèse est proposée pour expliquer la réponse diélectrique réduite dans les couches minces relaxeur, mettant l'accent sur la contribution quantitative des régions polaires dans les films couches minces comparé aux céramiques massives. Ces deux états de désordres peuvent évoluer vers un même état ordonné lorsque le traitement thermique appliqué est de l'ordre de 900°C pour des temps assez élevés.

Contents

List of Figures

List of Tables

Chapter 1

Introduction: Characteristics of Relaxor Ferroelectrics and the Reduced Thin Film Dielectric Response

1.1 Introduction and Motivation

Relaxor ferroelectrics have been a topic of interest since the late 1950's when Smolenski [8] observed a broad frequency dependent dielectric maximum in the Lead Magnesium Niobate (PMN) system. Surprisingly it was discovered that this diffuse permittivity maximum does not correspond to a structural phase transition but is reminiscent of dielectric relaxation phenomena. Furthermore, this "relaxor" phenomenon is not limited to lead based perovskites but is also found in some modified lead free ferroelectric perovskites [9] and layered tungsten bronze structures[10]. For a number of years the properties of these compounds were described by a compositional inhomogeneity model [11][12] where it was hypothesized that a small (100 Angstrom) non-equilibrium ferroelectric polar phase

appears and disappears under thermal fluctuations.

Hard experimental evidence for these polar regions came in the early 1980's when Burns and Dacol [13] observed deviations from the linear optic index of refraction occurring in PMN and PZN at T_b, now termed the Burns temperature, which is several hundreds of degrees above the temperature of the dielectric maximum. These changes were shown to be related to randomly distributed local polar regions whose presence gave an *average* index of refraction. Since for a normal cubic ferroelectric material this deviation in the index of refraction due to polar regions only exists after cooling through the phase transition to a macroscopically polar phase, the Burns temperature became analogous to the phase transition temperature in ferroelectrics, namely the onset of polarization. In this framework, relaxors at temperatures above the dielectric maximum could be viewed as composite materials of a cubic paraelectric phase with small regions of ferroelectric polarization, now commonly referred to as nano polar regions (NPR).

The main differences between conventional ferroelectrics and relaxor ferroelectrics are presented in figure 1.1, and these differences are directly related to the presence of NPR. The dielectric constant versus temperature behavior for a conventional ferroelectric shown in figure1.1a exhibits a sharp, narrow first or second order phase transition, with a macroscopic symmetry change at the transition temperature T_c. The dielectric constant (k) displays *no* shift of the dielectric maximum with measuring frequency and can be described by the Curie-Weiss law (k=C/T-T_c) which predicts a linear relation between 1/k and the measurement temperature [14]. The polarization behavior for a conventional ferroelectric is presented in figure 1.1b which shows the onset of spontaneous polarization (sharp according to first order transition, or gradual according to second order) at the phase transition temperature T_c, and the *absence* of any macroscopic polarization at temperatures above the phase transition. Figure 1.1c displays the polarization versus electric field response for conventional ferroelectrics at temperatures just below T_c indicating the switching of macroscopic size ferroelectric domains or regions of homogenous long range

polarization.
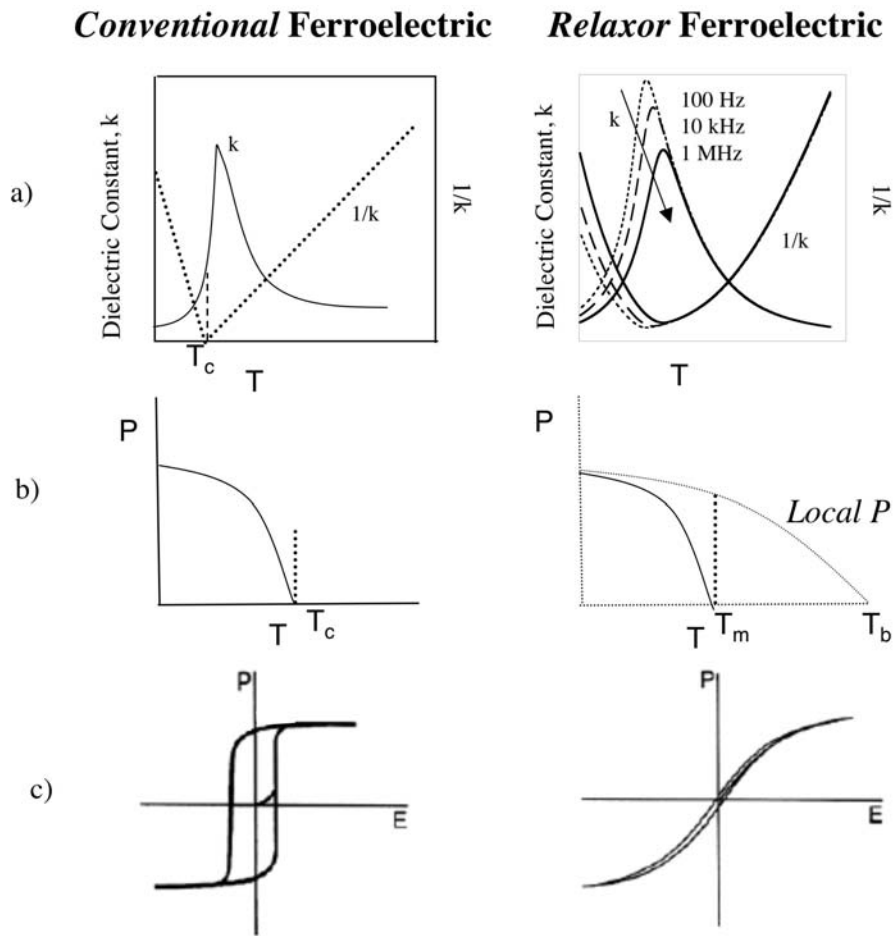
Figure 1.1: *Comparison between conventional ferroelectrics and relaxor ferroelectrics a) Dielectric constant (k) and 1/k versus temperature and frequency, b) Polarization versus temperature, and c) Polarization versus electric field at temperatures below the dielectric maximum. T_c in ferroelectrics, and T_m in relaxors stands for the temperature of the maximum permittivity and T_b stands for the Burns temperature, or onset of local polarization*

In contrast to conventional ferroelectrics, the dielectric constant in relaxors shows a shift of dielectric constant maximum with measuring frequency as shown in figure 1.1a . In addition, the response shows significant deviations from the Curie-Weiss law, and *no* structural phase transition is detected across the dielectric constant maximum T_m. This

is clearly reflected in figure 1.1b which shows that the dielectric maximum at temperature T_m is not associated with onset of polarization as in conventional ferroelectrics at T_c, and that nano-size polar domains NPR persist at temperatures well above the dielectric maximum as evidenced by measurements of local polarization. The behavior of these NPR at temperatures just below the dielectric maximum is also different from conventional ferroelectrics. Relaxors exhibit a slim loop polarization versus electric field response as shown in 1.1c, reflecting the non-cooperative nature and lack of long range polar order as compared to their conventional counterparts.

Qualitatively, the experimental observations of relaxors including their frequency dispersion and high permittivity maximum may be explained by involving the dynamics of NPR whose motion is responsible for the large extrinsic response in these materials[15]. The behavior of a relaxor material upon cooling from the Burns temperature towards the dielectric maximum is schematically presented in figure 1.2 as a competition between 1) a *relaxor state* -short range polar order, where the direction of polarization in NPR is in a random fashion with respect to the applied measuring field, thus raising the system energy due to mis-aligment or 2) a *ferroelectric state*- where long range polar order is developed along with the formation of domains (homogenous regions of polarization) and their interface called a domain wall, which increases the system energy.

Interestingly, it has been demonstrated in a large range of relaxor systems that long range polar order may be induced by application of an electric bias field upon cooling through T_m, thus stabilizing the polar phase in our composite picture of relaxor structure. Even more remarkable is that some relaxors such as PSN[16] and PST[17] exhibit a *spontaneous* relaxor to ferroelectric phase transition (with accompanying structural phase changes) at temperatures just below the dielectric maximum in *absence* of an external field. Furthermore, this spontaneous transition has been shown to be completely suppressed in the case of PST by the presence of lead vacancies, and the material remains a cubic relaxor well below the temperature of the dielectric maximum. It is emphasized
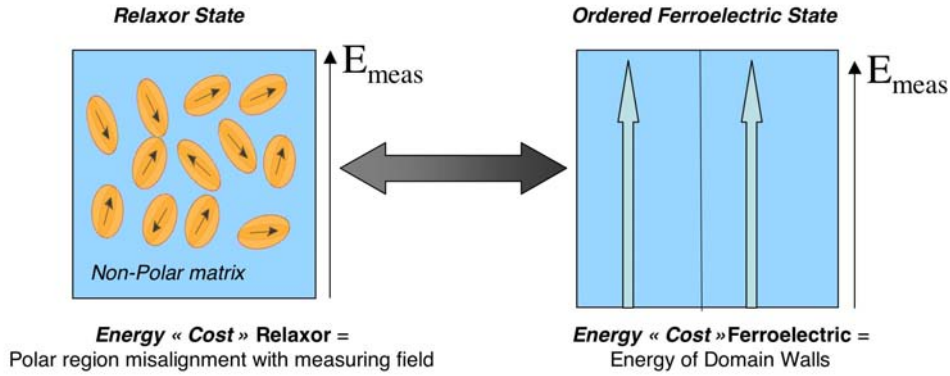
Figure 1.2: *Competition between relaxor and ferroelectric states as the material is cooled through the dielectric maximum: a relaxor state with* no *long range polar order, and a ferroelectric state*

that there is a spectrum of relaxor behavior between these two extremes, as evidenced by materials such as PZN[18] which undergoes a gradual transition to a long range polar ordered state in the absence of field.

The effects of pressure on the relaxor response have also yielded interesting perspectives on the relaxor to ferroelectric transition by examining the competition between long and short range interatomic forces in PLZT[19], and PZN-PT relaxor compounds[20]. At the composition studied (6/65/35 PLZT) and (PZT-9.5%PT), both materials exhibit a spontaneous relaxor to ferroelectric transition at some temperature T, below the dielectric maximum under zero applied electric bias field. The application of hydrostatic pressure during measurement inhibits this relaxor to ferroelectric transition and the material remains in the relaxor state at lower temperatures. This behavior has been explained in terms of a decrease in the correlation length between nano-polar regions with increasing pressure.

Recent work has focused on the *origin* of polar region formation at temperatures above the dielectric maximum at the atomic level, and how this microscopic level electrostatic

balance is maintained for different systems leading to the oberved dielectric response. With the proper understanding, it is hoped one can design materials with a large *reversible* non-linear response, within a certain specified temperature and frequency range.

The work presently available on thin film relaxor (TFR) materials [1] has a consensus on one major point, namely that the permittivity is drastically reduced by an order of magnitude as compared to bulk materials. The permittivity is in the range of $\approx 20,000$ for single crystal and ceramic relaxors to ≈ 2000-3000 typically reported for thin films with the maximum value reported for TFR being near 5000 [21],[22] for PMN and PST films respectively. This reduction in permittivity is commonly reported to be due to 1) film quality issues related to secondary phases, or entrapped porosity, 2) grain size effects[23], 3) clamping of the film by the substrate[24], 4) the presence of a low dielectric constant "passive" layer at the film electrode interface resulting in a series capacitor arrangement reducing the dielectric constant measured in films [25] [26], and 5) increased chemical disorder or the presence of defects (as a result of low processing temperatures of thin films as compared to bulk materials) which act as local pinning centers and reduce polar region response.

Thin films of conventional ferroelectrics such as BST[27] and PZT[28] have also exhibited a size effect, and it is theoretically estimated that there are size limits to ferroelectricity with film thicknesses decreasing further than about six unit cells ($\approx$24A)[29]. Since ferroelectricity is a cooperative phenomenon, these effects are related to the neighboring surface which cannot participate in the polarization response, thus all films should have a intrinsic "passive" or surface layer[30]. In addition there are effects associated with the presence of the top electrodes. If the dielectric response is measured "out of the plane" of the surface using a parallel plate capacitor method, the near by electrode layer forms a series capacitor connection due to the finite thickness layer of free charges in the electrode[31].

---

[1]Thin films are defined in this study as being less than 2 to 3 microns.

A recent review[32] using experimental data on BST films has quantitatively estimated the effective passive layer thickness from the blocking of surface polarization and from electrode effects resulting in values of less than 1 Angstrom, a value *less* than the unit cell parameter. Although these are clearly unrealistic physical values, it demonstrates the validity of the passive layer idea as a possible scenario for the reduction in permittivity. However, with increasing film thickness the surface response becomes negligible, and indeed ferroelectric films in the 1/2 to micron range exhibit exceptional properties, with recent work on PZT showing piezoelectric properties compatible with the electrostrictive coefficients and polarizations know from bulk ceramics [33]. These arguments beg the question, "How are relaxor materials impacted differently than conventional ferroelectrics in the thin film form, and what is the most efficient way to examine these differences?"

Direct comparisons between thin film and bulk materials are difficult for two main reasons, 1) the clamping (film constrained by substrate) and texture of the film which directly leads to 2) the domain pattern in thin films which determines the extrinsic response. However, in convential ferroelectrics it has been shown that the intrinsic, or lattice response is the same for nominally thick films (say in the 500 nm range), while the extrinsic response varies greatly due to domain formation. In thin film relaxors (TFR), the situation is more complicated because the origin, and dynamics of these nano polar regions (NPR) are still a source of controversy. In fact, the NPR are inferred to exist, yet they have never been directly observed. This makes it difficult to establish cause and effect relations as has been developed for ferroelectric domains. In fact, the onset of local polarization above the dielectric maximum at the Burns temperature has not until now been observed in thin films specimens. It is because of these issues that we pose the fundamental question which will be examined in the course of this thesis, *"Is the intrinsic nature of the relaxor the same in thin film form as in ceramics and single crystals?* Are we just unable to access the physical values, or is the material itself different, altered by defects or different on the scale of chemical homogeneity due to processing differences?

In order to examine this question we suggest the comparison of relaxor *thin films*, to convential ferroelectric *thin films*, in addition to the comparison of thin film relaxor materials to ceramic/single crystal specimens. The PST material system has been used as a "tool" for our investigation because by tailoring the arrangement of "B" site species Sc and Ta with processing, we can produce a thin film that behaves as either a conventional ferroelectric (ordered PST, PST-O), or a relaxor ferroelectric (disordered PST, PST-D). We shall proceed by studying 1) first the "Physical" effects thought to be responsible for the reduced permittivity including stress/clamping, grain size, surface and interfacial layers, 2) we will examine the regions where the response is expected to be the same, namely at low temperature 20K, and at very high frequencies to examine the lattice contributions to the dielectric response. By comparing this lattice or intrinsic response, with the extrinsic responses observed in ordered, and disordered PST thin films and bulk materials we will be in the position to comment on the "nature" of TFR.

1.2   Relaxor Characteristics

1.2.1   PMN

Figure 1.3a shows the real and imaginary part of permittivity as a function of temperature for the model relaxor system PMN showing significant frequency dispersion at temperatures near the dielectric maximum. Figure 1.3b shows results from Bovtun et al [1] of broadband frequency dependance of the complex permittivtiy in PMN from THz to the MHz range at temperatures between 500 and 110 K. The high and low temperature permittivity are frequency independent with a peak in the loss appearing near 10^{11} Hz range below 500K, which increases in intensity and slows to 10^9Hz at 290 K. This peak, termed a central mode (CM), further decreases into the MHz range near 260K, and below this temperature the relaxation broadens leading to frequency independent dielectric losses and which must be characterized with a distribution of relaxation times.
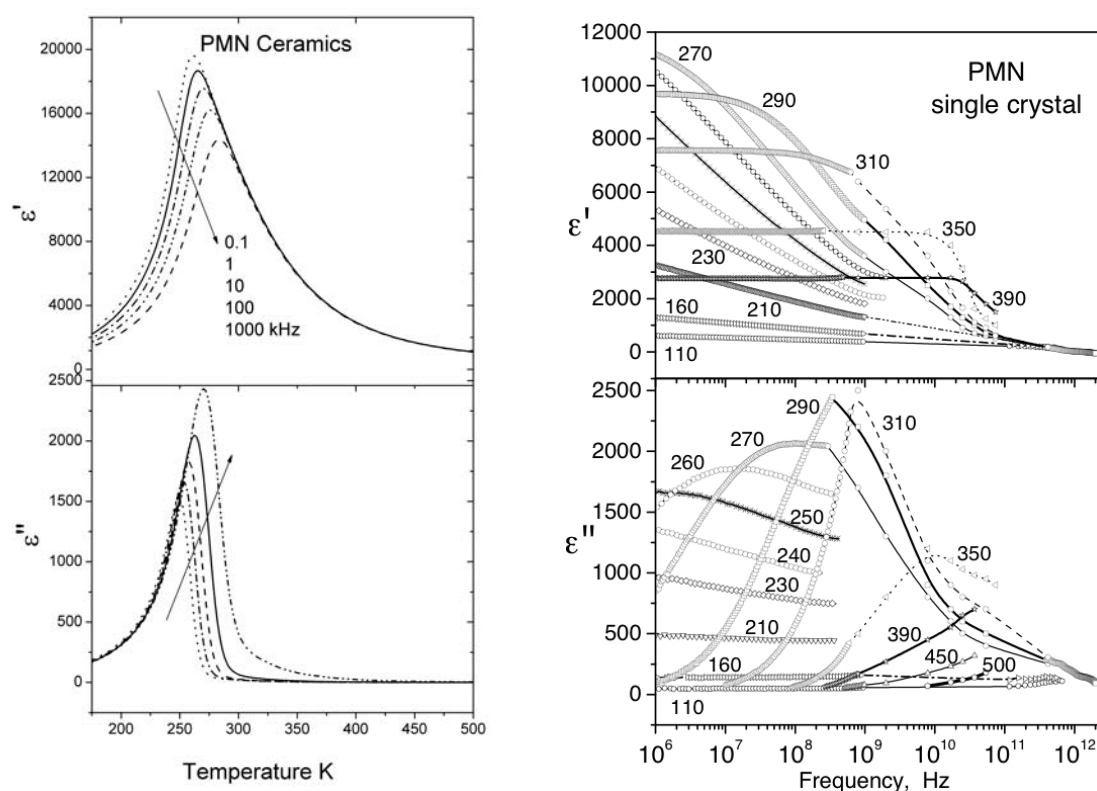
Figure 1.3: *a)Dielectric constant and loss of PMN ceramics as a function of temperature and frequency from 100Hz to 1MHz Courtesy of Dr. S. Gentil, b) Dielectric constant and loss of PMN single crystal from MHz to THz in the temperature range 500K to 100K, from reference [1]*

At temperatures well below the dielectric maximum PMN displays hysteresis in PE loop measurements indicative of long range polar order, however structural studies have surprisingly shown that there is no evidence of optical anisotropy [13], or x-ray line splitting which would indicate a phase transition to a polar phase. The structure of PMN at 5K was examined by Mathan [34] by X-ray and neutron powder diffraction revealing a rhombohedral symmetry in the local polar phase which occupies roughly 20% of the volume in the cubic host lattice. The correlation length of these polar regions NPR were estimated to be 100 Angstroms. The dielectric behavior above the temperature of the dielectric maximum deviates from the Curie-Weiss law, and this deviation is thought due

to the presence of local polarization as observed by the presence of RMS (root mean squared) polarization derived from thermal expansion measurements [10], and deviations from the linear optical index of refraction at temperatures below the Burns [15] temperature T_b, with the local polarization disappearing above this temperature. The observation of a structural phase change induced by a DC bias field has been observed by X-ray[34] and optical birefringence [35], with several authors observing a threshold field level of 2 kV/cm necessary for field induced transition upon cooling.

1.2.2   Other Materials with Relaxor Behavior

The model relaxor system PMN exists as a single phase. However relaxor behavior has been observed in solid solutions, particularly the PZT system with Lanthanum additions to the A site in the form $(Pb_{1-x}La_x)(Zr_yTi_{1-y})O_3$. Studies by Li [36] at y concentrations of y=0.65 (rhomobohedral) and y=0.40(tetragonal) indicated the disappearance of normal ferroelectric domains at high La contents ($\approx$8 at.% with y=0.65, and $\approx$14 at.% with y=0.40). Obviously these changes in domain structure are accompanied by changes in the dielectric response, including a remarkable *spontaneous* relaxor to normal ferroelectric transition in the case of 12 at.% La addition in y=0.40 tetragonal samples.

Of particular importance is that the onset of relaxor behavior in these systems is accompanied by a *reduction* in the permittivity (from near 40,000 at low La content x=2 at.% in y=0.65, to nearly 8000 in x= 10 at.%). This was understood to be a result of aliovalent La ion substitution resulting in A site vacancies. In addition, the inhibition of the spontaneous relaxor to ferroelectric transition in the systems PST [17] and PSN [16] have also been shown to be as a result of lead vacancies. The common link in all relaxor behavior is the appearance of local polarization at some temperature above the dielectric maximum. Materials differ as to their competition between this polar phase and the cubic parent phase, with some materials undergoing a spontaneouos phase transition (PST, PSN) to a long range polar state (non-symmetric crystal structure) and some

materials (PMN) persisting as a "composite" of polar and non-polar regions even down to a temperature of 5K. The behavior of these NPR was shown to be impacted by both *internal* changes such as the presences of lead vacancies and positional disorder on the B site, as well as by *external* influences such as pressure and bias electric fields. What is not clear is the origin of the local polarization. Only speculative until recently, we now have some insight into the microscopic origins which will be discussed in the next chapter, followed by a discussion of the role of "B" site disorder and its impact on relaxor phenomena.

1.3 Microscopic Origins

A discussion of the origins of relaxor behavior starts with the structure of the unit cell. Most technologically important ferroelectrics and the relaxor compounds discussed herein are multicomponent oxides with a perovskite structure. In ionic crystals, the main contribution to the binding energy is electrostatic in origin[37] with the balance between cohesive and repulsive contributions determining equilibrium positions. These simple ideas combined with geometrical factors from Paulings rules provided the first quantitative description of perovskite stability, crystal structure and the driving force for a phase transition to to a polar state[38]. However, a more detailed view of bonding is needed even to explain the nature of ferroelectricity in the model ABO_3 systems $PbTiO_3$ and $BaTiO_3$.

It was demonstrated by Cohen [39] that covalent bonding plays an important role in these systems. With atomistic level simulations it was shown that assuming only an ionic character of the atoms, short range repulsions favor the centrosymmetrical cubic phase, even though long range Coulomb energy favors a ferroelectric distortion. This repulsive force is decreased by the hybridization of unoccupied d orbital states in common B site transition metals with the surrounding oxygen, allowing the long range forces to dominate and stabilize the ferroelectric state. Furthermore, it was shown that the A-site cation can

impact the balance of short versus long range forces by increasing the strain due to the size and bonding of the ion, thus favoring a certain unit cell geometry with the lowest energy, as well as by hybridizing with surrounding oxygens which indirectly affects the B site repulsive terms.

In the model relaxor system PMN, the occupancy of the B sites must be 1/3 Mg and 2/3 Nb in order to maintain charge neutrality. However, the observation of 1:1 cation ordering in this system[40] evidenced by small (2-5nm) micro-ordered domains along the 111 unit cell direction led to a debate as to how the local unit cell doubling and accompanying charged regions are distributed and what was their role in relaxor behavior. It is now proven from atomic simulations and direct TEM observation of B site cationic order in PMN [41] and PMT[42] that the B site atoms are arranged according to the so called random layer model. It has been shown that the ordering occurs in the 111 direction composed of two alternating planes, one which contains only Nb^{5+} ions and a second type of plane which has a random distribution of Mg^{2+} and Nb^{5+} in a 2:1 ratio, thus maintaing the electroneutrality and stoichiometry of the overall composition. The role between these ordered regions in PMN and the development of a local polar state has not yet been unambiguously established. However, recent work points to the role of the lead (Pb) atom as being a source of the local polar state, with changes in B site ratios affecting the charge/force balance in the unit cell, leading to local Pb displacements [43].

The role of lead has been experimentally confirmed by replacing Pb with Ba in systems such as PSN which display relaxor behavior. With the substitution of Ba, a paraelectric phase exists at all temperatures in the BSN material. Why do Pb atoms and their bonding in perovskites lead to random local displacements, giving rise to a local polar state, but Ba based perovskites do not? This question was recently addressed by Cockayne[44] by performing plane wave pseudopotential calculations of total energies for *ordered* $AB_{1/3}B'_{2/3}O_3$ and $AB_{1/2}B'_{1/2}O_3$, which showed that there are lower energetic barriers to disordering the B sites in Pb based systems than in Ba based systems. For

example, BSN disorderes at 1400, whereas PSN disorderes at 1200°C . This behavior was again explained by the covalent character of Pb-O bonding and the balance of long range Coulomb forces, which are responsible for the ordered state, and short range repulsive forces which lead to disorder. The long range interactions which drive B site order in Ba systems due to its ionic character do not dominate in the case of lead based oxides with significant Pb-O hybridization.

It is now clear that relaxor behavior is a manisfestation of local displacements at the atomic level determined by the balance of long and short range electrostatic energy considerations, and thus ultimately on the electronic structure of the consituent atoms. In lead based systems the positional order or distribution of B site cations determines whether a long range ordered structure will develop which is stabilized by Coulomb forces, or whether repulsive interactions due to random B site occupation will inhibit this transformation. The experimental results on B site positional disorder in PST and PSN materials which support these arguments are well documented and will be discussed in the following section.

1.4   The Role of "B" Site Disorder

Initial studies on the role of B site order in PST and PSN materials [45][46][47] indicating a disordered state at high temperatures near 1500°C with a broad permittivity maximum near 15,000 at T=13°C ; while lower temperature sintering (1300°C) for longer time resulted in the appearance of superlattice reflections due to the increased periodicity of the B site Sc and Ta ions alternating in an orderly fashion along the 111 body diagonal direction as shown in figure 1.4a in real space and seen in figure 1.4b as a cut of the [110] plane. Accompanying the increased periodicity was an upward shift of the dielectric maximum to higher temperatures, a reduced value of the maximum permittivity and an observed heat effect from DSC measurements indicating a first order phase transition.

The role of defects in bulk ceramics and their effect on ordered ferroelectic PST and
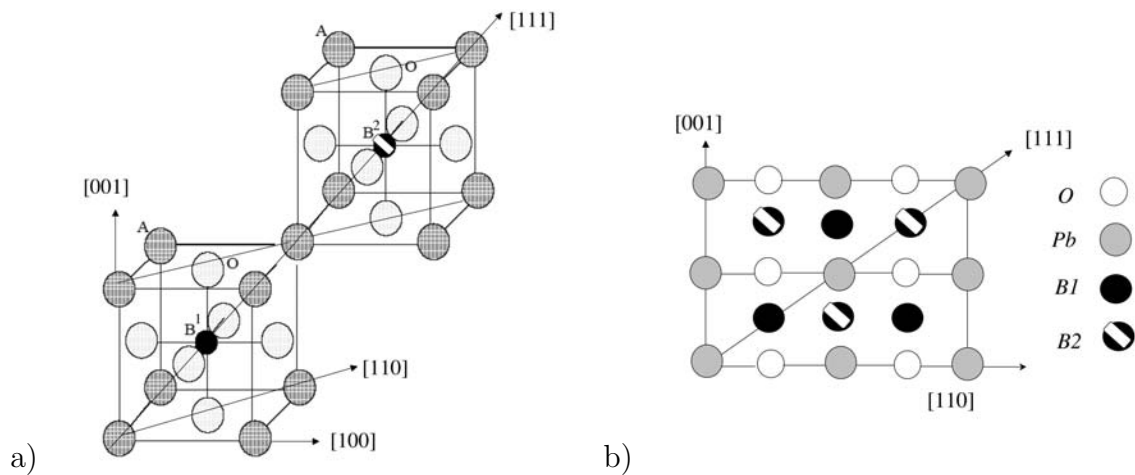
Figure 1.4: *Ordering on the B site along the 111 direction as seen from a) doubling of unit cells and b) cut of the (110) plane showing alternating planes of B_1 and B_2 in the ordered structure*

disordered relaxor PST was examined by Fan C. [17] and presented in figure 1.5 a and b. Stoichiometric disordered ceramics showed a high maximum dielectric constant near 25,000 with a spontaneous relaxor to ferroelectric transition near $=10°C$. The presence of lead vacancies *suppressed* the spontaneous relaxor to ferroelectric phase transition, shifted down the temperature of the dielectric maximum, and reduced the maximum dielectric constant by approximately half. Highly ordered ceramic samples displayed an upward shift of the dielectric maximum to higher temperatures as compared to disordered samples, as well as a *reduction* in the maximum value of the dielectric constant to near 8000. Of particular interest is that the ordered samples are impacted less by the presence of lead vacancies than their disordered counterparts, with a slight downward shift in the dielectric maximum to lower temperatures, and a more gradual transition to a ferroelectric state with the maximum value of dielectric constant remaining the same. Ordering of the B site species has also been observed in PST thin films[22][48], however very little dielectric data is available for comparison with the behavior observed in ceramics and single crystals.

In recent structural studies using neutron and synchrotron X-ray diffraction on PST[49]

ceramics it was shown that samples with high degree of B site order approaching 90% were found to have a significantly different average and local crystal structure, with deviations being greater for Pb and O than for the B site species. In addition, the local direction of polarization was found to be due to Pb displacements in the 100 direction, while the long range macroscopic polarization direction is in the 111 direction.
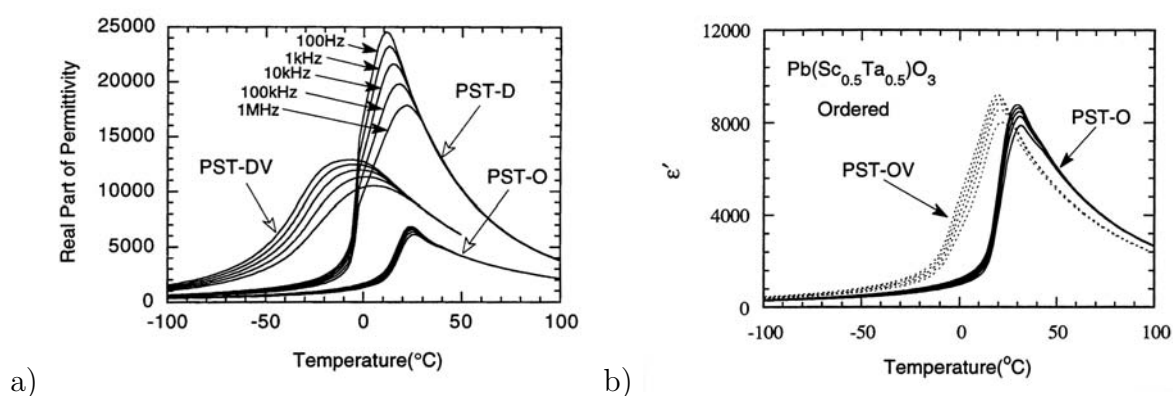
Figure 1.5: *Dielectric constant versus temperature for (a)disordered and (b) ordered PST ceramics with and without significant amounts of Pb vacancies, D-Disordered, O-Ordered, DV-Disordered with Lead Vacancies, OV- Ordered with Lead Vacancies.[2] From Chu F. Thesis Lausanne 1994,*

1.5 Models of Relaxor Behavior

There has been considerable debate in the literature as to whether the dynamics of PNR should be considered as a glassy state [50], or as nanodomain structures [35]. Proponents of the nano-domain state point to random fields induced by compositional heterogeneities such as local order in the case of PMN, and random B site arrangement in PSN and PST as possible origins of random fields. The observed Barkhausen jumps of a domain like structure support this idea, while proponents of models related a glassy state point out the advantage taking into account the *interactions* of local polar states as being similar

to the freezing process in dipolar glasses. Initially the dipolar glass model was commonly accepted based on the description of the dispersion of the dielectric constant maximum being experimentally described as a freezing process. However, initial examinations of the dipolar glassy state performed by measuring the non-linear dielectric response did not show the expected divergence of critical parameters extrapolated to the freezing temperature. In addition, models based on "flipping" or "spinning" of polar regions in analogy to super-paramagnetic moments were found not to represent the AC and DC non-linear behavior of relaxors [5].

In fact, a detailed examination of this non-linearity in the dielectric response which led to the two current models or pictures of relaxor behavior. The motion of inter-phase boundary regions as "breathing" rather than "flipping" or spinning was suggested by Tagantsev and Glazounov [51]. Within this framework a critical divergence of non-linear dielectric parameter was expected, but not observed [5] implying that no phase transition to a glassy state had occurred. Pirc [52] and Blinc however, *did* observe such a divergent behavior, and developed a model termed the Spherical Random-Bond Random-Field (SRBRF) to describe the interactions of NPR. The principle difference between a dipolar glass state and their SRBRF description is the introduction of a variable length parameter describing the dipole moment of local polar regions. In further studies [53], the calculated local polarization distribution by the SRBRF model was found to be in good agreement with the measured polarization distribution obtained from ^{93}Nb NMR measurements. The results of the polarization distribution confirming a glassy state, and the reported divergence of the dielectric non-linear coefficient, combined with the temperature and non-linear dielectric response prediction of the SRBRF model give strong evidence of a glassy state, at least in the model PMN relaxor system. It is emphasized that many models, or physical descriptions may produce the requisite frequency dispersion, however few can represent the non-linear dielectric data. Even with the apparent success of the SRBRF description of relaxors, there is no real model which can predict macroscopic

properties from atomic level strucure such as that in the thermodynamical LDG approach for the lattice response of ferroelectrics. One of the reasons is that local deviations at the atomic level create large extrinsic responses which may be influenced at a greater level than the lattice response of ferroelectics. This thesis does not seek to make an impact on the modeling of relaxor systems, but rather to qualitatively and quantitatively compare the dielectric response of relaxor and ferroelectric thin films and ceramic/single crystal specimens under similar conditions to comment on the origin of their difference.

1.6   Objective/Aim of Thesis

The ability to tailor the ordering of the B site species in PST provides the unique opportunity to study relaxor phenomena in thin film form, specifically by comparing its response with the corresponding ferroelectric film. This gives us a convenient "basis" on which to make our comparisons, since the behavior of conventional ferroelectrics in the thin film form is significantly better understood. The behavior we would like to understand is displayed in figure 1.6a based on results obtained in the course of this thesis. The dielectric constant of disordered PST thin films with thicknesses from 500 nm to 1.4 micron's are plotted versus temperature at 1 kHz in 1.6a, in comparison with a disordered ceramic PST. In figure 1.6b the polarization response is shown for a ceramic and a 500 nm thin film measured at room temperature. It is seen that at temperatures greater than 150°C the dielectric constant of all the samples converge to a value near 1000, with the greatest differences being exhibited near the temperature of the dielectric maximum. As it has been demonstrated in ceramic and single crystal relaxor materials the large dielectric response is extrinsic in origin stemming from the dynamics of NPR, the reduced thin film response could be due to the nature of the NPR in thin film form or external factors affecting their dynamics.

Specifically, to answer the question, "*Is the intrinsic nature of relaxor behavior the same in thin film form as in ceramics/single crystals?* we shall examine the following
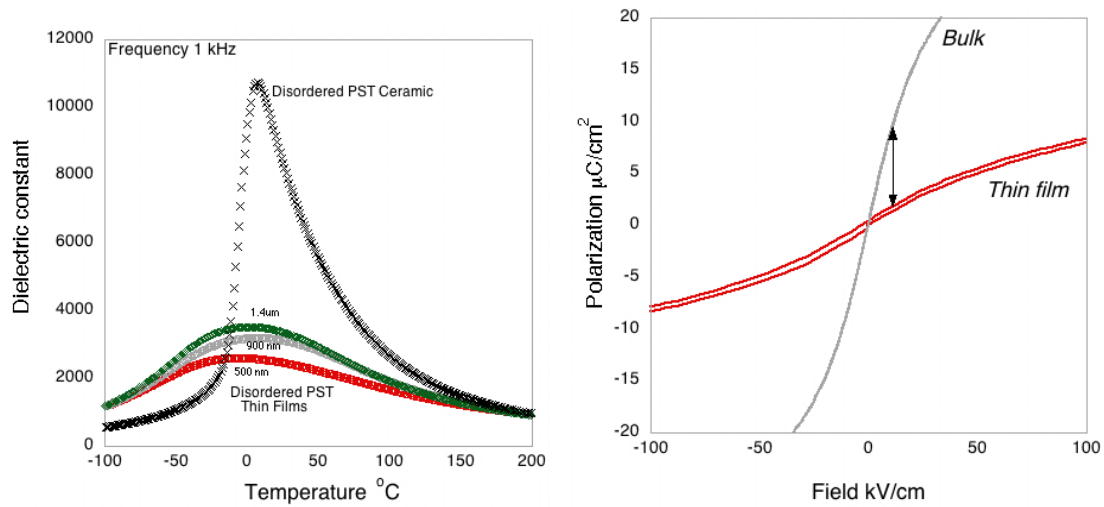
Figure 1.6: *Disordered PST thin films on Pt/Si substrates versus disordered PST ceramic*

points:

- Are there polar regions above the temperature of the dielectric maximum in thin film relaxors as in ceramics/single crystals?

- If yes, do their dynamics differ from that observed in ceramics/single crystals, or are they more sensitive to defects because of the thin film state?

- Is their quantitative contribution different? Are less NPR formed by lower processing temperatures in thin film as compared to ceramics/single crystals?

- To what extent may we attribute the reduction in dielectric constant in thin films to external factors such as passive layer, grain size and clamping/strain due to the underlying substrate?

With these general questions, the thesis is organized as follows:

Chapter2 Processing and Properties: State of the art in sol-gel PST films, and structure property relations

Chapter3 Dielectric Response including in-plane and out of plane response and thickness dependence of permittivity, dynamics of non-linear response probing polar region

dynamics, high frequency (GHz) and cryotemperatues 20K probing intrinsic dielectric response, and effects of bias fields.

Chapter4 FTIR investigations into the lattice dynamics and lattice contributions to static permittivity in model PMN system, and PST with varying degrees of "B" site order.

Chapter 5 Pyroelectric and Piezoelectric properties: Detection of fixed layer of "self-polarization" and impact on dielectric response.

Chapter 6 Discussion and synergy of the results for the Thin film Relaxor State

Chapter 7 Summary and Conclusions

Chapter 2

The Fabrication of PST Sol-Gel Derived Thin Films

2.1 State of the Art/Background

2.1.1 Literature Review of PST Thin Film Materials Processing

In contrast to traditional ferroelectric and relaxor compounds like PZT, and PMN, the reports on PST thin film fabrication are scarce and will be reviewed in this section starting with physical vapor processing methods, followed by solution derived films.

Early physical vapor deposition methods followed procedures similar to traditional ceramic processing. Reaney [54] developed a method of preparing PST in a two step procedure. Initially, a sputtered $ScTaO_4$ layer (annealed at 850°C) was deposited from metal targets followed by a lead oxide layer deposition and sample annealing from 800 to 900°C in order to promote diffusion between the two layers and eventually obtain the desired perovskite phase. One-step PST was fabricated by co-sputtering PbO with Sc and Ta metal targets followed by film annealing at 900°C [54]. Dielectric measurements of PST on sapphire substrates using Ni/Cr interdigitated electrodes revealed strong processing dependent properties [54]. For the two-step synthesized PST annealed at 825°C , the

"in-plane" dielectric constant maximum at 1 kHz was 7000 at a temperature of -5°C for a 1 micron thick film, compared to a "in-plane" dielectric constant less than 4000 at a temperature of 6°C for a 2.3 micron thick film. This discrepancy is explained by the thicker film having an unreacted $ScTaO_4$ phase at the PST/sapphire interface which was not present in the thinner specimen. Films of similar thickness (2 micron) were made from both one, and, two-step processes and annealed at 900°C to promote the PST reaction by liquid PbO diffusion, resulting in dielectric constants of around 5000. The varying diffuseness of the transition is attributed to different degrees of "B" site ordering [54].

A series of publications followed these initial works on the sputtering of PST films indicating that rapid thermal annealing, post deposition, to temperatures around 800°C for 850 nm thin films on $Pt/Ti/SiO_2/Si$ substrates resulted in a dielectric constant maximum of 1800 at 30Hz, and 0°C , and a loss tangent of 1% at room temperature measured with Au/Cr top electrodes in an "out-of-plane" configuration [55], [56]. Microstructural studies on these films deposited at 300°C and then slow furnace or Rapid Furnace Annealed (RTA) revealed the presence of both pyrochlore and perovskite phases. Lead deficient grain boundaries were observed in the case of furnace annealed films. The RTA processed samples showed only the presence of a perovskite phase according to X-ray and TEM analysis, and all films suffered from voids and porosity as well as apparent cracks [56], [57].

An additional study of PST [58] deposited by reactive sputtering at 525°C on $Pt/Si/SiO_2/Si$ substrates indicated perovskite grains with amorphous or secondary phase pyrochlore grain boundaries (which were tantalum rich and lead deficient). The "lines" or cracks were determined to be chemically and crystallographically similar to the grain boundaries. The PST was concave along the lines, with perovskite grains within the concave area. This implies that during film growth these lines act as stress release centers, but are not genuine cracks that extend to the film substrate interface. The microstructure of reactivally sputtered films was further investigated revealing lead rich perovskite grains

resulting from the large (30 to 50%) lead excess employed during the process to favor perovskite formation at low temperatures (525°C). Evidence from lattice parameter measurements points to Pb^{4+} in the B site of the perovskite structure [58] in sputtered thin films, similar to that reported for PZT [59].

Pulsed laser deposition has also been used to prepare 500nm PST on 200nm YBCO/LaAlO$_3$ substrates at 575°C resulting in highly (100) oriented PST with dielectric constant maximum of 900 at a temperature of-40°C and 1kHz, and a loss tangent of 2% at room temperature measured "out of plane" with Cu top electrodes [60].

Chemical solution processing of PST started in the early 1990's with work by Whatmore in which again, the thin film processing was similar to that of traditional ceramic processing of PST. A two step procedure was followed with first the synthesis of a ScTaO$_4$ layer and second, a reaction with the PbO layer [61],[62] facilitated by high temperature annealing. The Sc/Ta layer was made from a reaction of Scandium acetylacetonate and tantalum ethoxide in 2-Methoxyethanol (2-MOE) resulting in a Sc/Ta complex which was deposited by spin coating and pyrolyzed at 450°C before deposition of a lead layer formed from lead acetate in 2-MOE. Multiple layer films were prepared by alternating Sc/Ta and Pb layers after pyrolyzing at 450°C after each layer before annealing. Processing temperatures of 900°C were employed in order to melt the PbO layer leading to a liquid phase, which could diffuse through ScTaO$_4$ and react to form PST. Due to the high processing temperature, the deposition was made on sapphire, MgO and GGG ($Gd_3Ga_5O_{12}$) substrates. A typical thickness of 2.7 μm film on GGG had a random film texture, a slight degree of superlattice ordering as evidenced by X-ray diffraction, and a nominal grain size of 1.5μm. Dielectric measurements were performed using interdigitated electrodes (due to lack of bottom electrode/high processing temp) and gave values of around 4000 for the dielectric constant and a loss tangent of 0.2 % in the paraelectric phase (70°C). No frequency dependence of dielectric properties as a function of temperature confirming relaxor behavior were presented.

The Sol-gel processing of PST was continued by Liu [63] who in an initial publication prepared a MOE based PST solution from Sc acetate, Ta ethoxide, and Pb acetate precursors. Films were made using multiple thin layers on Pt/Si substrates, i.e., spinning followed by heat treatment at 700°C for 1 minute *for each layer* until arriving at the desired thickness, followed by a final anneal for 30 minutes at temperatures ranging from 800 to 900°C . The room temperature dielectric constant of 300 nm films was 1000 with a loss tangent of 2% at 100kHz using gold top electrodes and a bottom Pt electrode. Temperature and frequency dependence was not indicated. In addition, PST films of 500 nm were fabricated by the multiple thin layer technique, each layer to 700°C with a final layer anneal to 750°C on Pt/MgO (100) substrates. The grain size of the film was 700 nm with X-ray indicating preferred (100) orientation, although the films lacked an epitaxial relationship with the substrate. Dielectric properties were measured "out of plane" with Au top electrodes displaying a dielectric constant maximum near 4000 at 0°C and 1kHz (Eac=0.25kV/cm), and a room temperature loss tangent of less than 1%. The dielectric constant and loss tangent displayed frequency dispersion characteristic of relaxor behavior in the frequency range of 1kHz to 1MHz [64].

In a later publication Liu [22] reported multiple thin layer films made from a solution with 18%Pb excess prepared by pyrolysis at 300°C , and annealing at 600°C between each layer to arrive at the desired thickness, followed by a further high temperature annealing step. Ordered PST thin films were made by slow cooling (1°C /hour) from annealing temperatures near 700°C . The resulting films displayed also a preferred (111) orientation on Pt/Si substrates. No dielectric data was presented in this case. Dielectric data was presented however for a disordered, 300 nm PST film on Pt/Si measured out of plane at a AC field level of 3kV/cm at 3 frequencies (1kHz, 10 and 100kHz) indicating frequency dispersion of real and imaginary parts of permittivity and a dielectric constant maximum of 4500 near 0°C . However processing details of the film were not given and there is no mention as to why the dielectric constant increased from 1000 to 4500 between the first

[63] and subsequent report [22].

Fuflyigin [65] has fabricated PST films on Pt/Si substrates using MOE based sol-gel solution with Scandium nitrate as a precursor. Again, the multiple thin layer method was used where each layer was annealed at 700°C with the total film thickness ranging from 300 to 500 nm. No microstructure was presented, but the films displayed a bimodal (100) and (111) orientation with no evidence of secondary phases as determined by X-ray diffraction. Dielectric properties were measured *"Out-of-Plane"* using Pt/Ti top electrodes resulting in a dielectric constant of 1400 and 1800 for PST films on Pt/Si fixed substrates, and free standing membranes (fabricated by reactive ion etching) respectively. The loss tangent was less than 2% at room temperature and 10 kHz. Dielectric measurements as a function of frequency and temperature were not displayed.

A comparative study of 400nm PST post RTA annealed to 800°C processed by sol-gel, Chemical Vapor Deposition (CVD), and sputtering on Pt/Ti/SiO$_2$/Si substrates was recently reported by Huang [66]. CVD films (deposited at 600°C) had 500 nm grains with a dense microstructure although there were problems with pyrochlore formation and surface roughness. Au/Cr electrodes measured out of plane displayed a dielectric constant of 1700 with a loss tangent around 1% at room temperature and a Tc=0°C at 120Hz. Sputtered films were typically porous with large 1 micron grains and pyrochlore present at the PST/substrate interface. Strangely, these films resulted in the best dielectric properties with a dielectric constant maximum of 2200 at Tc=10°C and loss tangents just above 1% at room temperature and 120 Hz. Sol-gel films showed columnar grain growth (200nm grains) with voids/pores concentrated at the grain boundaries and a relatively temperature independent dielectric constant of 1500 with a loss tangent of 1% at room temperature and 120 Hz. The sol-gel and sputtered films indicated superlattice ordering peaks after RTA annealing while the CVD film remained disordered. Even with the presence of ordering in the films, the phase transitions all very diffuse and no frequency dependence of the dielectric permittivity was reported [66].

2.1.2   Sol-Gel

2.1.2.1   General

The modern study of solution processed materials is often attributed to Ebelmen [67] who in 1846 produced the first silica gels from a metal alkoxide that hydrolyzed upon exposure to air. Since the foundation of colloidal science in the late 19th century, the knowledge of ceramic colloidal suspensions and their structural evolution from a sol to a gel, amorphous network, or final crystalline compound has progressed rapidly [68].

Solution preparation of oxide materials usually begins by the dissolution of metallo-organic compounds in a common solvent. Typical starting compounds are of the type M-OR metal alkoxide compounds; with a partial (+) charge on the metal atom and partial (-) on the oxygen due to electronegativity differences, these molecules are highly suited to undergo reactions which facilitate inorganic polymer networks. Through the hydrolysis and condensation of these metal alkoxide starting precursors an inorganic network of M-O-M bonds are formed along with byproducts such as water and alcohol [69]. The basic reactions are indicated as follows:

i)   M-OR   + H_2O $\rightarrow$ M-OH   +   R-OH   (hydrolysis)

ii)   M-OH   +   M-OH $\rightarrow$ M-O-M   + H_2O (condensation by oxolation)

iii)   M-OH   +   M-OR $\rightarrow$ M-O-M   +   R-OH   (condensation by alkoxolation)

iv)   M-OH   +   M-OH $\rightarrow$ M-OH-M   + H_2O (condensation by olation)
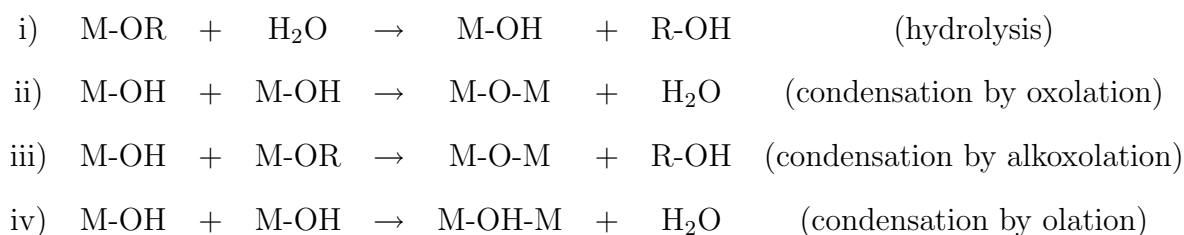
The metal species present M and the nature of the R group determine the starting compound reactivity. In addition, the choice of solvent may also affect the hydrolysis and condensation reactions through alcohol exchange reaction:

v)   M-OR   +   R'OH $\rightarrow$ M-OR'   +   ROH   (alcohol exchange)

Solvent characteristics such as polarity, and viscosity also play a role on the nature of the reactions, their rates and ultimately on the nature of the inorganic network that is formed; ie, the size of the oligimers/polymers, their shape, chemical composition and

distribution/bonding with each other in the solution, sol, or precipitate state. Through the tailoring of starting precursors, solvent and reaction conditions (pH, temperature, time) one can obtain a wide variety of final states such as gels, aerogels, precipitates, as well as stable solutions which can later be used by dip-coating or spin coating methods to produce films. For a general review see reference, "sol-gel science and technology" [68] .

2.1.2.2 Thin Film Ferroelectrics

In the solution processing of thin films, often termed "Chemical Solution Deposition (CSD)", there are three categories of solution routes generally referred to in literature; 1) sol-gel, 2) chelate, and 3) metallo- organic decomposition (MOD) which refer to the nature of the R groups and their solvent interactions.

For ferroelectric thin films the classic example of sol-gel processing is the method developed by Budd et. al., which uses lead acetate trihydrate, titanium isopropoxide, zirconium n-propoxide, and 2-methoxyethanol (MOE) as the solvent [70]. In this procedure the solvent MOE undergoes an alcohol exchange with the Zr and Ti precursors, thus reducing their sensibility to hydrolysis by an inductive effect of the oxygen in the methoxy group thus promoting solution stability as quick hydrolysis often leads to precipitation of metal oxide particles in solution. In addition to the alkoxide replacements, the acetate group of the lead precursor was shown to be partially replaced by MOE after refluxing and distillation steps used for dehydration [71]. The classic sol-gel process is characterized by a high starting precursor reactivity which allows for a large degree of control over the reaction pathway. Recently the more viscous and lower volatility solvent 1,3 propanediol has been used as a replacement solvent for MOE resulting in single thick layer depositions ranging from 0.5 to 1μm [72].

The chelate process is characterized by a molecular modification of the starting alkoxide precursors by chelating ligands such as acetates and β-diketonates. The chelating ligands may be the solvent, for instance in acetic acid based solutions, or the ligands

may be added in appropriate molar ratio's to metal alkoxide's in alcoholic solvents. An example of this process applied to ferroelectric thin films is the so called Inverted Mixing Order (IMO) process for PZT where titanium isopropoxide and zirconium butoxide are reacted with acetic acid in methanol to form chelated structures as evidenced by proton H^1 and carbon C^{13} Nuclear Magnetic Resonance (NMR) [73]. The chelate process in general renders the starting precursors less reactive.

The metallo-organic decomposition MOD process initially developed by Vest et al. utilizes large carboxylate ligands such as neodecanoates, and ethylhexanoates, and solvents such as xylene [74]. This process is the least flexible due to the relatively inert precursor structures. In addition, it requires the removal of a large quantity of organic matter during pyrolysis, however it is in practice the simplest technique in that one does not need to worry about hydrolysis or special solution synthesis procedures. It is in many cases a straightforward procedure that can even be used in aqueous solvents avoiding many of the health and processing hazards of common organic solvents [75].

Other approaches have also been used including the nitrate and Pechini process. These methods involve the dissolution of metal nitrates in water or alchol for the nitrate; and in citric acid/ethylene glycol mixture for the Pechini process [76],[77]. By controlling the citric acid to ethylene glycol ratio and solution temperature we can tailor the polymer molecular weight and viscosity for desired applications. In actuality, most of the routes used are hybrid techniques and the term sol-gel is used interchangeably with chemical solution deposition.

2.1.2.3   Chemical and Physical Solution Characterization

The characterization of the solution state and the subsequent "structural evolution" into the final crystalline phase can be divided into 1) chemical methods and 2) physical methods. Chemical methods include the determination of the bonding of the chemical species in solution by spectroscopy techniques such as Nuclear Magnetic Resonance (NMR) and

Fourier Transform Infrared (FTIR) to for example identify chemical shifts of H^1 and C^{13} in different chemical environments, and the frequency of absorption corresponding to vibration and rotation of chemical species respectively. NMR studies have been used to monitor ligand replacement reactions in the chelate processes described above and have shown that acetic acid completely replaces the starting alkoxy groups in the starting metal alkoxide precursors (zirconium butoxide and titanium isopropoxide in methanol solvent)[73]. This is also seen by FTIR with the appearance of two peaks near 1500 cm-1 corresponding to the asymmetric and symmetric stretching modes of the acetate group [78].

In addition to investigating ligand replacements, FTIR and NMR have been used to characterize the aging of solutions produced by a chelate process [78]. The ester content of the solutions were found to increase with time (until approx 30 days where esterification 75% complete) by a reaction of free acetic acid with the methanol solvent. The pH levels of the solution also increased (becoming less acidic) with time as the acid was converted into the ester. Although it was deemed unlikely that the ester content was influencing the reactivity of the metal centers, films made from aged solutions showed decreased dielectric constant values, with increased loss tangents, as well as lower spontaneous polarization than fresh solutions. High ester content solutions have also been related to secondary phase formation and the appearance of "rosette" perovskite phase microstructures in traditional sol-gel procedures [79].

Thermal studies such as Thermogravimetric Analysis (TGA) and Differential Thermal Analysis (DTA), sometimes in conjunction with gas analysis techniques such as mass spectroscopy provide information on decomposition behavior of the material with temperature which can be related to the proposed chemical structures. This type of analysis has been performed for example in the Lead Titanate system to correlate the effect of starting precursor on microstructure of thin films. A comparison of Lead titanium precursors [80] prepared from starting lead precursors 1) anhydrous lead acetate prepared by a reaction

with 2-MOE, 2) lead acetate, and 3) lead oxide showed that the lead oxide system had the lowest weight loss upon heating with 2.5% up to 200°C from water identified by mass spectroscopy, and 8.2% weight loss from 380 to 480°C corresponding the evolution of water and carbon dioxide. Lead titanium precursors prepared from anhydrous lead acetate lost 4.5% due to water upon heating to 200°C , followed by 2 decomposition steps (200 to 300°C , and 300 to 440°C , 5.5% and 4% weight loss respectively) attributed to the evolution of water, carbon dioxide and acetone (a byproduct of acetate group decomposition), before a final 4.2% weight loss up to 520°C from water and carbon dioxide.

The precursor prepared from standard lead acetate revealed the greatest weight loss, with 9.5% due to water up to 220°C with a complex 4 major weight loss steps above 200°C corresponding to water, carbon dioxide and acetone. Lead Titanium oxide films fabricated from lead anhydrous precursors resulted in thinner films after pyrolysis and more shrinkage upon densification, leading to a grain size 100 nm. Corresponding films made from lead oxide precursors resulted in a grain size of 75 nm, highlighting the impact of chemical precursor characteristics on the structural evolution of the resulting films.

More detailed chemical and structural information has been obtained with techniques such as EXAFS of Extended X-ray Absorption Fine Structure studies using high intensity synchrotron X-ray sources to examine the local chemical environment around specific elements, including coordination number, bond distances. A EXAFS study of PT, PZ and PZT [81], [82], [83] has been performed on sol-gel derived gels. In the case of lead titanium synthesized from lead acetate and titanium n-propoxide in n-proponal or n-butoxide in n-butanol, the local neighborhood within 3.4 Å is identical with the presence Pb-O-Ti bonding [81]. The titanium atoms were found to be pentacoordinated with a proposed trimeric structure of Ti-O units forming a distorted hexagonal ring; interesting as this is similar to the proposed structure for liquid titanium butoxide [84].

The presence of Pb-O-Zr bonding in an amorphous gel has been seen using a zirconium n-propoxide precursor. The results indicated an immediate neighborhood of 6

oxygen atoms around the Zr, and 2 oxygen around the Pb atom. However, studies of butoxide derived PZ amorphous gels showed only Zr-O-Zr linkages, with no evidence for heterometallic Pb-O-Zr bonding [82]. Studies of PZT gels prepared by a 2-MOE route according to Budd [70] with lead acetate, titanium isopropoxide and zirconium n-propoxide as well as from lead acetate prepared with transition metal n-butoxides in butanol showed evidence of high levels of heterogeneity with preferred homocondensation in zirconium species leading to Zr-O-Zr links [67]. This high zirconium reactivity is to be expected due to its lower electronegativity (thus more electropositive and more sensitive to hydrolysis) as compared to titanium, and raises a key point as how to balance the reactivity of starting precursors as to achieve a homogenous sol. Since the final crystal structure of the film is related to the homogeneity in the gel phase, significant zirconium clustering can lead to non-stoichiometry as well as to zirconium rich pyrochlore type phases. These studies point to the importance of molecular level mixing, and homogeneity for the final crystalline phase, as well as to the difficulty involved in investigating all the transformation mechanisms that occur from the precursor species, through the amorphous gel, to the final crystalline material.

For a more complete picture these chemical studies are often combined with "physical" studies to determine molecular weight, the size and shape of the polymers in solution and evolution upon hydrolysis to an amorphous gel state. Techniques such as viscosity measurements, and Small Angle X-ray Scattering (SAXS) provide information on the physical characteristics of our sols. SAXS measures the differences in electron density on a scale of around 0.1 to 50nm, at low angles which can be used to determine the radius of spherical particles, as well as the length and diameter of rod like particles [85]. Viscosity measurements are also useful to determine the shape of polymers produced in an alkoxide solution by examining the variation in viscosity with the solution concentration. The variation of viscosity is independent of the concentration and particle size for spherical particles, while it depends linearly on concentration of the polymer in chainlike or linear

polymers [86],[87].

A determination of the particle size and shape of PZT precursor solutions as they undergo hydrolysis in a chelate process by SAXS, and by using rheological data was recently performed [86]. This study showed that the polymers evolve from spherical 5nm particles in the sol state to linear chain-like polymers upon hydrolysis. Additional experiments were performed to examine the "mixing" order effects on sol-gel homogeneity [88] by comparing previous results of PZT sols synthesized by reaction of titanium isopropoxide with zirconium n-propoxide in 2-MOE before the addition of lead acetate; contrasted to the separate synthesis of lead zirconium (PZ) and lead titanium (PT) sols which were subsequently combined to form a PZT modified sol. Results from the latter experiment showed that they were in fact a heterogenous mixture of large PT 5nm center particles surrounded by small (less than 4nm) PZ particles; such heterogenous structures are expected to have higher processing temperatures and be prone to secondary phase formation as the heterogeneity extends into the crystal structure. This has been seen as well in PST, where mixing order effects were empirically studied showing that a mixture of Pb and Sc precursors before the addition of tantalum led to higher levels of pyrochlore secondary phase than Sc/Ta mixtures followed by later Pb addition [64]; again pointing out the role that "B" site homogeneity in the solution phase has on the final crystal structure and ultimately on material properties.

2.1.2.4   The Role of Excess Lead

As has been established for many lead containing perovskites fabricated by the sol-gel method [80], the addition of excess lead is necessary to compensate for surface lead loss as well as interface diffusion in some substrate systems. The lead loss in thin films is not unique to sol-gel derived ceramics but applies as well to films fabricated from physical deposition methods such as sputtering [58], [33]. Usually lead deficiency is accompanied by the appearance of secondary pyrochlore type phases, often leading to a fine grain py-

rochlore matrix and "rosette" type perovskite grains (this has also been reported however in solutions with high ester content) [79]. The lead loss from high surface area thin films is usually balanced in sol-gel processing by the addition of excess lead to the precursor solution in varying amounts depending on crystallization conditions but often in the range of 5 to 15% excess Pb.

Other methods have also been employed to reduce lead loss in thin film perovskites including the application of PbO cover coats first used by Tani [89] who found that the deposition of a 1 Molar (M) lead acetate trihydrate solution in MOE applied as a final layer before crystallization of PLZT (8/65/35) at 700°C for 5 minutes showed the absence of surface pyrochlore, an increased grain size by 100 to 200 nm, and improved dielectric and ferroelectric properties. Other researchers have utilized a combination method of lead rich first, and final layers combined with stoichiometric middle layers in order to optimize perovskite phase formation and maximize dielectric and ferroelectric properties [90].

In addition, a PbO rich atmosphere has also been investigated using both stoichiometric and lead excess solutions, with the proposal of a crystallization model based on the kinetic competition between lead loss and the nucleation and growth of the perovskite phase [91]. This work demonstrated for the first time the fabrication of dense and homogenous, columnar grain perovskite microstructure from stoichiometric lead solutions fired at 650°C for 30 minutes in a PbO rich atmosphere, while the control sample fired in air resulted in a two phase microstructure with rosette perovskite grains in a pyrochlore matrix. However, films made from a 10% excess lead solution and fired in a PbO rich atmosphere showed a near surface pyrochlore secondary phase.

Since in PZT the crystallization of the perovskite phase is reported to follow the sequence amorphous gel, pyrochlore intermediate phase, followed by heterogeneous (or film/substrate nucleation) and homogenous (nucleation and growth within the film) nucleation of the perovskite phase which preferably starts at the film/substrate interface and grows up in a columnar fashion to the free surface [3],[91]; stoichiometric lead precursor

solutions can be converted into stoichiometric fluorite which can then convert directly to perovskite as the phase grows up from the substrate. In the case of excess lead solutions processed in PbO atmosphere, the intermediate pyrochlore phase is lead rich, requiring a rejection of Pb at the growth interface for nucleation and growth of the perovskite phase. The pyrochlore to perovskite phase transformation in this case may be kinetically rate-limited by the Pb diffusion to the free surface, and further impeded by the high Pb vapor pressure which reduces the driving force for diffusion.

Previous reports in the PST system indicate that lead deficiency is also a problem for Lead Scandium Tantalum with reports of up to 20% excess lead added to obtain the pervoskite phase in some cases[64].

2.1.2.5   Film Nucleation and Growth

Film deposition is made by depositing solutions containing a polymeric network of metal oxide species using a syringe with a μm size filter onto a substrate, typically a electroded Si wafer. The wafer is covered with solution before spinning at 1000 to 7000 rpm. The resulting as-deposited film is amorphous and its physical state is determined largely by the reactivity of the starting precursor and solvent employed in the solution synthesis. The films may consist of a chemical gel, a physical gel, or a non-gelled film as defined by significant condensation and/or cross linking of chemical species during deposition, physical aggregation, and minimal precursor interactions respectively. An account of film consolidation behavior in Ti and Zr model systems, their structural evolution and impact on final crystalline phase has been studied [92] and recently reviewed [80].

The most common method of achieving the amorphous to crystalline transformation begins with a pyrolysis step of the as-deposited film at 200 to 400°C for short times promoting organic species removal. Studies have indicated that as-deposited sol-gel films contain short range order relating to the chemical precursor structure and bonding in solution. After pyrolysis, medium range order with nanometer scale chemical heteroge-

niety was observed, with higher pyrolysis temperatures leading to a more homogenous distribution of chemical species [93].

The transformation of the amorphous pyrolyzed film to the crystalline ceramic phase occurs by a nucleation and growth process in which the increased temperature during film annealing provides the energy to overcome the barrier heights for homogeneous and heterogeneous nucleation as is described in the literature of glasses [78] by equation 2.1 and 2.2:

$$\Delta G^*_{homo} = \frac{16\pi\gamma^3}{3\Delta(Gv)^2} \tag{2.1}$$

$$\Delta G^*_{hetero} = \frac{16\pi\gamma^3}{3\Delta(Gv)^2} f(\theta) \tag{2.2}$$

where γ is the interfacial energy, ΔGv is the free energy difference per unit volume for the amorphous film-crystalline film transformation, and f(θ) is a function related to the contact angle, θ, according to equation 2.3.

$$f(\theta) = \frac{(2 - 3cos\theta + cos^3\theta)}{4} \tag{2.3}$$

From equation 2.1 and 2.2 we see that with increasing driving force (Δ Gv) there is the probability of both homogenous and heterogeneous occurring simultaneously, despite the f(θ) term which favors interface nucleation. A typical free energy versus temperature curve shows as we increase the crystallization temperature near the melting point of the compound, the driving force (Δ Gv) decreases. Thus higher crystallization temperatures result in lower driving force for crystallization which favors heterogeneous, interface nucleation with the substrate often resulting in columnar growth. An example of this effect is presented in [3] where additions of 3 moles acetylacetonate (acac) per mol PZT in
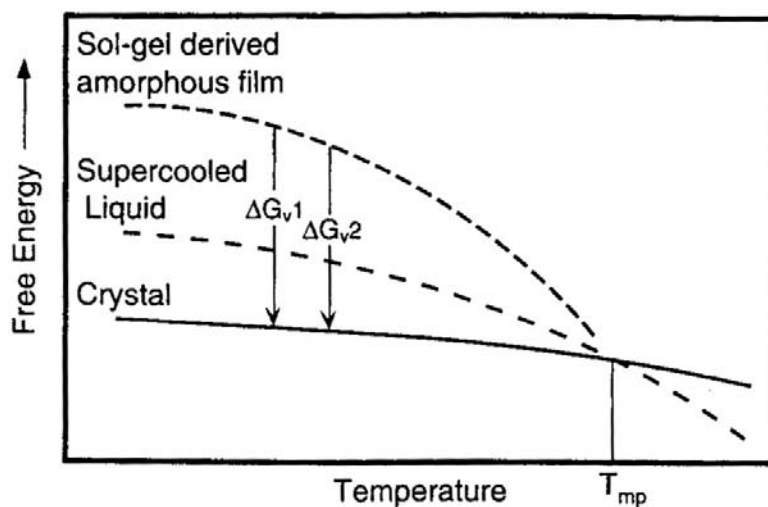
Figure 2.1: *Free energies of a sol-gel derived amorphous film, the ideal supercooled liquid, and the crystalline perovskite phase. $\Delta G_v 1$ represents the driving force for low pyrolysis temperature precursors; while $\Delta G_v 2$ represents the driving force for high pyrolysis temperature precursors. [3]*

a cheleate prepared solution resulted in an increase in pyrolysis temperature, and subsequent increase in crystallization temperature due to the additional organic content. Films prepared from the standard chelate solution and acac modified solution were annealed at 650°C for 30 minutes in air resulting in surface nucleated grains in the standard chleate indicitive of multiple nucleation events, in contrast to the acac modifed films which displayed a columnar grain strucure with no surface phase present. This analysis is somewhat simplified as treating the amorphous to perovskite transformation as a single step process, when in fact, intermediate phases such as pyrochlore or fluorite have been stabilized under certain processing conditions, and sol-gel films of lead containing perovskites such as PZT [94],[95], PMN [26],[4], and PST [22] are reported to transform via these intermediate phases to the final perovskite phase.

In traditional tube furnace annealing procedures, we pass through a distribution of

driving forces as we heat the sample leading to multiple nucleation events. By employing Rapid Thermal Annealing (RTA), one can in principle, heat to the final crystallization temperature without giving the intermediate phases time to form.

2.1.2.6 Microstructure and Texture/Orientation

Common applications of ferroelectric thin films including non-volatile memory storage and MEMS have required the integration of ferroelectrics (mostly PZT) onto silicon substrates and for this reason much work has been done on buffer, barrier, adhesion and electrode layers for PZT integration on Si. Lead containing perovskites can not be grown directly on Si because of Pb-Si interdiffusion [96], so that the most common substrate electrode system used is $Pt/Ti/SiO_2/Si$, with Platinum chosen for its inertness, good lattice matching properties (3.92 Å, resulting in 0.5% match for $PbTiO_3$), and high texturability in the (111) direction, and titanium serving as an adhesion layer[97]. Although a (111) texture of PZT grown on (111) Pt is expected, many researchers have shown that random, (111), and (100) PZT textures emerge in both sol-gel and physical vapor deposition methods depending on a large number of factors including chemical precursor characteristics, pyrolysis conditions, annealing conditions, and adhesion/buffer layer characteristics. Since ferroelectric properties are anisotropic, it is desired to control the orientation/texture of thin films growth.

Chen and Chen [98],[99] have reported that the formation of MOD sol-gel derived PZT(111) on Pt(111) ($Pt/Ti/SiO_2/Si$) was not due to the Pt itself, but due to the formation of lead rich intermediate phases in particular $Pt_{5-7}Pb$, a (111) oriented transient intermetallic phase that nucleates (111) PZT. The condition required for forming the intermetallic layer is a local reducing atmosphere to transform Pb^{2+} to Pb, found at $P(O_2)$ partial pressures of 10^{-5}atm between 400 and 700°C [98]; such conditions can be found at the buried film/Pt interface during the initial stages of pyrolysis where oxygen is consumed in the removal of organic species, but oxygen diffusion from the surround-

ings has not reached the interface, such conditions can also be found in fast heating to annealing temperatures [100]. The authors also correlated (100) PZT on (111)Pt with the appearance of a (001)PbO layer whose formation is possible under general conditions which do not favor Pb-Pt intermetallic compounds, experimentally obtained by heating slowly to intermediate temperatures. Thus processing conditions favoring (111), or (100) orientation amount to conditions which favor the formation of "seed" layers from which the PZT takes its orientation during subsequent growth.

Brooks [101] investigated the effects of pyrolysis temperature and post-pyrolysis thermal treatments on the microstructure and texture of PZT films on (111)Pt/Ti/SiO$_2$/Si substrates. Experiments had shown that textures of (111) and (100) were obtained by pyrolyzing sol-gel derived films at 350°C and 420°C respectively before rapid thermal annealing to 600°C , with (111) oriented films having a nominal grain size of 100nm compared to 500nm for the (100) orientation. In spite of these orientation differences, X-ray, TEM, and EDAX analysis had shown that the as pyrolyzed amorphous films at the two different temperatures were structurally identical, and no occurrence of the Pb-Pt alloy reported by Chen [100] was observed in any pyrolyzed or annealed PZT films. Further experiments on post-pyrolysis conditions indicated that films pyrolyzed at temperatures of 370°C usually leading to (111) orientation but post annealed in oxygen at 370°C for 30 minutes followed by rapid thermal annealing to 600°C changed their orientation to (100); with the converse experiment also true, ie, films pyrolyzed at 420°C in air normally leading to (100) orientation, showed a (111) orientation after post-pyrolysis annealing in argon for 30 minutes before annealing to crystallization temperature. These results indicate that the oxygen content of the pyrolyzed films before annealing affect the nucleation and growth of the perovskite phase, as well as the kinetics of the pyrochlore to perovskite phase transformation.

An explanation was given in terms of the stablility of the metastable pyrochlore type phases in different oxygen environments. At lower pyrolysis temperatures, less oxygen is

incorporated into the structure and a probable oxygen deficient pyrochlore with nearly identical structure to the perovskite phase leading to enhanced pyrochlore to perovskite transformation. At higher pyrolysis temperatures, higher oxygen content leads to more stable pyrochlore structures, thus slowing the pyrochlore to perovskite transformation. In both the (111) and (100) orientations of PZT films, TEM revealed heterogeneous nucleation events (film/substrate) occurring initially, and growing to the free surface; (111) films had better lattice matching and less nucleation energy to surmount so they had multiple nucleation sites and consequently small grain sizes, while (100) oriented films exhibited larger grain size related to less nucleation sites due to the large thermodynamic barrier, the stability of the increased oxygen pyrochlore phase is also evidenced by the residual pyrochlore in (100) films annealed in the same conditions as (111) counterparts. These results were valid for both 5 and 10% Pb excess amounts in solution.

Fe [102] has also evidenced chemical differences in pyrolyzed films as a function of processing conditions related to orientation selection in PZT sol-gel derived films on Pt/Ti/SiO$_2$/Si substrates. By using FTIR to monitor the organic, and OH hydroxyl content in pyrolysed films it was seen that films pyrolyzed in a one step process to 350°C for 10 seconds contained significant amount of acetate groups (and same OH content) as compared to films pyrolysed for 2 minutes. This led to bimodal (111) and (100) orientations for films pyrolyzed during 2 minutes, versus (111) orientation for 10 second pyrolysis times. Furthermore, two step pyrolysis procedures were examined with a "drying" step at 200°C before subsequent pyrolysis at 350°C which resulted in less OH incorporation. The reduced OH content indicates full condensation of OH bonds to yield a M-O-M metal oxygen network. The results of films crystallized at 600°C from the one and two step pyrolysis procedures to 350°C for 2 minutes indicate that the two step pyrolysis displayed (111) oriented growth, while the one step with OH hydroxyl incorporation showed bimodal (111) and (100) growth. These results are explained in terms of 2.1; where for the one step pyrolysis with short holding times, the incorporated organic shifts the crystallization

temperature to a higher temperature, thus promoting one heterogeneous nucleation event similar to acac additions in [3]. The one step pyrolysis for 2 minutes with OH incorporation, and incomplete condensation reactions shifts the amorphous free energy curve to higher energy thus promoting multiple nucleation events and mixed orientations.

For sputtered films, a variation of orientation was also seen with processing conditions, and especially different textured bottom electrodes. During reactive sputtering in oxygen atmosphere, the formation of Pb-Pt inter-metallic compounds is not likely, and preferred (111) PZT orientation was related with titanium on the Pt surface due to diffusion along Pt grain boundaries at high temperature. Experiments have shown that a thin (less than 5nm) layer of TiO_2 of rutile (110) serves as an epitaxial bridge between Pt (111) and $PbTiO_3$ (111); and that in sputtered as well as sol-gel films, growth conditions leading to (100) $PbTiO_3$ on bare platinum are switched to (111) with the presence of the titanium layer. The driving force for the texture development is explained by both the chemical effect; a lowering of nucleation energy for PbTiO3 in the presence of titania, as well as by the physical epitaxial relationship between the Pt(111), TiO_2(110) and $PbTiO_3$(111) growth planes [97]. Recently the use of 2nm TiO_2 and 10nm $PbTiO_3$ seed layers has been used on $Pt/Ti/SiO_2/Si$ substrates to seed (111) and (100) growth in PZT films prepared by sputtering [33], as well as sol-gel [103]. These same seeding layers have also been recently used to change the orientation and grain size of sol-gel derived PMN thin films [21].

The growth of perovskite compounds on single crystal substrates often leads to epitaxial growth for both sol-gel [104] and physical deposited films, especially on cubic substrates like MgO and STO which have similar lattice parameters to lead containing perovskite compounds, although the epitaxial mechanisms are in general different for solution and physical vapor processed films . Solution derived films with similar crystal structures led to heterogeneous film/substrate nucleation which grow through the film to consume randomly oriented grains in epitaxial grain growth, while high temperature processing can

also lead to liquid phase process. However, epitaxial films are possible even in relatively unrelated film/substrate systems via the film splitting into isolated epitaxial grains which can further be used as seeding layers for a continuous epitaxial film.

The epitaxial growth of sol-gel derived $PbTiO_3$ films on (001) STO was studied by Seifert [104] who found a similar mechanism as seen in polycrystalline samples of a pyrochlore or fluorite phase crystallizing from the amorphous precursor followed by epitaxial nucleation of the perovskite phase at the film/substrate interface and subsequent growth towards the free surface; in fact it was concluded that the intermediate pyrochlore phase promotes perovskite epitaxy by providing an additional driving force (pyrochlore to perovskite) for growth other than the elimination of grain boundary area. Epitaxial PMN films have been reported on STO [4], MgO and $LaAlO_3$ single crystal substrates, however the author is not aware of any previous reports of epitaxial PST thin films. Property measurements are accomplished by depositing an epitaxial electrode layer, or by suitable doping of the single crystal substrate (Nb doping in STO). A table of substrates utilized in PST film fabrication is given in table 2.1.

Substrate	Electrodes	Type	Process	Reference
Si	Pt	$Pt/Ti/SiO_2/Si$	sol-gel	[63],[64],[22], [65],[66]
	Pt	$Pt/Ti/SiO_2$	sputtering	[55],[56],[58],[66]
	Pt	$Pt/Ti/SiO_2/Si$	CVD	[66],[105]
	Pt	$Pt/Ti/TaO/SiO_2/Si$	CVD	[66],[105]
		Si (100)	CVD	[106]
	Pt	$LaNiO_3/Pt/Ti/SiO_2/Si$	CVD	[107]
MgO	Pt	Pt/MgO	sol-gel	[64]
		MgO	sol-gel	[62]
sapphire		sapphire	sol-gel	[62]
		sapphire	sputtering	[54][48]
GGG ($Gd_3Ga_5O_{12}$)			sol-gel	[62]
$LaAlO_3$	YBCO	$YBCO/LaAlO_3$	PLD	[60]

Table 2.1: *Substrates utilized for PST thin film fabrication*

2.1.2.7 Stress Effects in Thin Films

Stress development in Sol-gel thin films arise from three main contributions: 1) the evaporation of solvent and shrinkage of the oligomeric network during spinning and subsequent shrinkage upon pyrolysis and crystallization, 2) lattice mismatch creating strain between the film and substrate, and 3) differences in thermal expansion inducing stress upon cooling from crystallization temperatures.

The stresses in the first case are generally a function of solution chemistry, deposition parameters, pyrolysis, and crystallization conditions; however a few general rules may be presented. The tensile stress in the gel network arises as liquid in pores replaces the solid/vapor surface energy with the more favorable liquid/vapor so that the stress in the film is approximately equal to the tension in the liquid, often 200Mpa or greater [108]. Cracking in thicker films (around 500nm) is caused by the differential strain between the surface and interfacial layers due to different solvent evaporation rates and thus different contraction rates of the amorphous network.

The second cause of stress in thin films is the lattice mismatch between the film and the substrate as seen by equation (2.4) for tetragonal, pseudo-cubic and cubic materials [109]. The mismatch is of greatest importance in thin epitaxial films where film growth takes the orientation of the underlying single crystal or textured substrate. In thicker films, the stresses induced by the lattice mismatch are relaxed by dislocation formation. Residual in-plane strain, x, in the films present due to large differences in the lattice parameters can be related to the out of plane lattice parameter, c, determined by X-ray diffraction, and the Poisson ratio ν, by equation (2.5). For $a_{film} < a_{substrate}$, the film will be under tension at the interface.

$$LatticeMismatch = \frac{a_{film} - a_{substrate}}{a_{substrate}} \tag{2.4}$$

where a is the lattice constant

$$x = -\frac{1-\nu}{2\nu}(\frac{c-a_0}{a_0}) \tag{2.5}$$

Where x is the strain, ν is Poisson's ratio, c is the out of plane lattice parameter, and a_0 is the lattice constant of a mechanically free unit cell.

The third cause of stress in sol-gel derived thin films is the thermal expansion difference between the film and substrate; since high crystallization temperatures are necessary for perovskite formation (700°C) stress develops upon cooling to room temperature. This stress can be expressed in equation 2.6 where E_f and ν_f are the Young's modulus and Poisson's ratio of the film and ΔT is the temperature difference between the crystallization temperature and the final film temperature after cooling. For $\alpha_s < \alpha_f$ the film will be under tension (as is the case for PST on Si).

$$X = \frac{E_f}{1-\nu_f}(\alpha_f - \alpha_s)\Delta T \tag{2.6}$$

The effects of stress in ferroelectric films include microstructural features of cracking, leading to short circuiting with the bottom electrode, stress driven preferred orientation, and a shift of the dielectric peak temperature. In the case of 53/47 PZT it was shown by Tuttle that films deposited on Pt/ MgO ($\alpha_s > \alpha_f$) and thus under compression resulted in c-axis orientation, while the same films on Pt/Si ($\alpha_s < \alpha_f$) and thus under tension resulted in a-axis oriented films[110]. Although in general the film orientation is a complex function of nucleation and growth issues such as lattice mismatch and chemical compatibality; it is seen that stress can also play a role.

In the case of normal ferroelectrics, the Landau-Ginzburg Devonshire formalism provides a framework for understanding the temperature shift with stress. The effects of mechanical boundary conditions on epitaxial (001) oriented $PbTiO_3$ and $BaTiO_3$ films on cubic substrates were analyzed by Pertsev [111] who found that 1) the transition temperature in films were higher than in the corresponding bulk material, and 2) the *order* of the phase transition was changed to second order in films as compared to first order in

bulk materials. This theoretical work was later experimentally verified [112], and can be explained as follows: Upon cooling from the cubic paraelectric phase with electrostrictive constants $Q_{11}>0$ and $Q_{12}<0$, the equivalent (100) directions of polar axis will take the orientation which is energetically favorable with respect to the elastic contribution of the film free energy. The result is described in equation 2.7 for film under compression resulting in an "out-of-plane" polarization and in equation 2.8 for a film under tension leading to a "in-plane" polarization.

$$T_{outplane} = T_0 + 2C\epsilon_0 \frac{2Q_{12}}{s_{11} + s_{12}} x \tag{2.7}$$

$$T_{inplane} = T_0 + 2C\epsilon_0 \frac{Q_{11} + Q_{12}}{s_{11} + s_{12}} x \tag{2.8}$$

where $T_{outplane}$ is the transition temperature for the film under compressive stress resulting in polarization being oriented "out- of- plane", $T_{inplane}$ is the transition temperature for a film under tensile stress with the polarization oriented *"In-Plane"*, T_0 is the transition temperature for a mechanically free film, C is the Curie-Weiss constant of the material, ϵ_0 is the permittivity of free space, Q_{11} and Q_{12} are the electrostrictive coefficients, and s_{11} and s_{12} are the elastic compliance using common Voigt convention for matrix notation.

The values of the parameters in PT and BT are such that $Q_{11}+ Q_{12}$ is positive whereas Q_{12} is negative. In the case of compressive strain (-x), the polarization wants to be directed "out of plane", resulting in equation 2.7 predicting a higher transition temperature $T_{outplane}$ than T_0. It is important to emphasize that based on the analysis in [111] *both* compressive or tensile stress lead to an *increase* in the transition temperature with respect to the mechanically free bulk material.

In addition, the phase transition from the paraelectric state to the ferroelectric state can be described as a first order phase transition in bulk crystals who possess a negative thermodynamic coefficient β as described in the LGD expansion:

$$G_1 = \frac{1}{2}\alpha P^2 + \frac{1}{4}\beta P^4 + \frac{1}{6}\gamma P^6 + ... \qquad (2.9)$$

In mechanically constrained thin films, the addition of a strain term to equation (2.9) results in an effective β term described in equation (2.10) for the polarization directed "out of plane" of the film:

$$\beta^* = \beta + \frac{Q_{12}^2}{s_{11} + s_{12}} \qquad (2.10)$$

The second term in equation (2.10) is the same order of magnitude as β for PT and BT materials, making β^* a positive quantity and changing the order of the phase transition from first, to second order as a result of mechanical constraints.

The situation is somewhat different for relaxor ferroelectric thin films. First of all, due to their macroscopically cubic structure and the absence of any real structural phase transition, the effects of stress on orientation of a certain polar axis may not apply. Secondly, there are discrepancies in the literature as to the shift in the temperature of the dielectric maximum T_m. Although it has been suggested that the T_m of thin film relaxors is always shifted to lower temperatures as compared to bulk specimens [113] due to greater defect densities, there has been work refuting this idea [114]. PLD was used to deposit epitaxial thin films of PMN-PT(90/10) (100nm with LSCO top and bottom electrodes substrates) on substrates with smaller (LAO) and larger (MgO) lattice parameters than the PMN film, leading to an upwards shift of Tm with positive in plane strain (LAO) estimated from the out of plane lattice parameter , and a downwards shift of Tm with negative in plane strain(MgO) respectively [114]. In addition, the authors found that films under tension (MgO in this case due to lattice parameters) resulted in higher dielectric constant values (2000 on MgO) than films in compression (400 on LAO), however microstructural data as well as the frequency dependance of dielectric permittivity were not presented. In addition, it is not clear why measurements "out of plane" for (001) oriented films should show a higher dielectric constant in a compression

state as compared to a tensile state.

More recent studies have shown that PLD fabrication of 750 nm (001) oriented PMN on MgO with 200 nm LSCO electrodes resulted in compressive in plane strain according to equation (2.5), as well as by direct measurement of the in plane component [24] by X-ray diffraction. This suggests that 1)the tensile strain predicted by lattice mismatch is relaxed across the LSCO electrode and 2) the thermal expansion mismatch between the film and substrate is the dominating factor leading to the measured compressive in plane stress. Furthermore, an empirical relation was derived to account for the experimentally observed results of "in plane" compression leading to a downward shift which is opposite to that predicted by equation (2.7). This relation is based on a common experimentally observed quadratic temperature dependance of permittivity for lead based relaxors, and was used to indicate that according to the observations cited in reference [24], the temperature of the dielectric constant maximum can only *decrease* for thin films under stress, regardless of the sign of the in-plane strain. However, since it is known in bulk materials that the transition temperature may be shifted down with defects such as lead vacancies, the relation with stress/strain in the material to the dielectric temperature maximum of thin film relaxors is far from being completely understood. A detailed study of stress effects in PST thin films and subsequent effects on dielectric properties has not, as of yet, been proffered.

2.1.3 State of the Art: Summary and Challenges

For reasons elucidated in Chapter 1, it is necessary in this study to fabricate *both* ordered and disordered PST thin films in order to compare their dielectric properties. A review of the literature indicates that indeed, ordered films have been fabricated, however mainly structural data was presented and little comparison with disordered relaxor films was made. In fact, the ordered films were produced by drastically different methods and annealing conditions, including a traditional sol-gel procedure [63], and a hybrid sol-gel

and ceramic processing procedure requiring high temperature annealing [61]. What is desired for this study is a true sol-gel procedure as has been reported by Liu, so that disordered films may be initially produced, with further ordering controlled by post annealing conditions. The first challenge of this thesis is therefore to build on the available knowledge in order to produce a stable, repeatable solution chemistry with proper constituent stoichiometry. With this achieved, the work becomes a matter of optimization of processing conditions with the goal of being able to tailor the processing in such a way so that intentional changes can be introduced in the material such as orientation, grain size, tensile/compressive stress via substrate thermal expansion mismatch, and "B" site ordering in order to characterize these effects on the dielectric response of thin films. In the following section, the specific problems and challenges concerning the processing of ordered and disordered PST are presented, followed by a presentation of the principal questions concerning the properties of PST which have not been previously addressed in the literature.

2.1.3.1 Processing

1. The preparation of a stable solution chemistry yielding proper material stoichiometry.

2. What is the optimum concentration of excess lead necessary to compensate for surface lead loss during film annealing to achieve perovskite pure films?

3. Since it is desired to fabricate films over 1 micron in thickness in order to study a size effect, is the commonly reported "single layer anneal" where each deposited layer is fired to high temperature necessary?

4. Can the microstructure and grain size be controlled by the use of seed layers, annealing conditions, or by solution additives?

5. Can PST films be made epitaxially on single crystal substrates using a sol-gel

method?

6. "B" Site order has been observed in thin films undear variety of processing conditions. Can we establish the processing links which control B site order such as the time and temperature of annealing and choice of substrate?

2.1.3.2 Properties

1. While "B" site order has been structurally observed, no strong link between ordering and dielectric properties for thin films has been given in the literature. Can we see the development of a normal ferroelectric state with an ordered thin film as we see in the corresponding ceramic materials?

2. Is there a thickness dependence of the dielectric cosntant in the PST thin films as has been reported for other thin film relaxor systems?

3. Why is the reported dielectric cosntant measured "in-plane" using interdigitated electrodes different than that measured "out-of-plane"? Is this a manifestiation of a passive layer at the dielectric electrode interface, or a result of increased "B" site ordering in the observed samples? How do the "in" and "out of plane" measurements compare with films processed under the same conditions?

4. By strict control of the processing conditions can we comment on the contribution of external factors such as the effects of stress in the film, the presence of a low dielectric constant passive layer, and grain size on the position and value of the dielectric maximum?

5. How does PST thin film data compare with relevant relaxor models, including the frequency dependance, and changes in the dielectric properties under AC and DC electric fields, and can a phase transition be induced under DC bias for disordered thin films as in ceramic samples?

6. In the high frequency limit where lattice dynamics dominate the dielectric response, does there still remain a difference between the thin film and bulk specemins?

2.2   Experimental Techniques

Solution Preparation Techniques "Schlenk Line" Solutions and precursor prepa-
ration were carried out under inert atmosphere using Schlenk Line techniques con-
sisting of 2 glass tubes; one for inert Ar gas flow, the other for the application of
a vacuum. Tygon plastic tube was used to connect the apparatus to glass reaction
vessels which were pumped, and backfilled with inert gas before the introduction
of precursor species. This equimment enabled the refluxing, distillation and trans-
fer of precursor materials while protecting them from exposure to air which could
hydrolyze initial reaction species.

TGA Thermal-gravimetric Analysis (TGA) was carried out on a Mettler TA50 Thermal
Analysis System with powders heated at a rate of $10°C$ a minute to final temperature
in air. Typical sample weight was on the order of 10mg.

FTIR Fourier Transform Infrared FTIR spectra were obtained using a Nicolet 510 spec-
trometer equipped with ATR crystal for quick analysis of both liquid and solid
specimens. The background spectra was taken immediately before the sample runs
and typically 64 scans were made to obtain the final spectra.

Spin Coating Spin coating was carried out at 3000 rpm for 30seconds in a clean room
under a hood using a machine from Headway Research, Inc.

Pyrolysis and RTA Pyrolysis was perfomed on a hot plate with external thermometer
at $400°C$ for 1 minute before cooling and repeating to build up thicker layers. Rapid
Thermal Annealing (RTA) was done on a Process Products Corporation machine
under Oxygen atmosphere.

SEM/TEM/EDAX Scanning Electron Microscopy (SEM) was performed on a Philips
XL30 equipped with an Energy Dispersive X-ray Analysis (EDAX) detector.

X-ray diffraction X-Ray Diffraction (XRD) was performed on a Siemens with CuK α at 40kV and 30mA in a theta-twotheta configuration.

Stress Determination Direct measurement of thin film stress was analyzed by measuring the radius of curvature of the substrate using a laser reflection technique (Tencor FLX-2900) capable of measuring the curvature during heating up to 900°C. In-plane lattice strain determined from glazing angle X-ray measurements performed in collaboration with P. Petrov, South Bank University (London, UK).

Dielectric Property Measurement Au and Pt top electrodes were sputter deposited at room temperature and post-annealed at 350°C for 5minutes (Au) and 650°C for 1 minute (Pt). Electrical measurements were made through the film thickness using an impedance analyzer (HP 4284A precision LCR meter) connected to a temperature chamber (Delta 9023) with controlled cooling rates of 2°C /minute from 100 to -100°C .

2.3 Experimental Procedure: Thin Film

This section describes the overall solution synthesis procedure as shown in figure 2.2 including the preparation and dehydration procedures for two different scandium precursors, bottom electrode fabrication and substrates/seed layers prepared by sputtering, deposition, pyrolysis, and crystallization behavior including two different crystallization procedures, the effects of excess lead, substrate effects, and time/temperature and processing/property investigations.

2.3.1 Solution Synthesis

Two different scandium precursors have been used for PST synthesis; scandium isopropoxide, and scandium acetate. This section describes the procedures necessary for stable solution synthesis using these precursors as well as initial characterization of PST crystallinity
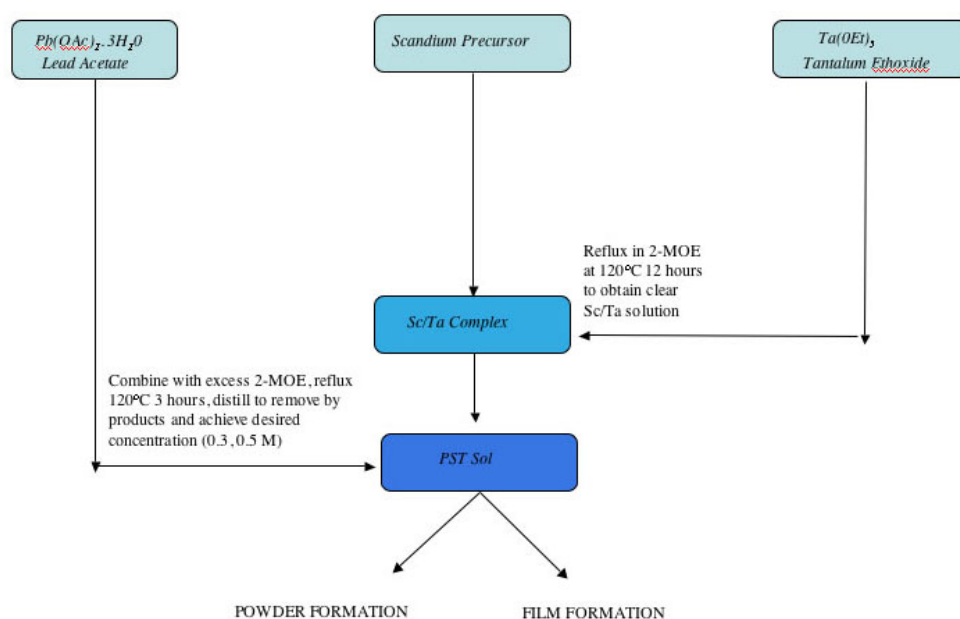
Figure 2.2: *Solution Synthesis: general procedure*

and stoichiometry.

2.3.1.1 "B" site complex Sc/Ta: Scandium Isopropoxide

A PST solution synthesis has been successfully accomplished using scandium isopropoxide as a starting precursor. In this case, the Sc/Ta complex in figure 2.2 is a result of combining Sc isopropoxide with 2-Methoxyethanol (2-MOE) and stirring at room temperature followed by addition of Ta ethoxide in MOE and refluxing for 12 hours at 120°C. As deposited films displayed scandium deficiency possibly related to starting precursor quality. The microstructure as determined by SEM and the crystal phases present via X-ray diffraction are presented in figure 2.3 for films rapid thermal annealed to 700°C for 1 minute.

2.3.1.2 "B" site complex Sc/Ta: Scandium Acetate

Stoichiometric control, as well as the tantalum precursor's sensibility to water necessitated a way to remove the hydrate from the starting precursor. Figure 2.4 shows the a) TGA
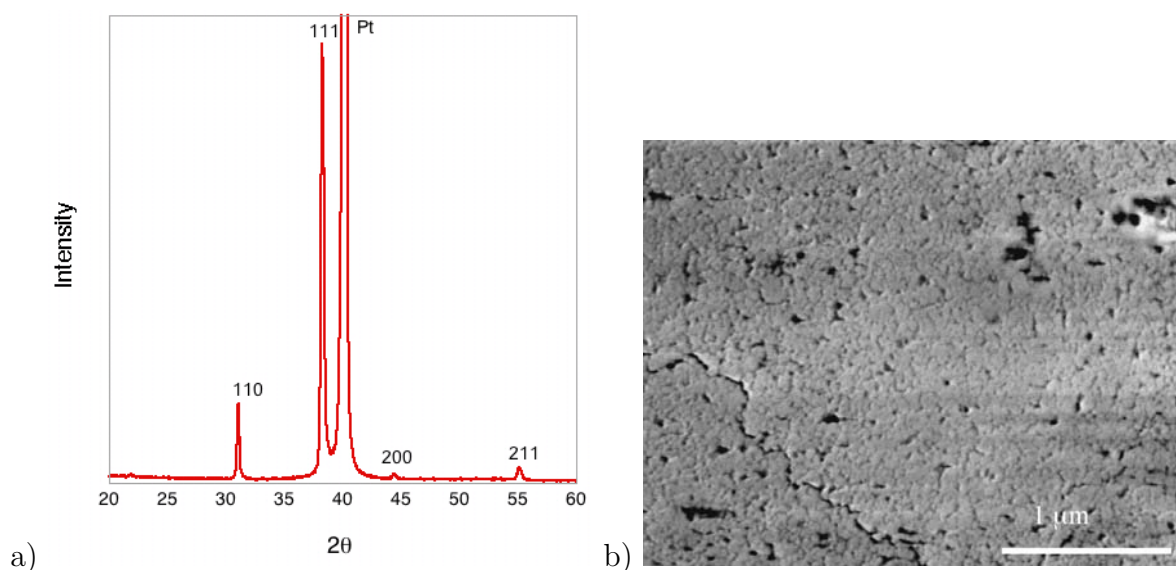
Figure 2.3: *(a) Xray and (b) SEM of PST/Pt/Ti/SiO$_2$/Si films made from scandium isopropoxide precursor*

and b) FTIR of the as received scandium acetate indicating two major decomposition steps; the first from approximately 150°C to 300°C , and the second between 300 and 400°C . The overall measured weight loss upon heating scandium acetate to scandium oxide was 63%, or 37% weight remaining; compared to the theoretically calculated value of 31% weight remaining. The 6% weight difference between the measured and calculated value is attributed to bound and absorbed water in the starting precursor as confirmed by FTIR studies. The FTIR of the scandium acetate powder displays a broad vibration band at 3500 cm^{-1} attributed to water, the symmetric and asymmetric acetate stretch bands centered at 1500 cm^{-1}, C-O-M stretches observed in the 1000 cm^{-1} region, and a generally broad and noisy M-O region around 500 cm^{-1}. Since the first decomposition step has a weight loss of 15%, and extends to near 300°C ; it is likely that this is a combination of weight loss from 1) water groups up until approximately 220°C (weight loss approximately 6%), followed by the start of the acetate decomposition from less strongly bound acetate groups. the second decomposition step from 300 to 400°C corresponds to acetate decomposition which finished at approximately 450°C. In fact, the presence of

a)   b)
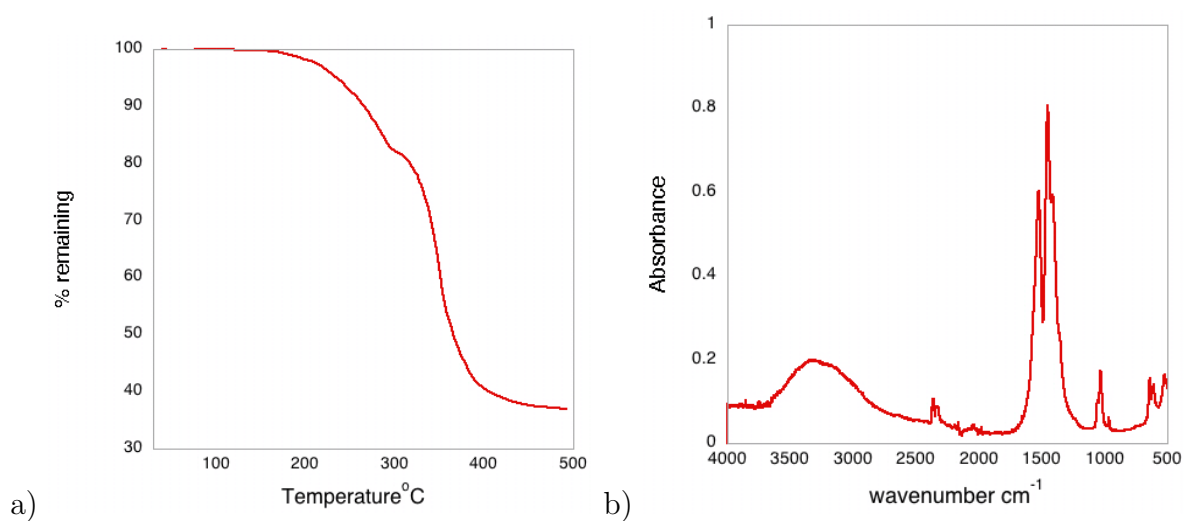
Figure 2.4: *(a) TGA and (b) FTIR of Scandium acetate precursor as received*

a two step decomposition indicates precursor inhomogeneity, and the precense of water indicates the need for a dehydration step before further solution synthesis.

Two methods were investigated for the dehydration of scandium acetate, 1) a reaction of scandium acetate hydrate with Methoxyethanol (MOE) at the boiling point of MOE (120°C) under argon (Sc-MOE) and 2) a reaction of the scandium acetate hydrate precursor with acetic anhydride for water removal (Sc-Acetic Anyhdride). In order to judge these procedures we should keep two points in mind; one, are they successful in the dehydration, and two, do they change the structure of the starting compound?

In the case of Sc-MOE, the water is removed upon distilling the minimum boiling point azeotrope which forms between water and the solvent. In figure 2.5a) the thermogravimetric analysis shows the behavior of Sc acetate after being refluxed 12 hours in MOE under inert argon, vacuum distilling and vacuum drying for 12 hours. We see a different decomposition behavior from the as received scandium acetate, with 4 major decomposition steps present in the precursor 1) from room temperature to approximately 240°C , 2) 240°C until approximately 320°C , 3) 320 until 400 °C , and 4) 400 to approximately 550°C .

The overall measured weight loss is 65% or 35% of the weight remaining after transformation into scandium oxide, compared to the 31% remaining weight theoretically calculated for decomposition of scandium acetate. The initial weight loss up to 200°C is attributed to the removal of MOE solvent present even after the vacuum drying step as well as bound and absorbed water; both evidenced by the room temperature IR spectra of Sc-MOE powder shown in figure 2.5.

The corresponding spectra of pure 2-MOE is indicated for comparison showing OH vibrations in the 3500 cm^{-1} range, alkoxy and aliphatic resonances from MOE in the 3000 cm-1 region, and C-O-M stretches (MOE) around 1000 cm^{-1}. The IR spectra of the Sc-MOE powder shared the same MOE vibrations at 3000 and 1000 cm^{-1}, and included as well as the acetate stretch region at 1500 cm^{-1}. The IR spectra of the same powder after vacuum drying and subsequent heating to 300°C and 500°C as well as the spectra of MOE for comparison indicating 1) the removal of water by MOE, and 2) the presense of MOE vibrations in the spectra at elevated temperature (above bp of MOE). The second decomposition step from 240 to 320°C is attributed to less strongly bound acetate groups as seen in 2.4, and similarly the decomposition from 330 to 400°C is attributed to bound acetate groups. The final decomposition from 400 to above 500°C may be attributed to a more stable species bound to the scandium than the acetate group (previous decomposition seen to finish at 400°C), presumed to be bound MOE.

The presence of MOE vibrations at elevated temperatures as seen by IR and the multiple step decomposition as compared to non-MOE modified scandium acetate suggests that the structure of the starting compound was modified by refluxing at 120°C for 12 hours in the solvent 2-MOE. This method is deemed capable of dehydrating the starting compound, however the change in precursor structure makes weight determination and resulting film stoichiometry difficult to control.

In the case of the Sc-Anhydride dehydration method, the water is removed by reaction with acetic anhydride to form acetic acid. Figure 2.6 shows the TGA and IR of scandium
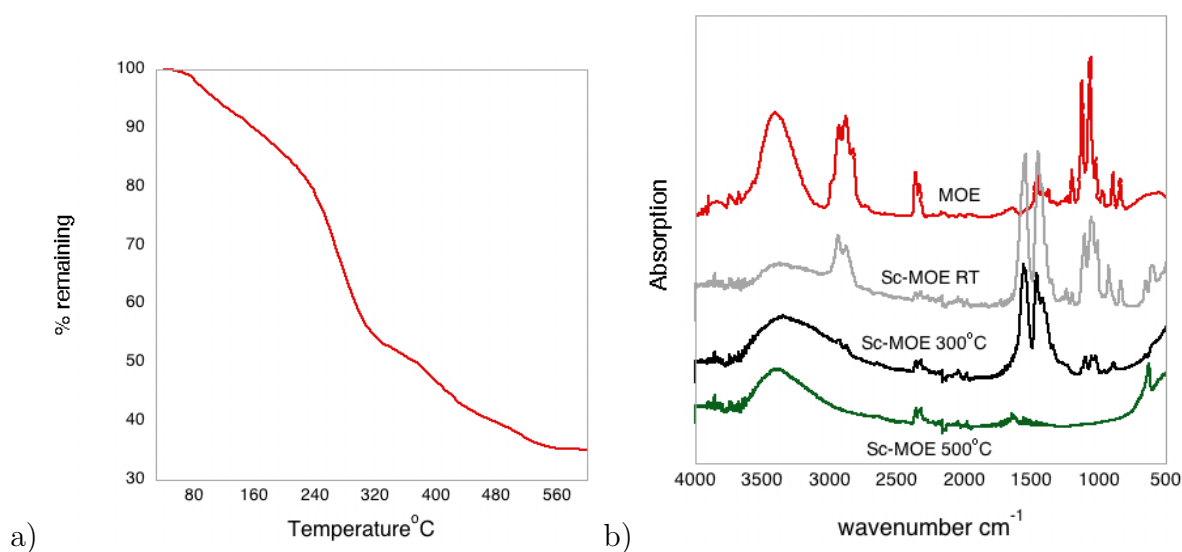
Figure 2.5: *(a) TGA and (b) FTIR as a function of temperature for ScMOE powders*

acetate after refluxing in acetic anhydride solvent at 130°C for 2 hours before vacuum distillation and vacuum drying at 60°C for one day. The TGA indicates a one step decomposition (suggesting one chemical species) with a measured weight loss of 68% or remaining weight of 32% compared with the calculated 31% theoretical remaining weight. The IR shows an absence of water vibrations at 3500 cm^{-1} and a slightly modified acetate stretch region including a sharper, less broad acetate absorption peaks than Sc-MOE and a change in the relative intensities of the symmetric and asymmetric acetate stretch peaks as compared to Sc-MOE and Sc-Acetate. The scandium anhydride method is successful in precursor dehydration and results in a homogenous starting precursor.

The Sc-Anhydride, and Sc-MOE precursors were subsequently reacted with tantalum ethoxide, forming a Sc/Ta complex which was combined with lead acetate (10% excess in this case) to obtain the final PST sol. Experiments showed that the use of the Sc-Anhydride directly with the tantalum precursor resulted in a quick reaction forming a clear/colorless Sc/Ta complex (after 4 hours at 130°C), and an unstable PST solution which quickly precipitated in a number of days. Sol-gel solutions were allowed to dry at 100°C in air to promote gel formation and were subsequently calcined in a box furnace at
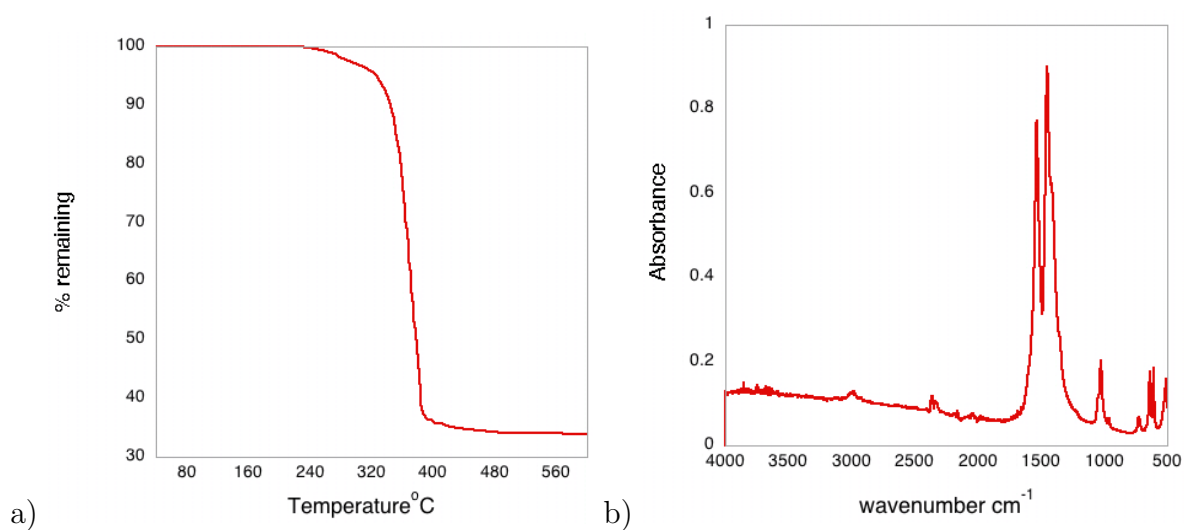
Figure 2.6: *(a) TGA and (b) FTIR of Sc acetate purified in acetic acid anhydride*

$1000°C$ for 2 hours in air, using a sealed crucible.

PST powders made from Sc-Anhydride precursor solutions led to high quantities of a pyrochlore secondary phase. In the case of PST prepared using a Sc-MOE precursor, the reaction to form a clear/colorless Sc/Ta complex took over 12 hours when refluxed at $120°C$ under Ar, and was stable upon cooling and storing in an Ar atmosphere for months after synthesis. Figure 2.7 shows the X-ray spectra of PST sol-gel derived powders made from Sc-Anhydride and Sc-MOE precursor species showing phase pure perovskite for the Sc-MOE, and pyrochlore mixed with perovskite for the Sc-Anhydride.

It is known in sol-gel processing that the solution structure and stoichiometry has a direct impact on the resulting crystalline phase. We have seen from TGA and IR studies that the starting precursor structure is modified in the case of Sc-MOE. This structural change was further seen to impact the reactivity and stability of the Sc/Ta complex (longer reaction times and more stable Sc/Ta complex as compared to Sc-Anhydride), which led to increased perovskite phase formation. Although this is empirical evidence and detailed chemical and structural studies have not been performed on the system, the link between perovskite phase formation and "B" site precursor homogeneity has been

previously established in other material systems [83]. Pyrochlore phases in the PST system are usually Ta rich and Sc deficient [57]. Since lead content and processing conditions were the same in the Sc-MOE and Sc-Anhydride derived PST solutions, the pyrochlore phase observed in our case is likely linked with the "B" site species. Therefore we can hypothesize than it was an in-homogenous Sc/Ta complex that led to a high degree of pyrochlore phase for Sc-Anhydride.

In light of these experiments, a modified solution synthesis scheme was developed in which the as-purchased scandium acetate was first dehydrated with acetic anhydride to form Sc-Anhydride for strict control of material stoichiometry. This precursor was subsequently reacted with MOE by refluxing at 120°C for 12 hours before vacuum distillation resulting in our Sc-Stoich precursor which was then used in further PST solution synthesis steps.
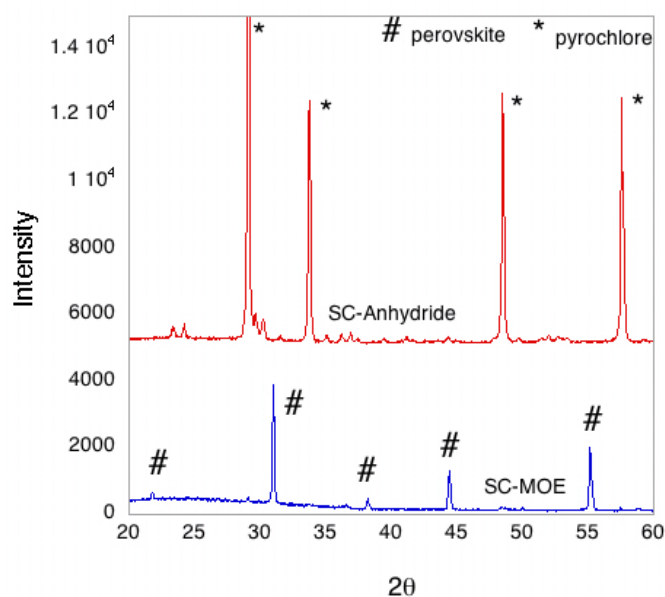
Figure 2.7: *X-ray diffraction of Sol-Gel Derived PST powders made from Sc-MOE and Sc-Anhydride heated at 1000°C for 2 hours in air*

In summary:

1)In order to obtain a stable solution, Sc acetate was reacted with MOE in an initial

Theoretical	Pb (M line)	Ta (L line)	Sc (K line)	O	Sc/Ta
Stoichiometric ratio	20	10	10	60	1
Sc-acetate(as received)	16.8	13.55	7.56	62.5	0.56
Sc-Stoich	23.04	8.84	8.57	59.55	0.97
Sc-isopropoxide	16.64	8.82	7.42	67.13	0.84
Bulk PST reference	19.94	10.8	9.75	60.05	0.90

Table 2.2: *EDAX stoichiometry analysis performed on Philips XL-30 SEM for Sc-acetate (as received powders), Sc-Stoich (from MOE process), Sc-isopropoxide and Bulk ceramic PST reference*

ligand replacement step, and subsequently reacted with Ta forming the B-site precursor.

2)In order to obtain proper stoichiometry, the as received scandium was first dehydrated in Acetic Anhydride, followed by MOE ligand replacement in order to obtain a stoichiometric, stable solution. Table 2.2 displays stoichiometric deviations of Sc/Ta ratio of 0.56 obtained from using as received scandium acetate without the dehydration step, as compared to 0.97 Sc/Ta ratio obtained by Sc-Stoich made with the modified synthesis procedure.

2.3.1.3 The Role of Excess Lead

Lead acetate tri-hydrate was used as a precursor and a standard method of MOE dehydration was used to remove the water (hydrated in crystal structure and absorbed) before reaction with the Sc/Ta complex. It has been reported that the MOE replaces the acetate ligands [71], however unlike the case of scandium acetate, we know the molecular weight of lead acetate tri-hydrate and subsequent changes of molecular structure with MOE did not adversely affect the final solution; in addition, because of "excess" lead, the necessity for such strict analysis is not as important as in the case of Sc/Ta where the homogeneity and distribution of the B site species has been seen to have a drastic effect on material

properties. Solutions with lead excess amounts of 10, 20 and 30% were synthesized.

2.3.2   Film Fabrication

2.3.2.1   Crystallization Behavior

The primary focus on film optimization was performed on Pt/Si substrates; one, because of cost, and two, because of the need for bottom electrodes conducive to dielectric property measurements. Bottom electrodes of Pt, and seed layers were sputter deposited on Ti/SiO$_2$/Si substrates in a Nordico sputtering tool, details of sputtering conditions are given in [33]. Rapid Thermal Annealing was employed in order to obtain dense microstructures, bypass the pyrochlore phase and limit the time exposed to high temperatures. The films were amorphous after the pyrolysis step and were annealed from room temperature to between 500 and 700°C in 1 minute, held at the annealing temperature for 1 minute, and cooled to room temperature in 10 minutes in order to preliminary investigate crystallization behavior. Figure 2.8 shows the X-ray scans of 4 layer films deposited from PST (acetate) 10% Pb on Pt/Si substrates. Only a pyrochlore phase is seen at 500°C (at $2\theta = 29°$) which slightly diminishes as we approach 700°C . The predominant perovskite (111) peak is seen at 600°C, along with the presence of a pyrochlore phase. Annealing temperatures of 700°C with rapid heating in 1 minute were chosen for further investigations.

2.3.2.1.1   Thin Layer vs. Thick Layer Anneal   In the construction of multiple layer thin films, initially, two methods were employed: 1) "*Thin* Layer Anneal" and 2) "*Thick* Layer Anneal" as depicted in figure 2.9. A common theme in previous publications on sol-gel PST thin films was the crystallization of each deposited layer. The results of 4 layer films made using these methods are presented in figure 2.10. The "Thin Layer Anneal" indicated phase pure perovskite crystallinity and a normal grain structure. However, the "Thick Layer Anneal" sample showed a broad pyrochlore peak, as well as a 2
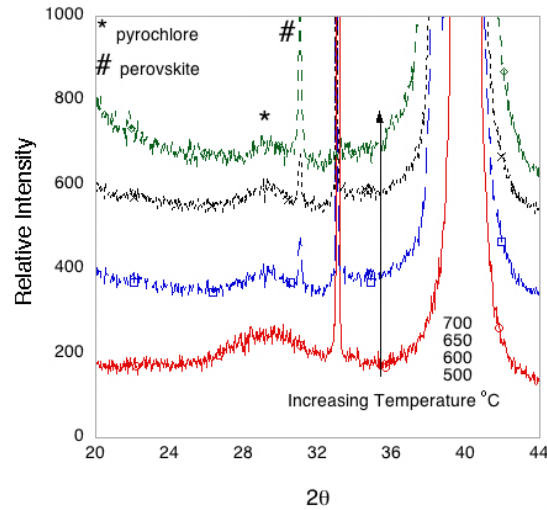
Figure 2.8: *X-ray diffraction determined crystallization behavior of 2 pyrolyzed PST layers with 10% excess lead on Pt/Si heated to annealing temperature in 1 minute with a 1 minute dwell time*
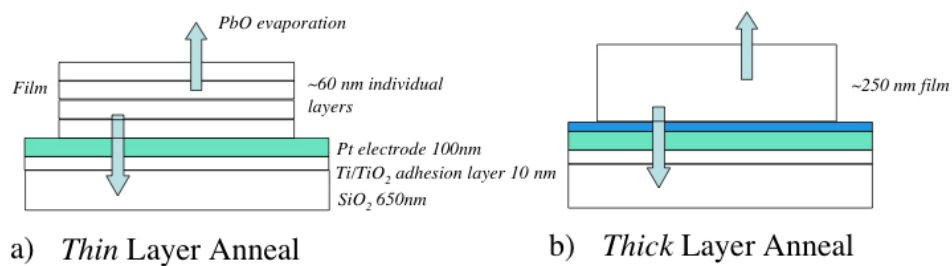
Figure 2.9: *Film deposition/crystallization methods employed in thin film construction: a)Thin Layer Anneal and b)Thick layer Anneal*
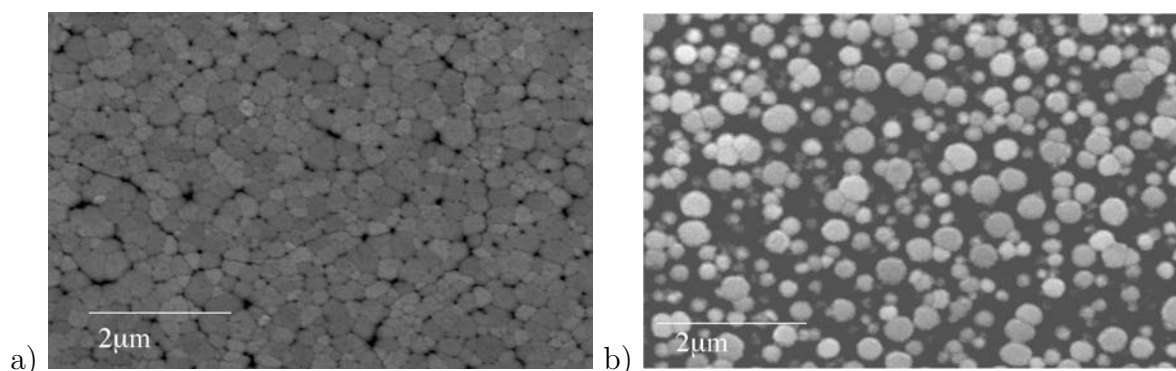
Figure 2.10: *SEM microstructure of (a) Thin Layer (b) Thick Layer annealing procedures in 4 layer (250 nm) films on Pt/Si with 10% Pb excess*

phase microstructure indicated by SEM in figure 2.10. Figure 2.11 shows TEM diffraction of the "Thick Layer Anneal" sample indicating the "rosettes" are the perovskite phase, surrounded by a polycrystalline matrix which corresponds to a FCC diffraction pattern with a lattice parameter of 6.4 Å, typical for lead deficient pyrochlore.

To further investigate the crystallization behavior between *Thin* and *Thick* layer annealing procedures, films were also fabricated from solutions containing 30% Pb excess lead. In the "*Thin* Layer Anneal" procedure no significant differences were seen between different excess lead contents in terms of X-ray and SEM investigations. However, TEM investigations revealed the presence of a secondary phase at the grain boundaries of 10%Pb which was not observed in the 30% case, as seen in figure 2.12. Due to the necessity of thick film fabrication (exceeding 1 micron) and the increased thermal load inherent in the "*Thin* Layer Annealing", this method was rejected from further film fabrication studies, and levels of 10% excess lead in the solution were deemed insufficient for phase pure perovskite formation.

2.3.2.1.2   Excess Lead Comparisons and Methods   Further experiments on excess lead content and processing conditions were performed. In order to compensate for lead loss from the surface of the films, we tried lead rich surface coatings similar to that
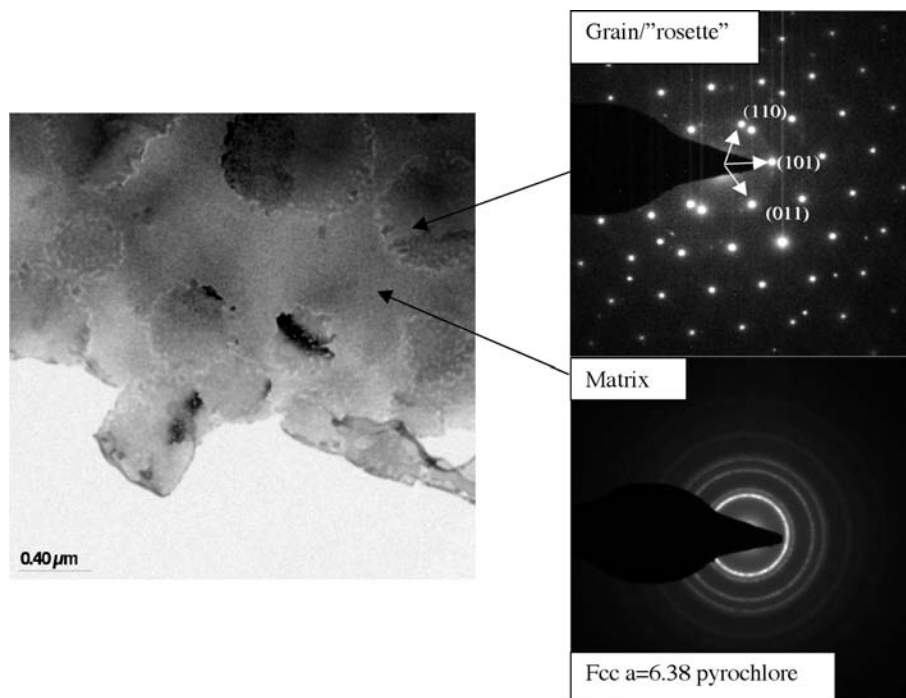
Figure 2.11: *Plane View TEM, Bright Field (BF) Image and Selected Area Diffraction (SAD) indicating a perovskite "rosette" grain structure in a pyrochlore matrix: sample "Thick Layer Anneal" (Dr. M. Cantoni)*
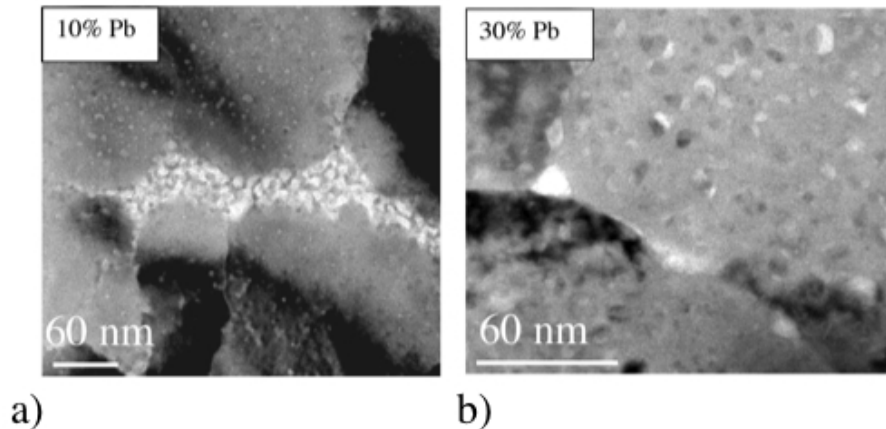
Figure 2.12: *Plane View TEM, Bright Field (BF) investigations of PST grain boundaries a) 10% and b) 30% excess Pb levels "Thin Layer Anneal" showing increased quantity of grain boundary phase with 10% excess lead addition (Dr. Marco Cantoni)*

previously performed in the PZT system [90]. The "*Thick* Layer Anneal" consisting of 4 layers with pyrolysis in-between, followed by a final anneal, was modified to include 3 interior layers of 10% excess lead, followed by a 30% Pb excess top coating before the final film anneal. This procedure was unsuccessful in our case, as we observed pyrochlore peaks in the X-ray spectra, as well as the two phase rosette microstructure, similar to the results seen in films processed with 10% Pb excess lead.

Figure 2.13 shows the X-ray spectra of 8 layer films (500 nm thickness) processed in the "*Thick* Layer Anneal" fashion on Pt/Si at 700°C for 1 minute with different excess lead contents (10, 10/30top, 20, and 30% excess Pb in solution). We can see that in the case of 10 and 10/30%Pb excess combinations the presence of a pyrochlore phase indicated by the broad peak at 29 degrees. Samples prepared with 20 and 30% lead excess indicated phase pure perovskite according to the X-ray analysis. The corresponding microstructures as observed by SEM are shown in figure 2.14 where we clearly see a perovskite phase in a pyrochlore matrix in the 10 and 10/30%Pb cases, and only perovskite grains in the films
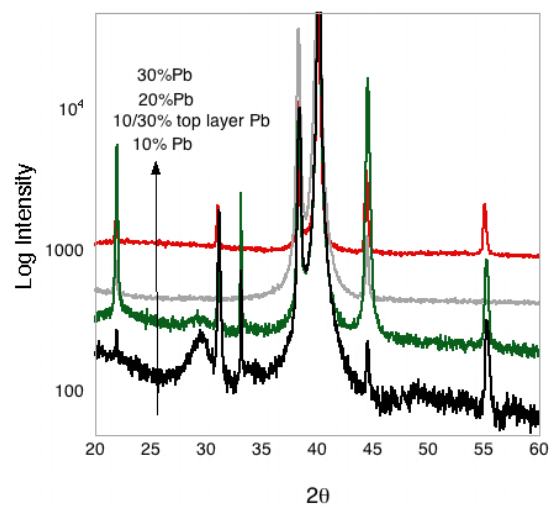
Figure 2.13: *X-ray Diffraction Spectra of 500 nm PST films on Pt/Si, RTA annealed (1 minute ramp rate) to 700° C for 1minute with 10, 10/30 combination, 20, and 30% excess lead*

prepared from solutions containing 20 and 30% Pb. The apparently observed "cracks" were determined not to be actual cracks because they did not extend all the way to the bottom electrode as evidenced by 1) our ability to perform dielectric measurements, and the films ability to withstand up to 500 kV/cm bias field during polarization measurements and 2) SEM and TEM cross sections in which there was never observed a "crack" that extended from the surface to the interface. They can be more aptly described as surface features which formed at the edges of the grain boundaries forming "secondary" grains. Similar microstructures have been observed in the PST system [56] with sputtered films, indicating the defects are not related to sol-gel processing, but more likely to enhanced lead loss at the grain boundaries. The corresponding dielectric properties of the films were measured at 1khz, and Eac 1kv/cm from 100 to -100°C and presented in figure 2.15. The reduction of the permittivity in films which contain only 10% Pb alone, or in combination with greater excess amounts can be attributed to the presence of a secondary pyrochlore phase. Although no pyrochlore phase is observed in films with 20% excess lead by SEM or X-ray investigations, the nucleation and growth determined microstructure of the perovskite phase is clearly affected by the lead content.

Figure 2.16 shows the results of TEM investigations on a film annealed at 700°C for 1 minute processed from a solution containing 30% excess Pb in solution on a Pt/Si substrate. TEM dark field investigations revealed a well developed columnar grain structure indicating the nucleation of (111) oriented grains at the Pt interface and subsequent growth to the free surface, color contrast indicated a change of "in-plane" grain orientation. Figure 2.16b and c display the results of an EDAX analysis as a function of film thickness revealing lead loss from approximately the first 80nm of the film closest to the surface, followed by a lead excess in the middle of the film, and finally a reduced lead levels approaching the stoichiometric value near the Pt interface. The lead profile indicates both lead diffusion with the Pt interface and lead loss from the surface of the film during annealing, both previously reported in the PZT Pt/Si material system [80]. The Sc/Ta
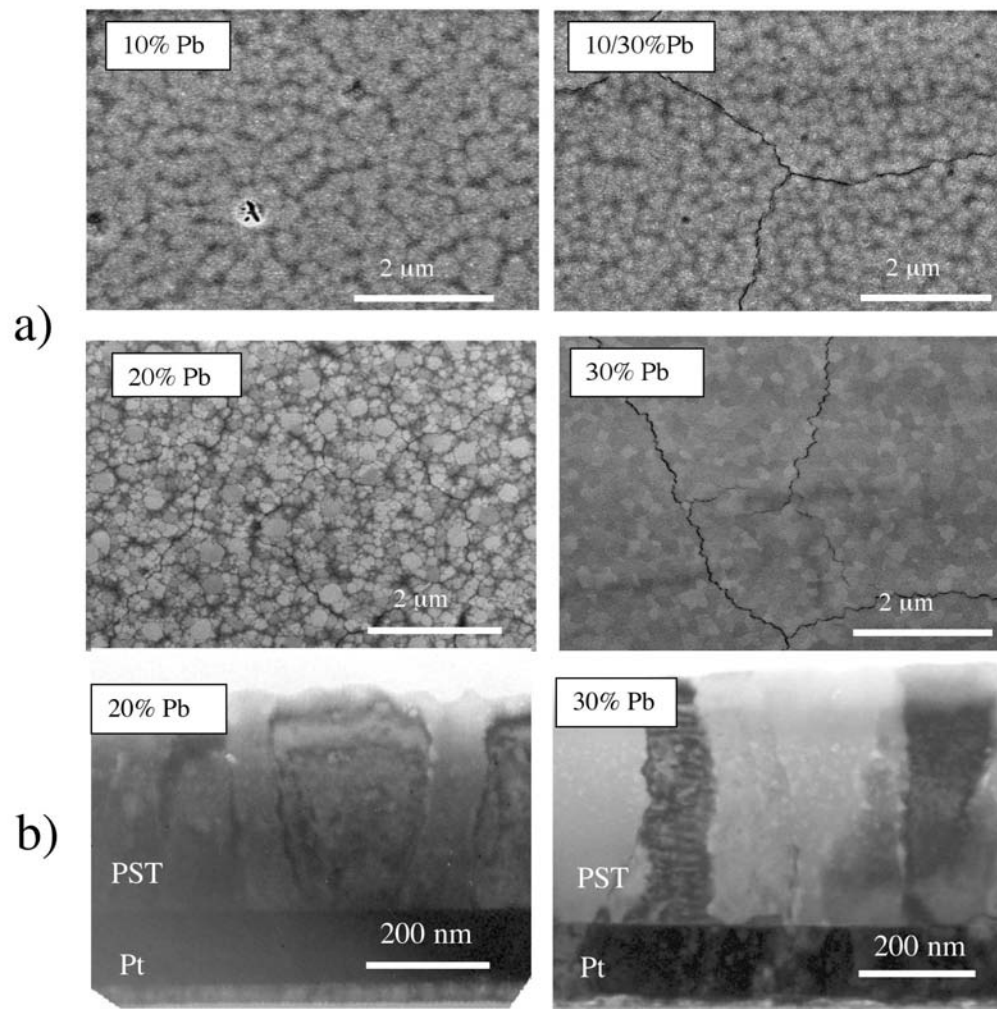
Figure 2.14: *a)SEM of 500nm PST on Pt/Si RTA annealed (1 minute ramp rate) in 1 minute to 700°C for 1 minute with 10, 10/30 combination, 20, and 30% excess lead and b) TEM BF of film cross sections: 20% Pb and 30% Pb (Dr. Marco Cantoni)*
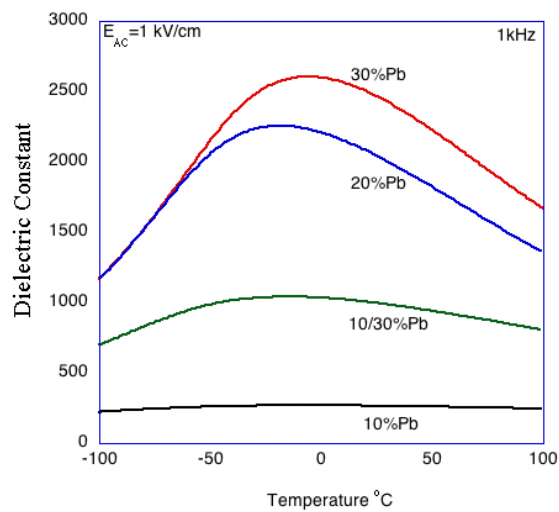
Figure 2.15: *Dielectric constant measurement at 1 kHz and E_{AC} 1 kV/cm of 500nm PST on Pt/Si RTA annealed in 1 minute to 700° C for 1 minute with 10, 10/30 combination, 20, and 30% excess lead*
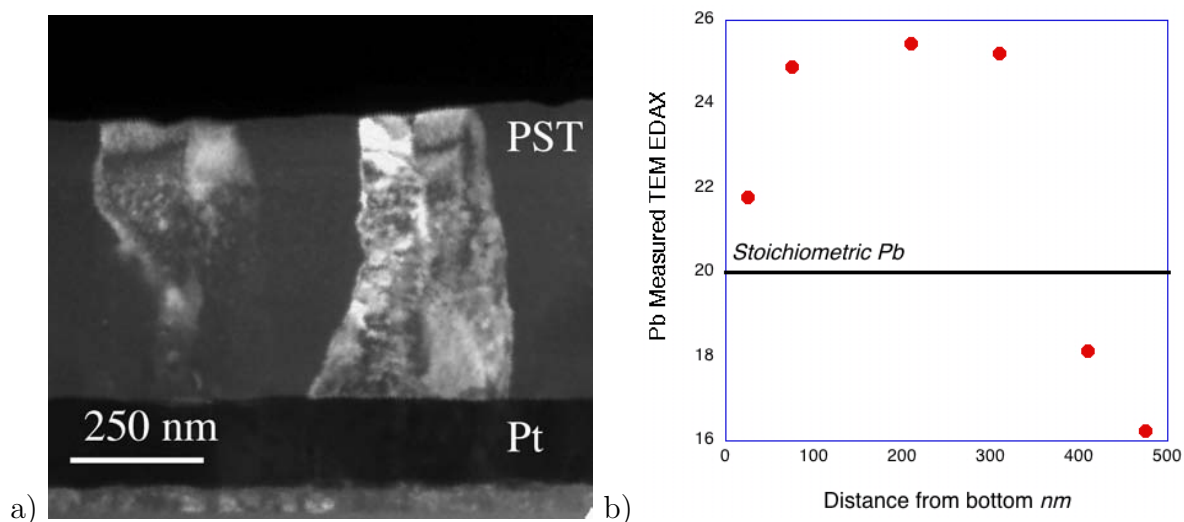
Figure 2.16: *(a) TEM Dark Field of PST/Pt/Si heated 700° C for 1 minute (b)TEM scanning mode for EDAX analysis, Pb stoichiometry as a function of film thickness (Dr. Marco Cantoni)*

ratio was seen to remain constant through the film thickness as examined by EDAX and XPS depth profiling experiments.

In Summary:

The "*Thin* Layer" processing was abandoned because of the large thermal load in the fabrication of films over 1 micron. The effects of excess lead in the solution was investigated using the "*Thick* Layer" method using amounts of 10, 20 and 30%, in addition to combinations of 10 and 30%. Phase pure perovskite films were prepared from solutions containing 20 and 30% excess Pb in solution processed by rapid thermal annealing to annealing temperatures of 700°C on Pt/Ti SiO$_2$/Si substrates.

2.3.2.2   Substrates

A number of different substrates were used for PST thin film fabrication in this study. The substrates influence the film through 1) their facility for nucleation and growth of the perovskite phase (either through nucleation directly, or on subsequent electrode/buffer or

seed layers) and 2) through the induced stress caused by differences in thermal expansion. A review of PST films on various substrates published in the literature has been already discussed and can be found in table 2.1 on page 41. Table 2.3 presents thermal expansion data for PST and the substrates used in this study along with the calculated stress in the film upon cooling from 700°C calculated using equation(2.6) on page 43. The calculated stress is compared with the measured stress on two substrate systems as verification of our assumption that thermal stress dominates in nominally thick films.

A wafer bending technique was used to examine the stress in PST films on Pt/Si substrates resulting in a measured stress of 700 MPa in tension, significantly greater than the estimated stress level of near 400 MPa. However this analysis is complicated by the presence of the Pt electrode which also exhibits thermal stress changes and this may account for the observed discrepancy in the present case. Film stress determined from measurements of the "In-Plane" lattice parameter indicated a compressive stress near 200 MPa as compared with the calculated 640 MPa. This apparent under estimate of the film stress may be due to the measurement technique which samples the surface layers which are indeed expected to be less strained that near by electrode layers thus skewing the data to lower stress levels. Overall, it is important to note that the *sign* of the calculated and measured stress is the same so that we may use the calculated stress levels to compare in general films that are in tension versus compression.

2.3.3 Film Optimization and Processing Property relations in the Pt/Si substrate system

2.3.3.1 Time and Temperature Studies

Since thin films fabricated by the Thick Layer method with 30% Pb at 700 °C for 1 minute gave satisfactory results, dwell time effects on crystallinity, microstructue and dielectric properties were investigated. No difference between relatively slow heating in

Material	TECα X$10^{-6}K^{-1}$	Calc. Stress MPa eq.(2.6)	Measured Stress MPa
PST	6.5		
Si	4	**+370 (tension)**	**+700 (tension)**[a]
STO	11.7	-380 (compression)	
MgO	13.6	**-640 (compression)**	**-180(compression)**[b]
Al$_2$O$_3$ (sapphire)	6.7	-20 (compression)	

[a]Stress measured using wafer bending technique upon cooling from crystallization temperature

[b]In-plane lattice parameter measured by grazing angle X-ray by P. Petrov, South Bank, London

Table 2.3: *PST and Substrate Thermal Expansion and Stress Data: Calculated stress determined from equation (2.6) with E_f=1 X 10^{11} N/m^2 and ν_f= 0.3*

10 minutes versus fast heating (rapid thermal anneling in 1 minute) was observed. Figure 2.17 displays the X-ray spectra and SEM determined microstructure of PST films made from solutions containing 30%Pb on Pt/Si substrates rapid thermal annealed to 700°C for 1 to 20 minutes. There was no difference seen in the microstructure, or film crystallinity and orientation between the films, however, figure 2.17d shows that the maximum value of the dielectric constant increases with longer annealing time up to 20 minutes, with no shift of the dielectric maximum.

Longer times at 700°C were performed in a tube furnace with flowing oxygen as post-annealing treatments at 5°C heating and cooling rates. Figure 2.18 shows X-ray and dielectric constant measurements indicating no change in crystal structure or orientation, however a reduction in dielectric constant (with constant loss tangent). Microstructural investigations by SEM revealed no differences, however TEM investigations indicated pronounced surface lead loss and evidence of "A" site vacancy ordering with annealing times in excess of 30 minutes. Figure 2.18c displays a plane view TEM bright field image of the sample annealed for 30 minutes showing small 5nm pores which were not annealed or repaired under long time heat treatment at 700°C . Therefore the increase in the dielectric constant with time up to 20 minutes does not seem to be associated
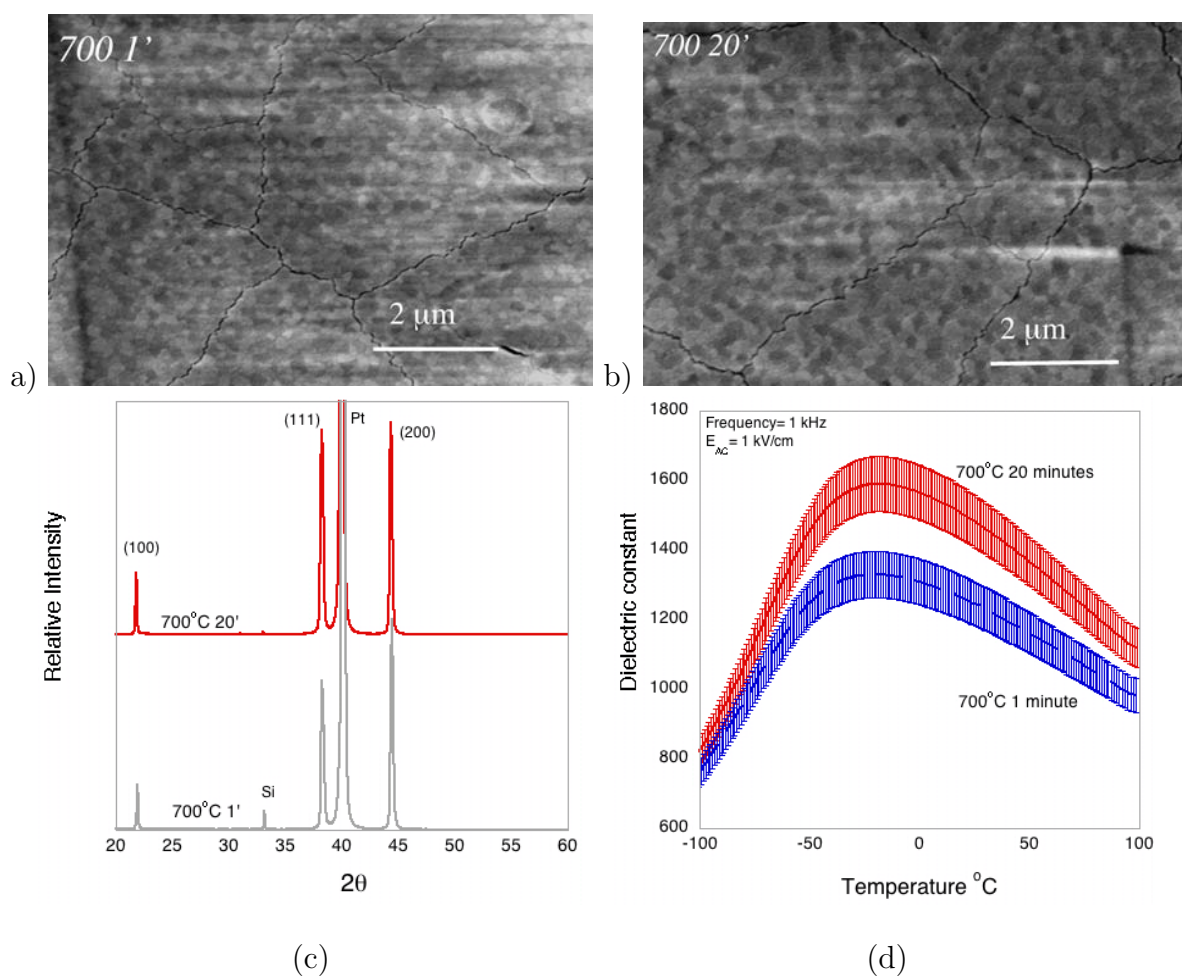
Figure 2.17: *(a) SEM of 500nm PST from 30% excess Pb on $TiO_2/Pt/Si$ substrates heated to 700°C for 1 minute (b) SEM microstructure for the same film annealed for 20 minutes (c) X-ray diffraction and (d) dielectric measurements at 1kHz and E_{AC} 1kV/cm*

with microstructural features such as pores as seen in the films, but maybe attributed to improved film homogeneity. Longer annealing times increase surface lead loss leading to dielectric property degradation.

As longer annealing times for the final anneal improved electrical properties at 700°C, higher temperatures of annealing for durations of 1 and 20 minutes were investigated for the final layer anneal. The X-ray spectra, SEM and dielectric measurements for the films annealed to 750°C are presented in figure 2.19. At longer annealing times we see the presence of a secondary phase at 22 and 46 degrees, however no parasitic phase is

a)

b)

c)
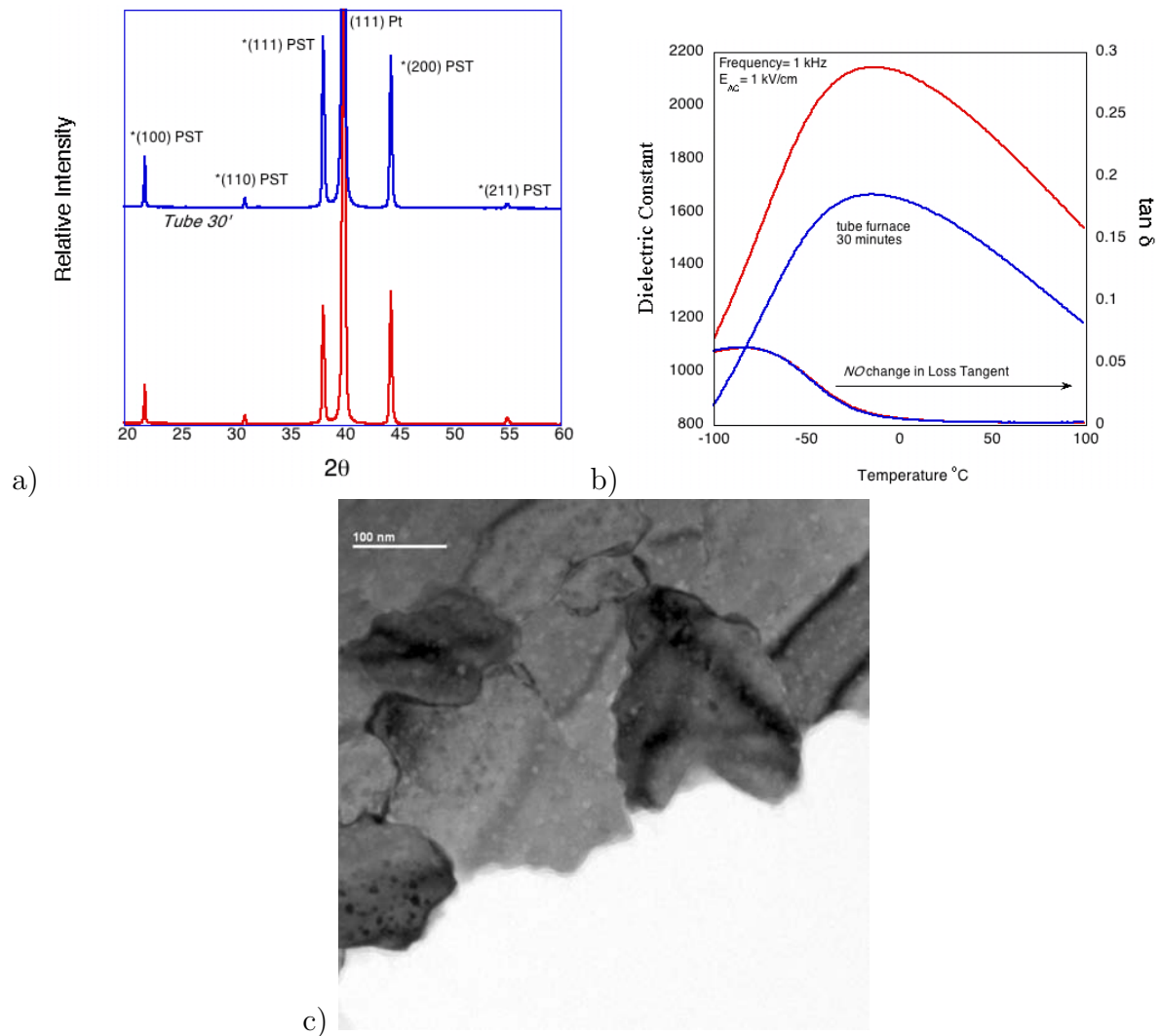
Figure 2.18: *(a) X-Ray diffraction spectra for 650 nm PST films with 30%Pb on TiO$_2$/Pt/Si substrates RTA annealed to 700° C for 1 minute and annealed to 700° C in tube furnace for 30 minutes (b)Dielectric measurements at 1kHz and E$_{AC}$ 1 kV/cm (c)TEM plane view of the film annealed at 700° C for 30 minutes (Dr. Marco Cantoni)*

detected in the microstructure. The average grain size of the films annealed at 750°C has increased to 500 nm with respect to those annealed at 700°C (grain size 250nm) on Pt/Si substrates. No change in the grain size is seen with longer annealing times, however the films heated for 1 minute shows a high level of surface defects and a "solid" surface structure in contrast with the sample annealed for longer times, which reveals a

"wavy" surface and less defects. High temperature diffusion seemed to heal the defects and promote an almost liquid like sintered microstructure. The dielectric properties of these films are displayed in figure 2.19d revealing that despite the healing of defects at longer annealing times the dielectric constant decreases, possible due to secondary phase formation associated with lead loss at high temperatures with a long time exposure.
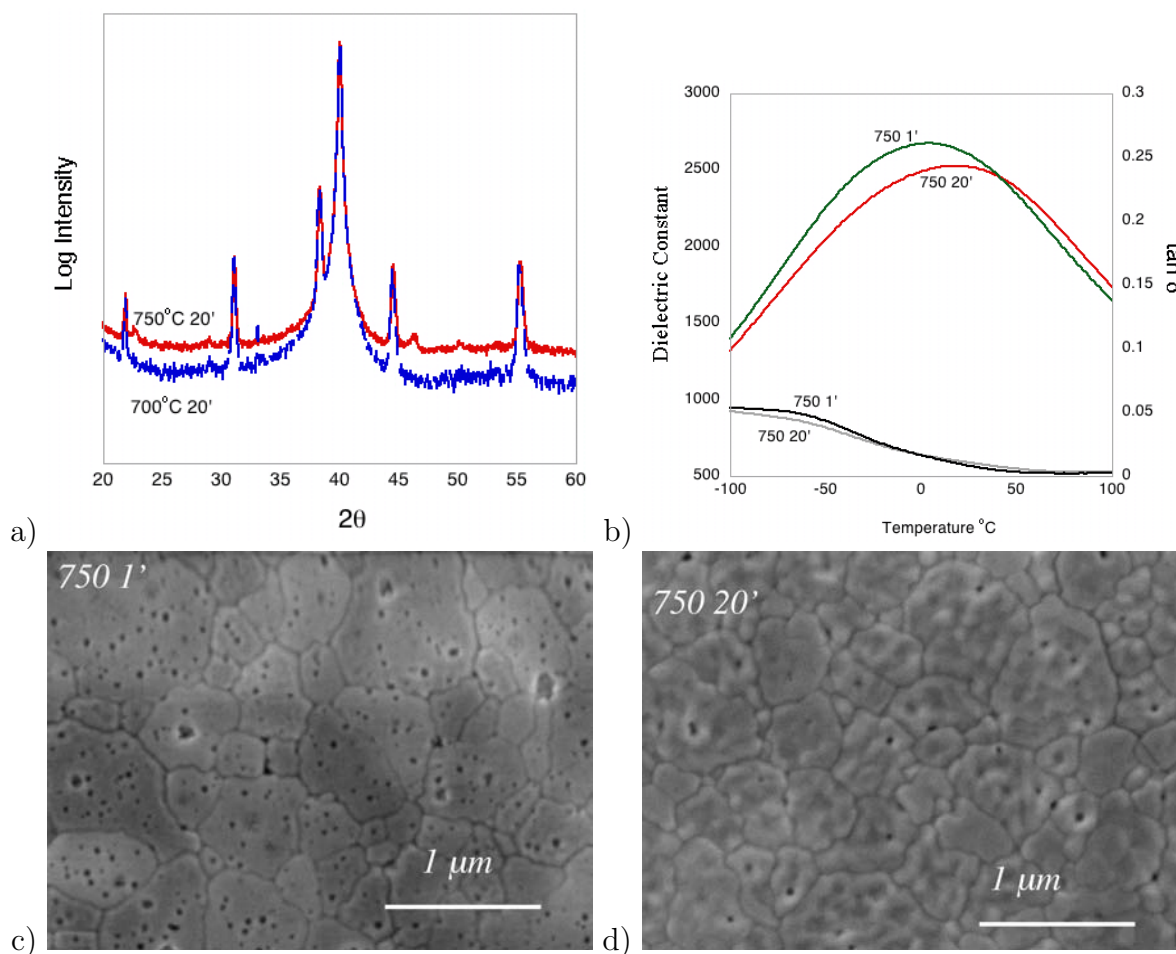
Figure 2.19: *500nm PST films on Pt/Si (a) Xray diffraction spectra for annealing at 750°C for 1 and 20 minutes (b)dielectric measurements at 1 kHz and E_{AC} 1 kV/cm (c) SEM microstructure for sample annealed to 750°C for 1 minute (d) SEM of film annealed to 750°C for 20 minutes*

Figure 2.20 displays the results for films annealed to 800°C for 1 and 20 minutes. Similar to the samples annealed to 750°C , the X-ray diffraction spectra indicate the

appearance of a secondary phase at 22 and 46 degrees in the sample which was held for 20 minutes at high temperature. The SEM microstructural investigations indicate that again the grain size has increased with processing temperature as compared to samples annealed at 700 and 750°C on Pt/Si respectively. The film heated to 800°C for 1 minute does not display the pores or surface defects that accompanied the film annealed to 750°C, probably due to enhanced surface diffusion at high temperature. In addition, the sample held for 20 minutes at 800°C displays round grain boundaries, and a cleaner surface probably due again to enhanced surface diffusion. The dielectric properties of these two films were indistinguishable, however the film annealed for 20 minutes displayed a higher defect density of top electrodes (only a few electrodes gave good dielectric measurements).

In summary: Rapid thermal annealing to 700°C for 1 to 20 minutes on Pt/Si substrates resulted in films with indistinguishable x-ray crystallinity and microstructure, however films held at temperature for 20 minutes displayed enhanced dielectric constant values. Further heat treatment at 700°C for 30 minutes led to a reduction in the dielectric constant with no apparent change in x-ray determined crystallinity or microstructure. A comparison of TEM studies of films processed for 1 and 30 minutes showed comparable levels of film porosity/defects, so that improvement of dielectric properties for films heated to 20 minutes *cannnot* be ascribed to the healing of defects at long annealing times, and is probably related to improved film homogeneity. Furthermore, annealing times longer than 20 minutes resulted in enhanced lead loss and a degradation of the dielectric constant.

Higher annealing temperatures of 750 and 800°C resulted in films with similar dielectric properties as a function of annealing time, however they exhibited more defects after 1 minute annealing duration (with phase pure perovskite) which improved with time at high temperatures. The temperature of the dielectric maximum increased from -10°C , to 19, and finally 30°C at 1kHz and electric field of 1kV/cm with annealing at temperatures of 700, 750 and 800°C respectively. The shift of dielectric maximum to higher temperatures is due to the increase in superlattice ordering with increased annealing temperature
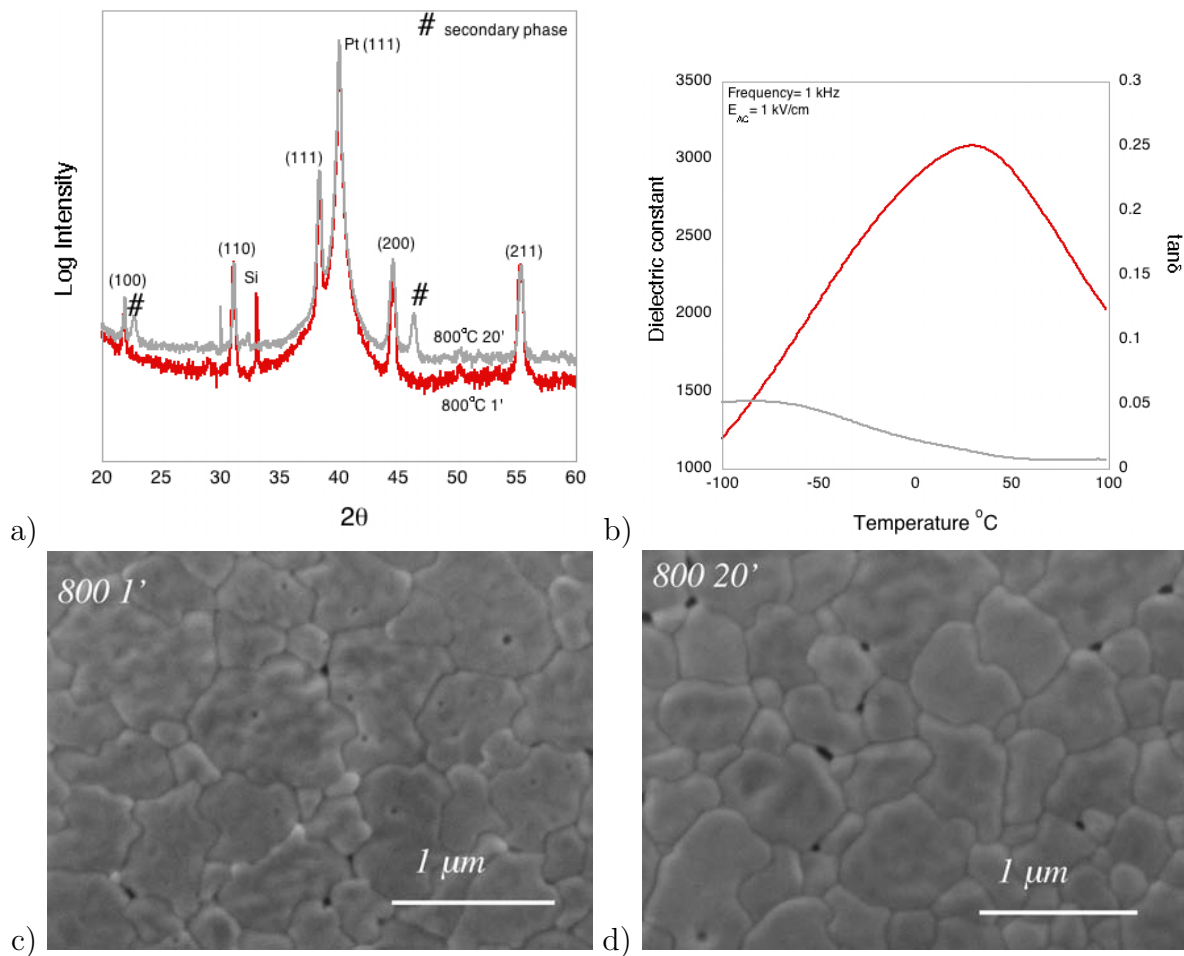
Figure 2.20: *500 nm PST film on Pt/Si (a) Xray diffraction spectra for samples annealed at 800°C for1 and 20 minutes, (b) Dielectric measurements at 1kHz and E_{AC} for sample annealed at 800°C for 20 minutes (c)SEM microstructure 800°C for 1 minute (d) SEM microstructure at 800°C 20 minutes*

and will be discussed in the following chapter. The grain size of the film increased from 250 (at 700°C), to over 500 nm with an increase of annealing temperature while annealing durations up to 20 minutes at temperatures between 700 and 800°C had no effect on the grain size. The dielectric constant maximum of films processed at 700 and 750°C is similar with values around 2500 at 100Hz, even though the the specimen annealed at 750 has an increasing degree of B site order. The subsequent increase of dielectric constant to over 3000 at 100Hz in films annealed to 800°C is probably due to a combina-

tion of increasing B site order, and improved film homogeneity due to high temperature processing. Annealing temperatures higher than 800°C on Pt/Si substrates resulted in conductive films making dielectric studies impossible due to bottom electrode degradation and film/substrate interaction. The effects of "B" site order on the position and value of the dielectric maximum will be examined in a later section.

2.3.3.2 Texture and Seed layer effects on Pt/Si substrates

The use of seed layers to control grain size and orientation were investigated following the work reported for PZT[97]. Figure 2.21a shows the X-ray spectra for films processed from solutions containing 30% excess lead deposited on Pt/Si, TiO_2/Pt/Si, and $PbTiO_3$/Pt/Si substrates and rapid thermal annealed to 700°C for one minute. All films showed phase pure perovskite, and similar orientation was observed for Pt/Si, and TiO_2/Pt/Si indicating a bimodal (111) and (100) growth modes. The fact that the two samples are similar is not suprising since it is reported that Ti, used as a adhesion layer in $Pt/Ti/SiO_2/Si$ diffuses to the surface at elevated temperatures and reacts with the oxygen environment creating an "in-situ" TiO_2 seed layer. Although the orientation dependence is opposite to that seen for PZT thin films, similar results were obtained for sol-gel derived PMN thin films[21]. The grain size is larger in (100) oriented films which indicates that under the processing conditions used, a seed layer of TiO_2, or Pt/Ti substrates used at high temperatures may result in a layer of titania which impedes heterogenous nucleation resulting in fewer nucleation sites and a relatively larger grain size of 325 nm as compared to (111) oriented films with grain size of less than 140 nm.

It is interesting to compare the results of PST films made from scandium acetate precursors with those made from isopropoxide precursors. Figure 2.22 displays the x-ray spectra of 600 nm PST made from solutions using scandium isopropoxide and 20% excess Pb. In contrast to the scandium acetate derived films, the isopropoxide derived films show (111) preferred orientation with (110) and (211) reflections not seen in the acetate
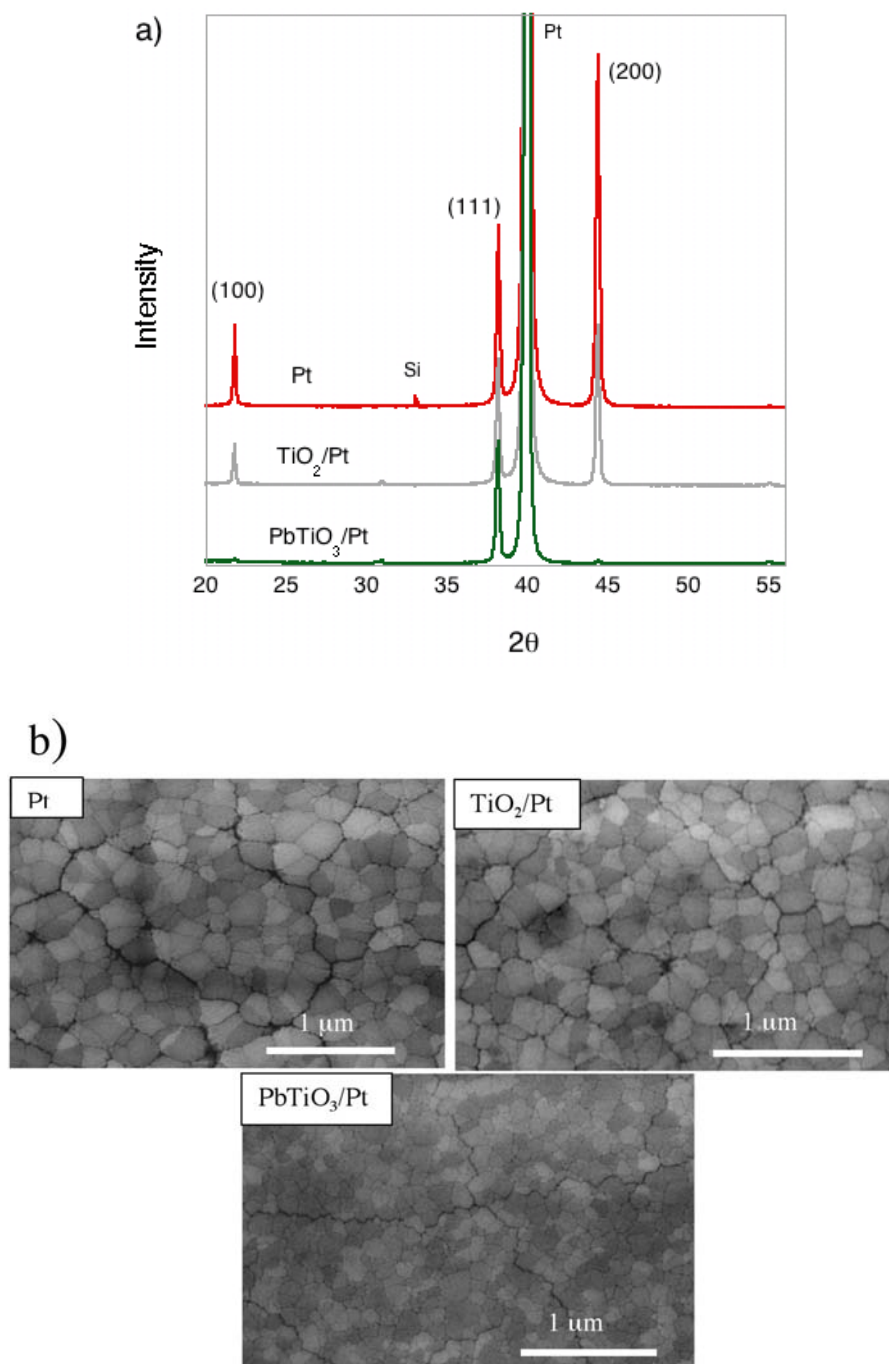
Figure 2.21: *Seed layer effects of 300 nm PST from 30% excess Pb solutions on Pt/Si substrates annealed 700° C for 1 minute (a) X-ray of PST on Pt/TiO₂/Pt and PbTiO₃/Pt electrode stacks (b) SEM microstructure*
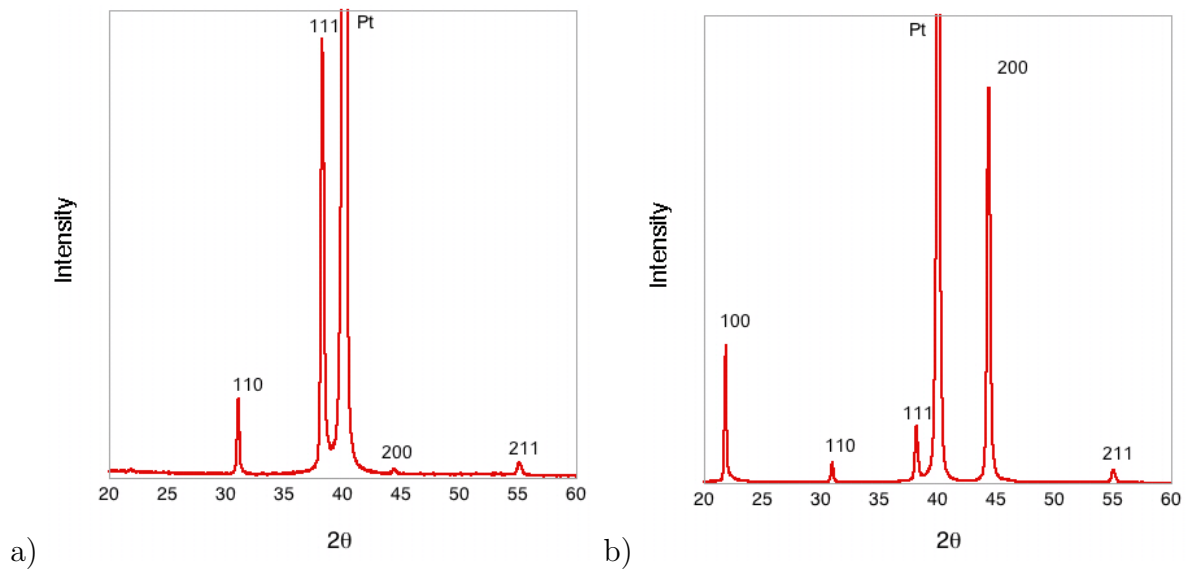
Figure 2.22: *X-ray diffraction of 600nm PST from Sc isopropoxide precursor, with 20% excess Pb annealed at 700° C for 1 minute on (a) Pt/Si, and (b) PbTiO$_3$/Pt/Si substrates*

derived samples when processed under similar conditions, on Pt/Si substrates, pyrolysis at 385°C and rapid thermal annealing to 700°C for 1 minute. Films from isopropoxide scandium precursors made on PbTiO$_3$/Pt substrates showed preferred (100) orientation as was seen in the PZT system, in addition to (110), (111) and (211) reflections. This gives further evidence of chemical effects on the orientation of sol-gel films which has been seen in other material systems and may result from the different organic content and precursor structure of the starting solutions[3].

The impact of the bottom electrode on film orientation is seen as well in the case of conductive oxide electrodes such as IrO$_2$ used in the PZT system for fatigue improvement. A 100 nm bottom electrode of IrO$_2$ was sputter deposited on TiO$_2$/Ti/SiO$_2$/Si substrates. The growth and microstrure of 600 nm films rapid thermal annealed to 700°C are presented in figure 2.24. We see a random film orientation with the most intense peak being the (110) reflection as in randomly oriented powder or ceramic samples. The microstructure was porus with surface defects, and a lack of any real grain development. Dielectric measurements showed a dielectric constant maximum in excess of 2000, but with very
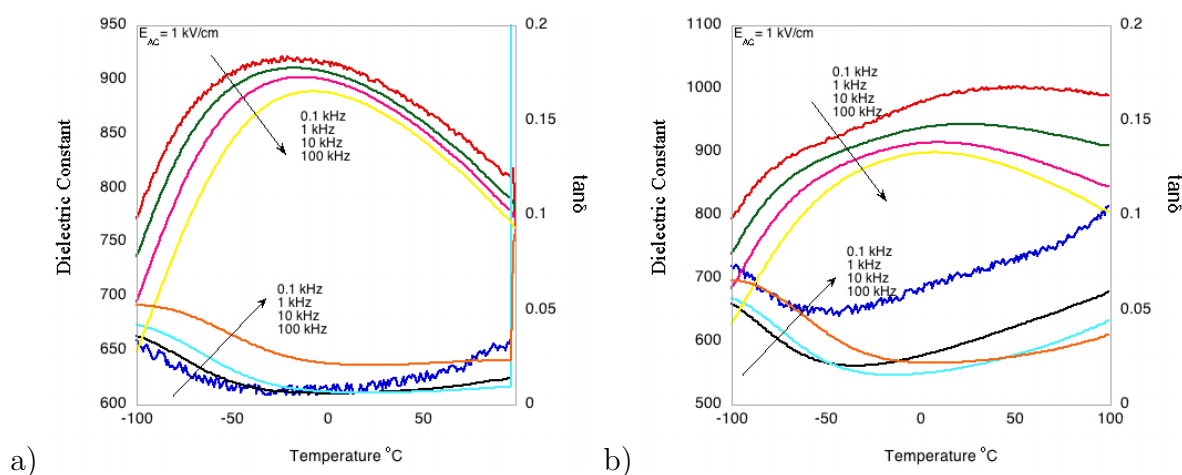
Figure 2.23: *Dielectric constant and loss tangent of 600nm PST films made from a Sc isopropoxide precursor, with 20% excess Pb annealed at 700°C for 1 minute on (a) Pt/Si, and (b) PbTiO₃/Pt*

large loss tangent values.

2.3.4   Other substrate systems for PST film fabrication

2.3.4.1   MgO

Films of PST from acetate derived 30% excess lead solutions were deposited on single crystal (100) MgO substrates resulting in phase pure perovskite with an out-of-plane orientation of (100) matching the underlying substrate. The X-ray spectra and pole figure of the (110) pole are shown in figure 2.25 for a 950 nm PST film rapid thermal annealed to 700°C for 1 minute. The position of the (110) peaks in figure 2.25b as the sample is rotated indicates an epitaxial relationship with the MgO substrate, and the single crystal nature of the thin film. Films prepared with thicknesses of 540, and 950 nm both resulted in epitaxial films with the rocking curve of (200) PST indicating an increasing FWHM from 1.54 degrees (540 nm) to 2.2 degrees (950 nm) as compared to 0.2 degrees for the (200) MgO substrate indicating a degradation of heteroepitaxial quality with increasing film thickness. Bright field TEM investigations and the diffraction
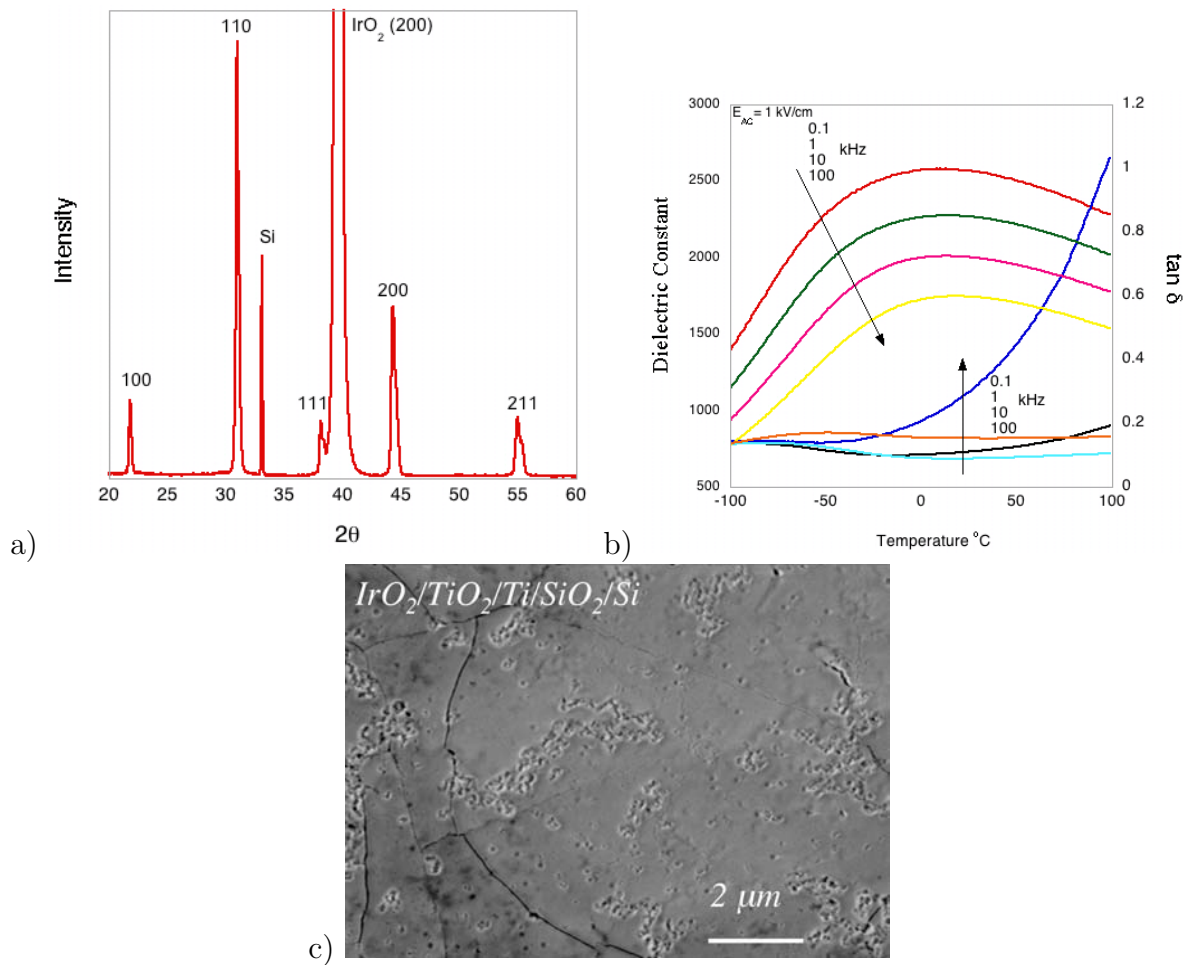
Figure 2.24: *600 nm PST films on $IrO_2/TiO_2/Si$ substrates from 30% excess Pb solutions annealed to 700° C for 1 minute*
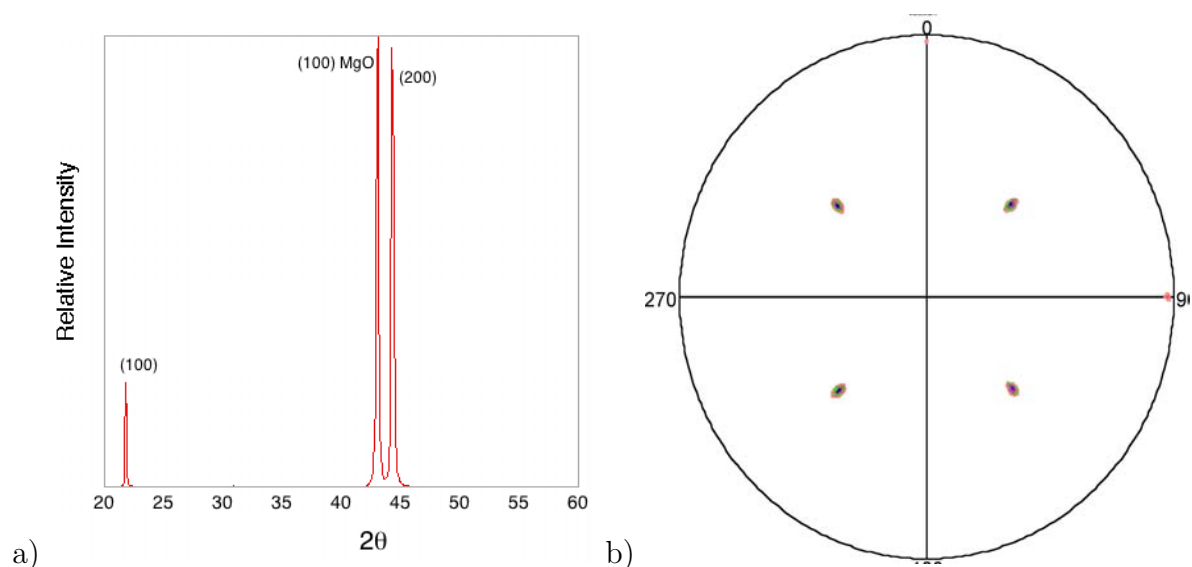
Figure 2.25: *X-ray Spectra and Pole figure of the (110) peak of 950 nm PST from 30% excess Pb on (100)MgO annealed at 700°C for 1 minute showing epitaxial nature of the film*

pattern shown in figure 2.26 also confirm the single crystal nature of the film. In addition, the bright field image in figure 2.26 reveals some degree of trapped porosity as is often the case with epitaxial films processed at temperatures much lower than their melting temperature [104]. Detailed studies of the interface by HRTEM are presented in figure 2.27 which reveal local deviations from epitaxy at the interface. Specifically, by taking a Fourier transform (FFT) of the HRTEM image in figure 2.27 we obtain the corresponding diffraction pattern. The result in the present case is a polycrystalline (rings) diffraction pattern indicating deviations from epitaxy at the PST/MgO film/substrate interface.

As bottom electrodes are needed for out-of-plane dielectric measurements, it was attempted to deposit PST on (100) Pt/(100)MgO substrates. A (100) Pt bottom electrode 100 nm thick was sputter deposited on (100) Ir/MgO with the Ir serving as an adhesion layer between the platinum and magnesium substrate. Figure 2.28 displays the X-ray spectra and SEM microstructure of a 500 nm PST film made from scandium acetate derived solution with 30% excess lead rapid thermal annealed to 700°C for 1 minute.
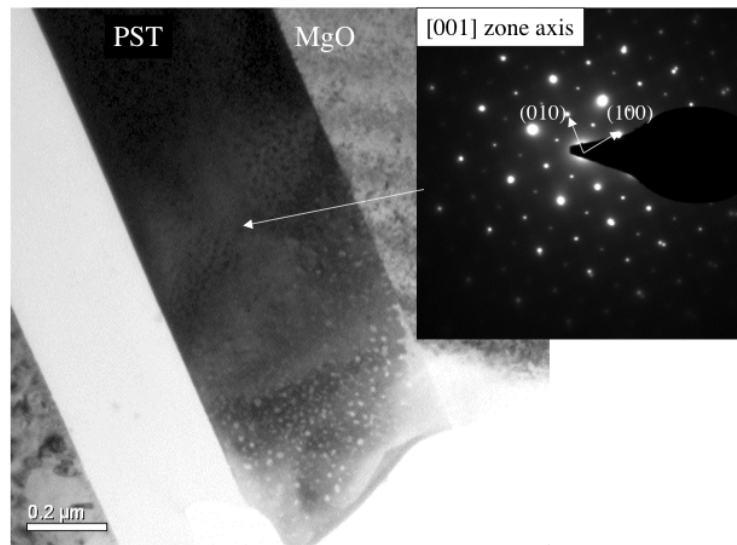
Figure 2.26: *TEM Bright Field Image and SAD of 540 nm PST film with 30% excess Pb on (100) MgO substrate annealed at 700° C for 1 minute indicating epitaxy and single crystal nature of the thin film (Dr. D. Su)*
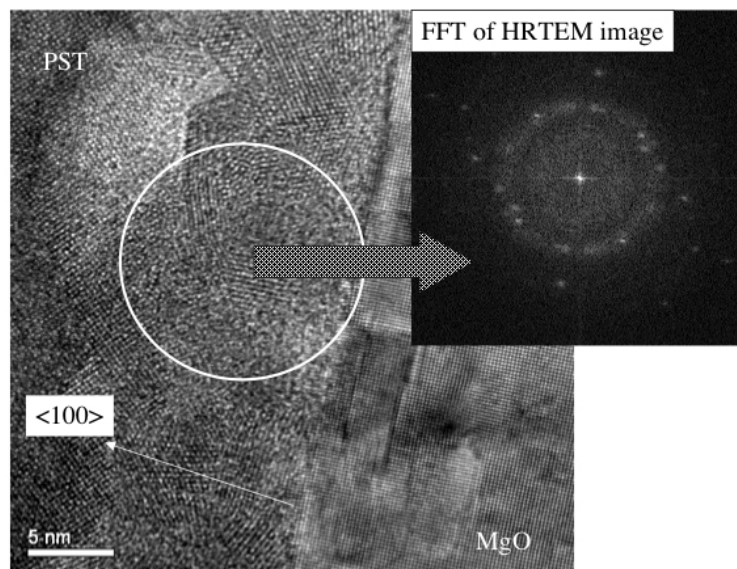
Figure 2.27: *HRTEM of 540 nm PST film with 30% excess Pb on (100) MgO substrate annealed at 700° C for 1 minute, and FFT Fourier Transform of film/substrate interfacial region showing polycrystalline nature of interface (Dr. D. Su)*

The X-ray spectra shows phase pure perovskite with highly preferred (100) orientation, including the peaks of (100) MgO substrate, (100) Pt electrode and Ir peak. The films display columnar grain growth, with large grains in excess of 3 microns.
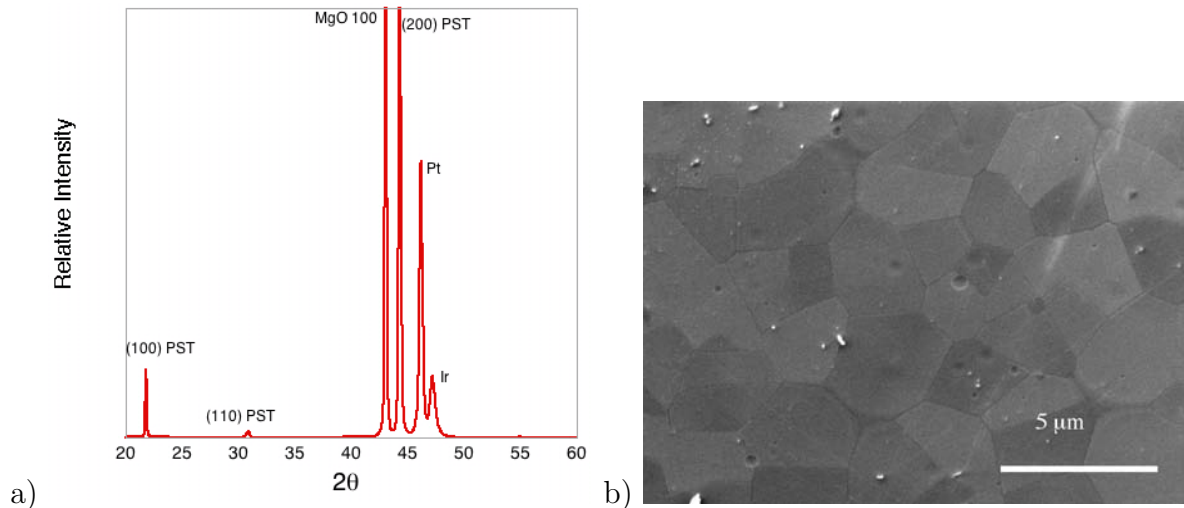
Figure 2.28: *a) X-ray-Spectra and b) SEM of 650 nm PST with 30% excess Pb on Pt/Ir/(100)MgO substrates annealed at 700°C for 1 minute*

2.3.4.2 STO

Single crystal (111) and (100) strontium titanate substrates doped with 1% Nb were used for the growth of epitaxial (100) and (111) PST films. Figure2.29a, and b show the X-ray spectra of (111) PST on (111) STO and (100) PST on (100) STO respectively rapid thermal annealed to 700°C for 1 minute indicating phase pure perovskite and highly oriented films. The global epitaxial relationship was confirmed by a pole figure of the (111) peak in "out of plane" (100) oriented PST shown in figure2.29d. The epitaxial relationship was also observed in TEM studies of (111) PST as shown in figure2.29c. The microstructure of a film annealed at 700°C for 1 minute investigated by TEM is presented in figure2.30. The dark field image presented in figure 2.30 shows some porosity in the bulk of the film consistent with previous observations of epitaxial film processed at such

low temperatures, while the contrast at the film/substrate interface shows evidence of strain induced by lattice mismatch.

2.3.4.3   Sapphire

Films were also fabricated on single crystal c-axis oriented sapphire substrates. In this case the low dielectric constant of the substrate (k=10) compared with the film (in excess of 1000) facilitated the calculation an in-plane dielectric constant by a planar capacitor method which eliminated the need for a bottom electrode. In the case of sapphire, the lattice constant and crystal structure was unfavorable for heterogeneous nucleation at the film/substrate interface and an often detectable amount of pyrochlore was observed under the same conditions leading to phase pure perovskite in other substrate/electrode systems. The nucleation could be improved however by employing the use of seed layers previously described for the Pt/Si system. Figure 2.31a shows the x-ray spectra of a 600 nm PST film deposited on sapphire and TiO_2/sapphire and rapid thermal annealed to 700°C for 20 minutes. The film without the seed layer displays pyrochlore at 29 degrees, and a random orientation indicative of homogenous nucleation in the bulk of the film. The film processed with the aid of a 2nm TiO_2 layer indicates phase pure perovskite with a high degree of (111) orientation, similar to the enhanced (111) PZT nucleation with the use of titania.

Lead Magnesium Niobate (PMN) thin films fabricated by a sol-gel method following [21] were also grown on sapphire substrates for the purpose of investigating the lattice response using FTIR spectroscopy in this model system as will be discussed in Chapter 4. Titania seed layers were also used to promote perovskite growth for PMN on sapphire substrates. Figure 2.31 shows an increase in the perovskite content from 74% to 97% and an increase in the (111) orientation of the film with the presence of a 2 nm TiO_2 layer for a 620 nm PMN film annealed at 800°C for 1 minute.
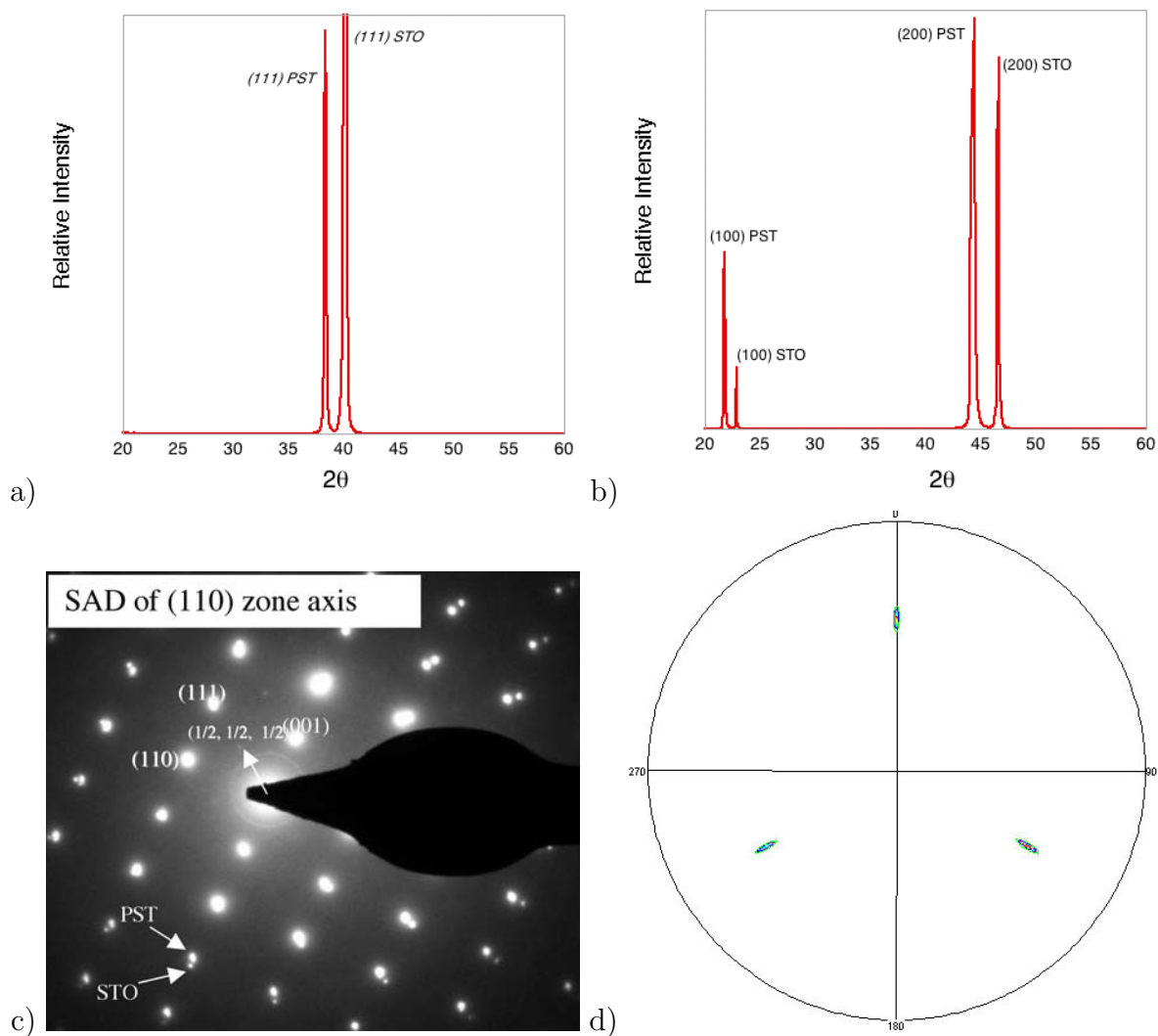
Figure 2.29: *X-ray and Pole figure of 600 nm PST on STO (a) 111STO (b) 100 STO (c) SAD of (110) zone axis in (111) PST/STO indicating local epitaxy and slight superlattice ordering (TEM by Dr. Marco Cantoni) (d) 111 pole of (100)PST on STO100*
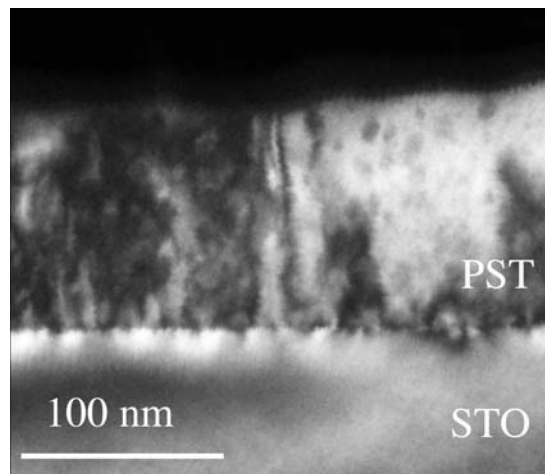
Figure 2.30: *TEM dark field image of 100 nm PST on (111) STO (Dr. Cantoni)*
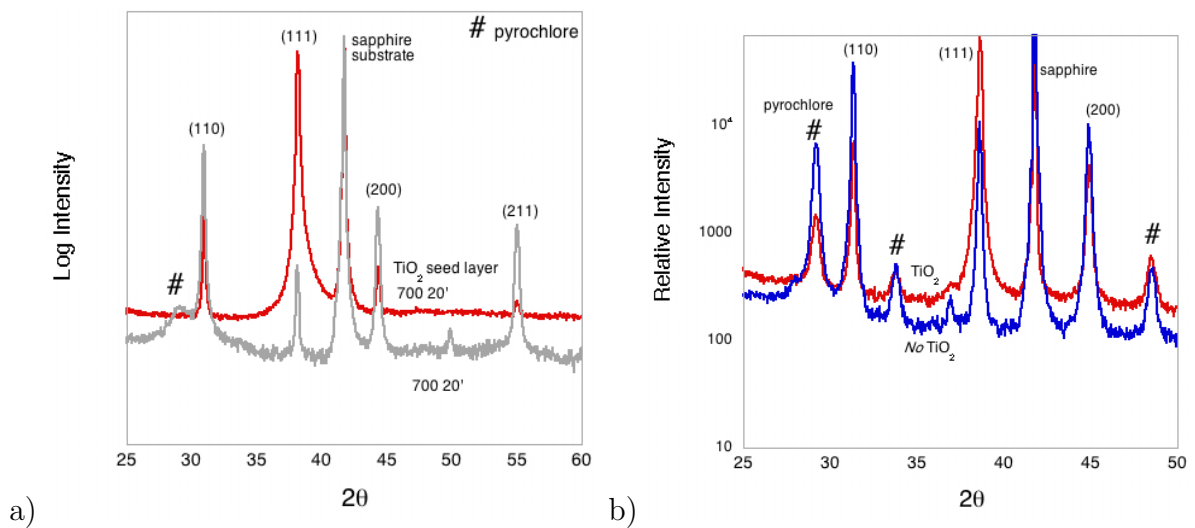
Figure 2.31: *X-ray diffraction spectra of (a) 500 nm PST film annealed at 700° C for 20 minutes and (b) 620 nm PMN film annealed at 800° C for 1 minute on sapphire substrates, with and without a 2 nm TiO_2 seed*

2.3.5   "B" Site Ordering

The effects of positional disorder in the PST system have been established for single crystal [115], and Bulk ceramics [6], however the structure property relations between ordered and disordered thin films have not yet been throughly investigated. While in bulk materials, the ordering occurs upon annealing at elevated temperatures (1000°C) for long times (62 hours), ordering in PST thin films has been reported at low temperatures of 700°C upon very slow cooling (-1°C /hour)[22]. The temperature/time requirements for thin film ordering on different substrates were studied.

In PST, with a cubic structure the ordered arrangement of Sc and Ta atoms leads to an additional periodicity (111) direction, a effective doubling of the PST unit cell, and the appearance of superlattice reflections from (h+1/2, k+ 1/2, l+ 1/2) planes. In bulk materials it is common to characterize the degree of order S by equation 2.11:

$$S^2 = \frac{I_{(1/2,1/2,1/2)}/I_{(100)} \ observed}{I_{(1/2,1/2,1/2)}/I_{(100)} \ calculated, for S = 1} \tag{2.11}$$

where S=1 for complete order and S=0 for a completely disordered material, and I is the integrated intensity area of the relevant diffraction peak. The degree of order is determined using the integrated intensity area of the superlattice peak compared to a reference peak in the material, usually the (100) for randomly oriented bulk materials. In textured thin films, the degree of orientation as seen by X-ray diffraction is best seen in films which have at least some degree of (111) reflections. In this case, there is a convenient basis to compare the intensity of the superlattice peak, to the principal (111) reference peak which removes any effect due to preferential orientation. In some cases, (100) oriented epitaxial films for instance, the degree of order cannot be estimated using normal theta-2theta diffraction techniques and must be examined by TEM studies. In addition to the order degree, the size of the ordered regions may be estimated from X-ray data by Scherrer's formula 2.12:
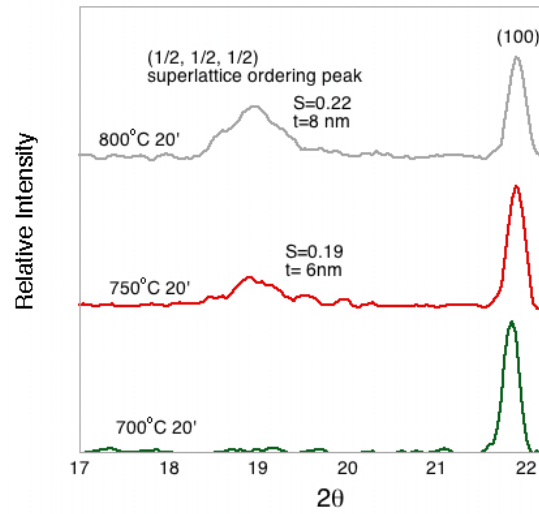
Figure 2.32: *500nm PST film from a solution with 30% excess Pb on Pt/Si (a) X-ray diffraction spectra for films annealed at 700, 750 and 800° C for 20 minutes; S is order degree estimated using equation (2.11) with the (111) peak as a reference, and t is the estimated size of the ordered region from equation (2.12)*

$$t = \frac{0.9\lambda}{\beta * cos\theta} \ where \ \beta = \sqrt{\beta_s^2 - \beta_p^2} \tag{2.12}$$

where t is the size of the ordered region, λ is the wavelength of X-ray radiation used, β is the peak broadening, β_s is the FWHM of the superlattice peak and β_p is the FWHM of a simple lattice reflection at similar diffraction angles to the superlattice peak.

2.3.5.1 Ordering on Pt/Si Substrates

Surprisingly, even annealing times as short as 20 minutes at 750 and 800°C resulted in an increase in B site ordering. Figure 2.32 shows the superlattice reflections, calculated size, and the order paramater S for a film heated at 700, 750 and 800°C for 20 minutes. The order parameter increased from S=0, to S=0.22 with a roughly estimated ordered region size of 8 nm. Longer time annealing at 800°C and higher temperature processing were not possible due to the degradation of the underlying Pt electrode.

2.3.5.2   Ordering on STO(111) Substrates

Doped single crystal substrates may serve as bottom electrodes and provide a unique opportunity to further study high temperature processing which is limited in the Pt/Si system. At elevated temperatures the processing limitations are not associated with bottom electrode degradation, but enhanced lead loss from the film surface. In studies with temperatures exceeding 800°C, films were first rapid thermal annealed to crystallinity at 700°C for 1 minute before being further heat-treated in a box furnace in a double shelled sealed ceramic container with a pellet of $PbO/PbZrO_3$ between the first and second ceramic cover providing a control of the processing atmosphere in the system, while eliminating PbO deposits on the film surface. Figure 2.33 displays the x-ray spectra of PST films made from 30% lead excess solutions annealed at 700, 800°C for 1 minute and 1050°C for 5 minutes. Figure 2.33 shows a detailed view of the superlattice ordering peak which increases with processing temperature as seen in PST on Pt/Si substrates. At an annealing temperature of 1050°C there is seen the development of a (110) perovskite peak, along with an altered surface morphology indicative of liquid phase development and subsequent re-crystallization leading to a broad (111) PST peak. The estimated order parameter S increased from S=0 at 700°C to S=0.37 at 1050°C for 5 minutes, with an estimated ordered region size of 26 nm.

2.3.5.3   Ordering on Sapphire Substrates

In addition to high temperature studies for short annealing times, longer annealing times at intermediate temperatures were also investigated. Figure 2.34 shows the superlattice and microstructure evolution upon heat treatment. After 1 minute at 850°C , no evidence of ordering was found by X-ray or TEM investigations. Samples annealed for 1 hour displayed a order parameter S=0.55, increasing to S=0.91 after 35 hours. The grain size of greater than 5 microns is maintained on annealing from 1 minute to 1 hour, accompanied by a homogenization of the surface/grain boundary structure which is highly evident after
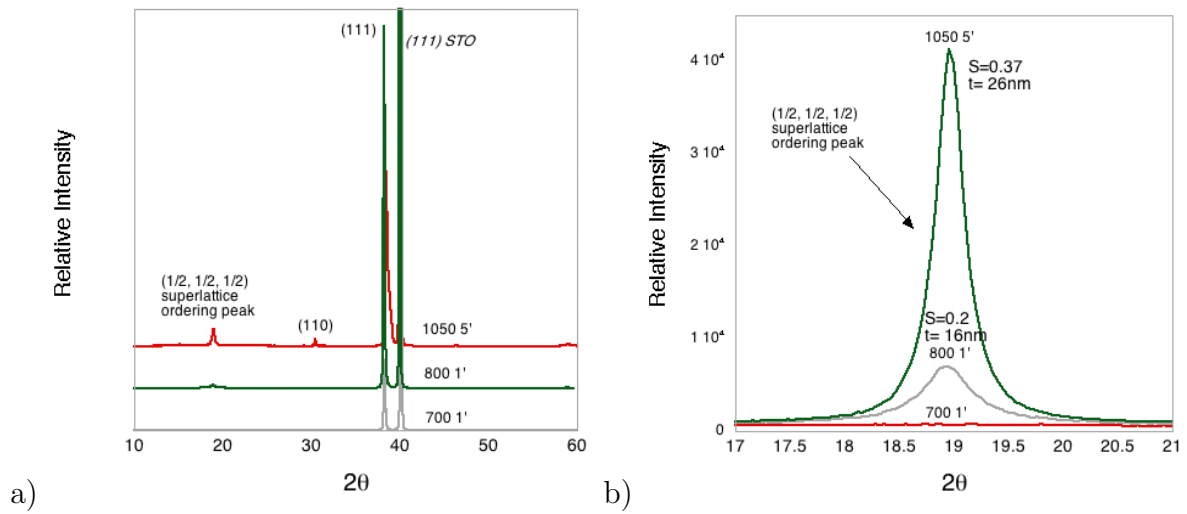
Figure 2.33: *X-ray spectra of 600 nm PST from solution containing 30% excess Pb on STO(111) annealed at 700, 800°C for 1 minute and 1050°C for 5 minutes; S is order degree estimated using equation (2.11) with the (111) peak as a reference, and t is the estimated size of the ordered region from equation (2.12)*

35 hours of annealing. TEM dark field investigations shown in figure 2.35 allow us directly see the degree of ordering as a volume percentage in a single grain and the size distribution of ordered regions. As seen in figure 2.35 the X-ray estimated order degree of roughly 50% is visually represented, with roughly half of the space being occupied by ordered regions. A higher magnification of the ordered regions allows us to see that while the volume of the material occupied by the ordered regions increases with time annealing time at 850°C , the *size* of the ordered regions are approximately the same as highly ordered the highly ordered sample (S=0.78) annealed at 800°C for 48 hours..

2.3.5.4 Ordering on MgO Substrates

The ordering of epitaxial films of PST on MgO (100) single crystal substrates was studied using only TEM dark field investigations because of the lack of (111) reflections in the standard theta-2theta diffractometer. Figure 2.36 shows the dark field image of superlattice reflections for a 550nm PST/MgO film annealed at 850°C for 24 hours. Although the
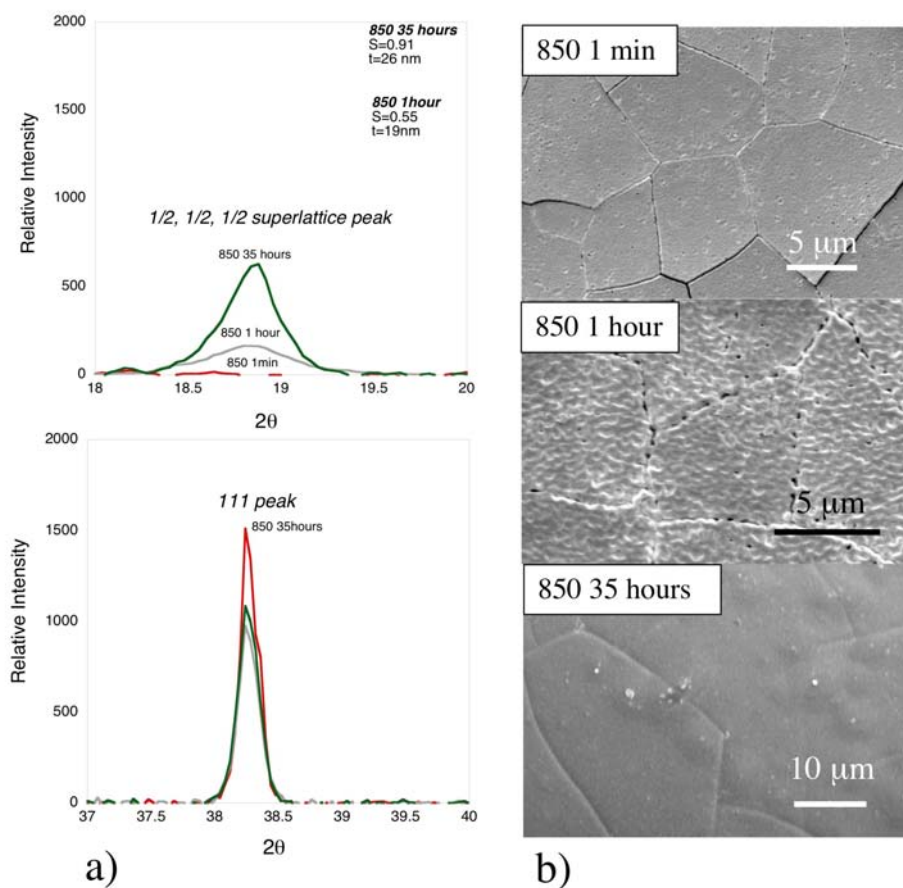
Figure 2.34: *650 nm PST film from 30% excess lead on (0001) sapphire substrate annealed to 850° C for 1 minute, 1hour and 35 hours (a) X-Ray diffraction of superlattice and (111) principal peak showing the increase in ordering with increasing time at 850° C and (b) SEM microstructure of the films; S is order degree estimated using equation (2.11) with the (111) peak as a reference, and t is the estimated size of the ordered region from equation (2.12)*
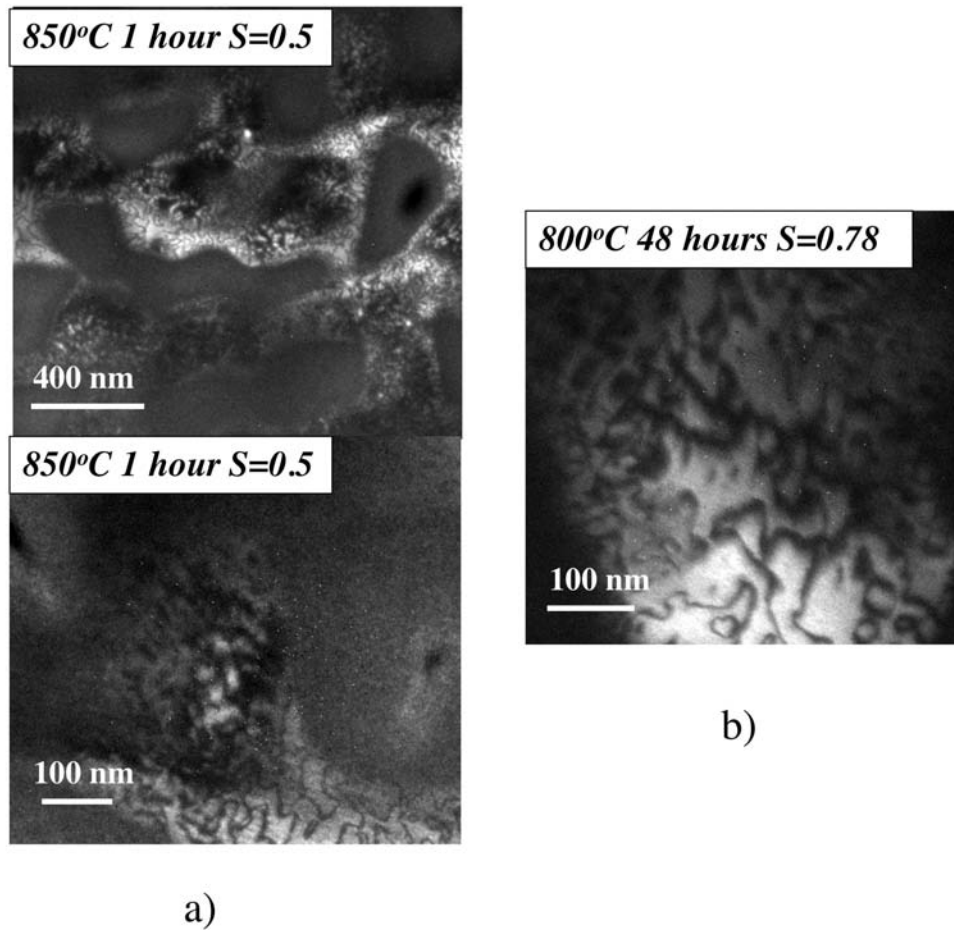
Figure 2.35: *650 nm PST on sapphire annealed at 850° C (a) Plane View TEM DF image from superlattice reflections at low and high magnification of film annealed for 1 hour, and (b) TEM DF image of film annealed at 800° C for 48 hours (Dr. D. Su), S is order degree estimated using equation (2.11) with the (111) peak as a reference as determined from X-ray diffraction*
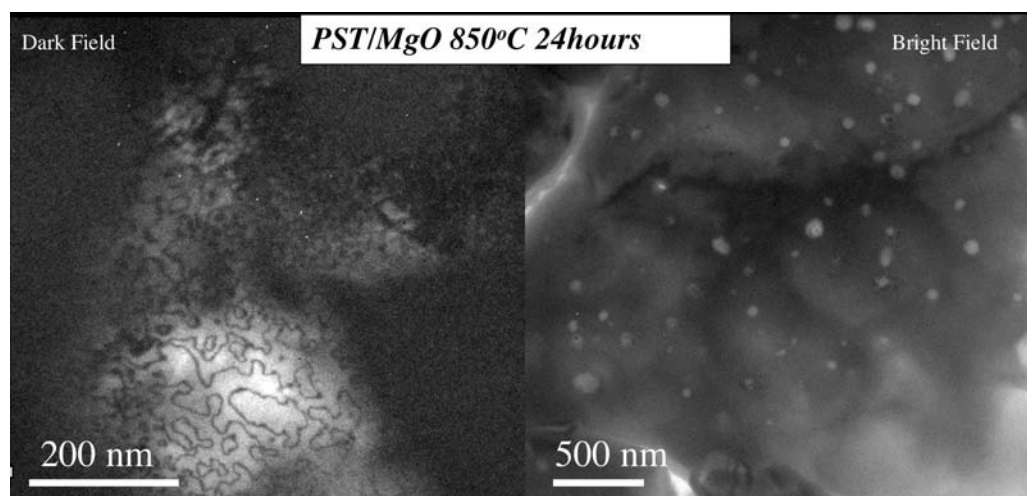
Figure 2.36: *550 nm PST on MgO annealed at 850°C for 24 hours, Plane View TEM* Dark Field *imaging showing ordered regions, and* Bright Field *image showing porosity/inclusions (Dr. D. Su)*

degree of order cannot be quantitatively estimated, there is seen a well developed ordered phase with a distribution of ordered regions, dispersed in a disordered matrix, similar to that seen in highly ordered specimens on sapphire. From examining the bright field TEM images we see evidence at the nanometer scale of porosity and/or inclusions inside the PST grains.

2.3.5.5   Ordering of PMN on sapphire

PMN films were fabricated from a Mg acetate/Nb ethoxide solution route with 20% excess lead and deposited onto TiO_2 seeded sapphire substrates. PMN does not display long range ordering (although small ordered regions of 2 to 3 nm form in bulk and thin film) and thus is an ideal tool to separate the effects of ordering and microstructural changes previously seen in the PST system. The X-ray spectra and SEM images are displayed in figure 2.37 for films annealed at 850°C for 1 minute and 24 hours. Extended annealing times resulted in an increase in pyrochlore content from 2 to 10% with the size of surface nucleated pyrochlore phase of 55 nm estimated from X-ray data using equation (2.12).

SEM images showed surface nucleated pyrochlore with a size greater than 100 nm, and an increase in the perovskite grain size with increasing time at 850°C from a very fine grained 60 nm after 1 minute annealing time, to a size in excess of 600 nm after 24 hours of annealing time.

2.3.5.6 A High Temperature Disordered State in Thin Films?

We have seen a disordered PST phase after annealing at 700°C, and various increased degrees of "B" site order upon increasing the annealing *time* at 850°C, and with increased *temperature* 1000°C for short annealing times. As disordered ceramic PST is sintered in temperatures in excess of 1500°C, is it possible in thin film systems to further increase the annealing temperature for short time durations in order to produce a disordered phase at high temperature?

PST film deposited on STO and sapphire substrates and annealed at 1000°C for short annealing times still displayed significant degrees of order, and attempts to increase the annealing temperature resulted in film degradation as seen in figure 2.38. These experiments raise an important point, namely that *the disordered state in bulk and thin films samples are different due to processing*. The following chapter will focus on a detailed analysis of the dielectric properties of sol-gel derived PST thin films discussed herein.

High temperature sintering to 1000 and 1300 in an enclosed Pb atmosphere was performed for 650 nm PST films on sapphire substrates pre-annealed at 700°C. Both films were disordered according to X-ray analysis, however TEM dark field imaging showed that the sample annealed at 1000°C has a distribution of small ordered regions from less than 4 nm in diameter to 20 nm. In contrast PMN films annealed at 1000°C for short annealing times possessed only short range order with homogeneously distributed 2 to 3 nm ordered regions as seen in figure 2.39.

a)

b)
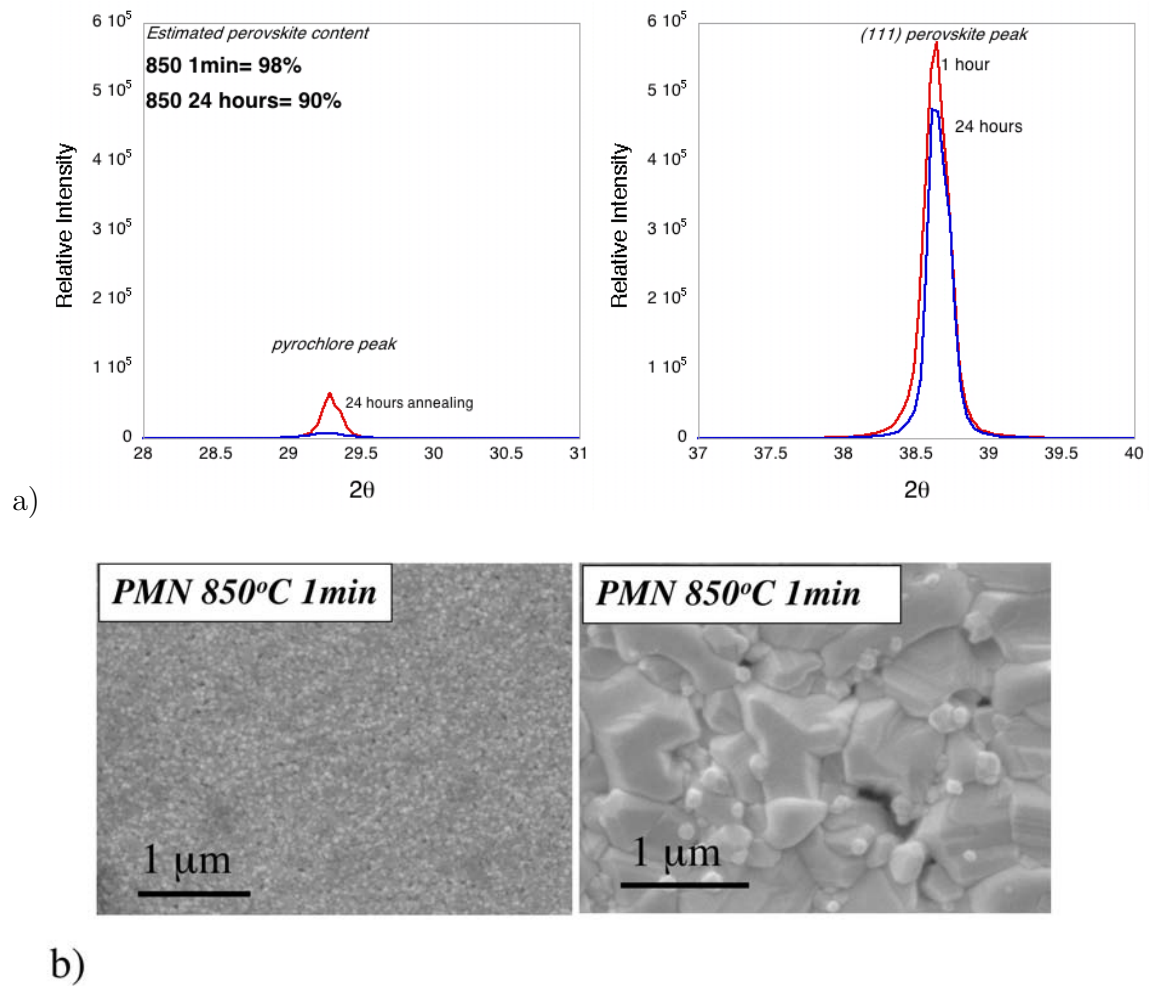
Figure 2.37: *620 nm PMN on sapphire substrates annealed at 850° C for 1 minute and 24 hours (a) X-ray diffraction showing the principal pyrochlore and perovskite peaks, and (b) SEM microstructure of films annealed for 1 minute and 24 hours at 850° C*
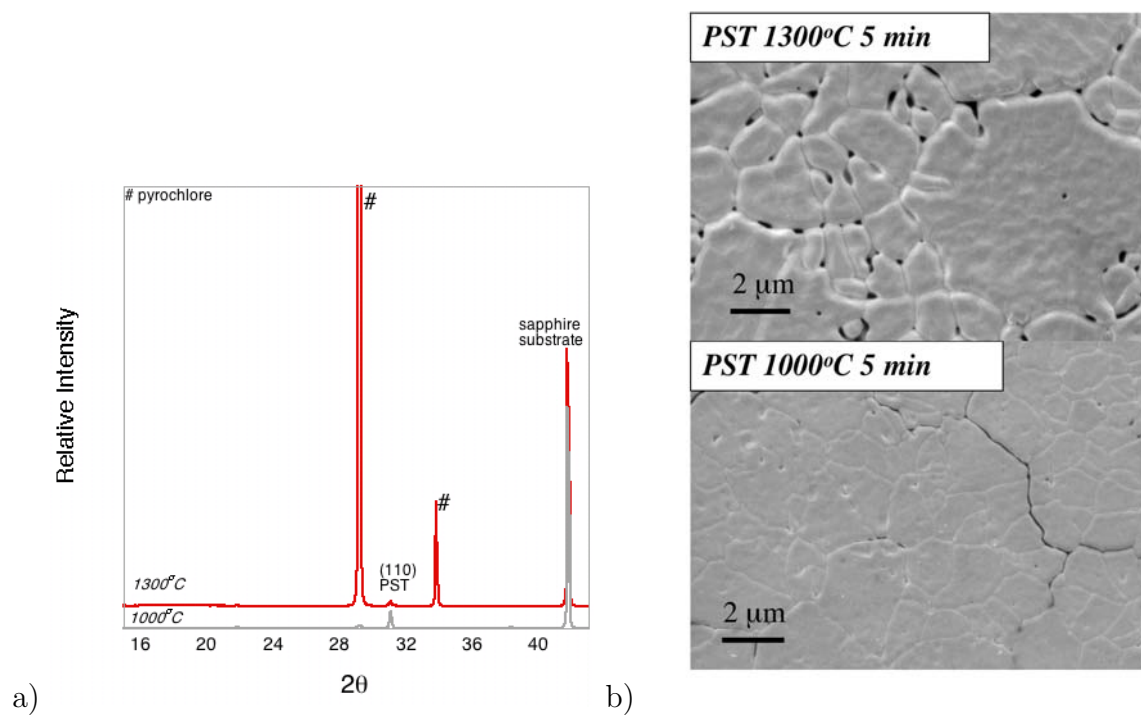
Figure 2.38: *High Temperature disorder in PST a) X-ray diffraction for films on sapphire substrates annealed at 1000 and 1300° C for 5 minutes, and b) SEM microstructure*
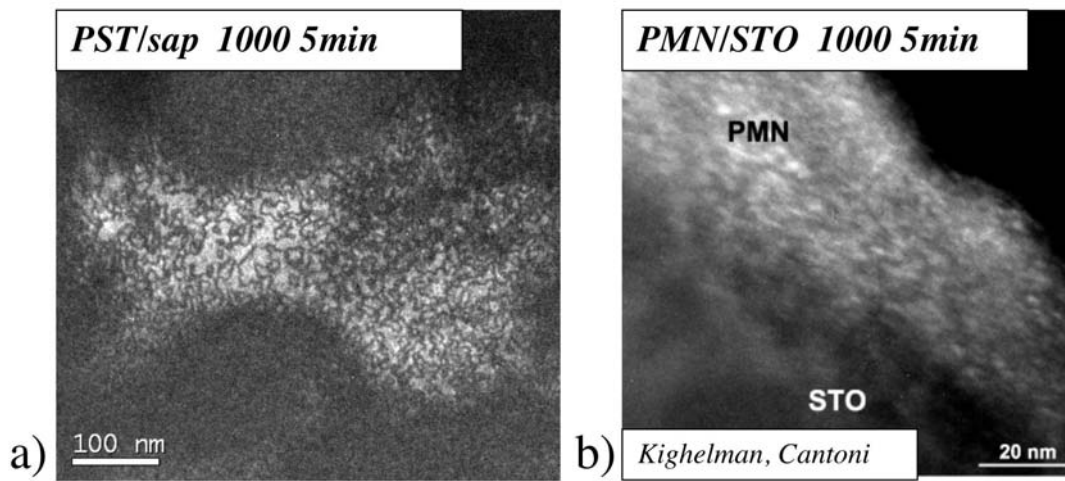
Figure 2.39: *High Temperature disorder in a) PST films on sapphire substrate annealed at 1000º C for 5 minutes versus b) PMN films on STO substrate annealed at 1000º C for 5minutes (Dr. Kighelman [4]); TEM ordered regions observation by Dr. Su and Dr. Cantoni*

2.3.6   Experimental Results: Analysis in Terms of Stated Processing Challenges (section 2.1.3.1)

The first challenge to produce a stable, repeatable solution chemistry with proper stoichiometry was accomplished by building on the synthesis procedure in reference [22]. It was found that dehydration of the scandium acetate hydrate precursor with acetic acid anhydride, followed by a reaction with the solvent 2-MOE resulted in a modified scandium precursor which easily combined with tantalum ethoxide to form a stable, stoichiometric "B" site complex. The reaction of lead acetate with the "B" site complex, followed by suitable annealing conditions resulted in perovskite phase PST films and sol-gel derived powders.

In terms of optimization of the processing conditions, it was found that excess lead concentrations greater than 20% were necessary to compensate lead loss during annealing,

and to avoid a surface nucleated pyrochlore phase. In addition, the commonly cited "*Thin* Layer" annealing procedure where each deposited layer is fired to the annealing temperature was found *not* to be necessary. The "*Thick* Layer" annealing procedure was used to fabricate films up to 2 microns in thickness. An annealing temperature of 700°C was found to be the optimum temperature for the fabrication of disordered thin films, as higher temperatures up to 1000°C resulted in significant degrees of ordering, and disordered films produced at temperatures near 1300°C possessed large amounts of pyrochlore phase and surface degradation. The dielectric properties of the films improved upon annealing time at 700°C from 1 minute to 20 minutes, however after 30 minutes at 700°C the films showed a degradation of properties.

The microstructure and grain size of the films were found to be impacted by the substrate, seed layers and on the annealing temperature. Epitaxial films were produced on STO (100), STO (111), and MgO (100) substrates. A seed layer of $PbTiO_3$ on Pt/Si substrates was found to increase the grain size of 300 nm PST films annealed at 700°C for 1 minute from 140 to 325 nm, while increasing the degree of (111) orientation as compared to bare Pt/Si substrates. In addition, the grain size was found to increase up to 500 nm for PST films on Pt/Si substrates annealed at 800°C, while annealing times from 1 to 20 minutes had no effect. The stress in the films was seen to be dominated by thermal expansion differences between the film and substrate as was verified for 1) Pt/Si substrates by measurements of the wafer bending indicating the presence of tensile stress, and 2) by glazing angle X-ray measurements for PST on MgO confirming the compressive nature of the stress.

The ordering of PST thin films was observed on a number of substrate systems. In the Pt/Si, system ordering was observed starting at temperatures as low as 750°C with an ordering degree S=0.19, increasing to a ordered degree of S=0.22 at 800°C for 20 minutes. Higher temperatures led to the degradation of the film/electrode interface and were not possible with the Pt/Si substrate system. To achieve higher levels of ordering,

it was necessary to use single crystal substrates *without* bottom electrodes. By long time annealing with a controlled atmosphere, ordering degrees up to S=0.91 at temperature of 850°C for 35 hours were achieved for PST films on sapphire substrates. The absence of a bottom electrode necessitates special techniques for dielectric property measurements which will be discussed in the following chapter.

The main objective of the processing work, which was to fabricate *both* ordered and disordered PST thin films on common substrates in order to compare their dielectric response was successfully achieved. The details of the dielectric measurements and comparison of the long range ordered state in thin film and bulk as compared with the disordered state will be presented in the following chapter.

Chapter 3

Dielectric Measurements and

Analysis of PST Thin Films

3.1 Dielectric Fundamentals

3.1.1 Polarization and Dielectric Constant

When an electric field E (V/m) is applied to an insulating material, a electric dipole per unit volume is induced, which is known as the dielectric polarization P (C/m^2) and can be expressed as [116]:

$$P_i = \chi_{ij} E_j \tag{3.1}$$

where χ_{ij} (F/m) is the dielectric susceptibility. The surface charge density is defined by the dielectric displacement D$_i$ (C/m^2) yielding:

$$D_i = \epsilon_o E_i + P_i \tag{3.2}$$

where ϵ_o (8.85 X 10^{-12} F/m) is the permittivity of a vacuum. Finally with:

$$\epsilon = 1 + \chi \quad \text{and} \quad k = \frac{\epsilon}{\epsilon_o} \tag{3.3}$$

we have the polarization of the material in terms of the permittivity (ϵ), or dielectric constant (k) of the material expressed as:

$$P = (\epsilon - 1)E = (k\epsilon_o - 1)E \tag{3.4}$$

For materials with large permittivities (like ferroelectric relaxors) $\epsilon_r \gg \epsilon_o$, D=P. Although in general ϵ and χ are second rank tensor quantities, in this analysis with a cubic material in thin film form we will consider them as average material properties equalivent in all directions, and we will discuss the unit-less dielectric constant (k), as compared to the permittivity (F/m).

If we apply a time varying field to the material, we can introduce a complex dielectric constant to describe the time varying polarization of the material as:

$$k^* = k' - ik'' \tag{3.5}$$

where the ratio of the real (k') and imaginary (k") parts of the complex dielectric constant result in a measure of the energy dissipated in the charging process expressed as:

$$tan\delta = \frac{k''}{k'} \tag{3.6}$$

In this study the real part is termed the "dielectric constant" and the imaginary part the "loss" (expressed as k' tanδ).

3.1.2   Frequency Dependance of Polarization in Dielectrics

Polarization mechanisms in dielectrics include (P_e) electronic polarization which is present at very high frequencies (10^{15}Hz) in the ultraviolet optical range, (P_a) atomic polarization which is present in the infrared region (10^{12}-10^{13} Hz), (P_d) dipole polarization, often termed "orientational" polarization which is present in a broad frequency range from 0.1

to 10^{11} Hz, in addition to interfacial polarization (P_i), often termed "space charge" polarization which is often present at low frequencies near 10^{-3} Hz depending on conductivity of the sample [117]. The dipole polarization region is of particular interest, as it is the motion of domains in ferroelectrics and polar regions in relaxor's which result in a large extrinsic dielectric response. The lattice or high frequency response may be measured by optical techniques and will be discussed in the following chapter. For dielectrics with defect induced dipole moments, the dielectric properties of the material at a given temperature as a function of frequency in the dipolar region can be expressed by the Debye equations[118], [119]:

$$k' = k_\infty + \frac{k_s - k_\infty}{1 + \omega^2 \tau^2} \tag{3.7}$$

$$k'' = (k_s - k_\infty)(\frac{\omega\tau}{1 + \omega^2\tau^2}) \tag{3.8}$$

where k_∞ is the high frequency dielectric constant, k_s is the static or low frequency dielectric constant, ω is the frequency and τ is the relaxation time. In a material with a single relaxation time or very narrow distribution, a plot of k" versus k', typically reffered to as a Cole-Cole plot gives a semicircle where the arc crosses the real part of the dielectric constant axis (zero loss) at k_s and k_∞ respectively.

The relaxation in relaxor dielectric systems can be described by using a distribution of relaxation times, where the total dielectric response of the material is considered as a sum of responses of individual Debye relaxators over the continuous spectrum of their relaxation times as [120]:

$$k^*(\omega, T) = k_s(T) \int_0^\infty \frac{g(ln\tau\omega_o, T)}{1 - i\omega\tau} d(ln\tau) \tag{3.9}$$

with the normalizing condition:

$$\int_{-\infty}^\infty g(z, T)dz = 1 \quad \text{and} \quad k_s(T) = k'(w = 0, T) \tag{3.10}$$

where ω is the ac measurement frequency, τ is the relaxation time, T is the measuring temperature, and k_s is the static real dielectric permittivity at temperature T. This distribution of relaxation times represents the frequency and temperature dependance of permittity in relaxor systems as schematically depicted in figure 3.1. In part a) of figure 3.1 the temperature is held constant at T_1 while the frequency is reduced so that $\omega_2 < \omega_1$. At temperature T_1 the *response* time is *slower* than the measuring frequency so that not all of the relaxors may contribute to the dielectric response. When the measuring frequency is decreased to ω_2 at temperature T_1, this allows more of the relaxation time spectrum to contribute, resulting in an increase in the dielectric constant.

Figure 3.1b shows schematically the temperature response for the distribution of relaxation times. At high temperatures T_2 above the dielectric maximum, there is a narrow distribution of fast relaxor species whose *response* time is *faster* than the measuring frequency, so that no frequency dispersion is seen in the paraelectric region. At temperature T_3, near the dielectric maximum, the distribution broadens, whilst maintaining relation 3.10, resulting in the characteristic relaxor dispersion of the dielectric response.

3.1.3 Frequency Dependence of the Dielectric Maximum in Relaxors

The Völgel-Fulcher (VF) law is commonly used to describe the frequency dispersion of the dielectric maximum and can be written in the following way [50]:

$$\omega = \omega_o \exp -\left(\frac{U_a}{k_B(T_{max} - T_f)}\right) \tag{3.11}$$

where ω_o is a constant (Hz^{-1}), U_a is an activation energy (J), k_B is the Boltzmann constant (1.38 x 10^{-23}J/K), and T_f is the freezing temperature (K). A similar equation based on τ_{max} versus T was also shown to represent the broadening of the relaxation time spectrum, while resulting in similar values for fitted parameters [121]. The physical meaning of the VF relation has been a subject of debate with Viehland [50] suggesting
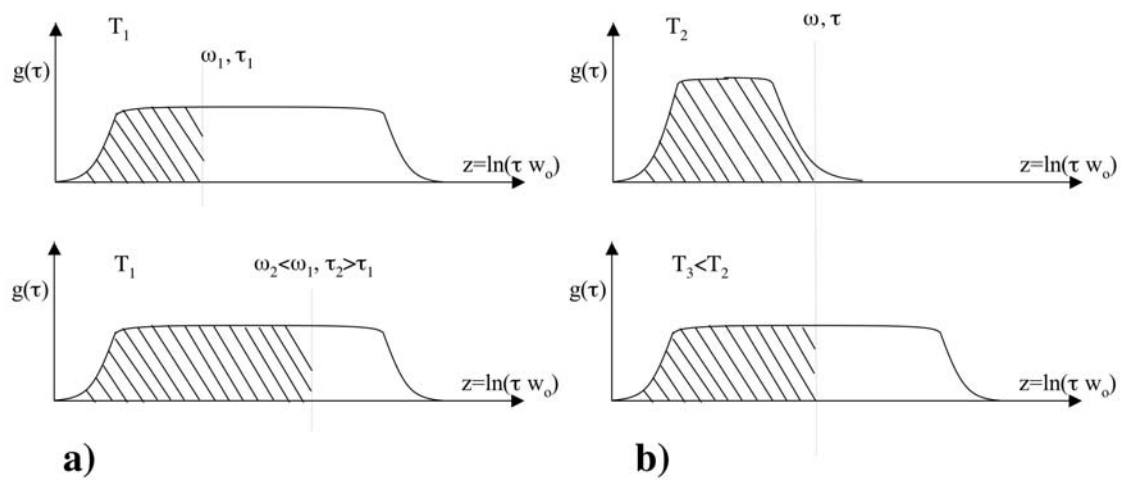
Figure 3.1: *g(z,t) function for frequency and temperature; dielectric constant is proportional to the shaded area (a)Temperature remains constant at T_1 while the frequency is reduced so that $\omega_2<\omega_1$ (b) Frequency remains constant while temperature is reduced so that $T_2<T_1$; In both cases a) and b) there is an increase in the shaded area and dielectric constant*

that at temperature T_f the spectrum becomes infinitely broad due to a critical variation of the activation energy. However, Tagantsev [121] showed that the VF relation can be used to describe a system with a maximum permittivity at T_f, followed by gradual broadening of the spectrum upon cooling, and does not necessarily imply "freezing" in the system. Regardless of the physical meaning of relation equation 3.11, it remains a tool for the quantitative description of relaxor properties. Typical values for fitting parameters from ceramic and single crystal specimens are $\omega_o \approx 10^{10}$ (Hz), $U_a/k_B \approx 171$ (K), and $T_f \approx 275$ (K) for PST, and $\omega_o \approx 10^{12}$ (Hz), $U_a/k_B \approx 910$ (K) and $T_f \approx 218$ (K) for PMN.

3.1.4 Effect of AC and DC Bias Field on the Dielectric Constant: Non-Linearity

A convient starting point for the analysis of non-linear properties is the LGD theory of ferroelectrics where the free energy of the material G1 can be expressed as a series expansion in terms of the polarization; in the cubic paraelectric phase resulting in [14]:

$$G_1 = \frac{1}{2}\alpha P^2 + \frac{1}{4}\beta P^4 + ... \tag{3.12}$$

where coefficients α and β are functions of temperature and only even powers of P are present due to the material symmetry. The polarization response to an applied electric field is obtained by taking the derivative of equation 3.12 with respect to polarization P to obtain:

$$E = \alpha P + \beta P^3 \text{ or } P = a_1 E + a_3 E^3 + ... \tag{3.13}$$

where a_1 and a_3 are function of temperature. Using this basis the non-linear components of permittivity can be found from experimental measurements of 1)Δk_{DC}=$k(E_{DC})$-$k(0)$; 2)Δk_{AC}=$k(E_{AC})$-$k(0)$; and 3) $P_{3\omega}(E_{AC})$ the resulting expressions for the small signal nonlinear response have been derived and can be expressed as [122]:

$$\Delta k_{dc} = -3\beta k_s^4 \epsilon_0^3 E_{DC}^2 \tag{3.14}$$

$$\Delta k_{ac} = -\frac{3}{4}\beta k_s^4 \epsilon_0^3 E_{AC}^2 \tag{3.15}$$

$$P_{3\omega} = \frac{1}{4}\beta k_s^4 \epsilon_0^4 E_{AC}^3 \tag{3.16}$$

where k_s is the linear static dielectric constant of the material, E_{AC} AC measuring field (kV/cm) level, and E_{DC} is applied DC bias field (kV/cm).

Within this framework, one can analyze the functional dependance of the dielectric constant versus applied field, specifically in the case of a cubic material $\Delta\,k \approx E^2$, and $P_{3\omega}(E_{AC}) \approx E^3$. However, the dielectric response in relaxor systems has been shown not to strictly conform to this approach. First of all, the phenomenological approach predicts the same sign of non-linearity for AC and DC field effects, and a quantitatively larger DC than AC field response. This is in contrast to experiments showing a decrease in permittivity with increasing applied DC field, and an *increase* in the dielectric response with increasing AC field [122], [51], [123], [21]; with the AC field response being greater than the DC response at the same field strength. Furthermore, there are a number of reports indicating a crossover, or deviation in the functional dependance of the non-linear dielectric response versus applied field at different temperatures above and below the dielectric maximum.

This crossover is unexpected based on the phenomological approach because relaxors have been shown to be macroscopically cubic/centrosymmteric both above and below the temperature of the dielectric maximum [34], and thus should display the functional dependance $\Delta\,k \approx E^2$ at all temperatures. It should be noted that some reports agree with the phenomigical prediction with a functional dependance of $\Delta\,k \approx E^2$ and $P_{3\omega}(E_{ac}) \approx E^3$ at all temperatures up to a relatively low field strength of 0.2 kV/cm, above which they observed a deviation from the expected dependance [124].

The negative observed linearity with DC bias has been explained by a coalescence of neighboring polar regions resulting in the diminishing of the total interface area which

contributes to the dielectric response. The AC field response, at least in the low field limit was thought due to the motion of interphase boundaries, therefore an increase in AC field resulted in the depinning of polar regions allowing more of them to contribute to the dielectric response [123]. This is seen schmetacially in figure 3.2 using the concept of a distribution of relaxation times due to a random distribution of pinning centers. At the same temperature and measuring frequency, an increase in the AC field is equilalent to a shift of the curve to lower relaxation time (faster response to applied field), while maintaining the normalizing condition in 3.10.
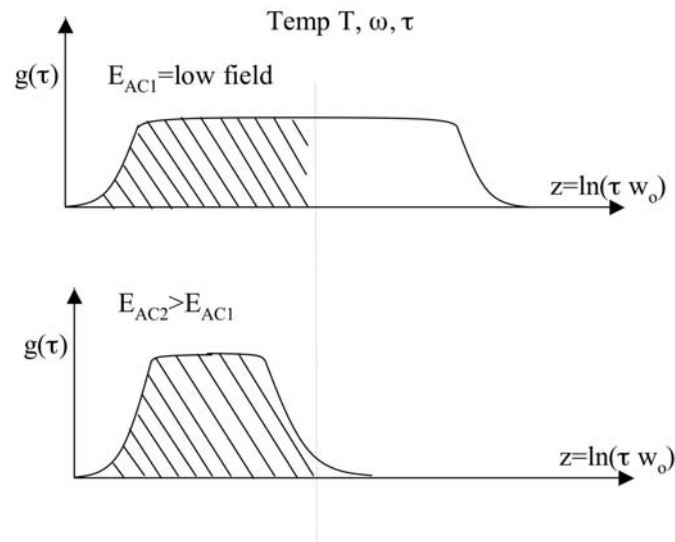
Figure 3.2: *g(z,t) function for Temperature T and frequency ω versus AC field strength; $E_{AC1}>E_{AC2}$; the shaded area corresponds to the dielectric constant, k*

The non-analytical behavior of the dielectric response and its "crossover" is a more difficult situation to analyze. It is instructive to begin with a normal ferroelectric such as PZT at temperatures below its phase transition in a non-centrosymmteric phase. An analysis of the non-linear dielectric permittivity and domain wall contributions at sub-switching fields showed that the functional dependance of the dielectic response may be *both* linear $k \approx E$ and quadratic $k \approx E^2$ depending on the sample history/aging and thus

the distribution of pinning centers which control domain wall motion [125].

In relaxor systems, no aging or hysteresis effects were observed after repeated measurements at a given temperature. This implies that the *temperature change* (in contrast to the electric field change in ferroelectrics) through the position of the dielectric maximum changes either 1) the distribution of pinning centers/defects, or 2) distribution of polar regions.

3.2 Dielectric and Polarization Measurements: Experimental

3.2.1 Parallel Plate Capacitor *"Out-of-Plane"*

3.2.1.1 Dielectric Measurements

Dielectric measurements were performed with a HP 4284A LCR meter over the frequency range 100 Hz to 1Mhz. The sample capacitance and loss tangent were measured as a function of temperature. For films measured *"Out-of-Plane"*, top electrodes were deposited with a nominal diameter of 600 microns, and the real part of the dielectric constant was calculated using:

$$k = \frac{C}{C_o} \ \ where \ \ C_o = \frac{\epsilon_o A}{t} \tag{3.17}$$

where C is the sample capacitance (F), ϵ_0 is the permittivity of free space, A is the electrode area (m^2) and t is the sample thickness (m).

Figure 3.3 indicates the parallel plate and planar capacitor sample geometries used for dielectric permittivity measurements. In the case of the film measured *"Out-of-Plane"*, the geometry of the electric field distribution is determined by the area under the top electrode and the dielectric constant values will vary on the uncertainty of the film thickness due to measurement and film roughness variations ($\approx$ 20nm) and the electrode area. For

films of 200 nm, the error in reported values are$\approx 10\%$, and decrease with increasing film thickness according to $\%error = \frac{\Delta t}{t}$. Note that this analysis does not take into account variations from electrode to electrode on film surface, and assumes a high degree of film homogeneity; it is imperative for the experimenter to measure multiple electrodes in different areas of the film in order to obtain a representative value.
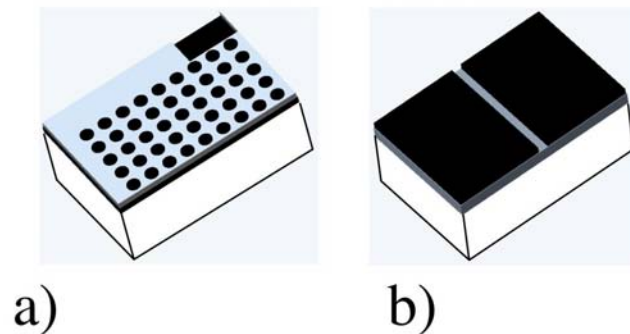
Figure 3.3: *(a)"Out-of-Plane" parallel plate capicator arrangement, and (b) "In-Plane" measurement geometry (two top electrodes separated by a photolithographically defined gap)*

3.2.1.2   Polarization Measurements

The large field polarization measurements were performed with a setup based on the standard Sawyer-Tower circuit using a triangular waveform and a nominal frequency of 1kHz. The harmonics of polarization were measured using a lockin amplifier. The AC driving field was applied to the samples from lockin and the voltage response for the harmonics was measured by using a resistor connected in series with the sample. The value of the resistor was chosen such that ωCR $\approx 10^{-2}$ so that the input voltage was completely applied to the sample. Details of these measurements are given in [5] and [103].

3.2.2 Planar Capacitor Structure *"In-Plane"*

3.2.2.1 Dielectric Measurements

Modeling of the planar capacitor structure shown in figure 3.3 involves an analysis of the electric field distribution between the ferroelectric layer, substrate and the air as depicted in figure 3.4. A conformal mapping techniques was used to seperate the measured capacitance across the gap into parallel capacitences of the individual layers given as [7]:

$$C_{meas} = C_1 + C_2 + C_3 \tag{3.18}$$

Electrodes and Air	$C_1 = w * \epsilon_o \frac{2}{\pi} ln(\frac{4l}{s})$
Film	$C_2 = \frac{w\epsilon_o(k_2 - k_3)}{s/h_2 + (4/\pi)ln2}$
Substrate	$C_3 = w * \epsilon_o(k_3 - 1)\frac{1}{\pi}ln(16\frac{h_3 - h_2}{\pi s})$

Table 3.1: *Partial capacitance components of equation 3.18 as described in reference[7]*

where in table 3.2.2.1, k_2 is the dielectric constant of the film, k_3 is the dielectric constant of the substrate, w is the width of the electrodes (m), l is the length of the electrode structure including gap (m), s is the gap width (10, 20 or 30 microns), h_2 is the film thickness, and h_3 is the thickness of the substrate. Under conditions that $h_2 < s \leq 10h_2$, $s \leq 0.25l$, $s \leq 0.5h_3$, $\frac{k_2}{k_3} > 100$ these equations provide accuray on the order of 1%. However the actual experimental accuracy in this case is similar to those encountered in the "out of plane" case, namely, uncertainty with the determination and or regularity/homogeneity of the gap width and the film thickness. The uncertainty associated with optical measurement and homogeneity of gaps is about +/- 1 microns which for a nominally 10 micron gap leads to an error of about 10%.

Microwave dielectric measurements were made using a microstrip resanotor employing the same sample geometry as low frequency measurements. The substrate/film/electrode stack capacitance was calculated from the resonant frequency, nominally 8.2 GHz, and
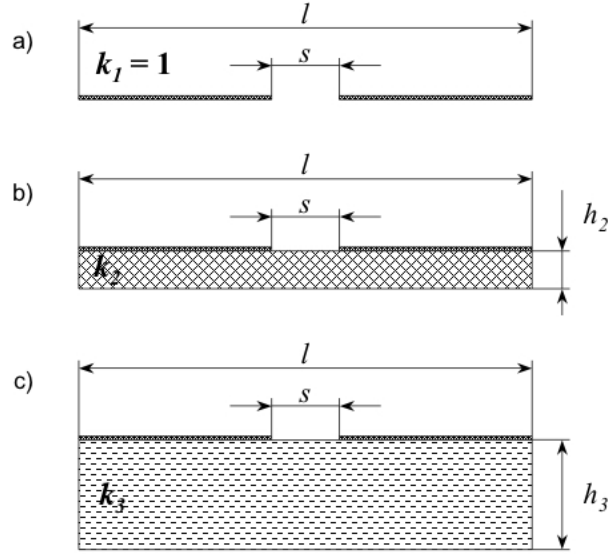
Figure 3.4: *Planar capacitor structure detail (a) Electrode and air geometry, (b) Film , (c) Substrate*

the loss tangent calculated from the width of the resonant frequency peak. Once the capacitance of the substrate/film/electrode structure was determined from the resonant frequency, the dielectric constant was calculated following the previously described procedure. For a detailed description the reader is referred to a recent review article by Tagantsev [32].

3.2.2.2 "In-Plane" Polarization Measurements

The "in-plane" polarization P has been calculated on the basis of the measured charge q by using the following equation:

$$P(E_{dc}) = \frac{1}{wh_2} \left[q - (C_1 + C_3)E_{dc}s \right], \tag{3.19}$$

where E_{dc} is the applied dc bias field. The equation 3.19 has been derived using Eqs. 3.2.2.1 and the assumption that $P \approx \varepsilon_0 k_2 E_{dc}$ and $q = (C_1 + C_2(k_2) + C_3) E_{dc}/s$.

3.3 *"Out-of-Plane"* Measurements

Relaxor like behavior with frequency dispersion of the dielectric constant was observed for all of the disordered films in this section. As a basis for comparison, properties will typically be presented in the frequency range from 100 Hz to 100 kHz under an AC measuring field of 1 kV/cm. The following paragraphs will briefly describe the basic features of the graphs including temperature of the dielectric maximum and its permittivity value at 1kHz, as well as the loss tangent values at 30°C (room temperature). As a basis of comparison, disordered ceramic (PST-D) samples typically have loss tangent values less than 0.3% at 30°C in the paraelectric region. Therefore, film loss tangent values in the paraelectric region may be taken as a measure of the intrinsic film/electrode stack quality since elevated values indicate conduction due to processing induced defects.

3.3.1 Pt/Si Substrates

Figure 3.5 displays the (a) dielectric constant, loss tangent and (b) the loss as a function of temperature from 100°C to -100°C and frequencies from 100Hz to 100kHz for a 1.4 micron PST film prepared from a 30% excess lead solution on a Pt/Si substrate annealed at 700°C for 20 minutes. The sample shows a maximum dielectric constant of 3520 at 2°C and a room temperature loss tangent of 0.8% at 1 kHz. The real and imaginary parts of the dielectric permittivity display relaxor behavior with the real part decreasing with increasing measuring frequency and the imaginary part increasing with increasing measuring frequency. Above 50°C the frequency dispersion in the real and imaginary permittivity disappears, and the deviation from the Curie-Weiss law can be seen in a plot of 1/k versus T (see figure 3.5c). Higher frequencies have higher y intercepts and thus a lower k, with an estimated high temperature Curie Weiss constant of 1.9E5, and an extrapolated curie temperature of 0°C obtained from fits of the linear region.

a)

b)

c)
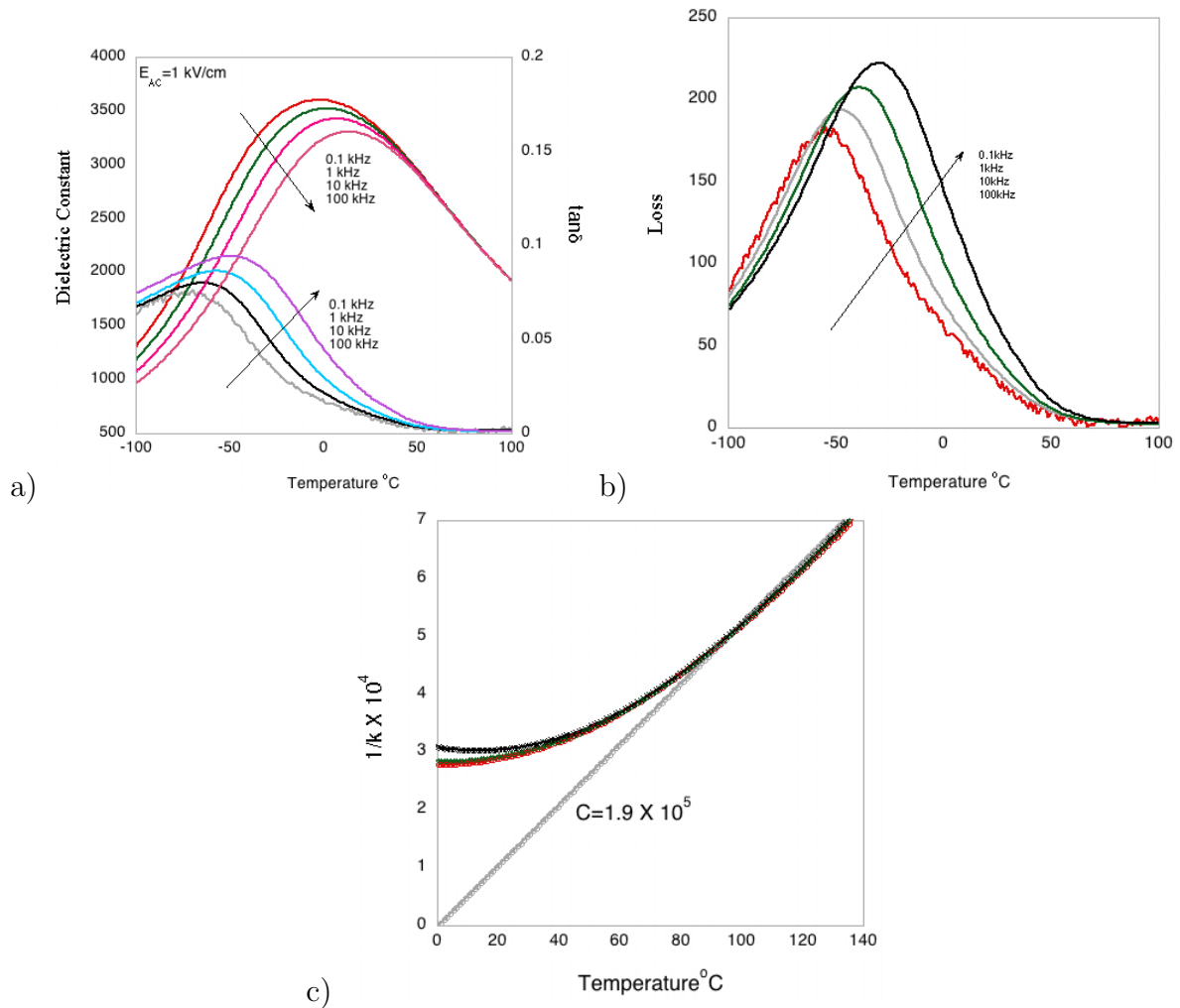
Figure 3.5: *1.4 micron thick PST film made from 30% excess lead solution on Pt/Si substrates annealed at 700°C for 20 minutes (a) Dielectric constant and loss tangent versus temperature, (b) loss versus temperature, (c) 1/dielectric constant versus temperature with Curie-Weiss constant from high temperature region ≈1.9 X 10⁵*

3.3.2　Pt/Ir/MgO Substrates

The dielectric response of 650 nm PST deposited from a solution containing 30%Pb on a Pt/Ir/MgO substrate annealed at 700°C for 1 minute is shown in figure 3.6. The sample displays a maximum dielectric constant of 1470 at -28°C and 1kHz, with a relatively high loss tangent of 1.3% in the room temperature paraelectric phase. The loss tangent

increases and exhibits frequency dispersion at higher measuring temperatures, in addition to slight frequency dispersion of the dielectric constant in the paraelectric region. As the film was phase pure with dense microstructure as shown in the experimental section, the relatively high loss tangent can be attributed to the sputtered Ir/Pt electrode stack and interface with the PST film. The reduced value of the dielectric constant in this sample as compared to samples produced on Pt/Si substrates under similar conditions is not understood. This is *not* thought to be due to issues such as film quality and microstructure given the results on these topics presented in section 2.3.4.1(page 80), but may be due to a passive layer effect or possible mechanical constraints.
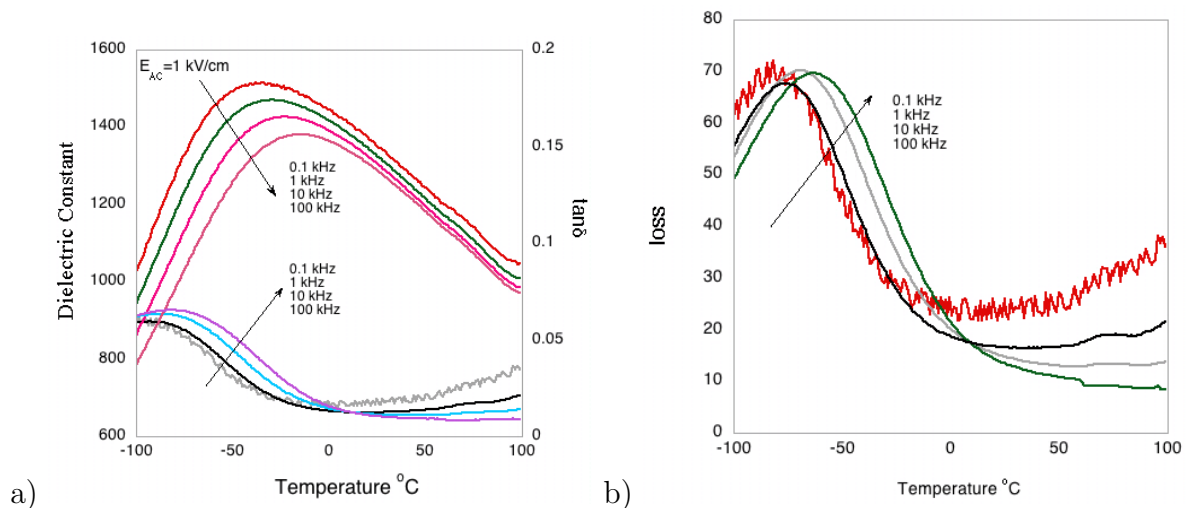
Figure 3.6: *650 nm PST films made from 30% excess lead solutions on Pt/Ir/(100)MgO substrate annealed at 700°C for 1 minute (a) Dielectric constant and loss tangent versus temperature, and (b) loss versus temperature*

3.3.3 STO Substrates

Figure 3.7 shows the dielectric constant and loss tangent as a function of temperature from 100 to -100°C from frequencies 0.1 to 100 kHz for 650 nm epitaxial PST films made from 30% excess lead solutions on STO (111) and (100) substrates annealed at 700°C

for 1 minute. The film on STO(100) displayed a 22% increase in the dielectric constant (within the error of measurement) with a maximum value of 1270 at -18°C and 1 kHz as compared to 1044 at -16°C for the (111) oriented sample. The room temperature loss tangent values at 1kHz are similar at 0.9% for (100) and 0.7% for the (111) oriented specimens reflecting relatively high film quality. The noise in the loss and the dielectric constant in the low frequency range of 100Hz has been observed primarily in samples deposited on doped STO substrates and could be due to an interfacial phenomenon as this behavior is not typically seen in films on traditional Pt/Si substrates. Although this issue remains unresolved, this does not impact the main ideas discussed herein.

The question remains as to 1) why do films with the same thickness, processing and measuring conditions display values of dielectric constant differing by more that 20%, and 2) why are the values of the dielectric constant in both specimens relatively low compared to the expected permittivity maximum values near 2000 for similar thickness specimens on Pt/Si and other substrates?

1) The apparent orientation difference exhibited in figure 3.7 between (100) and (111) epitaxial films may be attributed to changes in the rotation of polarization in the two samples. It is known that polar regions result from local Pb displacements creating a local polarization in the (111) direction (in the case of PMN [34]). In the case of PST on STO, the film is under a compressive stress due to thermal expansion mistmatch and it may be expected that the equivalent directions of the (111) polarization may be forced out of the plane in the direction of the measuring field. In contrast, the (100) epitaxial film has polar regions oriented at a 45° angle from the applied field, and there should be no re-orientation due to compressive stress. Since the polar region contribution is proportional to $cos^2\theta$ of the angle between the direction of polarization and the applied field, the (100) oriented sample would be expected to display a higher dielectric response[126].

2) An examination of the CV and PE curves for PST on Nb doped STO substrates reveals an asymmetry in the response due to the sandwich structure of a metal/ferroelectric/n-

type doped semiconductor. As a positive bias (positive terminal at the metal surface in ”Out-of-Plane” configuration) is applied to the sample we see an increase the capacitance, charge and thus the dielectric constant, and loss tangent values which reach a maximum at 25 kV/cm before decreasing and exhibiting a hysteric response as the field is decreased to zero. The internal bias thus applied to our ferroelectric material is estimated from the displacement of the CV curve to be approximately 25kV/cm, which can reduce our values of measured dielectric response by up to 20% (see non-linear DC measurement section) at temperatures near the dielectric maximum. A reduction of this magnitude combined with the 10% measurement uncertainty can account for the unusually low values of dielectric response in this work as well as those usually reported for doped STO substrates.

3.3.4 Thickness Dependance of PST on Pt/Si Substrates, the ”Passive Layer Scenario”

A blocking or passive layer has often been cited as being one of the factors responsible for the reduced permittivity of thin film relaxors. In order to investigate this phenomena in PST films, samples were prepared by varying the thickness from 300 nm to 2 microns on Pt/Si substrates from a solution of 20% excess Pb and annealed at 700°C for 1 minute. Figure 3.8 displays the X-ray spectra and SEM determined microstructure of characteristic films. No pyrochlore secondary phase was detected even after multiple annealings, and the films exhibited a global (111) orientation preferance, although an increase of (100) reflections was observed with increasing film thickness. A columnar microstructure with a *thickness independant grain size* distribution of 150 to 300 nm was observed.

Figure 3.9 displays the dielectric constant at 1kHz and 1kV/cm measuring field as a function of thickness measured out of plane on Pt/Si substrates. The temperature of the dielectric maximum is constant as a function of film thickness with a value of -17°C and all films displayed frequency dispersion characteristic of relaxor behavior. The difference between the dielectric constant of the 1.3 micron and 2 micron films were within
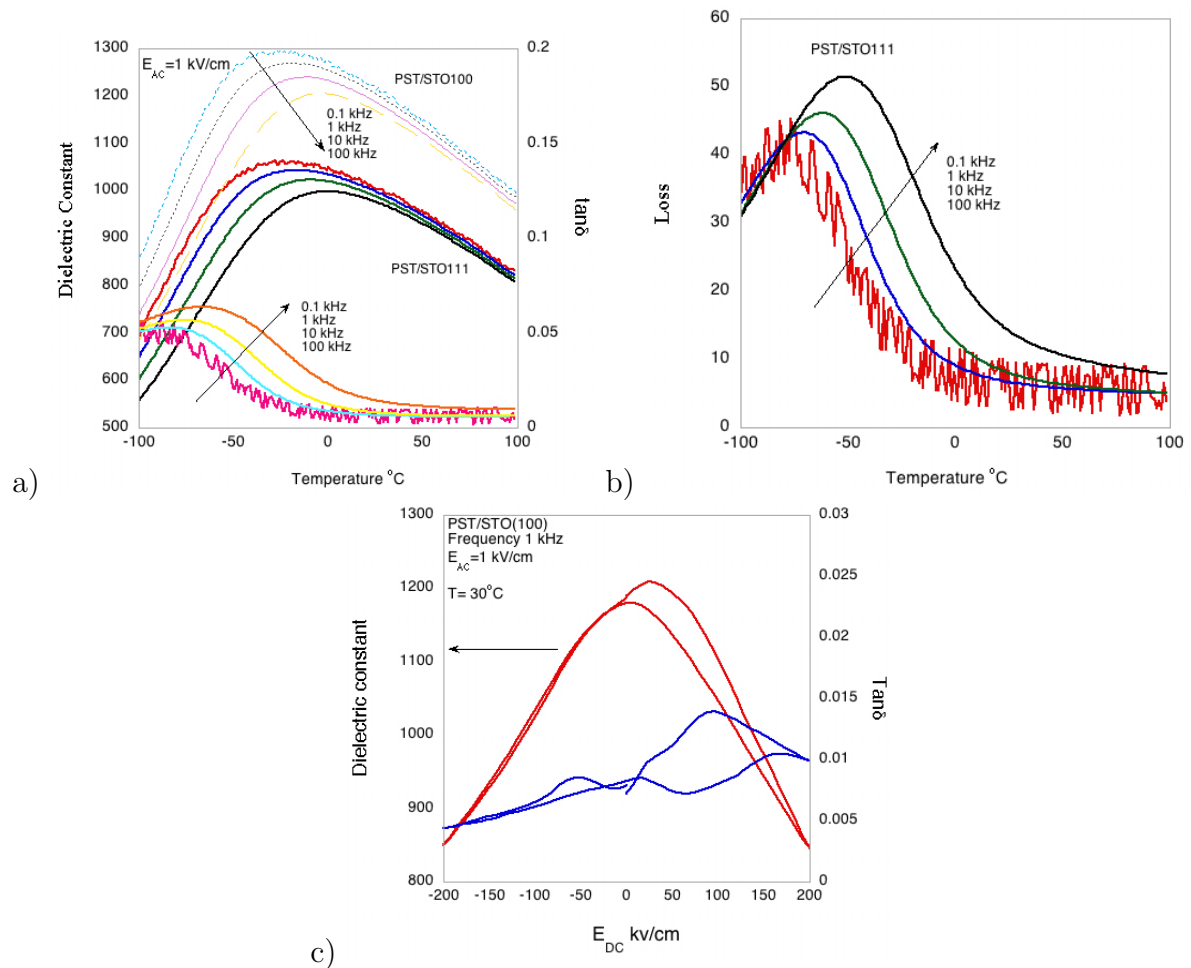
Figure 3.7: *650 nm PST film made from 30% excess lead solutions on STO (111) and (100), annealed 700° C for 20 minutes (a) Dielectric constant and loss tangent of PST on STO(100) and STO(111) versus temperature, (b) Loss versus temperature for PST on STO(111), (c) Dielectric constant and loss tangent of PST/STO(100) versus DC bias field at 1 kHz and 30° C temperature with E_{AC}=1 kV/cm*
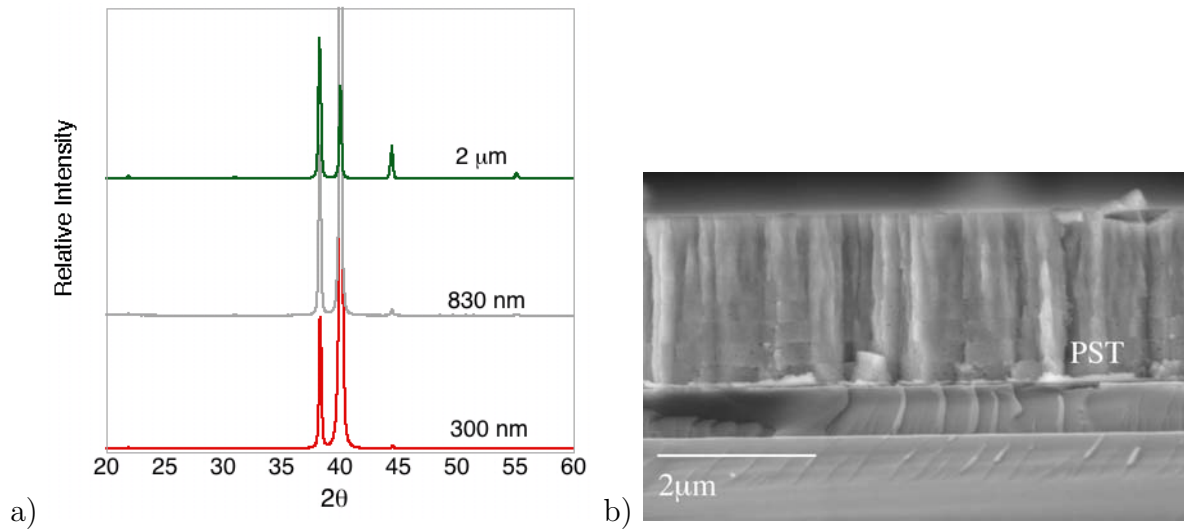
Figure 3.8: *(a)X-ray diffraction spectrum and (b) SEM determined cross section microstructure for disordered PST film made from 20% excess lead on Pt/Si substrates annealed at 700° C for 1 minute*

the measurement error and assumed equal in the following analysis. It is obvious that there is an increase in dielectric constant with increasing thickness, but does this increase conform with the passive layer scenario? Figure 3.10 and equations (3.20), (3.21), and (3.22) describe the experimental surface/passive layer scenario; where a plot of $1/\epsilon$ versus $1/d$ gives a straight line with an intercept of $1/\epsilon_f$, and a slope proportional to the difference in the inverse permittvities of the film and surface layer. For a temperature independent passive layer the slope from equation 3.22 may be plotted versus the intercept, resulting in a linear relation which directly gives the thickness and permittivity of the passive layer. The theoretical curves and graphical procedure are presented in figure 3.11.

$$\frac{1}{C_{tot}} = \frac{1}{C_1} + \frac{1}{C_2} \tag{3.20}$$

where C is the total measured capacitance and C_1 and C_2 are capacitances of the film and passive layer responses connected in series.
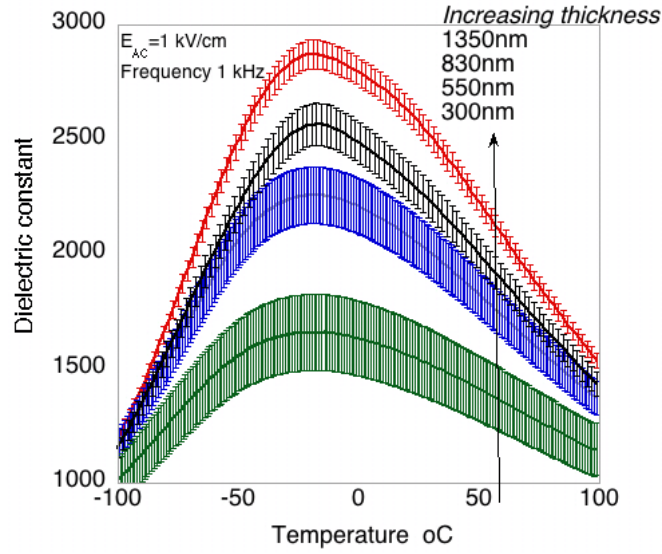
Figure 3.9: *Dielectric constant versus temperature at 1kHz and E=1kV/cm AC for PST/Pt/Si films annealed at 700°C for 1 minute with thicknesses from 300 to 1350 nm including estimate of error*
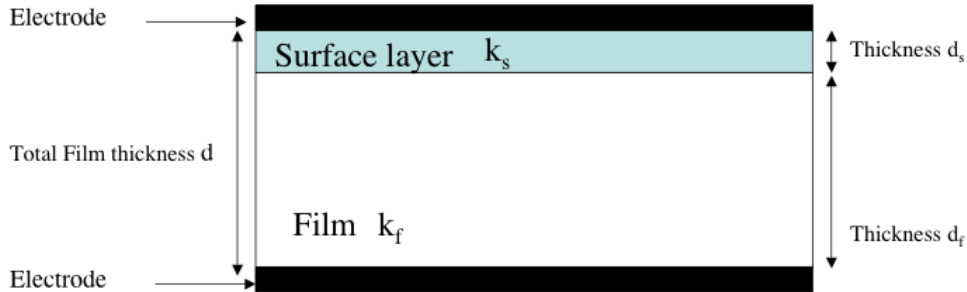
Figure 3.10: *passive layer scenario*

$$\frac{d}{k} = \frac{d_f}{k_f} + \frac{d_s}{k_s} \tag{3.21}$$

$$\frac{1}{k} = \frac{1}{k_f} + (\frac{1}{k_s} - \frac{1}{k_f}) * \frac{d_s}{d} \tag{3.22}$$

where k is the measured dielectric constant, k_s and k_f are the dielectric constant's of the surface layer and film respectively, d is the total measured thickness of the film

plus the surface layer, d_s and d_f are the thicknesses of the surface layer and the film respectively.
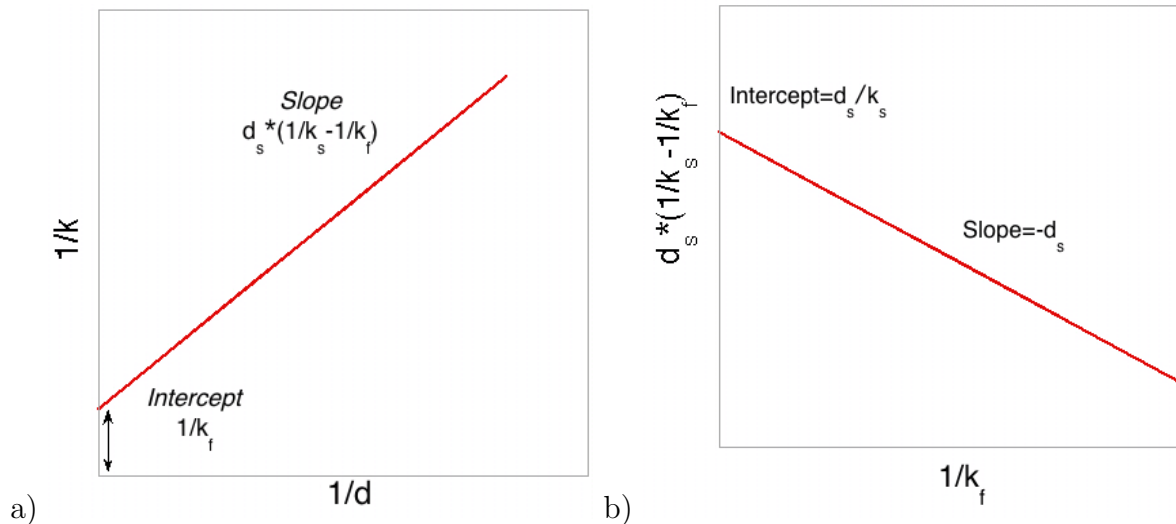
Figure 3.11: *Graphical procedure for determination of the temperature independent passive layer parameters from measurements of dielectric constant versus temperature and thickness (a) reciprocal dielectric constant versus reciprocal total thickness, (b) slope versus intercept of graph (3.11a) determined at different temperatures*

Figure 3.12 displays the measured inverse dielectric constant versus the inverse of film thickness from -100°C to 0°C , and from 0 to +100°C at 1kHz showing a linear dependance. The following qualitative features may be observed; upon heating from -100°C towards the phase transition the intercept decreases, while the slope increases as a result of the increasing film permittivity. With continued heating above the phase transition, the intercept increases and the slope decreases as a result of the decreasing film permittivity upon passing into the paraelectric region. A plot of the least squares determined slopes and intercepts is displayed in figure 3.12. A separate plot of these slope and intercepts at different temperatures results in figure 3.13 which displays a linear dependance from -100°C towards the phase transition where a strong deviation is observed. This implies our assumption of a temperature independent passive layer is not exactly valid.
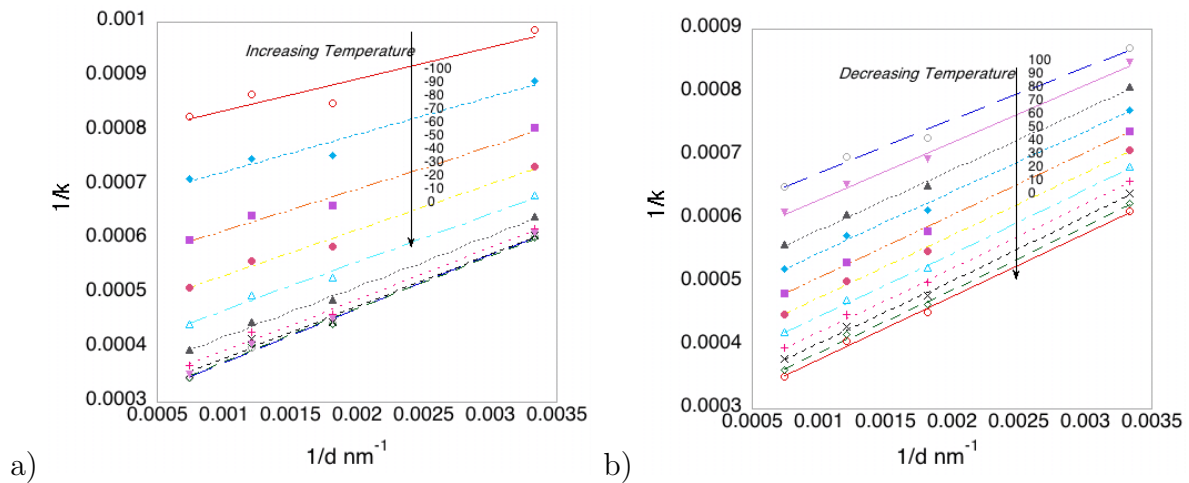
Figure 3.12: *(a) 1/k versus 1/d (nm^{-1}) from -100° C to 0° C at 1 kHz, and (b) 1/k versus 1/d (nm^{-1}) from 0° C to +100° C*
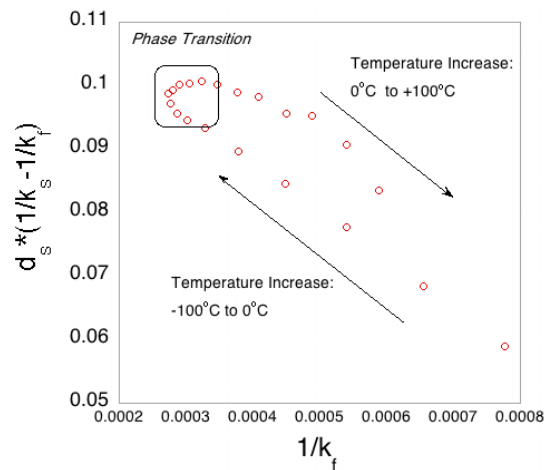
Figure 3.13: *slope versus intercept of graph 3.12 determined at different temperatures, with resulting model parameters of k_s=630, and d_s=74 nm*

However, one can still extract useful information from the temperature points above and below the phase transition which are asymmetrically distributed because of the -17°C phase transition. A fit of the low temperature data up to the phase transition in a linear fashion results in values of an approximately 70 nm passive layer with a dielectric constant of 630. These values most likely represent the effects of a lead deficient

surface layer with reduced permittivity which retains its temperature dependent dielectric response. Figure3.14 displays the results of the measured thickness dependance versus the calculated film dielectric constant using the experimentally determined passive layer parameters predicting a maximum dielectric constant value of 3500 for the film. In films above 2 microns the total measured capacitance due to the passive layer in series with the ferroelectric film will become indistinguishable and it can be assumed that true film values are being obtained.
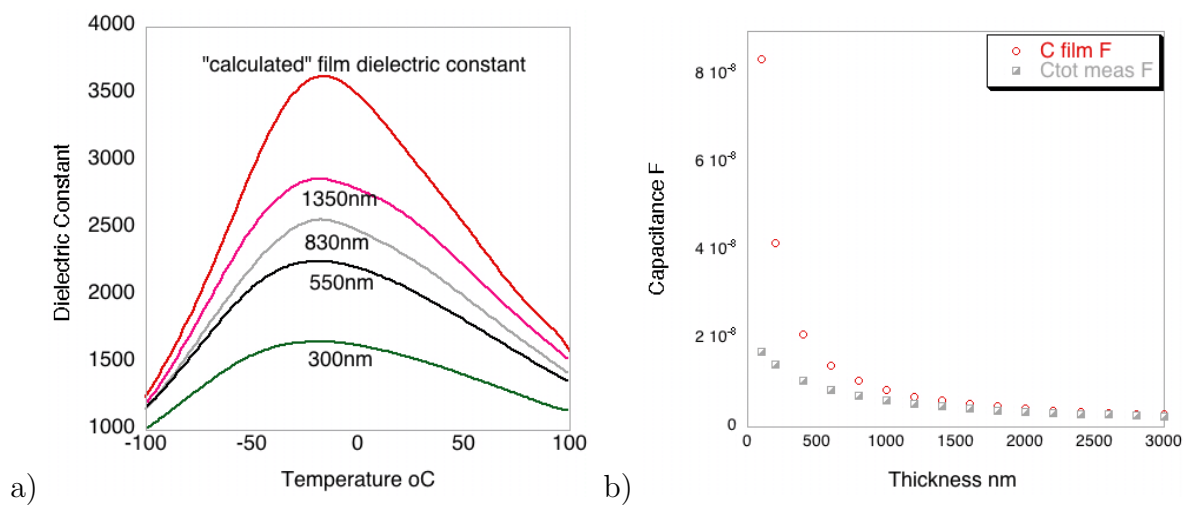
Figure 3.14: *(a) Calculated film dielectric constant using equation (3.21) with model parameters determined in figure (3.13), versus dielectric measurements as a function of thickness and (b) film capacitance versus measured total capacitance using model parameters and equation (3.20) indicating that above 2000 nm, there is no effect of the ”passive” layer*

However in traditional ferroelectrics such as PZT the theoretical passive layer is due to changes in the polarization response near a free surface and the subsequent *hardness* of the lattice[30], so are we investigating the same physical phenomena as has been theoretically proposed? The answer is no, as our data is not extensive enough in the low thickness range (below 300 nm due to difficulty in obtaining thin sol-gel derived films), and the obtained values point to processing induced defects rather than a true intrinsic passive

layer inherent in all thin film ferroelectrics. Nonetheless, the extracted values can still be extremely useful for examination of low dielectric response in relaxors, and point out that at film thickness over 2 to 3 micron's even a low dielectric constant surface layer induced by processing may not drastically deteriorate the measured film dielectric response.

3.4 "*In-Plane*" Measurements

Dielectric Measurements "in the plane of the film" provide important information on the behavior of the film without a bottom electrode and allow an additional examination of the passive layer scenario for dielectric response reduction. In the "*In-Plane*" configuration, any surface layer present is now connected in *parallel* with the film capacitance which may even result in an *increase* in the measured total capacitance (if the passive layer formed is not at the expense of the ferroelectric thickness). In the following sections the dielectric response is presented for disordered PST films fabricated from 30% excess lead solutions on MgO and Sapphire substrates annealed at 700°C . Low frequency measurements in the Hz range suffer from high noise levels due to the low capacitance of the "in plane" samples (often less than 0.3 pF) resulting in high impedance values, and a large error in capacitance; results below 10 kHz are not presented.

3.4.1 MgO Substrates

The dielectric constant, loss tangent and imaginary part of the loss are presented in figure (3.15a) for a 540 nm thick PST film made from a solution containing 30% excess lead and annealed at 700°C for 1 minute. The dielectric maximum for this sample was 1392 at -12°C and 100 kHz with a room temperature loss tangent of 0.6%. The sample exhibited frequency dispersion typical for relaxors in the dielectric constant and in the loss (figure 3.15b).

Of particular interest is the examination of the thickness dependance of the dielectric
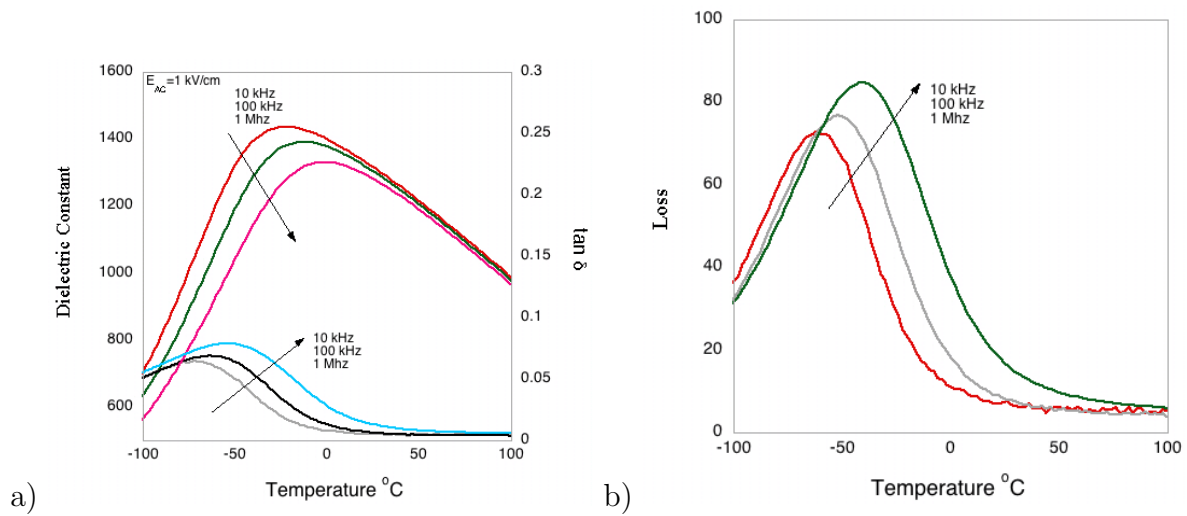
Figure 3.15: *540 nm PST film made from 30% excess lead solutions annealed at 700° C for 1 minute on MgO substrate measured "In-Plane" (a) Dielectric constant and loss tangent as a function of temperature and frequency, (b) Loss as a function of temperature and frequency*

constant as measured *"In-Plane"* of the film, as the effects of any passive layer should be negligible. Figure (3.16a) shows the dielectric constant versus temperature for PST films on MgO with thicknesses of 540 nm and 950 nm. As seen in the figure, the dielectric constant as measured at the same frequency, and electric field are the *same* for both thicknesses within the range of error. This demonstrates, as clearly expected that there is no thicknesses dependance for the dielectric constant when measured in the "In-Plane" configuration.

The question then arises, "How does the dielectric constant measured in the *"In-Plane"* and the *"Out-of-Plane"* configuration compare for films processed on the same substrates under similar conditions?" Figure (3.16b) displays the dielectric constant versus temperature for 950 nm PST film on MgO measured "In-Plane" and a 650 nm PST film on Pt/Ir/MgO measured "Out-of-Plane" under the same measuring conditions displaying *essentially the same values* within the range of error. This measurement provides strong evidence against the "passive" layer scenario, since a low dielectric constant layer between

film and electrode interface would be expected to reduce the "Out-of-Plane" dielectric response, and not affect the *"In-Plane"* response. It is stressed that in *very* thin films (below 100 nm), the effects of such a passive layer may be apparent, especially in the *"Out-of-Plane"* measurement configuration. However, for films in the micron thickness level, a passive layer scenario *does not* account for an order of magnitude reduction in the dielectric constant for thin films as compared to ceramics.
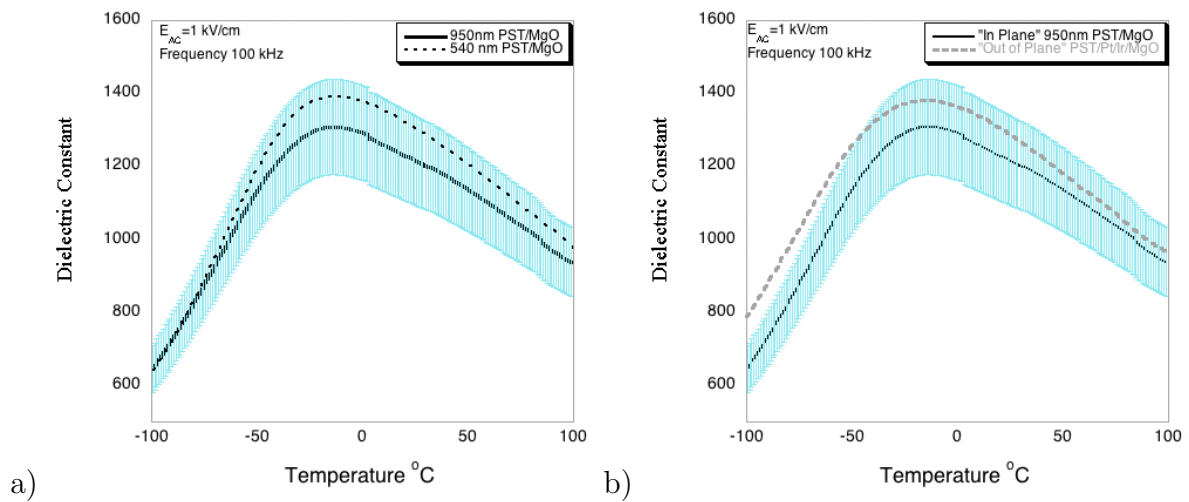
Figure 3.16: *(a) Thickness dependance "In-Plane", Dielectric constant versus temperature for 540 and 950 nm PST film on MgO substrate (b) 950 nm PST/MgO "In-Plane" compared to 650 nm PST/Pt/Ir/MgO "Out-of-Plane"; measurements performed at 100 kHz and $E_{AC}=1$ kV/cm, error bars indicate +/- 10% of measured values for 950 nm PST/MgO "In-Plane"*

3.4.2 Sapphire Substrates

Figure 3.17 displays the dielectric response of a 650 nm film of disordered PST on a sapphire substrate annealed at 700°C for 20 minutes. The dielectric maximum of 2110 occurs at 10°C at 100 kHz and a 1 kV/cm field level, with a paraelectric phase loss tangent at 50°C of 1.2%. Differences are seen as to the position of the dielectric maximum of films

on MgO or sapphire substrates, with a higher temperature of the dielectric maximum occurring for films on sapphire.
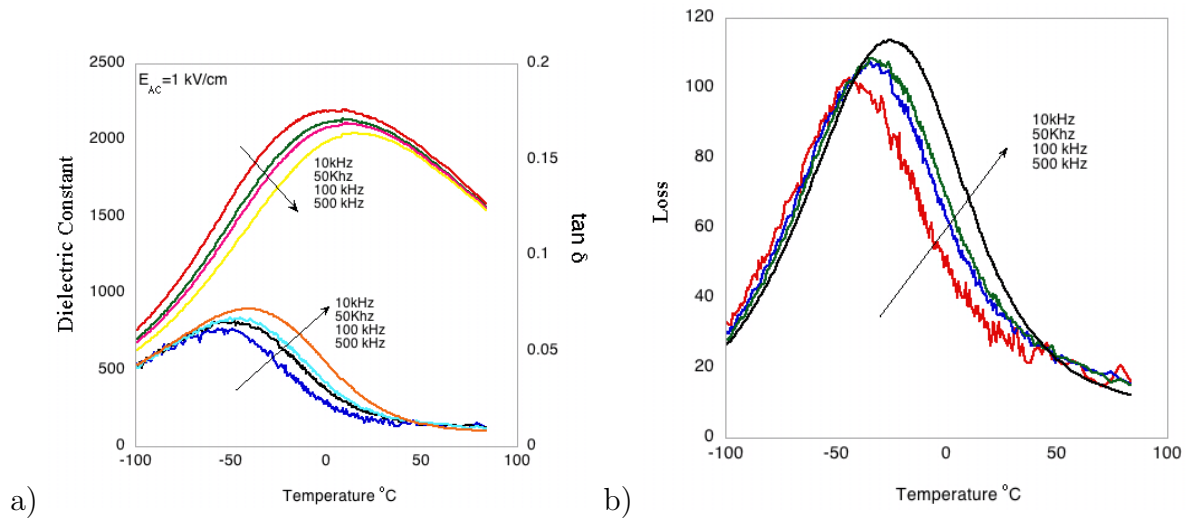
Figure 3.17: *650nm PST film on sapphire substrate annealed at 700°C for 20 minutes (a)Dielectric constant versus temperature and frequency, (b) loss versus temperature and frequency*

3.5 Ordered Thin Films

In this section we will examine the effect of "B" site chemical ordering on the dielectric response of PST thin films measured both in the *"Out-of-Plane* and *"In-Plane"* configurations.

3.5.1 Pt/Si Substrates *"Out of Plane"*

The mechanism of ordering which requires elevated temperature annealing for long times is particularly unsuitable for the processing of thin films on bottom electrodes such as platinum. It was possible however, to achieve small degrees of ordering at temperatures between 750 and 800°C with 20 minute annealing times as evidenced by an increase in

the ordering paramater S=0.2 presented in the experimental section. As an increase in ordering in bulk samples leads to normal ferroelectric behavior with an absence of the shift of the dielectric maximum, and the appearance of ferroelectric hysteresis at temperatures below the dielectric maximum. The thin film polarization response was also verified and presented in figure 3.19.
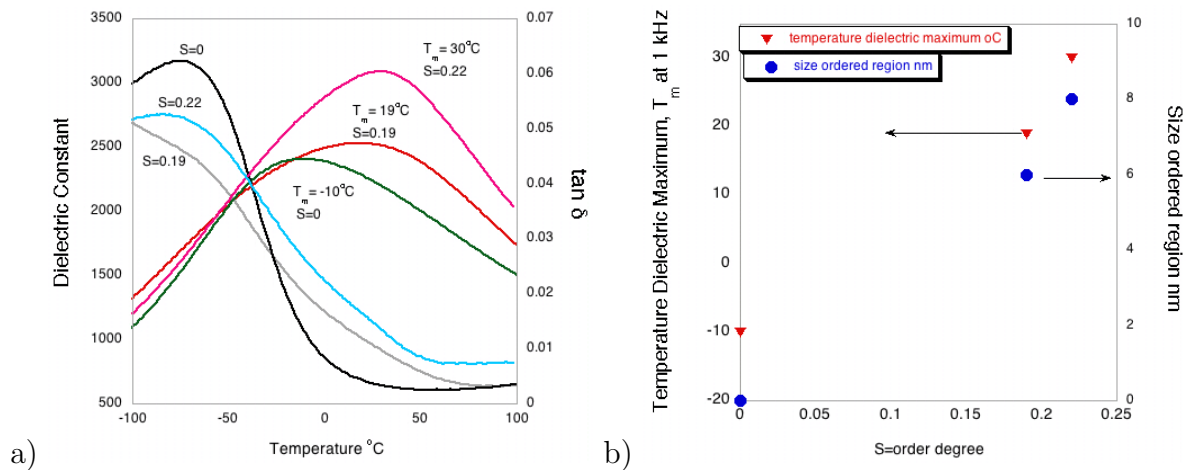
Figure 3.18: *500nm PST film on Pt/Si substrates with increasing degrees of order due to higher annealing temperatures from 700 (S=0), 750 (S=0.19) to 800° C (S=0.22) for 20 minutes (a) Dielectric constant versus temperature at 1 kHz and E_{AC}=1 kV/cm and (b) Temperature of the dielectric maximum at 1 kHz and estimated size of the ordered regions versus the degree of order, S*

It was observed that an increase in the annealing temperature increased the degree of order, the size of the ordered regions, the *temperature* of the dielectric maximum and the *value* of the dielectric maximum. However, coupled to the ordering are accompanying microstructural changes which make it difficult to propose exact cause and effect relationships. For instance, the grain size increases from approximately 300 nm to over 500 nm with an increase in temperature from 700 to 800°C , along with the elimination of "cracks" or grouping of grains due to higher diffusion at elevated temperatures. One can pose the question as to whether the shift in the temperature from -10 to 30°C of the

dielectric maximum, and the increase in the values of the dielectric maximum from 2400 to 3088 at 1 kHz for samples annealed at 700 and 800°C is due to "B" site ordering or to changes in microstructure and homogeneity?

The shift in the dielectric maximum in thin film relaxors is a dynamic phenomena and thus easily influenced by processing conditions inducing defects. Therefore, films annealed at different temperatures, or fabricated with different amounts of excess lead may exhibit differences in the value and temperature of the dielectric maximum. In addition, stress or strain effects have been shown to play a role[114], [24]. In the present case, the films were identically processed from 30% excess lead solutions on Pt/Si substrates with only the annealing temperature altered, resulting solely in an increase in grain size. From studies of similarly processed films using different seed layers on Pt/Si substrates (experimental section), an increase in grain size from 140 to 325 nm resulted in *no* significant change in the value or position of the dielectric maximum. As in bulk materials, the presence of defects such as lead vacancies or "disorder" in the system, as well as stress/strain in the film tends to shift *down* the temperatures of the dielectric maximum, while increasing "B" site order shifts the temperature *up*. One can therefore conclude in this case, that the shift of the dielectric maximum to higher temperatures is due to "B" site ordering. However, it is not clear if the increase in the value of the dielectric constant maximum results from the ordering itself, or from microstructural changes accompanying the ordering process.

Polarization measurements presented in figure 3.19 display the large field PE response at temperatures 40 degrees above Tmax in the paraelectric region and 90 degrees below in the relaxor/ferroelectric region for a disordered and S=0.22 degree of ordered film. In the paraelectric phase, both films show linear like polarization response in the low field region up to 100 kV/cm with the steeper slope of the ordered sample reflecting its higher permittivity, saturating to similar values of 24 and 26 $\mu C/cm^2$ for disorderd and ordered samples respectively. The low temperature polarization response shows a typical slim loop relaxor hysteresis with remanent polarization of 2.5 $\mu C/cm^2$ for the disordered relaxor.

A more developed hysteresis indicating additional response from domain switching was observed in the case of the ordered film, with an increased remanent polarization value of 6.5 μC/cm^2. Similar to bulk materials, an increase in ordering (even small degrees, S=0.2) results in an upwards shift of the dielectric maximum and the development of a long range polar state at temperatures below Tmax evidenced by PE measurements.
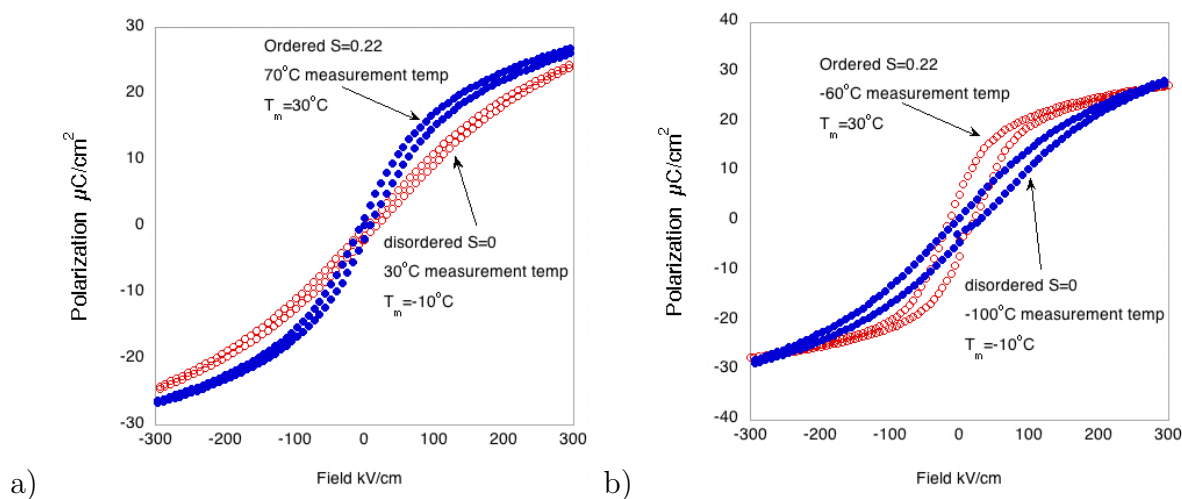
Figure 3.19: *500 nm PST film on Pt/Si disordered (S=0) versus ordered (S=0.22) measured in the "Out-of-Plane" configuration (a)PE loops in paraelectric region + 40°C above dielectric maximum temperature (T_m) of the material, and (b)in the temperature region -90°C below T_m*

3.5.2   STO (111) Substrates *"Out-of- Plane*

Figure 3.20 displays the dielectric constant and loss tangent at 1 kHz for 600 nm PST films on doped STO(111) substrates annealed at 700 (1min), 800(1min) and 1050°C (5min). Again we see an upwards shift in the position and value of the dielectric constant maximum, with the relatively low values due to the nature of the film/substrate interface and built in field previously discussed.
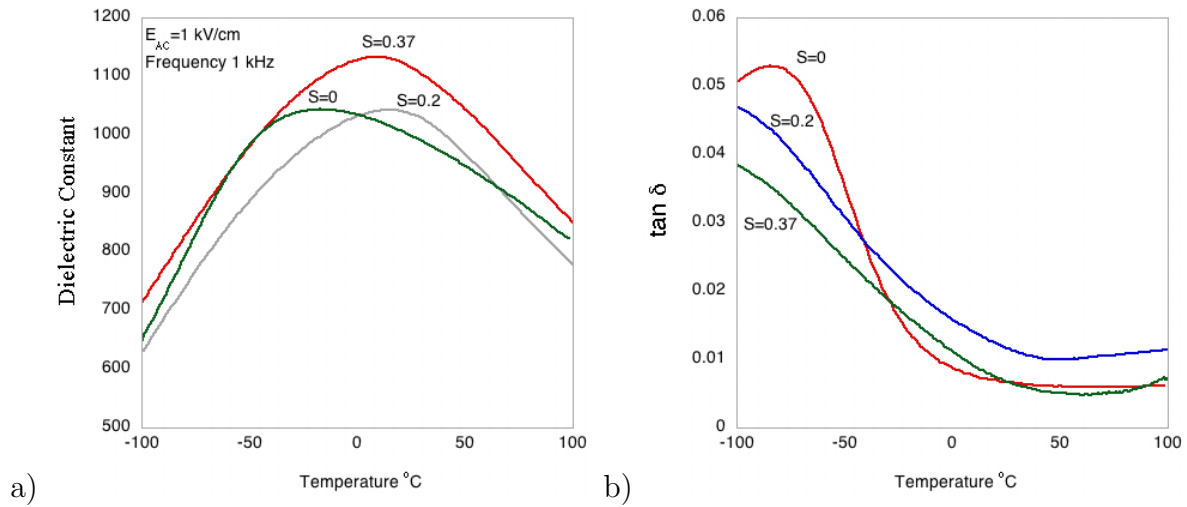
Figure 3.20: *600nm PST film on STO(111) substrates annealed at 700 (S=0), 800 (S=0.2) and 1050°C (S=0.37), (a) Dielectric constant versus temperature and (b) loss tangent versus temperature at 1 kHz and E_{AC}=1 kV/cm*

3.5.3   Sapphire Substrates *"In-Plane"*

In plane dielectric measurements present the opportunity for the examination of ordered films without the worry of damage to the bottom electrode due to high annealing temperatures. Figure 3.21 displays the real and imaginary part of the dielectric constant for films with varying degrees of "B" site order at 10 kHz and 1kV/cm measuring field. Again, there was observed an increase in the temperature and the value of the dielectric maximum with an increase in the degree of "B" site order, similar to what was observed in low degrees of ordering on Pt/Si substrates measured "out of plane." The dielectric constant shifts from 2210 at 0°C for the sample annealed at 700°C to 6750 at 30°C for the highly ordered (S=0.91) sample annealed at 850 for 35 hours.

Another interesting facet of this figure is although the films processed at 700°C and 850°C for 1 minute are disordered according to the absence of X-ray superlattice reflections, they have a significant difference in the dielectric response. A close examination of the real and imaginary parts reveals a "composite" type behavior showing phase transi-
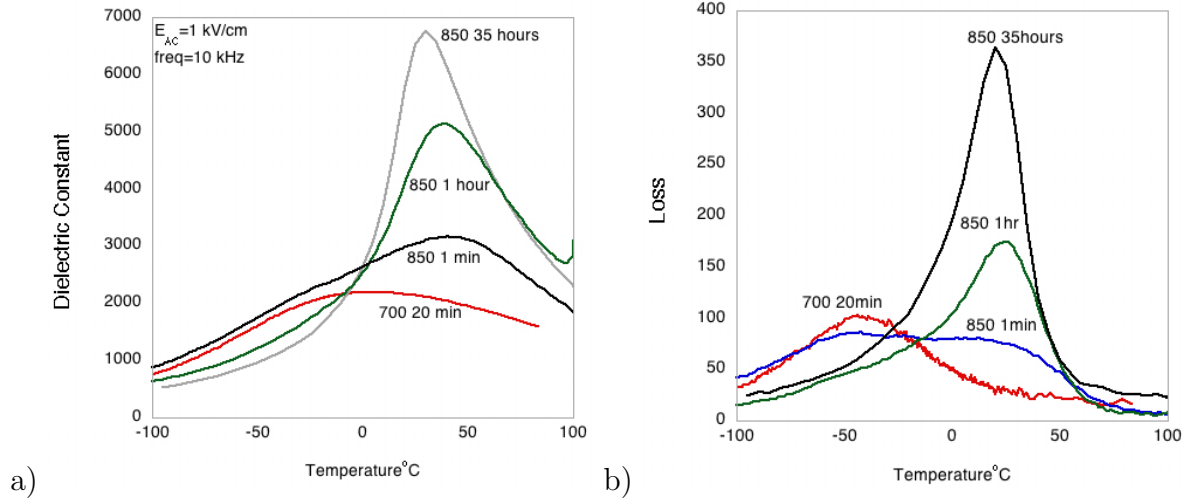
Figure 3.21: *650 nm PST on sapphire substrates annealed to 700°C (S=0), 850°C for 1 minute (S=0), 850°C for 1 hour (S=0.55) and 850°C for 35 hours (S=0.91) (a) "In-plane" dielectric constant versus temperature and (b) loss versus temperature at 10 kHz and E_{AC}=1 kV/cm*

tion characteristics of both ordered and disordered samples. In the sample annealed at 850°C, the real part reaches a maximum near 30°C as in highly ordered samples, however, its subsequent drop below Tmax is more gradual. The imaginary part also shows an increased loss near 30°C, but only decreases near -50°C coinciding with the decrease of the loss from the disordered film annealed at 700°C . This sample seems to *feel* the presence of disordered *and* ordered regions at the same time; even though the ordered regions are undetectable by X-ray and TEM investigations. Similar behavior has been recently observed in BST thin films and was also explained by the coexistence of ferroelectric and relaxor properties [127].

The polarization measurements "in the plane of the film" are shown in figure 3.22 for the disordered sample annealed at 700°C, and for the highly ordered specimen (S=0.91). The disordered sample displays a linear type polarization response at +100 (paraelectric) and -100°C with no evidence of hysteresis. This is similar to the case for disordered thin films measured at such small field levels (10 to 20 kV/cm *"Out-of-Plane"*). The range

of *"In-Plane"* polarization measurements is limited by the gap width in the tens of microns level, which defines the electric field, instead of fraction of microns film thickness for *"Out-of-Plane"* measurements. The highly ordered sample which displayed a sharp drop in dielectric constant after Tmax displayed a linear like hysteresis in the high temperature paraelectric phase (50°C), a slim loop hysteresis near the temperature of dielectric maximum of 30°C with a remanent polarization Pr=1 $\mu C/cm^2$, and a well developed hysteresis loop with Pr=5.8 $\mu C/cm^2$ at -60°C .
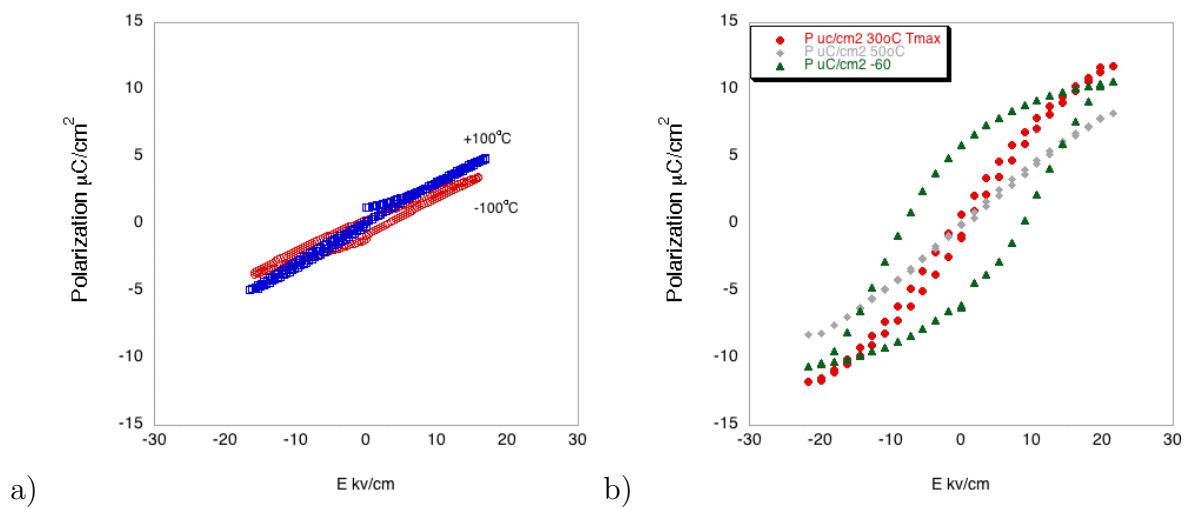
Figure 3.22: *"In-Plane" polarization measurement versus electric field (a) 650 nm PST film on sapphire substrates annealed at 700° C for 20 minutes (S=0) measured at 250 Hz, +100° C and -100° C and (b) annealed at 850° C for 35 hours (S=0.91) measured at 250 Hz, 50° C , 30° C and -60° C*

3.5.4   MgO Substrates *"In-Plane*

Similar observations of the ordering effects on the "in-plane" dielectric properties were observed for PST on MgO substrates including an upward shift of the temperature and value of the dielectric maximum. In the case of epitaxial PST films on (100) MgO the superlattice reflections cannot be observed with normal theta, 2theta X-ray scans but were

observed by TEM DF investigations and reported in the experimental section. Although the exact degree of order cannot be calculated, the large size and proportion of the ordered species in the DF TEM images combined with our previous experience of similarly processed specimens suggests a highly ordered sample. Figure 3.23 displays the real and imaginary dielectric constant measured *"In-Plane"* with a field level of 1 kV/cm. There was an increase in the dielectric maximum from 1110 at T=-12°C to 3546 at T=16°C for the 550 nm PST film on a MgO substrate after annealing at 850°C for 24 hours. The reduction of the dielectric constant of ordered films on MgO substrates as compared to sapphire may be due to entrapped porosity in the microstructure as seen in the processing chapter, or to a different degree of order as this value cannot be estimated directly from X-ray data for comparison.
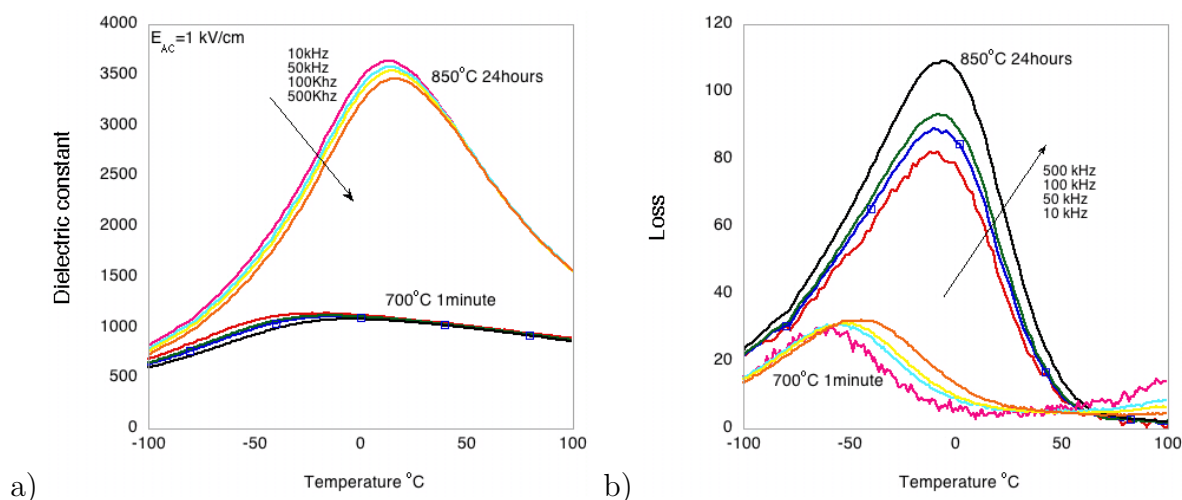
Figure 3.23: *550nm PST film on MgO substrate processed at 700° C 1 minute, and 850° C for 24 hours (a) Dielectric constant versus temperature and frequency and (b) loss versus temperature and frequency at E_{AC}=1 kV/cm*

3.5.5   A High Temperature Disordered State?

Instead of the moderately high temperatures and extended annealing times leading to "B" site ordering, it is interesting to examine whether higher temperatures of annealing

for short durations can produce a high temperature disordered state, *without* destroying the integrity of the film. As shown in the experimental section, films annealed to 1000°C for short times (5 minutes) lacked superlattice reflections from X-ray analysis, but TEM DF investigations indicated a distribution of small ordered regions from 4 to 20 nm in diameter. The dielectric response of this film is shown in figure 3.24a which indicates a dielectric constant maximum of 3400 at T=32°C and 10 kHz. This behavior shows how sensitive the dielectric maximum is to local order. It is shifted upwards on the temperature axis, with an increase in its value as compared to disordered samples, even with very small ordered regions which are not detectable from X-ray analysis.
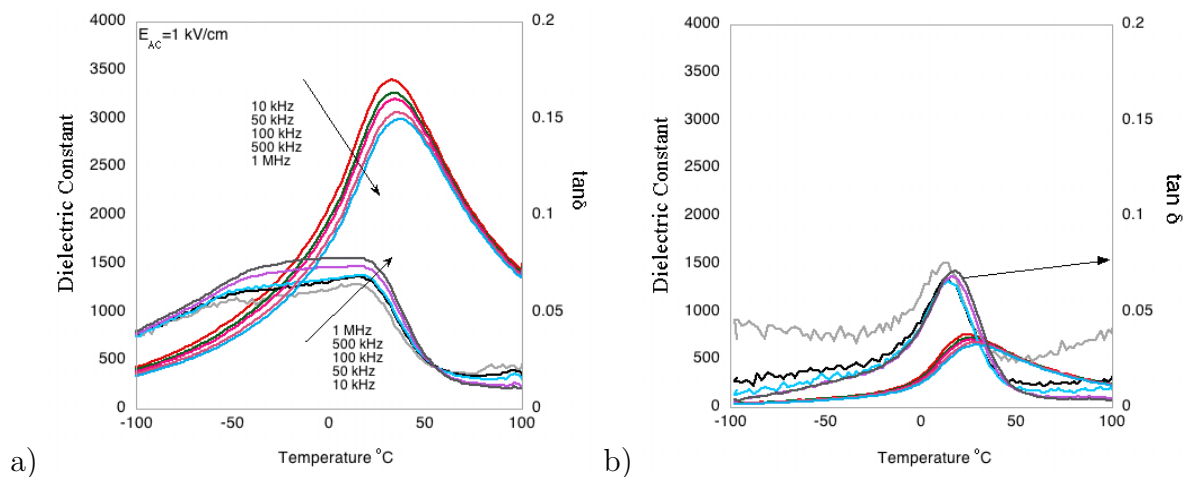
Figure 3.24: *High Temperature Disordered State: Dielectric constant and loss tangent for 650nm PST films on sapphire substrate annealed at (a)1000°C for 5 minutes and (b)1300°C for 5 minutes*

The behavior below the dielectric constant maximum also shows sensitivity to the presence of ordered regions. A rapid decrease in the dielectric constant was observed in figure (3.24a), in contrast to samples without ordered regions detectable by TEM analisys, as in figure 3.21 processed at 850°C for 1 minute. Even a small degree of small size (20nm) ordered regions undetectable by X-ray, but observed by TEM has a drastic effect on the dielectric properties of films on the same substrate with similar microstructure.

Increased annealing temperatures led to film degradation shown in the experimental section with large quantities of pyrochlore phase, and increased film porosity. This resulted in the expected decrease in the film dielectric constant shown in figure 3.24b. These studies point out the difficulty in obtaining a high temperature disordered state in thin film specimens, namely film deterioration. Unlike their bulk counterparts where the surface defects and imperfections may be polished away, thin films are merely destroyed by high temperature processes.

3.5.6   Ordering or Chemical Homogeneity/Microstructure: A Comparison with PMN Thin Films

Due to the complications of separating the effects of ordering, microstructural and chemical homogeneity changes with long annealing times in PST, we synthesized thin films of the classical relaxor PMN and submitted the samples to the same processing conditions. Since unlike PST, PMN does not form long range order (due to mixed charged "B" site species) it is an ideal tool for analysis. Figure 3.25 shows the dielectric constant and loss tangent versus temperature for a 620 nm PMN/sapphire film measured "in-plane" after annealing at 850°C for 1minute and 24 hours. Although the temperature of the dielectric maximum T=28°C at 10kHz is the same for both samples, the sample annealed for 24 hours displays a 36% reduction in the dielectric constant (from 2330 to 1495 at 10 kHz and 1 kV/cm measuring field).

Microstructural changes accompanying the annealing process shown in the experimental section include an increase in grain size from 70 nm to over 500 nm and the appearance of fine grained surface pyrochlore with an estimated secondary phase content of 10% estimated from X-ray analysis. The positional stability of the dielectric maximum after microstructural changes, and processing induced defects provides additional evidence that the upwards shift of the temperature of the dielectric maximum in PST is indeed due to an increase in "B" site order. However, in the case of PMN, the reduction of the dielectric
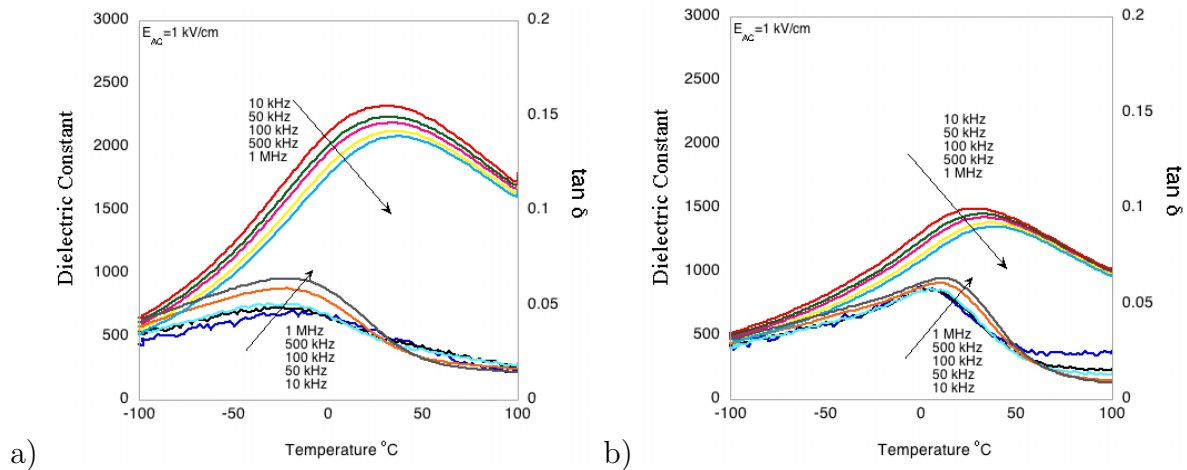
Figure 3.25: *Dielectric constant and loss tangent of 620 nm PMN film on sapphire substrate with TiO$_2$ seed annealed at (a) 850°C for 1minute and (b) 850°C for 24 hours*

constant may be attributed to secondary phase formation and does not therefore give us the information necessary to separate ordering from microstructrual changes on the value of the dielectric maximum.

3.6   Field Dependance

3.6.1   General Features

Figure 3.26 depicts the AC and DC field dependence of the dielectric constant as a function of temperature for a disordered 500 nm PST/Pt/Si film. All measurements were made at 1 kHz and the "baseline" measure is at a low AC field value of 1 kV/cm. It is seen that with increasing AC field strength from 1 to 20 kV/cm the dielectric constant increases displaying *positive non-linearity*, while the maximum shifts towards lower temperatures. This is consistent with reports in PMN thin films [21], which also indicated this behavior exhibits a maximum and decreases after some threshold field nominally 40 to 60 kV/cm depending on temperature and the material. In the case of an applied DC field superimposed on a low level AC field, our samples displayed a *negative non-linearity*, or a decrease
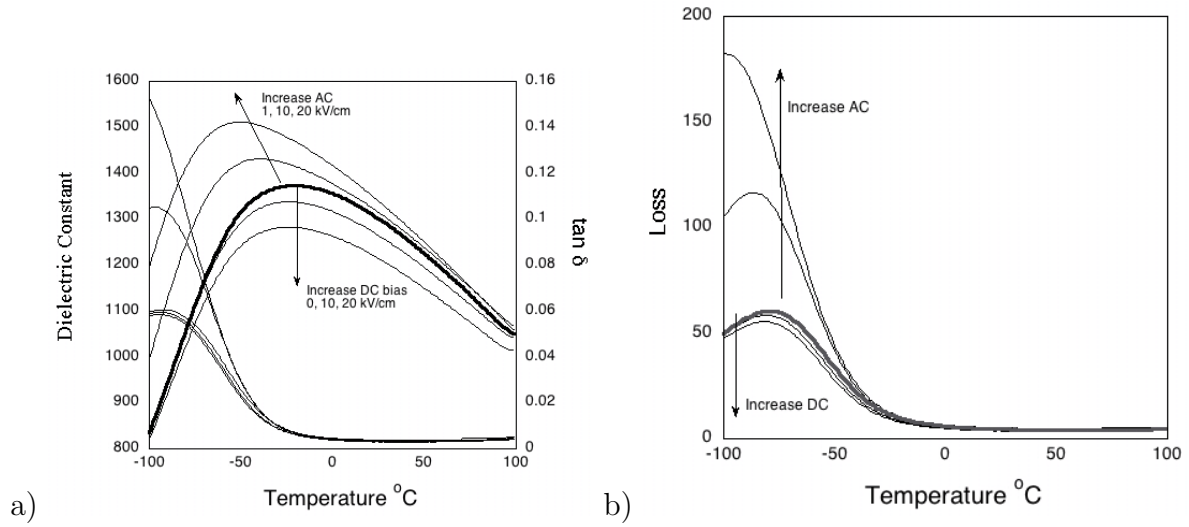
Figure 3.26: *500nm PST thin film of Pt/Si substrate: Effect of AC measuring field level from 1 to 20 kV/cm and DC bias fields from 0 to 20 kV/cm on (a) Dielectric constant and loss tangent versus temperature at 1 kHz and (b) loss versus temperature at 1 kHz*

in the dielectric constant with increasing applied DC bias from 0 to 20 kV/cm, and no change in the temperature of the dielectric maximum. The loss tangent behaves in a similar fashion with an increase in the losses with increasing AC field strength, and a decrease in the losses with increasing DC bias field. Higher field response is shown in figure3.27 up to AC and DC field levels near 100 kV/cm as a function of temperature. There is seen the maximum AC non-linearity at low temperatures, whose response saturates and decreases at fields in excess of 40 kV/cm, while the maximum DC non-linearity occurs at temperatures near the dielectric maximum (partly due to the higher permittivity).

A previous report in bulk PST also showed a positive non-linearity in low AC field levels from 0.1 to 1kV/cm [128] at temperatures near the phase transition. Results obtained during the course of this thesis on bulk ceramic PST also indicated a positive non-linearity near the phase transition for the AC field effect for PST-Disordered at low fields from 0.02 to 1.2 kV/cm with a shift down in temperature of the dielectric maximum.

Thin films provide a tool to explore the high field dielectric and polarization response
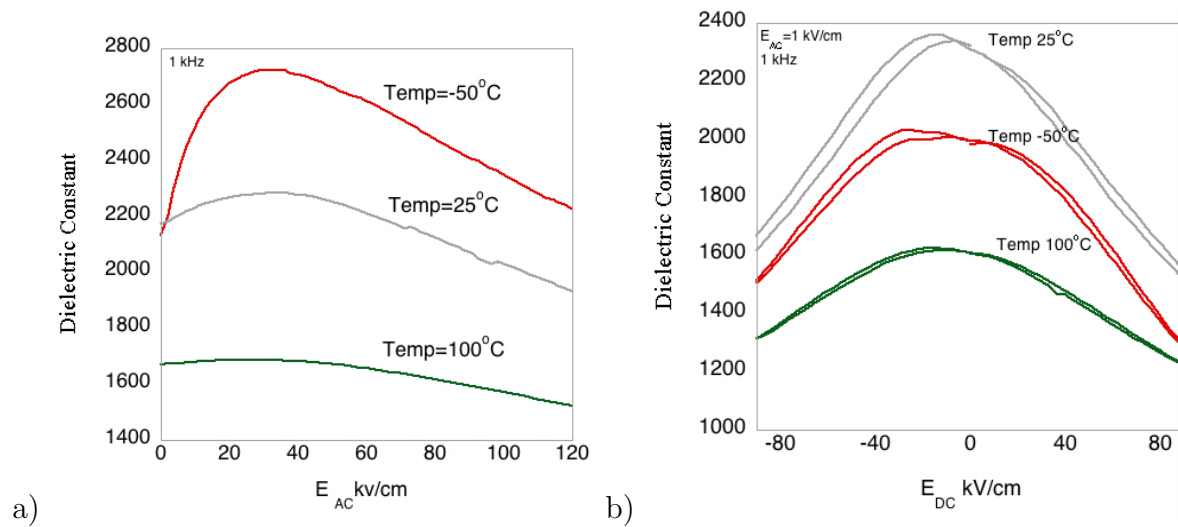
Figure 3.27: *650nm PST thin film on Pt/Si substrate, (a) Dielectric constant versus AC field level at 100, 25 and -50°C and 1 kHz, (b) Dielectric constant versus applied DC bias at 100, 25 and -50°C and 1 kHz*

because of their small thickness. In addition to this new range of field data available, an analysis of their non-linear behavior at field levels in comparison with their ceramic and single crystal counterparts gives insight into polar region dynamics in thin film versus bulk form.

3.6.2   Ordered and Disordered Films on Pt/Si Substrates

Figure 3.28 shows the low field dielectric response versus temperature, the large field normalized nonlinear AC and DC response at 1 kHz for 500 nm disordered PST film on Pt/Si substrates (T_m=−10°C) and an ordered film with S=0.2 (T_m=30°C). The non-linear measurements are presented at the Tmax for each specimen including temperatures 90 degrees above and below the dielectric maximum. The AC response is qualitatively similar for both samples with the maximum non-linear response at low temperatures displaying a decrease after some critical field. The disordered sample displayed a 60% increase in the normalized AC nonlinearity, with a slow decrease after the maximum at

−100°C, while there was a sharp decrease/saturation in the case of the ordered sample. Since the disordered sample is thought to be composed of frozen in/interacting polar regions at temperatures below the dielectric maximum, an greater quantitative non-linear response would be expected. Since the slightly ordered sample is expected to have ferroelectric domains at low temperature this quantitate lower non-linear response is expected, as well as the sharp reduction after some critical field due to the reorientation of domain patterns.

The difference in order and corresponding differences in polar-region versus some degree of normal domain behavior is also seen in the DC non-linear response. While both samples have their expected maximum reduction in permittivity with DC field at temperatures near the dielectric maximum, the disordered sample exhibits a reduced non-linear response in the low temperature regime as compared to the ordered sample. The extrinsic mechanism of the reduction in permittivity with DC field is 1) domain reorientation/alignment in the ferroelectric case (ordered) and 2) field induced coalescence of nano-polar regions in the case of the relaxor sample. One can speculate that the experimentally applied fields were sufficient to cause domain alignment in the ordered case, but too small to coalesce the frozen in polar regions in their low temperature state.

It should be noted that the large field AC response seen in this work and in Kighelman [4] is particular to relaxors, as in normal dielectrics or ferroelectrics the non-linear response should increase with no predicted maximum and decreasing branch. The response of the loss tangent in figure 3.29 exhibits analogous behavior with a low temperature maximum ac non-linearity and subsequent decreasing branch. This behavior has not been seen in ceramic and single crystal specimens because of the high fields required.

3.6.3   Low Field "Crossover"

We have seen that thin films provide us new information in the high field regime, however it is also of interest to compare the non-linear dielectric behavior at low fields comparable
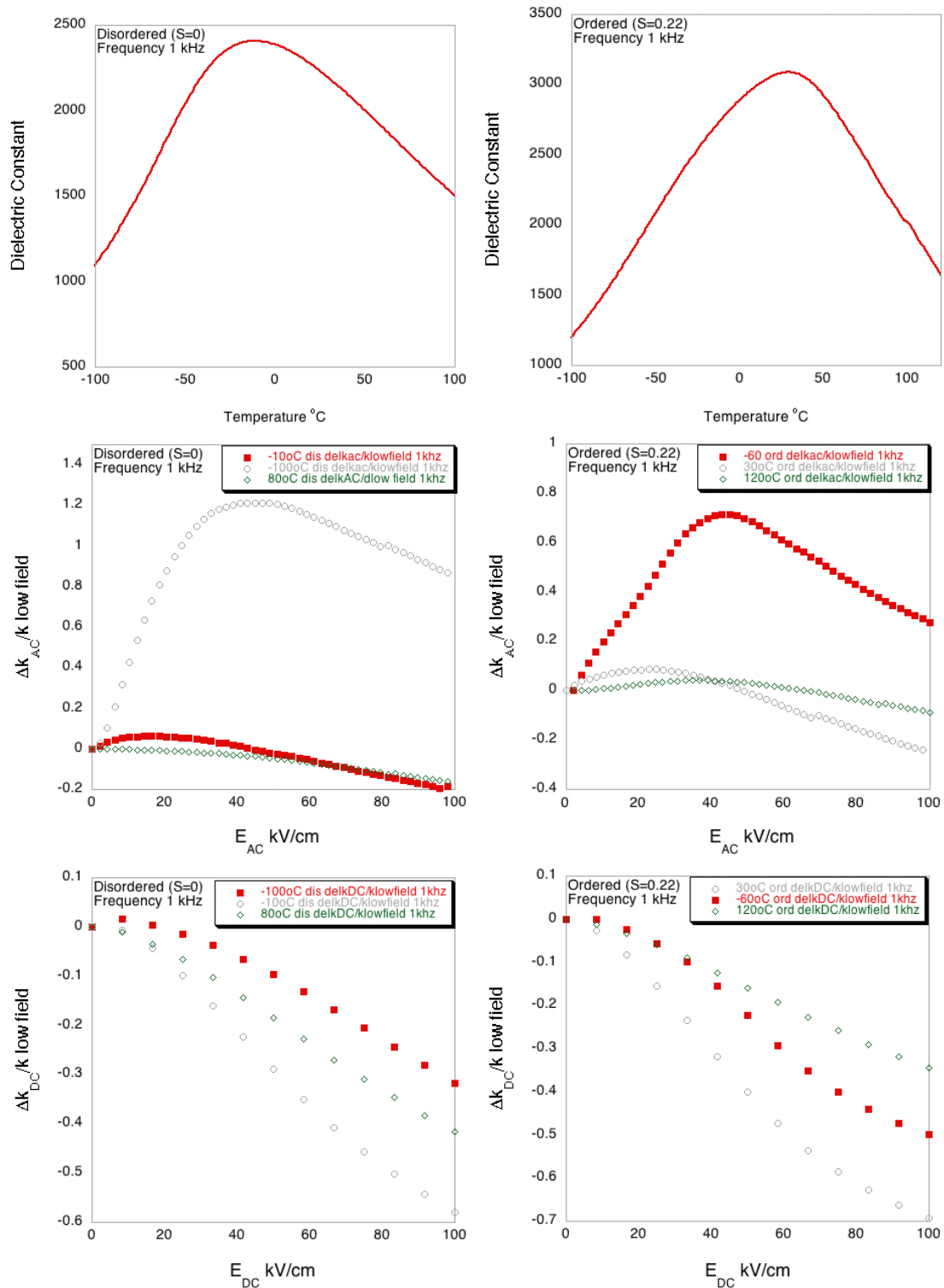
Figure 3.28: *500nm Pt/Si films ordered S=0.2 and disordered (S=0) with the dielectric constant measured "out of plane" versus temperature at 1kHz, AC and DC field dependance*
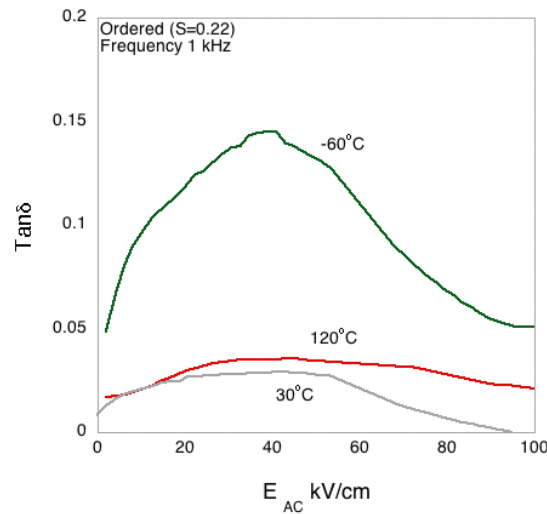
Figure 3.29: *500nm PST film on Pt/Si ordered with (S=0.2): AC field dependance of the loss tangent "out of plane" at 1 kHz, and 120, 30 and -60° C*

to that studied in ceramic and single crystal specimens. In order for a reliable response due to low applied fields, specimens were studied over 1 micron thick in the "out of plane" configuration. The examined sample was 1.4 micron *disordered* (S=0) PST film on Pt/Si substrate annealed at 700°C for 20 minutes. The low field study of the AC non-linear dielectric measurements was performed on the bridge as well as on a lock-in amplifier by collecting the voltage drop across a resistor.

3.6.3.1   AC Non-Linearity

Figure3.30 presents the normalized AC field non-linear response at field levels of 0.5 to 2kV/cm from -100°C to 70°C . Error bars are indicated and calculated from $d\epsilon/dT$ the slope of the dielectric versus temperature curve multiplied by the temperature stability of the measurement (0.01 to 0.1 °C). It is seen that at temperatures above the dielectric maximum there is an unexpected linear relation between the AC non-linearity and the driving field. However, at temperatures near 50°C below the dielectric maximum (Tm=5°C at 100 kHz, Tcrossover≈-50°C) a change in the functional dependance of Δk versus Electric

Field occurs from linear to quadratic. This observation of a "crossover" in the non-linear field dependance has been previously observed in single crystal PMN samples, however the origins of this phenomena are still, as of yet, not understood. As the normal ferroelectrics should show a quadratic field dependance for this non-linear behavior, both above and below the dielectric maximum; the observations in relaxor ferroelectrics indicate yet again a deviation from normal ferroelectric behavior at temperatures above the dielectric maximum. This crossover phenomenon has just recently been confirmed in BST thin films which displayed a shift of the dielectric frequency maximum characteristic of relaxor behavior [127].

3.6.3.2   P(3ω) Field Dependance and Phase Angle Measurements

In order to confirm the "crossover" behavior observed with non-linear AC measurements performed on the bridge, measurements were made of the third harmonic of polarization as a function of temperature on the same sample. Figure 3.31 presents the third harmonic and its phase angle as a function of AC driving field at 1 kHz from 0.5 to 2 kV/cm at temperatures above and below the dielectric maximum. As the plots are in the log scale, the slope of the fitted line corresponds to the exponent in the power law description of the observed behavior. It is clearly seen that measurements of the third harmonic of polarization show a crossover in functional dependance equivalent to that observed in measurements on the bridge, namely a decrease in the exponent by approximately 1 unit as the temperature passes from above to below the dielectric maximum (from 1 to 2 in the case of non-linear AC bridge, and 1.7 to 2.8 in the case of third harmonics). The phase angle of the third harmonic was seen to be 180 degrees independent of temperature or driving field.
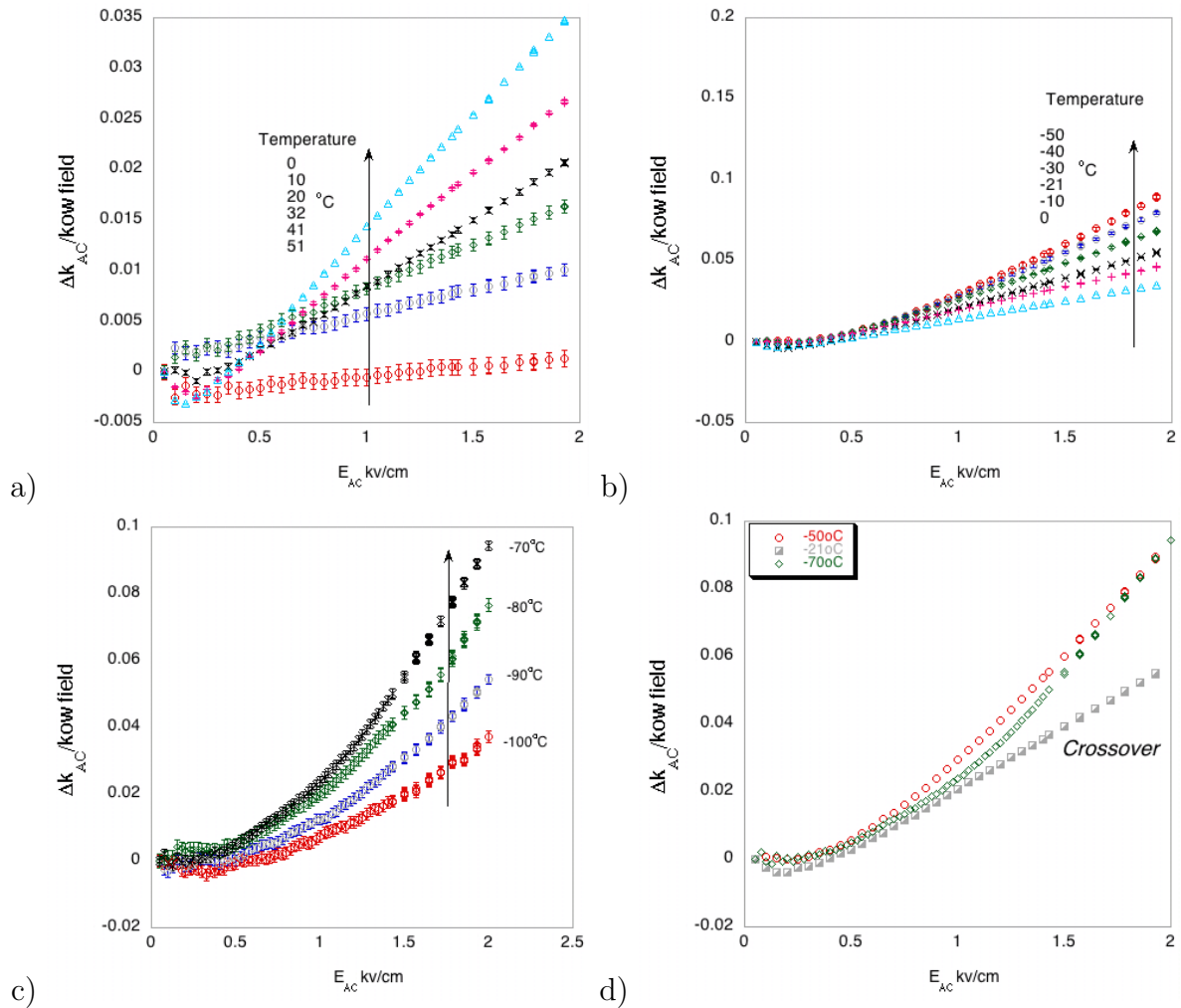
Figure 3.30: *Low Field AC dependance at 100Hz for 1.4 micron disordered (S=0) PST film on Pt/Si substrate measured "out of plane" (a) change in dielectric constant versus AC measuring field up to 2 kV/cm from 50 to 0° C , (b) 0 to -50° C , (c) -70 to −100°C, and (d) "Crossover" region where field dependance changes from linear to quadratic at low temperatures*
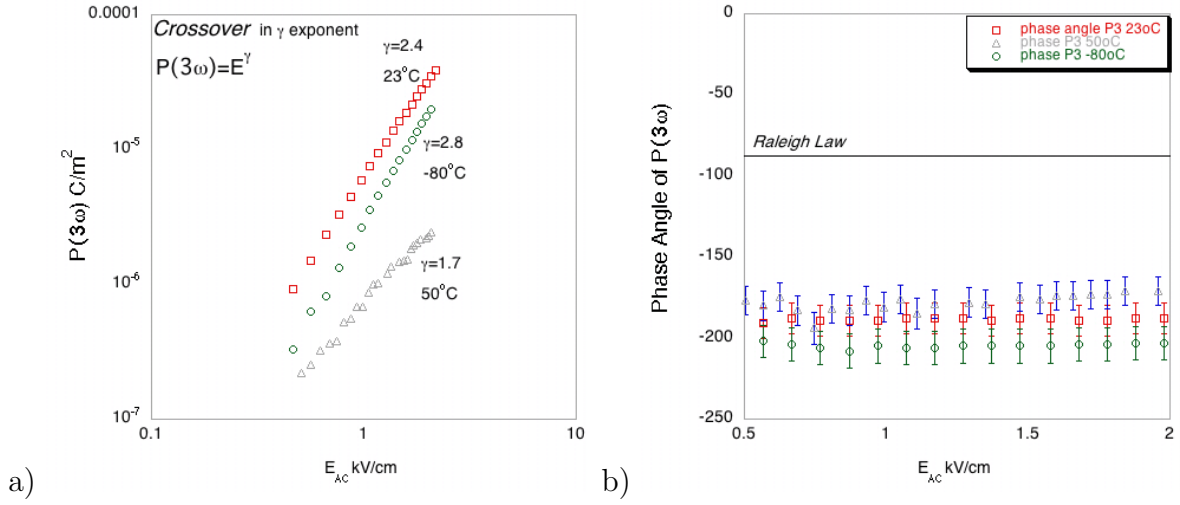
Figure 3.31: *1.4 micron disordered (S=0) PST film on Pt/Si substrate measured "out of plane"(a) Third harmonic P(3ω) of polarization as a function of AC measuring field at 50, 23 and -80° C at 100 Hz, and (b) Phase angle of P(3ω)*

3.6.4   Non-Linearity and Polarization Behavior: Raleigh law?

As we have seen the extensive non-linear behavior in relaxor thin films, once can pose the question "how is the non-linearity related to hysteresis in these materials?" In other words, since it is known that polar regions exist above the dielectric constant maximum for relaxors, and a number of authors have seen a crossover and linear dependance of dielectric constant versus E_{AC} at temps above T_m, it is of interest to compare the polarization behavior at low fields to give insight into the switching or motion of polar regions. According to the Raleigh law, domain walls or mobile interfaces (polar regions) interacting with randomly distributed pinning centers and whose distribution of potential energy barrier heights is broad and uniform contribute to the nonlinear dielectric response of the material according to:

$$k(E_o) = k_{init} + \alpha E_o \qquad (3.23)$$

$$P(E) = (k_{init} + \alpha E_o)E \frac{+}{-} \frac{\alpha}{2}(E_o^2 - E^2) \tag{3.24}$$

A fit of the dielectric permittivity under AC field yields the paramaters k_{init} and α which then can be used in equation 3.24 to calculate the PE loop. A comparison of the measured and calculated PE loops at the same field strength (low field, since Raleigh analysis does not predict saturated loops, and the k versus AC field should be linear) indicates if the observed non-linearity in the dielectric constant contributes to low field hysteresis. This gives indirect information on the potential energy barrier for polar domain motion.

3.6.4.1 Low Fields

Raleigh paramaters were extracted from a fit of dielectric constant versus increasing AC field strength at 1 kHz for a 1.4 micron disordered PST film measured in the "Out-of-Plane" configuration. The measured PE loop at 5 kv/cm indicated a Pr of 0.013 $\mu C/cm^2$, close to the calculated Raleigh offset parameter corresponding to theoretical Pr=0.02 $\mu C/cm^2$; in other words, not all of the observed non-linearity contributes to the hysetersis of the system according to the Raleigh Law. However, at such low field and hysteresis levels a more thorough examination of Raleigh behavior is given by the phase angle of the 3rd harmonic. The 3rd harmonic was seen to deviate from Raleigh law as was shown in the previous section with values $\approx$180 degrees at all temperatures and driving fields from 0 to 2kV/cm. We can thus conclude that the non-linearity in thin film relaxors is distinctly non-Raleigh in nature as was previously observed for PMN single crystal materials. The non-linear behavior of thin films and single crystal materials have been shown to be qualitatively the same, with deviations from Raleigh law indicating the large *reversible* component in polar region movement.

3.6.4.2 High Fields

The question remains as to the mechanism according to which relaxor ferroelectrics display slim loop hysteresis at temperatures above the dielectric maximum, and how is the hysteresis connected with the non-linearity, a question which has not been investigated in bulk and single crystal samples because of the high fields that are necessary. Therefore, thin film samples are an ideal candidate for this study. Figure3.32 shows the polarization response under low electric field levels up to 5 kV/cm with a small remanent polarization $P_r \approx 0.02$ μC/cm^2, as well as the polarization response under large fields up to 200 kV/cm with a remanent polarization $P_r \approx 1.5$ μC/cm^2. In a conventional ferroelectric in the paraelectric phase (no long range coherent polarization), this increase in remanent polarization with increasing electric field may only be understood in terms an increase in the dielectric loss with increasing bias field. In relaxor ferroelectrics at temperatures above the dielectric maximum, this phenomena may also be explained by an increase in dielectric loss, or it could be due to local switching of polar regions under high fields resulting in increased values of remanent polarization.

From studies of the dielectric constant and loss tangent under large AC fields, it was seen that above a certain threshold field of 20 to 40 kV/cm, there was a reduction in the dielectric constant (figure 3.27) *and* in the loss tangent (figure 3.29). This behavior was attributed to a reduction in polar region boundary area, creating orientable polar regions. Therefore the increase in the remanent polarization with increasing electric field as seen in figure (3.32) may not be attributed with loss in the samples, but may be due to the coalescence of polar regions which are able to be switched with a changing AC field.

3.7 The Position of the Dielectric Maximum

As the position of the dielectric maximum varies in the literature with differences in processing condition, and the nature of the substrate it is instructive to take a comprehensive
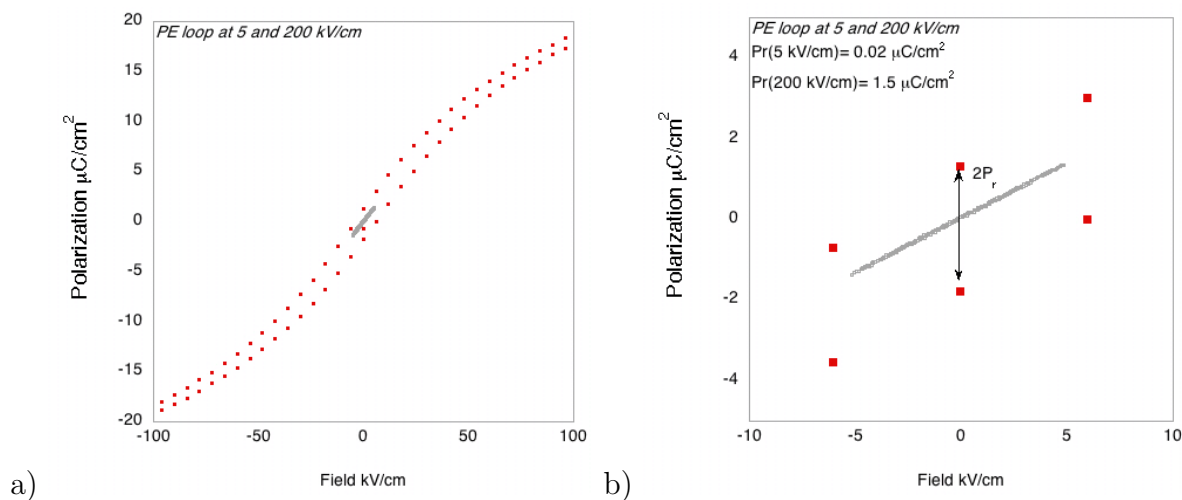
Figure 3.32: *Low and high field PE response at 250 Hz and 30°C (a) large view (b) close up of P_r remanent polarization as a function of applied field*

look at this behavior in PST thin films processed in a similar fashion.

3.7.1   Disordered Films

3.7.1.1   Thickness and Processing

Excess lead content was shown in the processing chapter to affect the microstructure and phase content as well as the dielectric properties of thin films. From figure (2.15, page 68) it was seen that films of the same thickness annealed at 700°C for 1 minute on Pt/Si substrates, showed the temperature of the dielectric maximum shift to higher temperatures with increasing excess lead content. Since less excess lead in solution is expected to produce lead vacancies, this is consistent with the observations in bulk materials with the presence of lead vacancies leading to a downward shift in the dielectric maximum. For films with a high excess lead content of 30% on Pt/Si substrates, the position of the dielectric maximum is relatively stable with variations in annealing time, in fact even after 1 hour post-annealing in a tube furnace at 700°C leading to lead vacancy formation as observed by TEM (A site vacancy ordering), the position of the dielectric maximum is

Material	TECα X$10^{-6}K^{-1}$	Calc. Stress MPa eq.(2.6)	Measured Stress MPa
PST	6.5		
Si	4	**+370 (tension)**	**+700 (tension)**[a]
STO	11.7	-380 (compression)	
MgO	13.6	**-640 (compression)**	**-180(compression)**[b]
Al$_2$O$_3$ (sapphire)	6.7	-20 (compression)	

[a]Stress measured using wafer bending technique upon cooling from crystallization temperature

[b]In-plane lattice parameter measured by grazing angle X-ray

Table 3.2: *PST and Substrate Thermal Expansion and Stress Data: Calc. stress determined from equation (2.6, page 43) with E_f=1 X 10^{11} N/m^2 and ν_f= 0.3*

unchanged although the value is reduced as seen in figure (2.18b) section(2.3.3.1).

Why do Pb vacancy defects lead to a downward shift in the dielectric maximum in the case of different levels of excess lead added to the solution, but processing induced defects from long time annealing result in little to no change? It is believed this is due to the *distribution* of defects, in the case of excess lead additions to the solution and subsequent annealing of thin layers the defect distribution is expected to be more homogenous than in high excess lead content film subjected to increased time annealing and surface lead loss. In the case of long time annealing, the defects should be concentrated in the surface layer which would lead to a reduction in the "Out-of-Plane" dielectric response but have little effect on the position of the dielectric maximum. In addition, an examination of the position of the dielectric maximum as a function of film thickness with the same annealing conditions showed similar values within +/- 2°C between films of 300 nm up to 2 microns.

3.7.1.2 Stress Effects

Figure 3.33 displays the temperature of the dielectric maximum at 10 kHz versus the Calculated Stress (MPa) induced by thermal expansion mismatch summarized in table (3.2). All films were fabricated from solutions containing 30% excess lead and were annealed
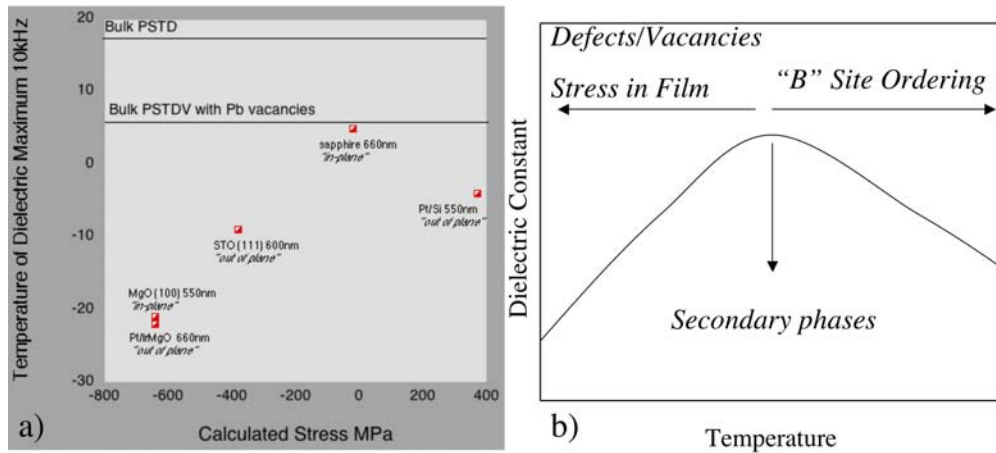
Figure 3.33: *(a) Stress effect on the temperature of the dielectric maximum at 10 kHz and (b) Schematic of the impact of different factors on the position of the dielectric maximum*

at 700°C for 1 minute. Although the thickness varies by 100 nm, studies in the previous section revealed a weak thickness dependance for the position for the dielectric maximum and may be assumed to be negligible for the present discussion. Indicated on the graph are the position of the dielectric maximum at 10 kHz for PST-D and PSTDV with lead vacancies taken from ref [17] showing that the presence of vacancies/defects reduces the temperature of the dielectric maximum. In addition, measurements were carried out in both the "In-Plane" and "Out-of-Plane" configuration, with both type of measurements giving a similar value for the position of dielectric maximum for a given substrate system as seen by comparing PST/MgO in-plane versus PST/Pt/Ir/MgO out of plane in figure 3.33. Since the grain size of PST/Pt/Ir/MgO is nominally 3 microns and PST/MgO is epitaxial with no observable grain boundaries, changes in the position of the dielectric maximum cannot be attributed to grain size effects in the present case.

In light of these factors, the differences in the position of the dielectric maximum are attributed to substrate effects, specifically the stress/strain induced from the thermal expansion mismatch upon cooling from the crystallization temperature. It is seen that PST film on sapphire which has the least thermal induced stress has its dielectric maximum

position equilivant with the bulk ceramic samples with lead vacancies (PST-DV). As the substrate is changed and stress levels move into compression *or* tension, the temperature of the dielectric maximum decreases. These observations are in agreement with [24], where PMN-PT films showed a decrease in the temperature of the dielectric maximum under *both* tensile and compressive stresses.

3.7.1.3 Völgel-Fulcher (VF) Frequency Dependance

The "freezing" behavior of polar regions as the material is cooled has been shown to follow the VF law for a wide variety of relaxor materials in ceramic and single crystal form. A few reports have indicated VF behavior for thin film materials in PMN and PMN-PT system, however the analysis was based on the very narrow frequency range from 100Hz to 1MHz where the behavior can essentially be considered Arrhenius, but with very big pre-exponential factor ($\omega_o \approx 10^{30}$) which makes this description void of any physical meaning. The author is not aware of any publications describing VF behavior for thin film relaxors in a wide frequency range from mHz into the GHz or THz range. There are a few reasons for this, 1) Microwave data for thin film relaxors near the dielectric maximum are difficult if not impossible to obtain from accurate resonance measurements due to their high loss, and 2) there is very little work on the high frequency response using Infrared techniques (FTIR) into the THz range to determine permittivity in thin films. FTIR measurements conducted on PMN and PST thin films during this thesis and presented in the following chapter thus provide a unique opportunity to study the freezing of polar region movement in thin film samples. Figure 3.34 displays a semi-log plot of frequency (Hz) versus 1/Tmax (K) for PMN thin films measured both *"In-Plane"* and *"Out-of-Plane"* versus commonly cited VF fitting parameters from ceramic and single crystal materials [50]. Firstly, it is interesting to see that the VF parameter predicts the same value of Tmax as that measured for thin films in the THz range, an expected result at the intrinsic response of the material should be the same. However, as we decrease in

measuring frequency we see significant deviations from VF behavior in thin film samples particularly in the case of the dielectric constant measured *"In-Plane"*. Specifically, we see a shift in the transition temperature to higher temperatures in thin film PMN specimens as compared to bulk ceramics, in agreement with recent results by Kighelman [21] and in contrast to the behavior predicted in reference [24]. In addition, thin films display a lesser shift of the permitivity maximum with changing frequency as compared to bulk materials. In other words, thin film relaxor behavior as defined by the shift of the dielectric constant maximum with measuring frequency is *"underdeveloped"*.

The previous section indicated that disordered thin film PST specimens are similar to reported PST-DV ceramics with lead vacancies (figure 3.33), with the closest resemblance for PST on sapphire substrates. Unfortunately there are no published VF fitting parameter studies on PST-DV materials, presumably because these materials showed deviations from the VF law. Figure 3.34b displays the frequency versus $1/T_{max}$ for disordered PST thin films on sapphire substrate as compared to that observed for PMN thin films on sapphire substrates. It was not possible to fit the thin film data to a VF relation due to the "underdeveloped" relaxor behavior at low frequencies.

3.7.2   Ordered Films

The position of the dielectric maximum is very sensitive to even small degrees of order, jumping from 0°C or below (depending on substrate), to near 30°C corresponding with the dielectric maximum of highly ordered ceramic samples. Figure 3.35 shows the temperature of the dielectric maximum at 1 kHz and size of ordered regions (from X-ray analysis) versus S, the ordering degree of the material for 500 nm PST films on Pt/Si substrates. This trend is the same for ordered PST on all the studied substrates, an upward shift of the temperature of the dielectric maximum with increases "B" site order, the same behavior as commonly observed in ceramic and single crystal samples.
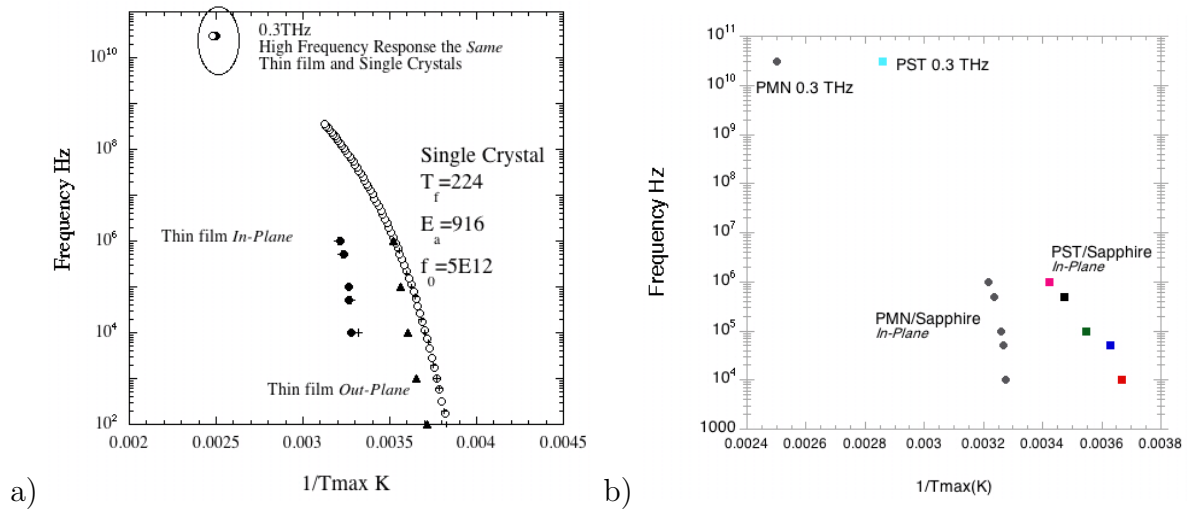
Figure 3.34: *Frequency versus $1/T_m$ (a) PMN Single crystal measurements and fitting parameters $T_f=224$ K, $E_a=916$ K, $f_o=5X10^{12}$ Hz, from reference [5] as compared to PMN thin films measured both "In-Plane" and "Out-of-Plane", and (b) PST and PMN thin films measured "In-Plane" on sapphire substrates from 10 kHz to 0.3 THz*
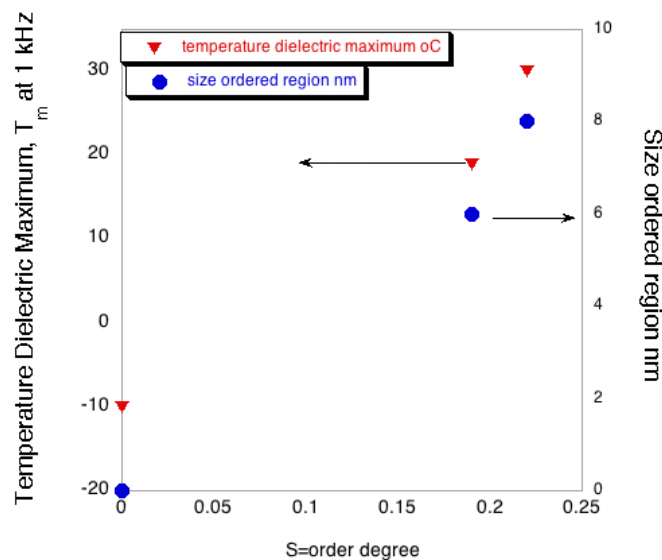
Figure 3.35: *Transition temperature and size of ordered regions for 500nm PST/Pt/Si*

3.7.3   Summary: Position of the Dielectric Maximum in Thin Film Relaxors

Disordered films show some similarities to their ceramic counterparts, including a shift *down* of the dielectric constant maximum to lower temperatures with lead deficiency (controlled by the quantity of excess lead added to the solution). In the case of PMN (considered a disordered material), the high frequency (THz) position of the dielectric maximum corresponds with that predicted from VF fitting of single crystals (from data in the range Hz to GHz). However, at lower frequencies the thin film behavior strongly deviated from the single crystal measurements (and fitting). Disordered PST films could not be compared directly with ceramic samples, however, they also showed strong deviations from VF functional dependance. In addition, the position of the dielectric maximum was found to shift *down* in temperature with tensile or compressive stress introduced by thermal expansion differences between the film and substrate. Ordered samples showed the same behavior as their ceramic and single crystal counterparts, an *upward* shift of the dielectric maximum with increasing B site order. In fact, the shift was found to be very sensitive to small degrees of order, indicating the ordered regions have a greater influence in thin films than the regions of disorder.

3.8   Low Temperature (20K) behavior of PST-O and D in MHz and GHz frequency range

A study of the low temperature behavior of ordered and disordered relaxors gives us an important reference, that of their intrinsic response. At 20K, most of the polar region response in PSTD and domain response in PSTO should be significantly reduced, there should be no frequency dispersion, and we should be able to take a rare look at a region where the properties are the *same*. This important reference can be used as a tool to

examine the different dielectric behavior we have been observing and discussing.

What should we expect for the dielectric response in this region? An estimate can be provided by Landau theory, using the Curie-Weiss constant determined above the phase transition to predict the low temperature lattice response of a PST ordered bulk specimen assuming a second order phase transition. This analysis gives a Curie Weiss constant of $C=2X10^5$ with Tc=-4°C . Estimation using $k = -\frac{C}{2*(T-Tc)}$ at 50K gives an estimated dielectric constant of 460. Measurements of a PST-O bulk specimen at 1 MHz resulted in a dielectric constant of 140 at 50K, significantly less than the estimated value. This difference can be understood as a deviation from the assumed 2nd order phase transition. As seen in figure (3.36), the transition of the ordered ceramic more closely resembles a 1st order phase transition, with a sharp drop of the dielectric constant at temperatures just under the phase transition due to the quick onset of spontaneous polarization. The theoretical ratio given by Landau theory for the slope of 1/k vs T below and above the transition temperature is 8, close to that observed in the ordered ceramic with a ratio of 6. Observations such as these, combined with the observed linear dependance of the transition temperature versus applied bias field has led several authors to conclude the PSTO posses a first order phase transition [128], [129].

There is however, one experimental discrepancy regarding a first order phase transition that needs to be addressed. Specifically, for a first order transition, the parameter β in the Landau expansion (equation 3.12) should have a *negative* value. In other words, the dielectric constant of the material should *increase* with increasing applied electric field in the paraelectric region. Experimental observations shows exactly the opposite effect, namely a *decrease* in the dielectric constant with increasing applied bias. However it may be possible that the β coefficient in the direction of polarization (111 in rhombohedral unit cell) can be *negative*, but that measurements on ceramics give an effective *positive* value due to: 1) residual disorder in the system, and 2) averaging behavior over many orientations in the ceramic sample.
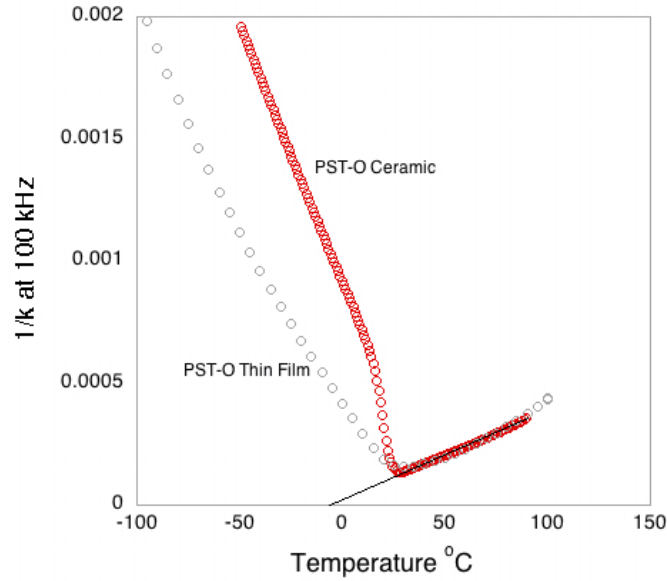
Figure 3.36: *1/k versus temperature at 100 Hz, Curie-Weiss behavior for a highly ordered PST ceramic data from [6] and an ordered PST thin film (S=0.9) on a sapphire substrate*

The other important issue regarding figure (3.36) concerns the nature of the phase transition in *ordered* thin film and ceramic samples. The thin film sample seems to more closely resemble a second order phase transition. The experimentaly determined slope of 1/k versus temperature is 3.5 for the thin film, closer to the prediction of *2* for a second order transition than of *8* for a first order transition provided by Landau theory. This raises the question, is there a physical mechanism which can account for a change of order in a phase transition between ceramic and thin films samples? This situation was investigated by Pertsev [111] and presented in the state of the art section (section 2.1.2.7, page 42), with the result being that *yes*, mechanical clamping of the film by the substrate may effectively change the order of the phase transition by making an effective β positive, when the original β parameter was a negative quantity. It should also be noted that such changes in the dielectric response below the dielectric maximum could be due to differences in domain patterns.

The dielectric constant values of both ordered and disordered PST films are near 400

at 20 Kelvin, close to the estimate provided by Landau theory for the lattice response from a second order phase transition. Figure 3.37a shows the dielectric constant and loss tangent versus temperature down to 20K at 1MHz. It is seen that at frequencies in the MHz range, and low temperatures near 20 K, the dielectric constant and loss tangent are the same for both ordered and disordered samples. However, in the Microwave range as shown in 3.37b there is a lower dielectric constant and a higher loss tangent exhibited in disordered samples.

An extended view is presented in figure 3.38a for disordered films and figure 3.38b for the ordered sample where the frequency dispersion of the dielectric constant is clearly seen between the MHz range and GHz range in the case of disordered PST. This experiment shows that at extremely low temperatures where the dielectric response is expected to be similar, the intrinsic difference between ordered and disordered PST thin films lies in the high frequency region. This dispersion in the high frequency region and intrinsic differences at the level of lattice vibrations will be explored further in the following chapter.
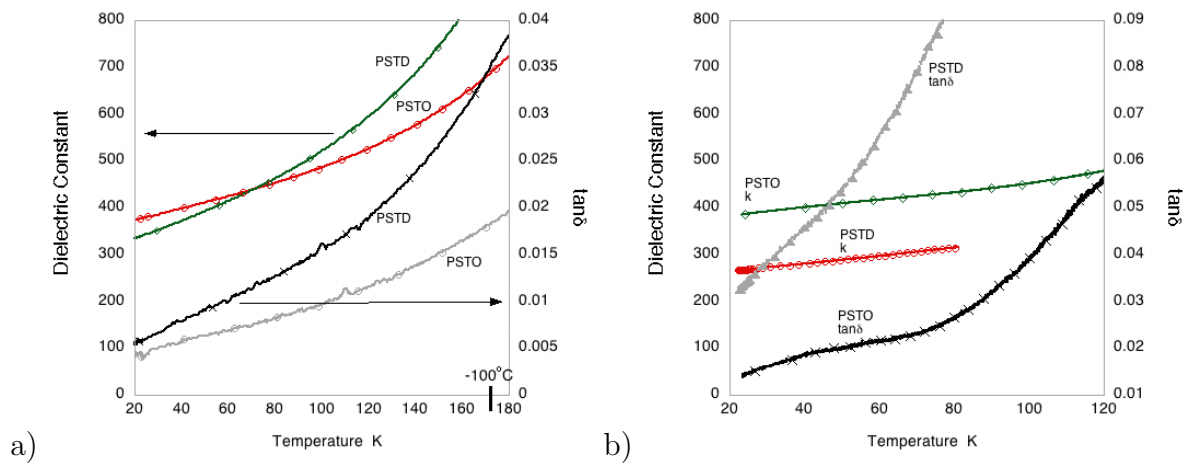
Figure 3.37: *(a) Dielectric constant and loss tangent for ordered (S=0.91) and disordered (S=0) PST films on sapphire substrates measured "in plane" using cryostat down to 20K at 1MHz and (b) 8GHz*
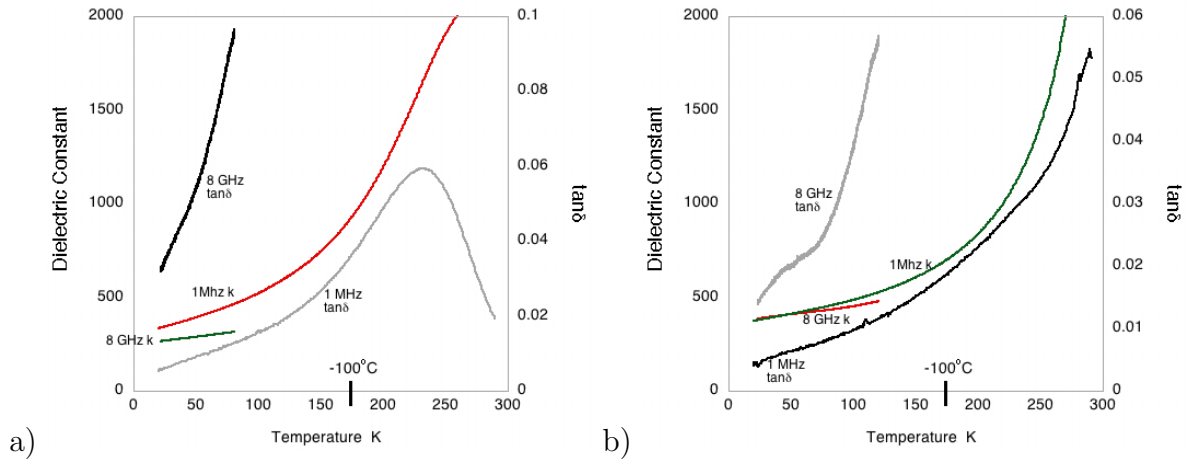
Figure 3.38: *Extended view from 300 to 20K of measured dielectric constant and loss tangent for (a) Disordered PST films (S=0) on sapphire substrates and (b) Ordered films (S=0.91) on sapphire substrates*

3.9 Field Cooling Investigations

PMN and PST relaxors have been shown to have induced phase transitions with the application of an electric field during cooling through the temperature of the dielectric maximum. The phase transition results in a long-range polar state with extrinsic contributions diminished from the formation of a monodomain state under large bias fields. Therefore, by studying field cooling, one can comment on the intrinsic versus extrinsic contributions to the observed permittivity. In the case of thin films, no phase transition has been observed on cooling, even under field levels greater than 100 kv/cm [4]. This section will explore the following questions by examining ordered and disordered PST films on sapphire substrates cooled to 20K through the dielectric maximum temperature under a DC bias: 1) can we induce a phase transition in relaxor thin films, and 2) if not, can we eliminate reduce the extrinsic effects by polar region alignment?

In both of the studied samples, *no* thermal hysteresis of the permittivity was observed upon cooling from room temperature to 20 K and back up to ambient temperatures. The results of field cooling on the disordered sample is presented in figure 3.39a where there is

seen a 20% reduction in the dielectric constant at 20K after cooling under a field level of 30 kV/cm (3 times higher than the coercive field of ordered samples at low temperature). Upon heating under zero field ZFH (zero field heating), the permittivity is lower than that observed during FC, indicating a reduction of polar region/extrinsic response. Near 220 K the aligned polar regions again become active and are seen to contribute to the dielectric response. However the room temperature permittivity is still 12% less than the value before application of the field. From these experiments it is seen that in disordered PST thin films, the application of an applied bias field during cooling *cannot* induce a long range ordered state. Even high field levels are insufficient to eliminate the NPR, or relaxor nano-domains which are supported by strong random fields.

The response of ordered PST is presented in figure 3.39b where it is seen the permittivity during FC is significantly less than the ZFC near the transition, although the low temperature 20K value remains the same. Upon heating under zero field (ZFH) the permittivity follows the FC curve until 225K where it again shows a higher response. The behavior in the case of the ordered sample is reminiscent of the removal of domain pattering and the formation of a single domain state under an applied bias. In the case of a single domain state induced by ZFH after FC, the dielectric response is due solely to the lattice, which may be evaluated using the previously discussed Landau parameters. However, an exact comparison cannot be made in this case because, although the film behaves qualitatively as second order phase transition, the value of the extrapolated transition temperature from the Curie-Weiss fit does not correspond to the actual transition temperature as in a conventional second order transition. Therefore, at temperatures close to the phase transition where differences are seen between ZFH and FC in figure 3.39b, the estimated values from the Landau expansion do not match those of the measured films.
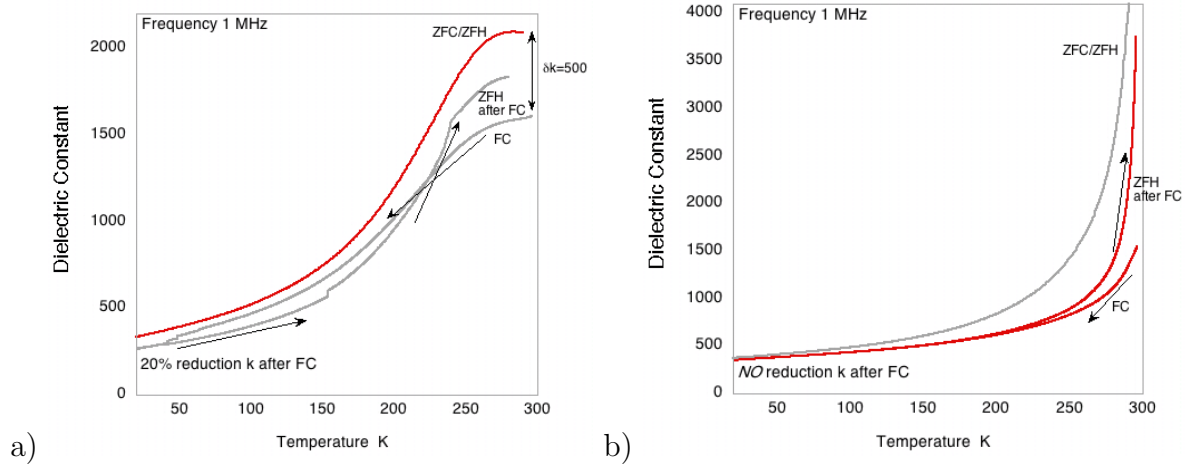
Figure 3.39: *Field Cooling investigations: (a) Dielectric constant of disordered (S=0) PST films on sapphire substrates measured upon 1) cooling under zero bias field (ZFC), and heating under zero bias field (ZFH), 2) cooling under bias field of 30 kV/cm, field cooling (FC), and 3) heating under zero bias field after field cooling (ZFH after FC), (b) Dielectric constant of ordered (S=0.91) PST thin films on sapphire substrate under condition: ZFC, ZFH, FC and ZFH after FC*

3.10 Summary of Dielectric Measurements: Analysis in terms of Challenges Posed in State of the Art section 2.1.3.2

An examination of the dielectric response of ordered and disordered PST thin films indicated that the dielectric maximum was significantly impacted by the level of "B" site order. In contrast to ceramic and single crystal samples which display a *decrease* in the value of the dielectric constant with an increase in "B" site order, thin film samples on a variety of substrate systems showed an *increase* in the dielectric constant with an increase in order. Highly ordered films also showed the development of a ferroelectric state comparable to their bulk counterparts.

The position of the dielectric maximum in ordered films was similar to that of ceramics

and single crystals *even* with low degrees of order and small ordered region size on a variety of substrates. However, the position of the dielectric maximum in disordered films was shown to be impacted by processing induced lead deficiency, as well as by stress in the films induced by thermal expansion mismatch between the film and substrate. Disordered films fabricated on sapphire substrates with the least amount of thermal induced stress showed a dielectric maximum temperature near that observed for ceramics with lead vacancies. The temperature of the dielectric maximum was shifted down for film under *both* tensile and compressive stress.

A thickness dependance of the dielectric constant was observed for disordered PST films on Pt/Si substrates measured *"Out-of-Plane"* with maximum dielectric constant values near 3000 for films over 1 micron in thickness. Analysis in terms of a passive layer indicated that this was probably due to processing induced lead deficient surface layers. These layers may reduce the observed dielectric constant in very thin films, but may not account for an order of magnitude reduction in the dielectric constant for micron thick films as compared to ceramic samples. Further studies showed that the *"In-Plane"* and *"Out-of-Plane"* dielectric constant was effectively the *same* for films near 700 nm in thickness. Since the *"Out-of-Plane"* response should be reduced compared to the *"In-Plane"* response in the presence of a passive layer, these experiments showed that the commonly observed low values of dielectric constant in relaxor thin films cannot be explained by a passive layer, at least in nominally thick films near 1 micron in thickness. With regards to the question posed in the State of the Art section (section 2.1.3.2, page 48), it seem that the large values of dielectric constant previously reported for PST thin films were due to ordering and not to effects such as a passive layer.

Extrinsic effects such as grain size and stress in the film were found to have little impact on the value of the dielectric constant in disordered PST thin films. Specifically, films with ≈ 140 nm grain size showed comparable properties with ≈ 3 micron grain size and even epitaxial films. Films processed on sapphire substrates with the least amount

of thermal induced stress showed higher values of dielectric constant as compared to similarly processed films on MgO or STO substrates, however, these small differences are insignificant when compared with an order of magnitude reduction of the dielectric constant of thin films as compared to ceramic and single crystal samples.

Analysis of the non-linear dielectric response in disordered thin films revealed a similar "crossover" in the field dependance of the dielectric constant as a function of temperature which was previously reported in PMN single crystals. In addition, the AC and DC field dependance of the dielectric constant was consistent with that observed in relaxors. However, unlike in ceramics and single crystals, a phase transition to a long range polar state could *not* be induced by the application of DC bias. Also, the position of the dielectric maximum as a function of measurement frequency did not follow the VF law as has been well documented for ceramic and single crystal relaxors.

The values of the dielectric constant at very low temperature (20 K) were the *same* for ordered and disordered thin films at 1MHz. However, disordered films exhibited a reduction in the value upon moving into the GHz region. Overall, highly ordered films showed dielectric behavior similar to their ceramic or single crystal counterparts. Their differences, such as a change in the order of the phase transition, could be explained in terms of mechanical effects due to the thin film state, and differences in domain patterns. Therefore, it seems that disordered PST films display essential features of relaxor behavior including the frequency dependance of the dielectric maximum and AC and DC field dependance, however it seems that their relaxor nature is "underdeveloped" as compared to ceramics, at least in the low frequency region and that the observed extrinsic factors do not account for these differences.

Chapter 4

Infrared Transmission Measurements of PST and PMN relaxor Thin Films

4.1 Introduction

By an examination of the high frequency dielectric response of thin films we would like to see if the "intrinsic" or lattice response is the same in thin film and bulk ceramic materials. Lattice dynamics of relaxors have recently been investigated in the classical PMN material system by inelastic neutron scattering (INS), where Naberezhnov [130] observed a transverse optic (TO1) phonon branch which softens on cooling to the Burns temperature $T_b \approx 620K$, along with the appearance of a strong central peak attributed to the formation of short range ferroelectric clusters (nano-polar regions). Subsequent INS experiments by Gehring [131],[132] on PMN single crystals revealed the TO1 branch dropping and merging with the transverse acoustic (TA) branch at a wavevector $q \approx 0.20$ Å^{-1}. At lower q values the TO phonon cannot be resolved from INS data and this rapid decrease/merging with the TA branch at a critical q was termed the "waterfall" effect, and was explained by the presence of polar clusters of a comparable size with the wavelength of the TO mode resulting in a critical overdamping of the mode. Wakimoto [133] [134] looked

at this behavior at lower temperatures and found the soft TO mode recovers/re-appeares below 220K with its frequency hardening according to the Cochran law (Curie-Weiss law for soft mode frequency behavior) with decreasing temperature according to:

$$\omega_{sm}^2 = A(T_b - T) \tag{4.1}$$

where ω_{sm} is the soft mode frequency in cm^{-1}, A is a constant cm^{-2}K^{-}1, T_b is the Burns temperature K (onset of polar nano-regions) and T is the measurement temperature K.

Hlinka recently [135] made measurements revealing one of the assumptions in the "waterfall" effect was not fufilled; namely, that the critical wavevector depended on the Brillion zone in which it was measured. The waterfall effect was then explained in terms of coupled damped harmonic oscillators and different dynamical structure factors in different Brillouin zones. However, whatever the origin of the unresolved TO phonon using INS, the question remains as to its behavior between T_b and T_f or T_c; that is between the onset of polarization fluctuations by polar nano regions T_b, and the temperature of freezing T_f inferred by the Völgel-Fulcher relation, or T_c the temperature at which PMN undergoes a phase transition upon heating after cooling under a critical bias field. Kamba measured FTIR reflectivity of PMN, PMN-PT and PZT-PT single crystals and found a well defined *underdamped* TO1 phonon from the center of the Brillouin zone between 10 and 530K [74]. As the wavelength of the probing IR radiation is long (Brillion zone center) q$\approx$10^{-5} Å^{-1} compared with the size of polar clusters, interactions such as in the INS measurements are not expected. However, FTIR data from reflectivity are difficult to fit in the range of the soft TO phonon due to noise and limited spectral resolution. Time-domain THz spectroscopy can give more reliable data with the amplitude *and* phase provided, but due to the thin samples (micron level thickness of single crystals) required for transmission, and the experimental difficulties, this area has only been recently investigated.

FTIR reflectivity has been used to study PST ceramics [136], both "B" site ordered and disordered between 20 and 500K. Interestingly no softening of the low TO mode was observed near the phase transition in either the Ordered or Disordered samples, and

the transition was inferred to occur thorough a order-disorder mechanism, whereas most ferroelectric perovskites proceed through a displacive mechanism. This is in contrast to the dielectric behavior, where the curie weiss constant C≈3X10^5 for ferroelectric PST-O is closer to values typicaly reported for displacive transitions (displacive transitions normally have up to 2 orders of magnitude greater C values)[14]. As in PMN studies, Pb anharmonicity was the most important cause of disorder, with the distribution of B site species not drastically affecting the lattice dynamics other than a weak mode near 315 cm^{-1} assigned to Sc-Ta vibrations.

The use of FTIR to study thin films has been performed on a variety of material systems including PZT, PLZT, and BST systems [137]. It is of interest for the present study that similar lattice dynamics were found in thin film PZT and PLZT as observed in the ceramic specimens. Specifically for PZT 75/25 there was observed similar softening of the TO1 mode (soft mode) near the the phase transition for thin films as compared to bulk ceramics. Softening of the TO1 phonon to the Burns T$_b$ temperature was observed in ceramic relaxor PLZT (8/65/35) compositions [138] and the behavior of this mode was attributed to the appearance of polar regions near the Burns temperature (620 K). The relaxation of these polar regions are thought to be responsible for the strong dielectric dispersion in the microwave and radio frequency regions below the Burns temperature and which give rise to to a new feature in the IR spectra below the frequency of the soft mode; the so called "central mode" or peak previously observed in neutron scattering experiments.

Studies of PMN single crystals [1] have shown that the central mode appears at the Burns temperature and splits into two components below room temperature; the first appears in the THz range and is attributed to IR activated phonon density of states due to the breaking of the local symmetry due to the presence of polar clusters, while the second relaxation arises from polar region motion which broadens upon cooling and leads to the frequency independent dielectric loss and broad distribution of relaxation times

discussed in the dielectric section. Due to experimental difficulties this central mode behavior has not, as of yet, been observed in thin film specimens.

Thin film specimens, therefore provide a opportunity for Transmission FTIR measurements to 1) fill in the gaps in data concerning fundamental relaxor behavior, and 2) compare the lattice dynamics in thin films with ceramic and single crystal specimins.

4.2   Experimental

In order to perform transmission FTIR measurements of the thin films a transparent substrate with no electrodes is required. As the soft TO phonon modes occur below 100 cm^{-1}, MgO, LaAlO$_3$, and sapphire are commonly used substrates which are possible candidates. Sapphire provides the best transmission characteristics with an upper transmission limit of at least 250 cm^{-1} depending on the temperature. PST films with varying degrees of "B" site order and PMN films were prepared on sapphire substrates with a nominal thickness of 500 to 600 nm.

The spectra were taken using a FTIR spectrometer Bruker IFS 113v at temperatures between 20 and 900K with a resolution of 0.5 cm^{-1}. A highly sensitive helium cooled Si bolometer operating at 1.5K was used as a detector. Temperature control was accomplished using an Optistat CF cryostat with polyethylene windows for cooling, and a commercial high-temperature cell SPECAC P/N 5850 for heating.[1]

Figure 4.2 displays the transmission spectra of a bare sapphire substrate showing appreciable IR transmission even at elevated temperatures in the region of the low frequency TO phonon. The interference pattern is produced from the interference of transmitted and reflected waves and with the periodicity inversely proportional to the index of refraction of the material. The spectra of the bare sapphire substrate and substrate with

---

[1]All of the measurements and fitting of the experimental data presented in this chapter were done in collaboration with Dr. Stanislav Kamba and colleagues at the Institute of Physics, Prague, Czech Republic

film were taken measured for each of the studied temperatures. The transmission spectra were first fitted with a sum of harmonic oscillators using Fresnel formulae for coherent transmission of the sample including interference effects. The resulting parameters of the sapphire at each temperature were then employed in the fit of the Film/Sapphire two-layer system. The complex transmittance of the two layer system was calculated using the transfer matrix formalism method including interference effects [139].

The complex dielectric response [2] determined as the sum of damped quasi-harmonic oscillators was calculated using expression4.2:

$$\varepsilon^*(\omega) = \varepsilon'(\omega) - \mathrm{i}\varepsilon''(\omega) = \varepsilon_\infty + \sum_{j=1}^{n} \frac{\Delta\varepsilon_j \omega_j^2}{\omega_j^2 - \omega^2 + \mathrm{i}\omega\gamma_j} \tag{4.2}$$

where ω_j, γ_j and $\Delta\varepsilon_j$ denote the eigenfrequencies, damping and contribution to the static permittivity from the j-th polar mode, respectively. ε_∞ describes the high-frequency permittivity originating from the electronic polarization and from polar phonons above the spectral range studied.The high-frequency permittivity ε_∞ resulting from electronic absorption processes was obtained from the frequency-independent room-temperature reflectivity above the phonon frequencies. The temperature dependence of ε_∞ is usually very small and was neglected in the fit.

4.3   PMN Spectra and Fitting

The FTIR transmission spectra of a PMN film on sapphire substrate is presented in figure 4.2 at selected temperatures between 20 and 900K. The oscillations in the spectra are due to interference phenomena in the substrate (see bare substrate figure 4.2) whereas the broad minima correspond to frequencies of polar phonons in the PMN film. The transmission decreases on heating due to the increase of phonon damping in the sapphire substrate resulting in opacity at high temperatures and high frequencies (above $150 \, \mathrm{cm}^{-1}$).

---

[2]In this chapter the notation for dielectric constant k, is changed to relative permittivity ϵ; and the loss k", is changed to ϵ"
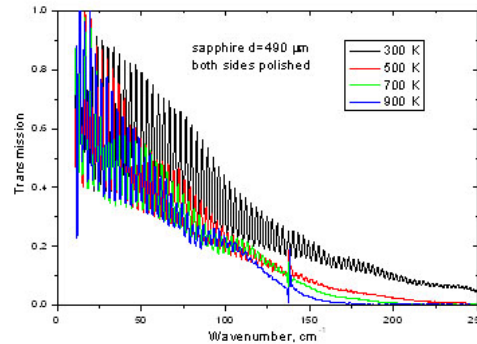
Figure 4.1: *Tranmission spectra of 0.5mm thick sapphire substrate from 300 to 900K*

The real and imaginary dielectric response calculated using equation (4.2) are displayed in figure 4.3. As the absorption of incident radiation corresponding with the energy of a phonon creates a peak in the dielectric loss spectrum, let us first look at the loss spectra as it evolves from a high temperature to a low temperature state. Two absorption peaks termed TO1 and TO2 appear at 55 and 230 cm^{-1} in the 900K loss spectrum. The high frequency phonon TO2 intensity increases upon cooling due to reduced phonon damping and finally splits into three parts below room temperature probably due to the change of infrared selection rules in polar clusters combined with the further decrease of phonon damping.

The TO1 low frequency phonon decreases in frequency or "softens" from 900 to 700K at which temperature there was observed a new excitation below the TO1 frequency termed a Central mode (CM). Between 700 and 400K the TO1 frequency levels off near 55 cm^{-1} before following the Cochran law below 400K as seen in figure 4.4. The estimated Burns temperature T$_b$ from the soft mode behavior is 703K, slightly higher than the commonly reported value of 620K for single crystal specimens. The damping of the soft mode remains constant at 50 cm^{-1} with respect to temperature variations. Although heavily damped, it remains *underdamped* and observable in the observed temperature range, in contrast to neutron scattering experiments.
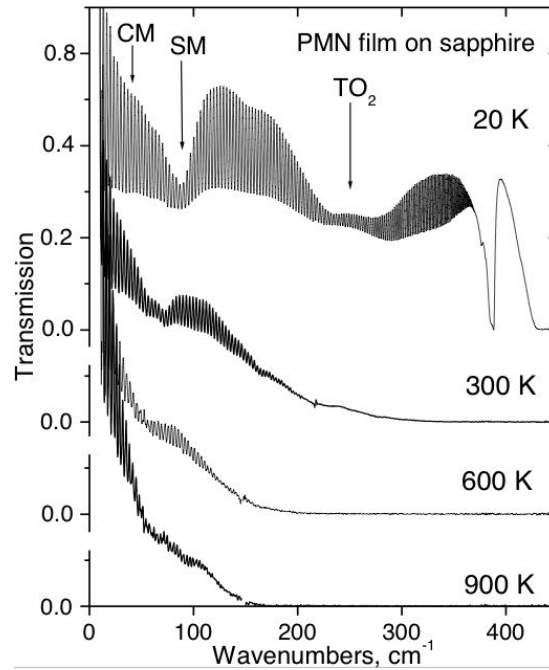
Figure 4.2: *500 nm PMN film on sapphire substrate, transmission spectra from 20 to 900K*

The CM appearing at the Burns temperature was fitted with an overdamped oscillator, and is seen to be the dominating factor for the observed increase in ϵ' and ϵ'' upon cooling to 300K analogous to previous observation with neutron scattering. The origin of this peak is the relaxation and motion of polar regions formed upon cooling below the burns temperature. At temperatures below the dielectric maximum the CM rapidly decreases as the relaxation freeze out to a broad frequency independent distribution of relaxation frequencies at low temperatures. Since our FTIR studies at low q revealed an underdamped soft TO1 phonon at temperatures between T_b and T_c, and Hlinka [135] showed that the waterfall effect is not necessarily related to scattering from polar regions, It is believed that this phenomena is related to the screening of the SM by the CM peak. Figure 4.5 presents the recalculated INS spectra from our FTIR data following $I(\omega)$ which is proportional to $\epsilon''(\omega)/\omega$. It is seen that a phonon peak is seen near 7meV at 900 K but is screened by the CM mode contribution until the CM contribution freezes out at lower
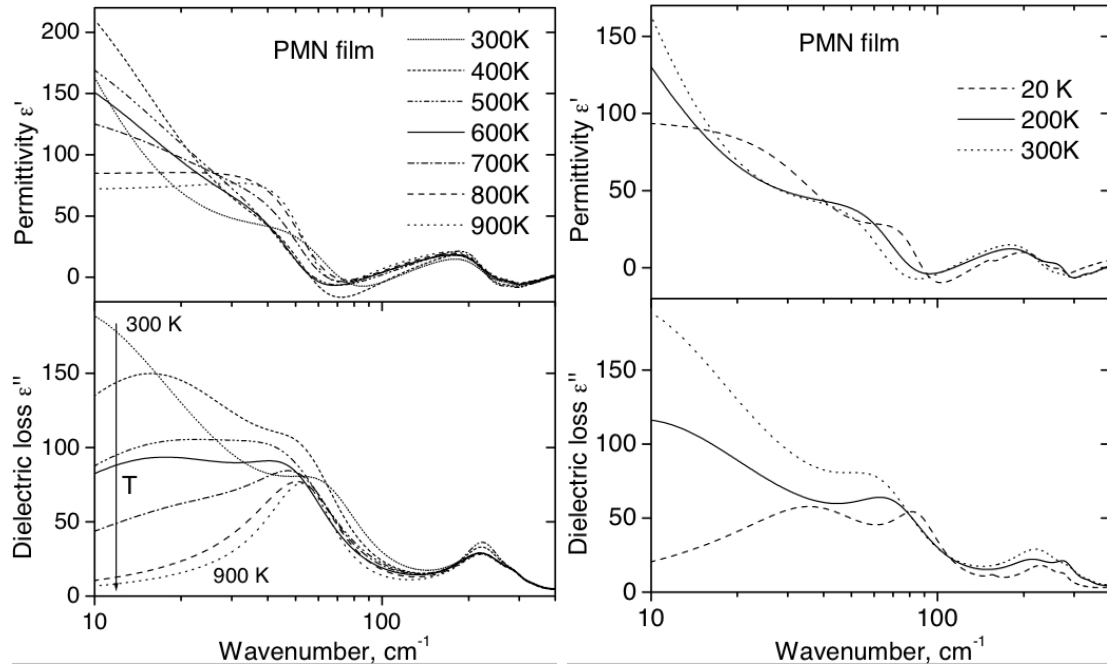
Figure 4.3: *500 nm PMN thin film on sapphire substrate, real ϵ' and imaginary ϵ'' permittivity at high and low temperature*

temperatures allowing the SM to be again resolved and re-emerge in the spectrum at 11 meV at 20K. Although this simple analysis does not include temperature and structure factor influences on the intensity of INS spectra, it clearly shows the impact of the central mode and polar regions as the source of the experimental discrepancies between the two techniques.

The picture of relaxor dielectric response as a hypothesized relaxation of polar nanoregions which contribute an enormous extrinsic portion to the measured permittivity at low frequencies, is seen to extend all the way to THz frequencies just below the lattice response. In normal ferroelectrics the lattice contribution to the permittivity increases upon cooling to T_c as the low frequency phonon softens. Below T_c the permittivity is comprised of *intrinsic* lattice (Curie-Weiss behavior with P_s) and *extrinsic* domain wall contributions, however the extrinsic contribution is absent in the high frequency range (above 1 GHz). To understand relaxor ferroelectrics from a dynamic standpoint in this framework,

we replace T_c by T_b, and extend the extrinsic contributions into the THz range. In other words, we have softening of the low frequency phonon to T_b burns temperature (and NOT to the phase transition temperature) where there is the appearence of polar regions whose dynamics create the central relaxation peak. The motion of the polar regions are responsible for the deviation in Curie-Weiss behavior for relaxors and their large low frequency contribution to the dielectric permittivity. The intensity of the central relaxation peak decreases at temperatures below the dielectric maximum , however there is still an extrinsic contribution to permittivity and loss even at 20K in relaxors where normal domain wall motion in ferroelectrics would be frozen out.
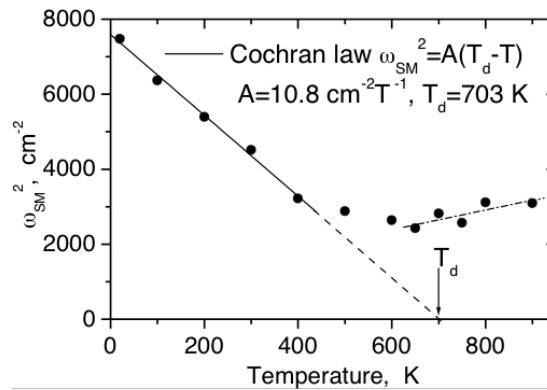
Figure 4.4: *Soft mode behavior corresponsing to the Cochran law in PMN thin film on sapphire substrate*

In Summary: FTIR transmission of PMN thin films allowed the observation of the soft TO1 phonon mode at temperatures between T_b and T_c where it was previously 1) difficult to observe in Bulk/Ceramic reflectivity measurments, and 2) where is was un-observed by neutron scattering. The experiments showed the phonon as underdamped at all the observed temperatures, and who obeys the Cochran low below upon heating to 400K, with subsequent hardening above the Burns temperature T_b. The appearance of a new mode at frequencies below the soft TO1 mode was observed at the Burns temperature and related to the dynamics of polar regions. The behavior above T_b and below T_c is similar
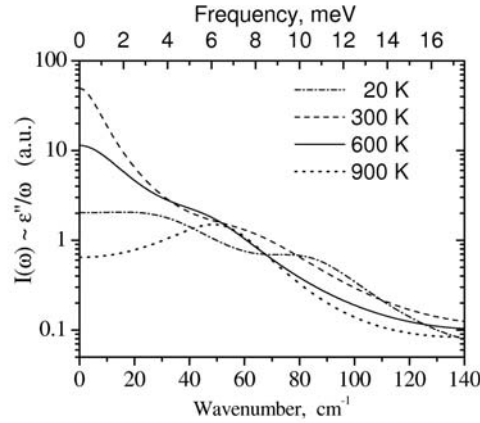
Figure 4.5: *The simulation of INS neutron scattering from FTIR data as $\epsilon"(\omega)/\omega$ of PMN thin films on sapphire substrate*

neutron scattering results of single crystals, and the waterfall effect where the soft TO1 is not observed in neutron scattering is explained as a result of CM screening of the SM response. Next let us consider how PST materials fit with this picture, and examine the link with chemical ordering and relaxor characteristics at the level of lattice vibrations.

4.4   PST Spectra and Fitting

4.4.1   PSTD

Figure 4.6 shows the spectra of disordered PST-D films on sapphire substrate, showing the same general features of substrate oscillations and broad minimum corresponding to phonon absorption as seen in the case of PMN. Figure 4.7 displays the fitting or real and imaginary parts of permittivity as a function of temperature. Let us again look at the phonon behavior via the dielectric loss upon cooling from 900K. At high temperatures there are two major phonon modes observed TO1 near 50 cm^{-1} and TO2 near 210 cm^{-1}. The TO2 phonon is stable with respect to position as a function of temperature and like the PMN sample, displays increased intensity with cooling due to lower damping.

The low frequency phonon TO1 decreases in frequency (softens) with decreasing temperature from 900 to 700 K, where a new broad central mode CM absorption appears near 30 cm^{-1}. The TO1 phonon then hardens upon decreasing from 500 to 200K according to the Cochran law with an estimated Burns T$_b \approx$737 K as seen in figure 4.8. A convenient way to see the mode frequency temperature behavior is presented in figure 4.11, presented for both PST-O and PST-D for low frequency modes below 100 cm^{-1}.

As seen in figure 4.11 below 200K the TO1 phonon split into two branches with one branch continuing to follow the Cochran law. The CM which appears near the estimated T$_b$=737 K, decreases in frequency (softens) upon cooling eventually disappearing from the spectra near the estimated freezing temperature for the system 275 K. Below this temperature a new absorption appears at 30 cm^{-1} which is temperature independent down to 20K and thought to be associated with the activation of phonon density of states.

The features seen in disordered PST thin films are therefore similar to those observed in PMN thin films and PMN single crystal relaxors, with the appearance of a Central mode at the estimated Burns temperature associated with polar regions, and the subsequent decrease of the central mode, eventually disappearing form the spectrum at the freezing temperature of the system. In addition, a new temperature independent mode near 30 cm^{-1} was observed in both systems thought to be a result of an activation of phonon density of states as a consequence of the breaking of translational symmetry in the low temperature polar phase. Thus from the standpoint of lattice dynamics, our disordered PST thin films resemble the traditional PMN relaxor system in both thin film and single crystal material forms. Let us next look at the effect of "B" site ordering on the lattice dynamics of PST.
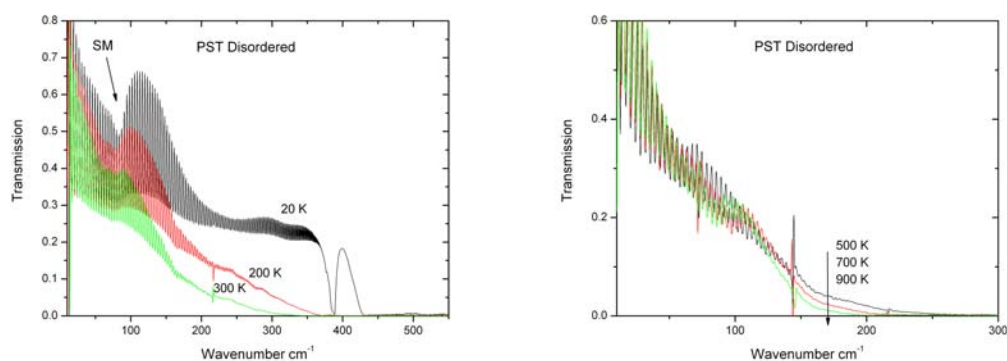
Figure 4.6: *High and low temperature spectra for 550nn PSTD at 700°C for 1 minute on sapphire*
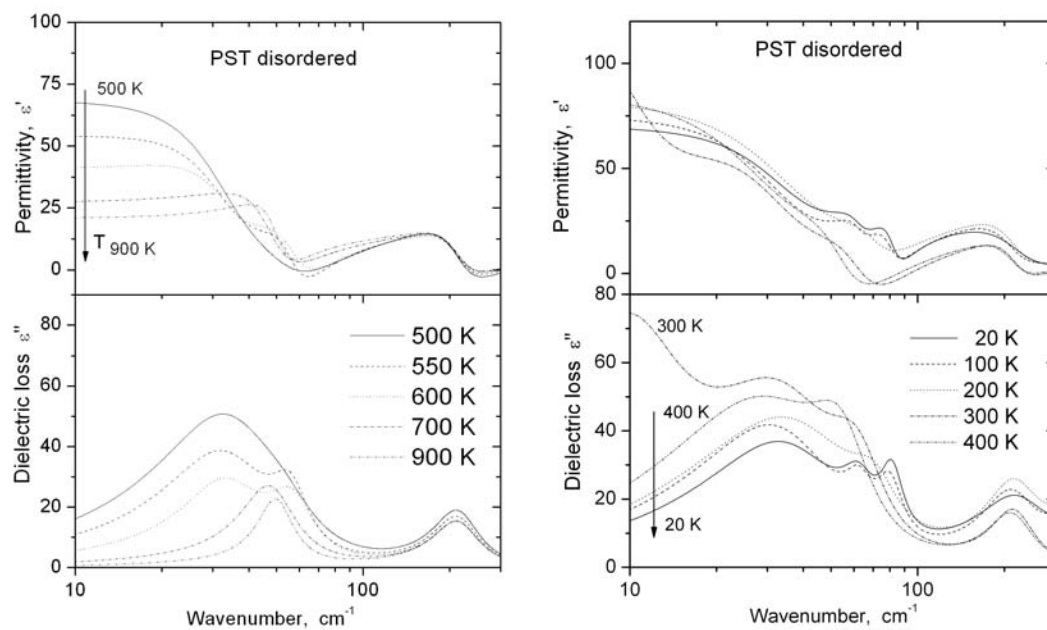
Figure 4.7: *High and low temperature fits of ε' and ε'' 550nm PSTD thin film annealed at 700°C for 1 minute on sapphire substrate*
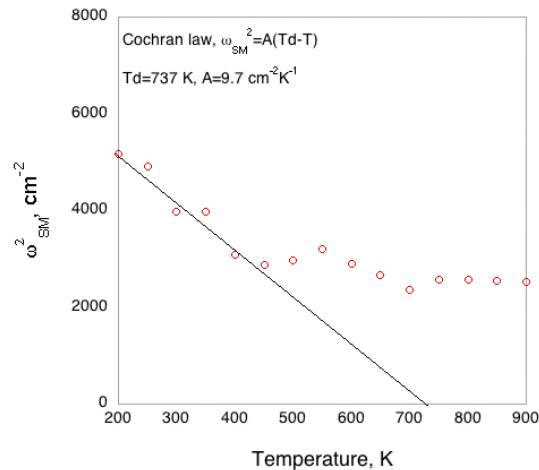
Figure 4.8: *Soft mode behavior for 550nm PST-D thin film, corresponding to Cochran Law from 500 to 200 K*

4.4.2   PSTO

In the case of perfectly ordered PST materials, we would expect normal ferroelectric behavior, that is Curie Weiss behavior down to the transition temperature with the appearance of spontaneous polarization resulting from a macroscopic transition to the polar rhombehdral state. In terms of the lattice response this would translate into a softening of the low frequency phonon towards T_c for the case of a displacive transition. From previous studies using FTIR reflectivity, we have seen a relatively temperature independent "soft mode" in the case of both ordered and disordered samples, however transmission measurements which are more sensitive below $100cm^{-1}$ in the range of the soft mode reveled a low frequency phonon softening to the burns temperature and Cochran law behavior below 500K; the origins of this discrepancy are not completely resolved, however the striking similarity of the PST-D thin film response (observation of CM, SM behavior etc..) in comparison with PMN in the thin film and single crystal form suggest that the transmission measurements are indeed more reliable than reflectivity and allow for a clearer picture of the phonon response below 100 cm^{-1}.

Figure 4.9 displays the spectra for 80% ordered PST-O on sapphire substrate pro-

cessed at 800°C for 48 hours. New spectral features are observed in comparison with the "disordered" PST and relaxor PMN samples including 1) a more pronounced broad minimum near 50 cm^{-1} in the high temperature range above 500 K, and 2) an absorption near 350 cm^{-1} which is forbidden in a disordered material. The more pronounced minimum is due to the increased phonon absorption intensity in ordered samples, while the peak near 350 cm^{-1} is attributed to coherent Sc-Ta vibrations [136].

The spectra of dielectric loss as a function of temperature reveal 1) a temperature independent TO2 phonon near 210 cm^{-1} which splits into two components at low temperature due to a change in local symmetry, 2) Surprisingly in a highly ordered material the appearance of a broad central mode CM at 700K. As the fitting results are a sum of individual mode contributions, again a look at the individual mode components in figure 4.11 allows for a clearer perspective. It is striking that a comparison of highly ordered and disordered materials display such similar qualitative lattice dynamic behavior including a low frequency mode softening to a temperature where there is the appearance of a broad central mode.
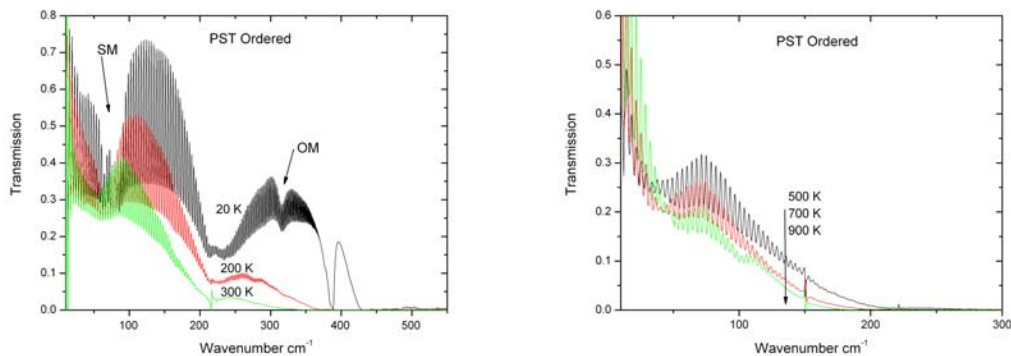
Figure 4.9: *High and low temperature spectra 550nm PSTO (S=0.78) thin film annealed at 800°C for 48 hours on a sapphire substrate*

A more detailed look at the TO1 and CM mode contribution are presented in figure 4.12 displaying the damping of the TO1 mode, and the dielectric strength of both the TO1
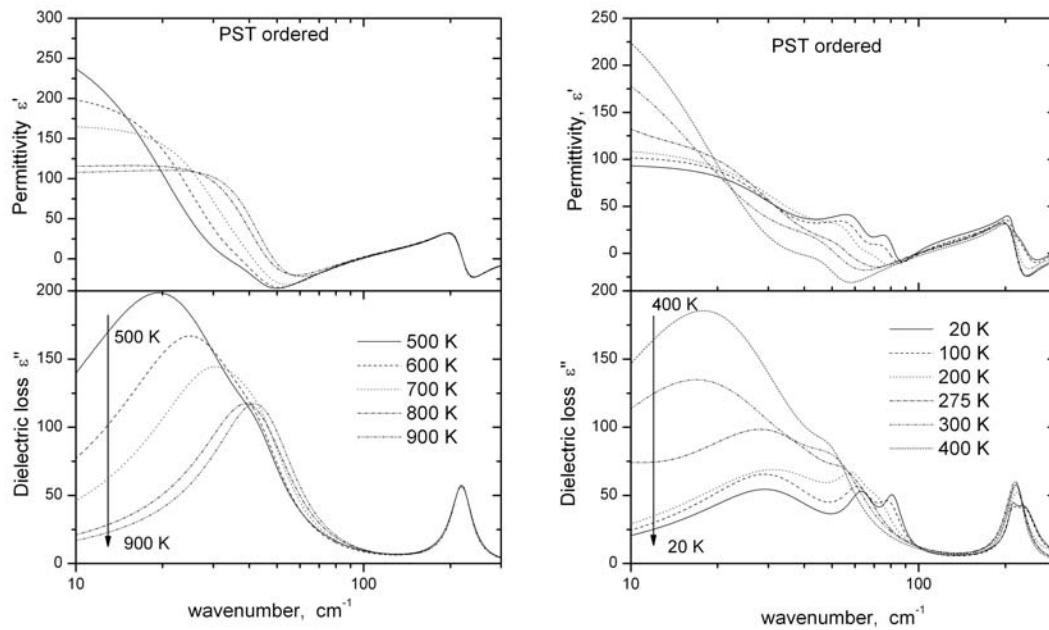
Figure 4.10: *High and low temperature of ϵ' and ϵ' ' for PST-O (S=0.78) on sapphire*

and CM mode as a function of temperature. The damping of the TO1 mode decreases with decreasing temperature exhibiting only a peak near 350 K due to the appearance of the new mode near 30 cm^{-1} in the case of ordered PST-O. In contrast the disordered sample exhibits an increase in the TO1 damping, with an relatively constant value near 40 cm^{-1} between the burns (T$_b$=737 K) and 200 K, below the freezing temperature of the system. The dielectric strength of the TO1 soft mode also displays significant differences as a function of ordering. The highly ordered PST-O sample shows the maximum dielectric strength of 110 near 800 K as the mode softens to T$_b$ Burns temperature, below which it decreases to values near 20 independent of further cooling. As expected, the disordered PST-D sample in contrast displays a lower soft mode contribution, possessing values below 20 at all temperatures. Again, a surprising result arises from looking at the dielectric strength of the central mode CM. As was expected in the case of the disordered PST-D

sample the CM contribution arising form polar regions at the Burns temperature increases with cooling until rapidly slowing down at the freezing temperature. However, rather unexpectedly is the result of the ordered sample display similar CM and SM dielectric strength at 700 K (Burns temp), with the CM contribution being 12 times greater than the SM at 400 K. This striking feature provides insight into the nature of the "disordered" regions.

In the case of the highly ordered sample (80% ordered) only approximately 20% volume is occupied by disordered regions. If we assume that the polar region response is concentrated in these polar regions (with ordered regions behavior as a normal ferroelectric), it is seen that quantitatively the disordered regions in the ordered sample which was processed at higher temperature show a much greater response than disordered regions processed at a lower 700°C , and below the temperature of formation (T_b Burns temp) of these regions they completely dominate the dielectric response, even though they only comprise 20% of the material.

In summary: while low frequency dielectric measurements revealed normal ferroelectric behavior in highly ordered samples, FTIR studies probing the lattice and high frequency response showed that in fact they have characteristics of both ordered and disordered materials, with qualitatively similar lattice response to traditional PMN relaxors in bulk and thin film including the formation of polar regions at temperatures above the dielectric maximum leading to a broad central peak relaxation which dominates the high frequency dielectric response between T_b and T_f.

4.4.3   An Ordering Study

In addition to highly ordered and disordered samples, varying degrees of order induced by processing at 850°C for 1 minute and 1 hour (low frequency dielectric measurements presented in section 3.5.3, page 131) were investigated below room temperature and the spectra are presented in figure 4.13. In both samples the low frequency soft mode absorp-
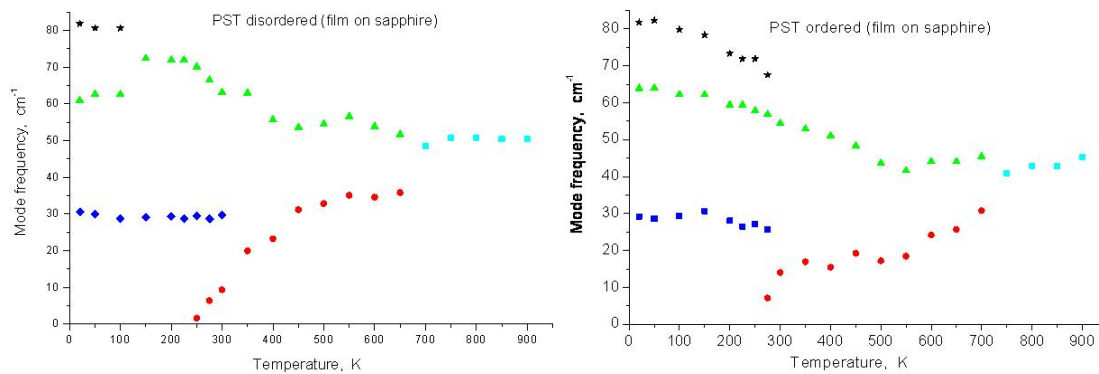
Figure 4.11: *Mode frequency as a function of temperature for PST-O and PST-D*
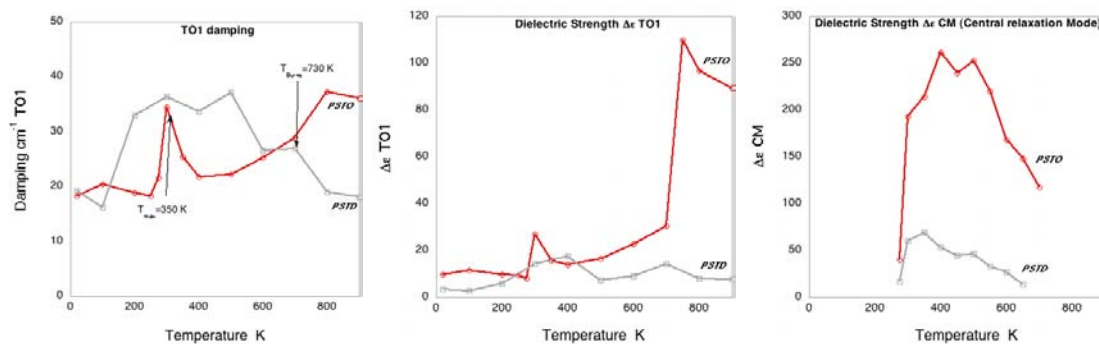
Figure 4.12: *Dielectric strength of TO1 and CM, and damping of TO1 versus temperature for PSTO and PST-D*

tion hardens all the way to 20K and the main spectral difference is the ordered absorption peak near 300 cm^{-1}in the sample with 50% order heated to 850°C for 1 hour. Fits of the spectra are shown in figure 4.14 above 100 cm^{-1}. It is clearly seen that the disordered sample's response (700°C) is relatively featurless in this range, while the sample processed at 850°C for 1 minute (disordered according to X-ray, with a temperature shift characteristic of an ordered sample from low frequency dielectric measurements) shows an absorption at 200 cm^{-1} not seen in the disordered sample, as well as a shoulder absorption below 200 cm^{-1}. As in the dielectric section presenting low frequency loss of this sample, it seems to *feel* the presence of both ordered and disordered regions even into the THz range (this

composite type effect was seen in low frequency dielectric measurements in section, 3.5.3, page 131). As the ordering increases, the damping of the 225 cm^{-1} phonon absorption decreases and the intensity of the peak near 300cm^{-1} corresponding to coherent Sc-Ta vibrations increases.
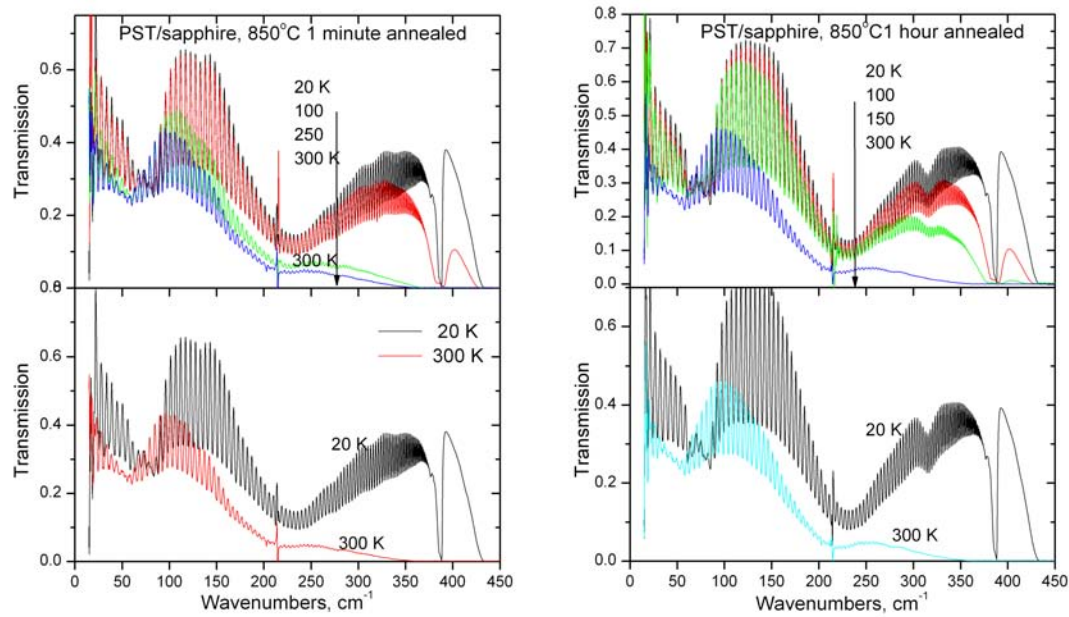
Figure 4.13: *Intermediate ordering states in PST thin films on sapphire substrates annealed at 850°C for 1minute and 1hour*

4.5   Discussion and Comparison with Low Frequency Measurements

It is interesting to compare the low temperature 20K measurements at THz with those in the GHz and MHz range presented in the dielectric chapter. In the case of the disordered sample (700°C) the real part of the permittivity decreased 20%, from 334 to 266, and as
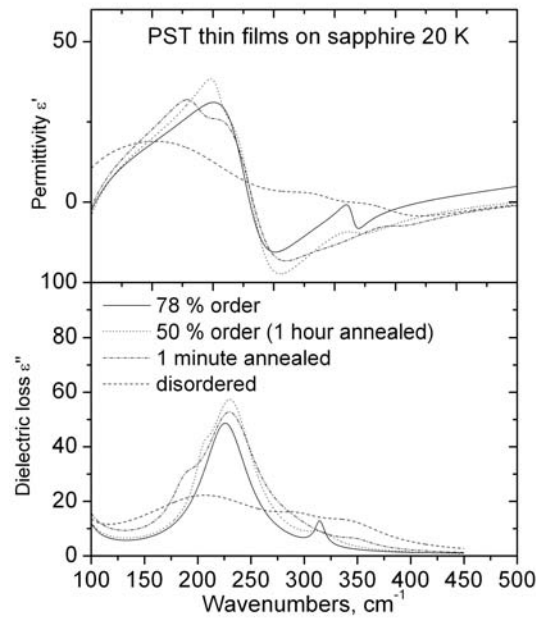
Figure 4.14: *Fits of ϵ' and ϵ'' for PST thin films on sapphire substrates with varying degrees of B site order*

the frequency increased from 1MHz to 8 GHz at 20K. From fits of the spectra measured at 20K the 3THz value of the permittivity was estimated to be near 70, which is over a 70% decrease from the value in the GHz range. This surprising result suggests significant dispersion in the GHz range, even as qualitatively the central mode CM responsible for polar region dynamics is freezing out at this temperature.

In the case of the highly ordered sample the permittivity was 400 independent of frequency below 8 GHz at 20K, consistent with estimates of the lattice contribution to permittivity for a second order phase transition. However, the THz permittivity was estimated at just less than 100, a 75% reduction in value as we move from 8 GHz to 300 GHz. This remarkable dispersion in the high GHz range suggests that the ordered regions lattice response dominate the low frequency dielectric response, but at the THz level
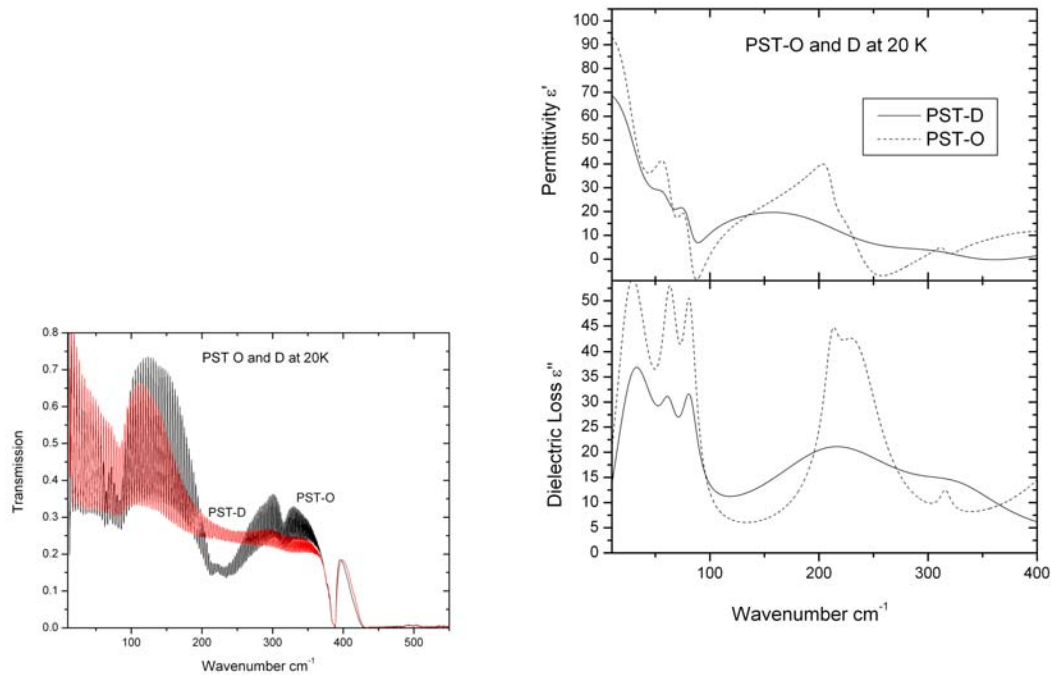
Figure 4.15: *PST-O (S-0.78) and PST-D at 20K spectra and fits of ϵ' and ϵ' '*

where the overall behavior was seen to be qualitatively similar to a disordered material, the residual 20% of remaining disordered regions and their dynamics dominate at high frequencies.

In terms of lattice dynamics, *both* ordered and disordered PST thin films showed unexpectedly the *same* features including TO1 mode softening to the Burns temperature wtih the simoltaneous appearance of a central mode (CM). Higher processing temperatures were shown to increase the dielectric strength of the central mode attributed to the dynamics of nano-polar regions (NPR).

Chapter 5

Pyroelectric and Piezoelectric Properties

5.1 Pyroelectric, Piezoelectric and Electrostrictive Fundamentals

5.1.1 Pyroelectricity

Pyroelectric measurements are a convenient way to measure the inherent polarization in a material, and the pyroelectric effect has been the basis for a number of applications such as photoacoustic gas detection, and thermal IR radiation/motion sensing[140]. In traditional pyroelectric elements, a non-centrosymmetrical material (ferroelectric phase) is exposed to a change in temperature, which produces a current through the variation of the materials spontaneous polarization. However, a pyroelectic current can also be induced by the application of a DC bias in a centrosymmetric (cubic) material. This effect is especially large near the phase transition due to the large change in dielectric constant with temperature ($\frac{\delta k}{\delta T}$). Formally, the pyroelectric coefficient in this case is described by:

$$p = \frac{dP_s}{dT} + \epsilon_o \int_0^E (\frac{dk}{dT})_E dE \qquad (5.1)$$

where p is the pyroelectric coefficient C/m^2K, P_s is the spontaneous polarization, T is the temperature, ϵ_o is the permittivity of free space 8.85×10^{-12} F/m, k is the dielectric constant of the material, and E is the electric field bias V/m.

An additional advantage to working above the transition temperature (paraelectric phase) in ferroelectric materials under DC bias is the lower loss values, and higher figure of merit/responsivity due to the absence of domain wall motion. The detectivity figure of merit F_D is commonly used to describe the signal to noise ratio since in the low frequency range (100Hz) where the noise is dominated by the lossy capacitance of the detector element, and is defined by [61]:

$$F_D = \frac{p}{c(k\epsilon_o \tan\delta)^{1/2}} \tag{5.2}$$

5.1.2   Piezoelectricity

The development of charge from mechanical stress, or an electric field defines a piezoelectric material. In thin films the converse piezoelectric effect describes the strain that is developed in a piezoelectric material due to the applied field by:

$$x_{ij} = d_{kij}E_k \tag{5.3}$$

where x is the strain developed in the material, d is the converse piezo coeff m/V, and E is the electric field V/m.

The electrostrictive effect is present in all materials and results from a coupling of elastic and electric fields described as:

$$x_{ij} = M_{ijmn}E_mE_n = Q_{ijmn}P_mP_n \tag{5.4}$$

where M (m^2/V^2) and Q (m^4/C^2) are the electrostrictive coefficients, P is the polarization (C/m^2), and E is the electric field (V/m).

From equation (3.1, page 101) we arrive at the relationship between the coefficients M and Q as:

$$M_{ijpq} = \chi_{mp}\chi_{nq}Q_{ijmn} \tag{5.5}$$

There is a piezoelectric analogue to the induced pyroelectric effect; a DC bias superimposed on a weak simultaneously applied AC field results in a electric field induced piezoelectric effect, regardless of the material symmetry. This is seen by writing equation 5.4 as [116]:

$$x = M(E_{DC} + E_{AC})^2 = ME_{DC}^2 + 2ME_{DC}E_{AC} + E_{AC}^2 \qquad (5.6)$$

where the term $(2ME_{DC})E_{AC}$ behaves like the piezoelectric effect, with an effective piezocoefficient d$\approx$2ME_{DC}, and a linear strain response with respect to the AC field, including a change of sign with the direction of applied field. Contrary to most material systems where this induced piezoeffect is small, relaxor ferroelectric systems display a large response and are of particular interest because of the linear response due to their lack of hysteresis.

5.1.3   PST Pyro and Piezo Properties

PST has long been a candidate for the bolometer mode/induced pyroelectric effect due to its near room temperature phase transition. Table 5.1 displays the major publications for pyroelectric properties for PST thin films in comparison with PbTiO$_3$ and PZT thin film materials employing the ferroelectric phase pyro effect. A recent review by Muralt is an excellent source of information for bulk and thin film pyroelectric properties, including device physics and processing of infrared detectors[140]. There are only two reports on the piezoelectric properties of PST thin films the author is aware of, both reporting AFM determined local piezo coefficients of 13-15 pm/V at applied fields near 100kV/cm [141], [142].

A striking feature of table 5.1 is the column labeled p_{self}, the pyroelectric coefficient at 0 applied bias which is forbidden in a centrosymmetric crystal class (PST above its phase transition). This effect is often termed "self-polarization" or "internal-bias" and has been seen in a number of thin film systems. Most recently, Kighelman reported on the effects of self polarization on the piezo and electrostrictive properties of PMN thin films[21] with

unbiased pyroelectric coeffcients of 50 μC/m²K. Shvartsman [143] used Scanning force microscopy on PMN-PT films to image piezoelectrically active regions (those under self bias) which indicated self polarization occurs in only part of the grains (20 to 25%). In table 5.1 we see significant a differences of p$_{self}$ versus processing conditions. In the case of sol-gel processed films the authors observed a fixed polarization layer with a polar direction *opposite* to that of the applied field, while in CVD and sputtered films the direction of the fixed polarization layer is in direction with the applied field with very large values (at time 3/4 of the reported true pyro response for PST). If one defines a effective pyroelectric coefficient p$_{eff}$ as:

$$p_{eff} = p - p_{self} \tag{5.7}$$

one sees that the effective pyrocoefficient for sputtered and CVD films are the same at 360μC/m²K, with the low value for sol-gel derived film of 279 probably due to poor film quality as evidenced by its low dielectric constant ($\approx$ 500) and high loss tangent (>4%).

Another important feature of table 5.1, is the induced pyroelectric coefficient of $\approx$6000 μC/m²K at 40 kV/cm bias reported in [48]. This unusually high value was reported for 1.5 micron sputtered PST on sapphire substrates annealed at 900°C , measured "in-plane" with 100 micron gaps in an interdigitated electrode structure (applied DC bias 400V). By high temperature annealing inducing an un-estimated degree of B site order the authors produced a film with a dielectric maximum of near 7000 at 2°C (low frequency Hz level). The S=0.91 ordered films synthesized in this work of PST/sapphire also displayed zero field bias dielectric constant near 7000 with the dielectric temperature maximum near 30°C (similar to bulk ceramic materials). A comparison of the dielectric constant versus temperature behavior above the phase transition in this work versus [48] reveals a ratio of Curie Weiss constants C$_{thesis}$/C$_{ref}$[48] of 1/2, or in other words a greater drop in permittivity as one moves above the phase transition by a factor of 2. Such a steep $\frac{dk}{dT}$ would be expected to result in an even higher induced pyroelectric coefficient. However, due to experimental limitations, such high field values were not measured, nor confirmed

in the present case.

Material Electrode *ferroelectric/induced*	p(μC/m^{2}K)	p$_{self}$	ϵ	tanδ%	F$_D$(Pa$^{-1/2}$ X 10^{-5})	Ref.
PST(sol-gel) Pt/Si *induced* 100kV/cm	270	-10	500	4%	1	[66]
PST(sputtered) Pt/Si *induced* 80 kVcm	743 500	363 50	2100 1600	1.5% 0.7%	4 2.5	[66] [56]
PST(CVD) Pt/Si *induced* 100 kV/cm	576	356	1700	1%	3.2	[66]
PST(sol-gel) sapphire *induced* 30kV/cm	900 (no information on ordering) 6000 (highly ordered from X-ray)		4500 7000	0.7% 0.4-0.6%	6 10	[61] [48]
PbTiO$_3$ Pt/Si *ferroelectric*	130-145		180-260	1.4- 3.5%	(0.7-1.1)	[144] [145]
PZT (30/70) (sol-gel) Pt/Si *ferroelectric*	200		340	1.1%	1.3	[146]

Table 5.1: *Thin film pyroelectric properties at $\approx$100Hz*

5.2   Results: Pyroelectric PST thin films

Dynamic pyroelectric measurements were made a room temperature to avoid thermally stimulated conduction. The temperature of the sample was cycled at 10 mHz in the form of a triangular signal with an amplitude of 1°C by using a Peltier element. The pyroelectric coefficient was calculated from the induced pyroelectric current and actual measured temperature rate as:

$$p = \frac{i}{A\frac{dT}{dt}} \tag{5.8}$$

where i is the induced pyro current (A), A is the sample area (m^2), and dT/dt is the rate of temperature change(°C /s).

Figure 5.1 displays the pyroelectric measurement results for a 500 nm PST/Pt/Si thin film and a ceramic at zero bias field, with the temperature oscillating 1°C about $\approx$22°C . The ceramic displays zero pyroelectric current as expected for a cubic material above the phase transition, while the thin films sample displays pyro current signal due to a layer of polarization/or internal bias.

Figure 5.2 displays the pyroelectric coefficient and figure of merit F_D as a function of applied DC bias field at room temperature. Displayed are the pyroelectric coefficients of 550 nm film PST/Pt/Si annealed at 700°C for 1 minute, 500 nm film annealed at 700°C 20 minutes (both with Au electrodes) and a 650 nm PST/Pt/Si film annealed at 700°C for 1 minute. The results indicate relatively processing independent values of pyroelectric coefficient saturating at $\approx$ 150kV/cm bias field with p=350 μC/m^{2}K. These results are in good agreement with the p_{eff} results for CVD, sol-gel and sputtered PST films on Pt/Si substrates measured in the "out-of-plane" configuration. It is interesting to see differences in the value of self-polarization in figure 5.2a between films with Au and Pt electrodes, which undergo different annealing conditions. It was routinely seen that films with Pt electrodes post-annealed at 650°C in an O$_2$ atmosphere, displayed a reduced self-polarization response, suggesting the film/top-electrode interface as the origin of self polarization, at least in this case.

The figure of merit versus DC field response in figure 5.2b is displayed for the films annealed at 700°C for 1 minute and 20 minutes respectively. It is clearly seen that while the pyroelectric coefficient is often insensitive to processing conditions, this is not necessarily the case for the figure of merit. As reported in the experimental and dielectric chapter, the lower dielectric constant for films annealed for 1 minute reflects in the higher figure of merit; in addition as the loss tangent is a strong function of film microstructure and processing, so is the figure of merit. The maximum figure of merit shown F_D=1.6 at 100kV/cm is greater than that previously reported for sol-gel PST on Pt/Si in the bolometer mode, greater than that for PbTiO$_3$ in the ferroelectric phase, and comparable
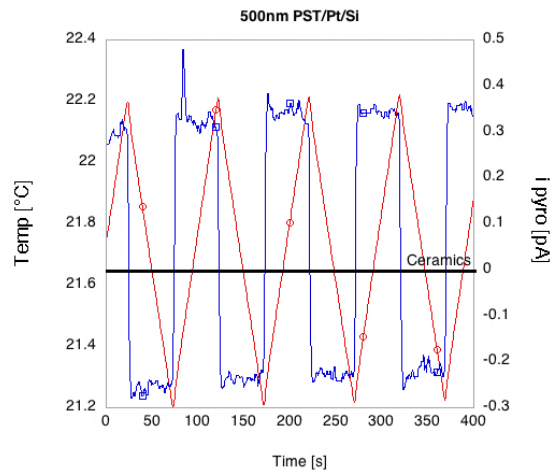
Figure 5.1: *500nm PST film on Pt/Si substrates, and bulk ceramic pyro-response at 0 bias field and room temperature*

with PZT pyroelectric sensors in the ferroelectric phase.

5.2.1 Dielectric Contribution

It is interesting to quantitatively compare the contributions in equation 5.1. Dielectric data was collected on a 500 nm PST film processed at 700°C for 1 minute at a low AC field level of 1kV/cm to determine its dielectric constant versus temperature response under increasing DC bias fields. The slope of the dielectric constant versus temperature curve $\frac{dk}{dT}$ was taken at the temperature of pyroelectric measurements (22°C) and the dielectric contribution to the pyroelectric coeffieicnt was calculated according to equation 5.1 and plotted versus the measured response in figure 5.3. It is seen that at low bias field near 10 kV/cm, the measured pyroelectric coefficient is approximately equal to the self polarization contribution plus the dielectric contribution, whereas above 10 kV/cm the measured response reflects an additional contribution believed to be the result of the reorientation of polar regions (known to exist in relaxors at temperatures above the dielectric maximum) under applied bias. This suggests the presence of nano-polar regions in a non-polar matrix above the transition temperature of the material as has been hypothesized for a
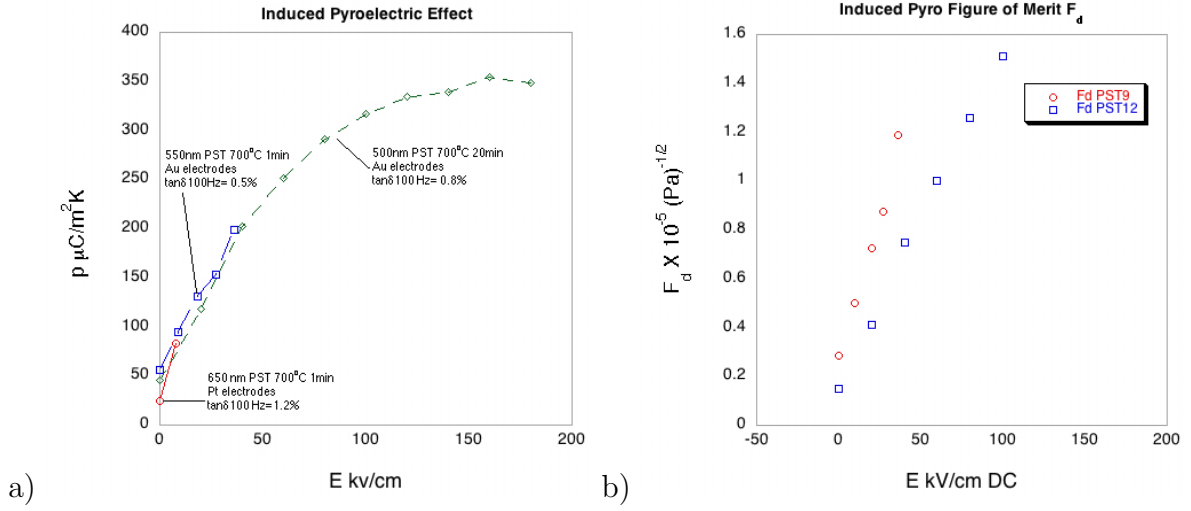
Figure 5.2: *PST/Pt/Si induced pyroelectric coefficient and figure of merit Fd*

wide variety of relaxor materials.

5.3   Results: Piezoelectric PST thin films

The converse piezoelectric effect (electric field induced) was measured using a double beam laser interferometer [147] and is presented in figure 5.4. It is seen that the curve is offset along the positive d axis, or that is displays a piezoelectric response in the absence of an applied field due again to the self-polarization/or internal bias previously discussed. The curve saturates near 100kV/cm to a value of 60 pm/V, comparable to previous reports in the PSN (58 pm/V at 100kV/cm) neighbor system [148], and slightly less than those reported in PMN (90 pm/V at 40kV/cm) [21]. The hysteretic response is indicitave of polar region switching at temperatures above the dielectric maximum, seen in large field PE measurments (section 3.6.4.2, page 147), and the measured versus dielectric contribution to the dielectric response.

Electrostrictive coefficients may be extracted from the data using equation 5.4 and 5.4 to arrive at:

$$d_{eff} = \frac{dx}{dE} = \frac{d(QP^2)}{dE} = 2QP\frac{dP}{dE} = 2Q\epsilon P \tag{5.9}$$
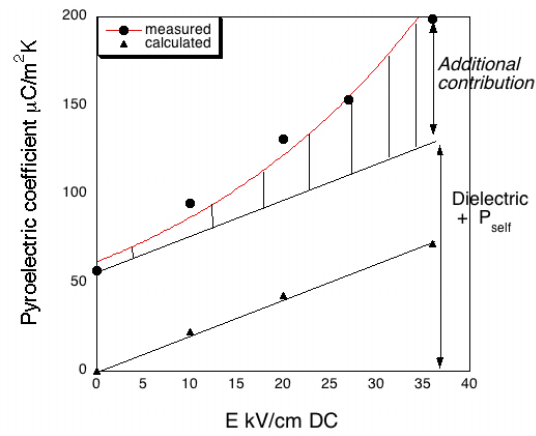
Figure 5.3: *500nm PST/Pt/Si* measured *pyroelectric coefficient versus the calculated dielectric contribution at room temperature*
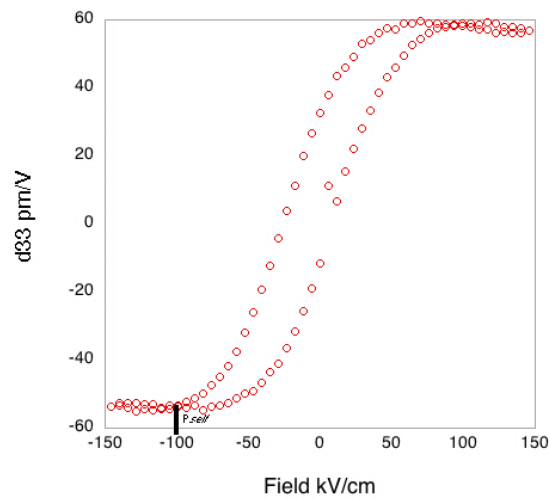
Figure 5.4: *550nm PST on Pt/Si substrates: bias piezoelectric response*
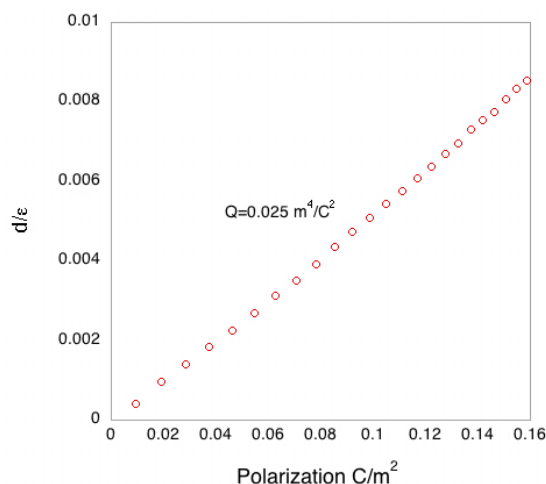
Figure 5.5: *550nm PST film on Pt/Si substrates: electrostrictive coefficient determination, a plot of d/ε versus the field induced polarization with the slope corresponding to 2Q, at room temperature*

where d is the piezoelectric coefficient (m/V), x is the strain, Q is the electrostrictive coefficient (m^4/C^2), P is the polarization (C/m^2) and ϵ is the dielectric permittivity.

Thus a plot of d/ϵ versus field induced P should result in a linear relation with the slope equal to 2Q. Figure 5.5 shows the results of this analysis for a 550 nm PST/Pt/Si film with the calculated electrostrictive coefficient Q=0.025 m^4/C^2. This is slightly higher than the reported values for PMN thin film (Q=0.0118$^4/C^2$) and single crystal (Q=0.00115$^4/C^2$) [4], and well within the range of reported values for PMN-PT thin film, single crystals and ceramics from (0.01-0.09$^4/C^2$)[149]. The reported value for Q in PST thin films, which is similar to related perovskite relaxor compounds such as PMN and PMN-PT lends credence to the claim that the reduced strain response in thin films is ultimately linked to the reduced permittivity. It is seen by equation 5.5, that Q in thin films and single crystal/bulk are of the same order of magnitude, however M is significantly different due to differences in the dielectric constant. These differences result in the induced strain variation from 0.3% in thin films to over 1.4% in single crystals.

5.4 Self Polarization: A Fixed Layer?

Is this "self-polarization" seen in a number of relaxor and ferroelectric thin films systems a fixed or switchable layer, and how can we see these changes? From figure 5.6 it is seen that the sign, or phase of the pyroelectric coefficient is determined by the direction of the current, and thus the polarization direction in the film (top down, or bottom up). This provides an easy way to monitor the switching of the polarization. Attempts were made to bias/pole the film in direction opposite to the polarization direction at various field levels up to 400 kV/cm at 100°C for 10 minutes and monitor the subsequent pyroelectric response of the self polarization, results are presented in figure 5.7. The results showed a coercive field like behavior for the reduction of the pyroelectric signal, with no reduction seen at field levels below 200kV/cm. At this field or higher there was a reduction of the pyroelectric current from 0.2 pA to $\approx$zero pA, but *not a phase change.*

The results of this experiment suggest that there is indeed a *fixed* layer of polarization which cannot be switched, and the subsequent reduction to zero under poling conditions is due to a switchable layer thus compensating the contribution of the fixed layer. This result is also represented in polarization loop measurements in figure 5.7 where before poling the loop is shifted along field axis due to self polarization, and after poling it is re-centered. The total switchable polarization remains constant, with only a change in the initial state of polarization. Similar phenomena was observed by Abe [150] in epitaxial sputter deposited $BaTiO_3$ thin films, and was attributed to the relaxation of the lattice misfit strain in the heteroepitaxial thin film.

5.5 Self Polarization: Impact on Dielectric Response

The presence of a fixed layer of polarization, or an equivalent internal bias field which could produce such a polarization response is detrimental to the dielectric properties of the film. As seen in the dielectric chapter, relaxors under DC bias show a negative
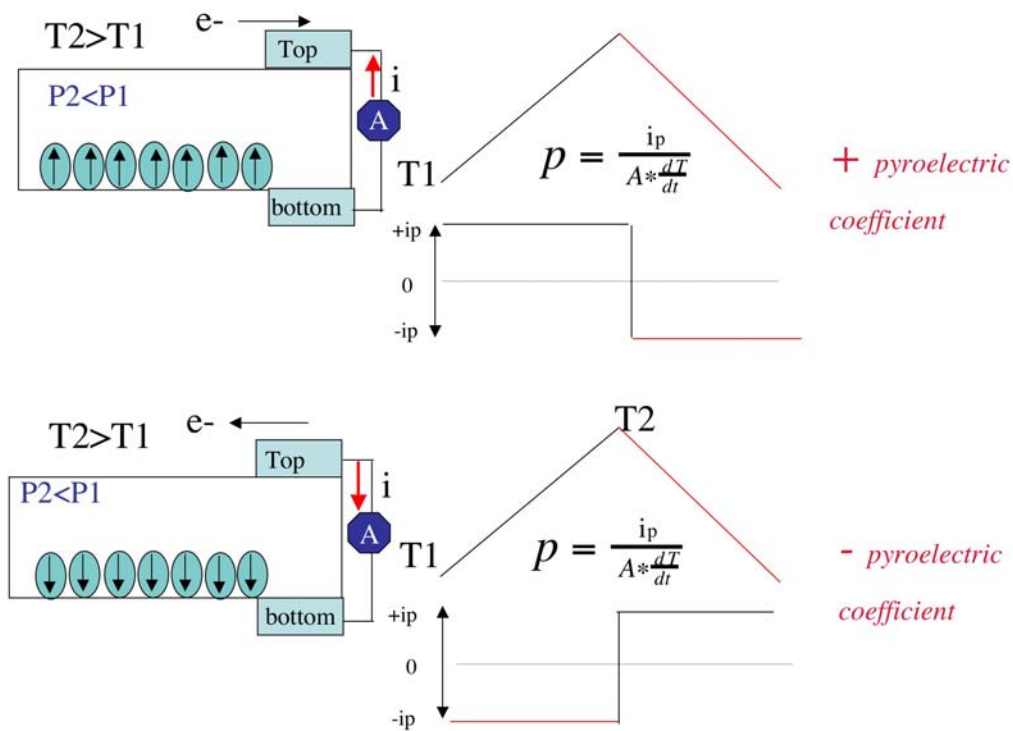
Figure 5.6: *Phase/sign of the pyroelectric coefficient reflecting the direction of polarization*

non-linearity, or a reduction in the dielectric constant (charge produced at a given field $k=C/C_0$ where $C=Q/A$). The quantitative impact of self-polarization on the dielectric response can be estimated by taking a common value of $50\mu C/m^2 K$ reported in PST and PMN relaxor systems, and calculating the electric field required for the equivalent polarization response at the measuring temperature, resulting in a nominal value of ≈ 20 kV/cm, comparable with the voltage offset seen in CV loops taken from similar samples. From the DC bias field response in the dielectric chapter this corresponds to a reduction in the dielectric constant due to self-polarization of less than a 10% at temperatures near the dielectric maximum. Therefore in our case, although self-polarization clearly has a demonstrated impact on pyroelectric, piezoelectric and the dielectric response, it in of itself cannot account for the drastically reduced permittivity of thin films as compared to bulk relaxors.
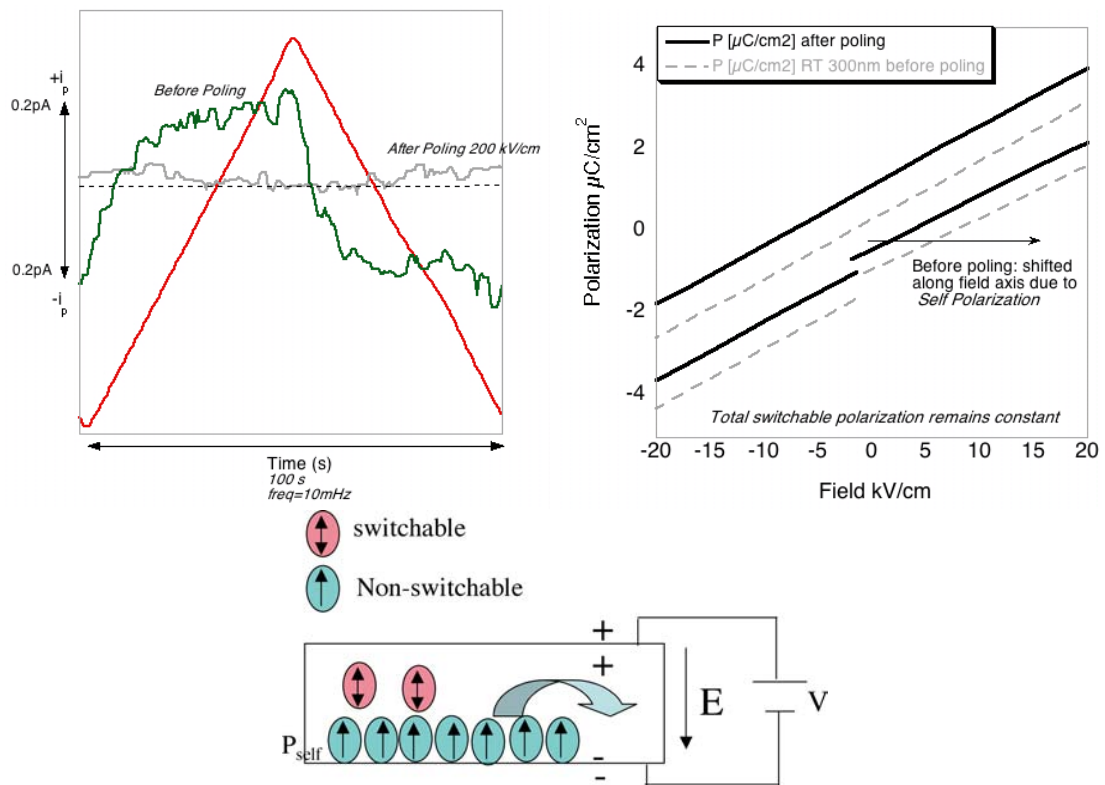
Figure 5.7: *300nm PST/Pt/Si with Au electrodes, zero bias pyroelectric response before and after poling at 200kV/cm and 100ºC for 10 minutes*

Chapter 6

Discussion

6.1 Ordered and Disordered Thin Films: The Basis of Comparison

The fabrication and study of ordered PST thin films produced by long time annealing at temperatures in excess of 800°C has shown that a long range polar state is formed upon cooling through the dielectric maximum, and that the dielectric properties of these films are comparable with ordered ceramics and single crystals. Furthermore, these materials behave as conventional ferroelectric materials, at least at frequencies below the level of lattice vibrations (THz). It was also found that the fabrication of disordered thin films required relatively low annealing temperatures near 700°C . All of the disordered films produced in this study displayed the essential feature of relaxor behavior; the shift of the dielectric maximum to higher temperatures with increasing measuring frequency. In addition, the presence of nano polar regions (NPR) at temperatures above the dielectric maximum were found in disordered thin films and their motion/dynamics was seen to be qualitatively the same as that observed in the model relaxor system PMN as evidenced by the study of non-linear dielectric properties. In spite of these similarities, a comparison of disordered PST in thin film and in ceramic form as shown in figure (6.1a) reveal that

disordered thin films display a drastically reduced dielectric constant, while *ordered* PST films shown in figure (6.1a) display a dielectric constant maximum near to that of ceramic samples. The deviation below the dielectric constant maximum may be accounted for by a change in the order of the phase transition induced by mechanical boundary conditions of the thin film state, as well as by differences in domain patterns as discussed in the chapter on dielectric properties (section 3.8, page 154). The purpose of this section is to summarize the effects of commonly cited extrinsic factors for the reduction of the Thin Film Relaxor (TFR) response and to propose a new hypothesis of the TFR state.
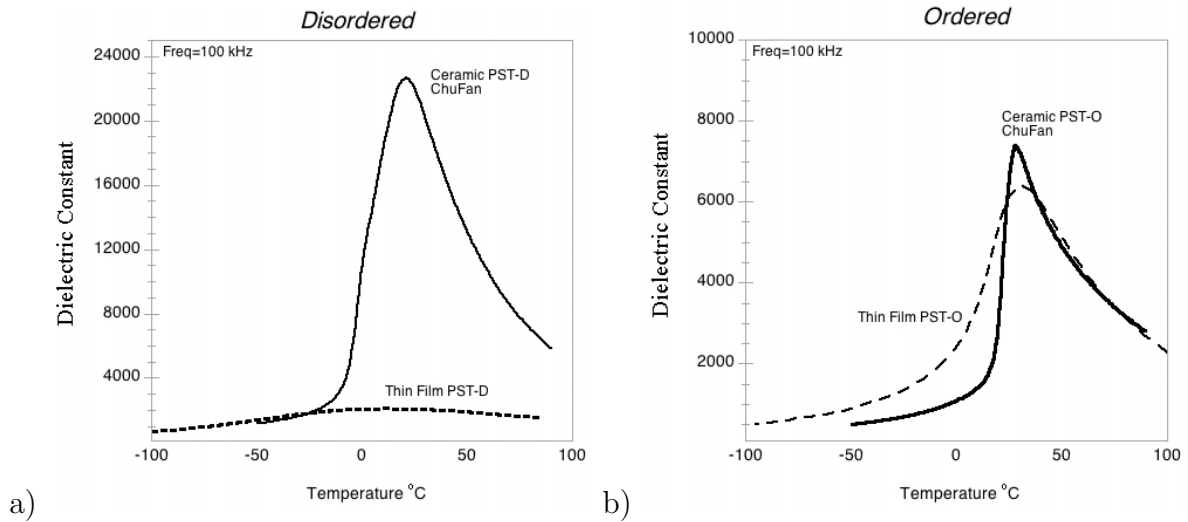
Figure 6.1: *(a)Dielectric Constant versus temperature for PST disordered ceramics annealed at 1520° C for 20 minutes, thin film on sapphire substrate (annealed at 700° C 1 minute) and (b) Ordered PST ceramics(S>0.9) annealed at 950° C for 62 hours, and thin films (S=0.91) on sapphire substrates annealed at 850° C for 35 hours. Ceramic data from reference [2]*

6.2 Impact of External Contributions: Summary

6.2.1 Film Quality

Perhaps the most important topic to begin the discussion of commonly cited external factors for the reduced TFR response may be termed *film quality.* It is true that thin films often have numerous defects, including stress induced cracking and entrapped porosity which may impact the dielectric response. A recent study by Ostapchuk [151] showed that such microstructrual defects could be responsible for an order of magnitude reduction in the permittivity at low frequencies, as well as a harder soft mode and lower dielectric response at high frequencies. In addition, the procedures for producing ordered and disordered thin films involve changing the annealing temperature and time which may cause changes in microstructure and defect levels in the films. It therefore of interest to take a closer look at the microstructural evolution accompanying the ordering process by examining 1) a disordered thin film processed at 700°C and 2) comparing with an ordered film typically annealed for greater than 24 hours at temperatures in excess of 800°C .

The X-ray diffraction spectra for an ordered and disordered thin film on sapphire substrates are shown in figure (6.2). In terms of crystal structure (ordered peaks at 19 degrees 2theta are not presented for clarity of the other parts of the spectrum), there are slight changes in the degree of orientation, with ordered samples displaying enhanced (100) and (111) reflections. No secondary phases were detected in either sample, so that by X-ray analysis the only major difference is the presence of superlattice peaks indicating increased "B" site order.

The microstructure of the films as seen by TEM bright field investigations is presented in figure (6.3a and b). An initial view shows that the grain size increases greatly with the long time annealing used to order the films and has been presented by SEM investigation in section (chapter 3 ordering section). Entrapped porosity is seen inside the grains in the disordered film in figure(6.3a) and in cross section TEM presented in the processing
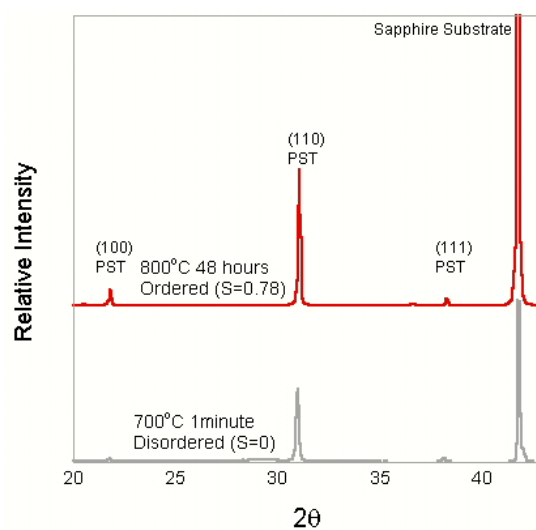
Figure 6.2: *X-ray diffraction for Disordered (S=0) annealed 700°C 1 minute and Ordered (S=0.78)PST thin film annealed at 800°C for 48 hours on Sapphire substrate*

chapter (figure 2.14). After the annealing procedures utilized to produce ordered films, the local homogeneity is seen to improve as evidenced by the high magnification image in figure (6.3b). However, larger local defects are also seen to be introduced, although some of these may be introduced during TEM sample preparation. In any case, local defects were seen not to have a major impact on the dielectric response of ordered thin films as they possessed values of dielectric constant similar to ceramic samples.

Furthermore, it is clearly seen that a film annealed at 850°C for 1 hour (S=0.55) shows a microstructure characterized by surface defects and local cracking/porosity but *still* had a larger dielectric constant than disordered films as shown by bright field TEM figure (6.4a) and dielectric measurements presented in figure (6.4b). It is the direct comparison of ordered thin films which have defects, and still display an enhanced response as compared to disordered samples which permits the conclusion in the case of this study that the films are of sufficiently high quality, and that these issues do not dominate the measured dielectric properties.
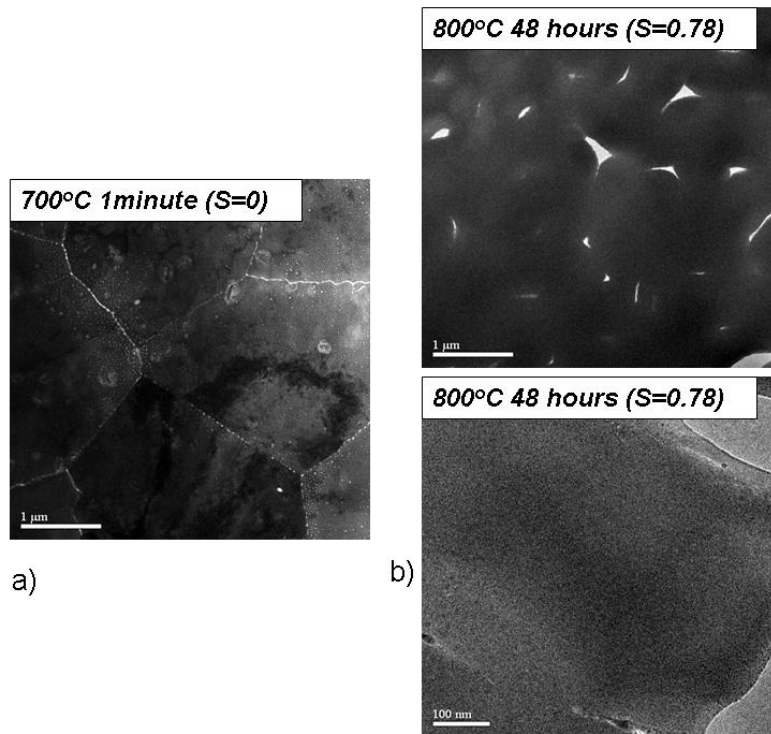
Figure 6.3: *a) TEM Bright field for Disordered PST thin films on Sapphire substrate annealed at 700° C for 1 minute b) Ordered (S=0.78) PST thin film on sapphire substrate annealed at 800° C for 48 hours (Dr. D. Su)*

6.2.2 Passive Layer

Studies comparing the *"In-Plane"* and *"Out-of-Plane"* dielectric response in the dielectric chapter revealed that they were effectively the *same* for films near 700 nm in thickness. Since the *"Out-of-Plane"* response should be reduced compared to the *"In-Plane"* response in the presence of a passive layer, these experiments showed that the commonly observed low values of dielectric constant in relaxor thin films cannot be explained by a passive layer, at least in nominally thick films near 1 micron in thickness.
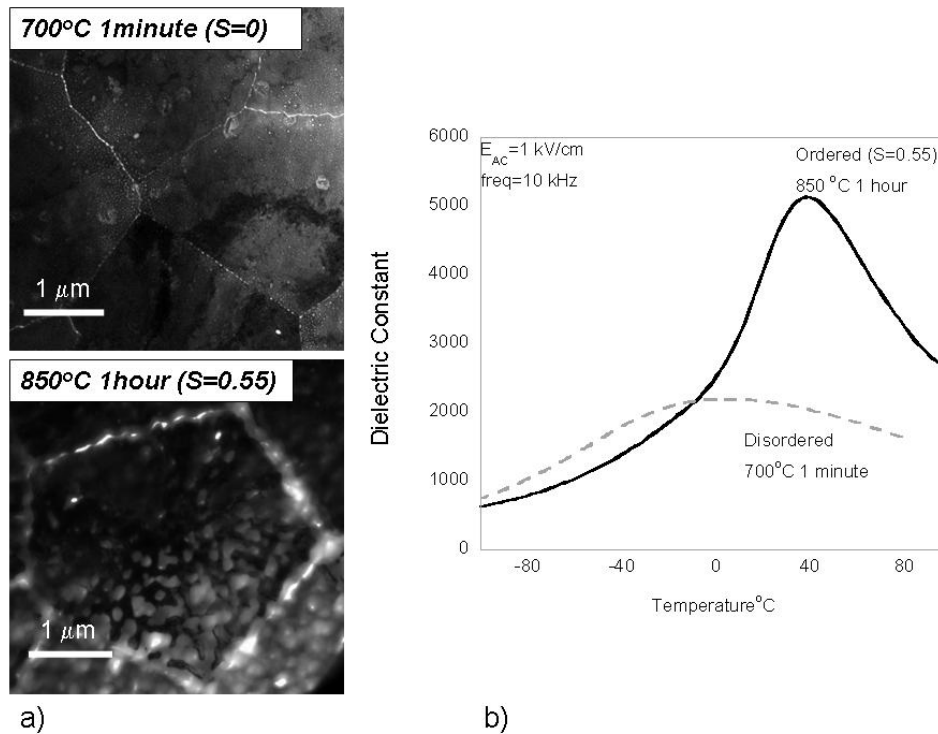
Figure 6.4: *a) TEM Bright field for Disordered PST thin films on Sapphire substrate annealed at 700°C for 1 minute, and film annealed at 850°C 1 hour (S=0.55) PST thin film on sapphire substrate annealed at 800°C for 48 hours (Dr. D. Su) (b) Dielectric constant versus temperature at 10 Khz and E_{AC}=1 kV/cm*

6.2.3   Stress/Clamping

It was seen that stress impacted the dielectric constant of disordered thin films with films on sapphire with the least thermal induced stress possessing the highest dielectric response. In addition, a report by Fluflygin [65], who made freestanding films, saw an increase in the dielectric constant by 10% after membrane fabrication. However, these changes are very small and relatively insignificant as compared to the order of magnitude reduction in the dielectric constant of thin films prepared in this study as compared to ceramics as presented in figure (6.5).
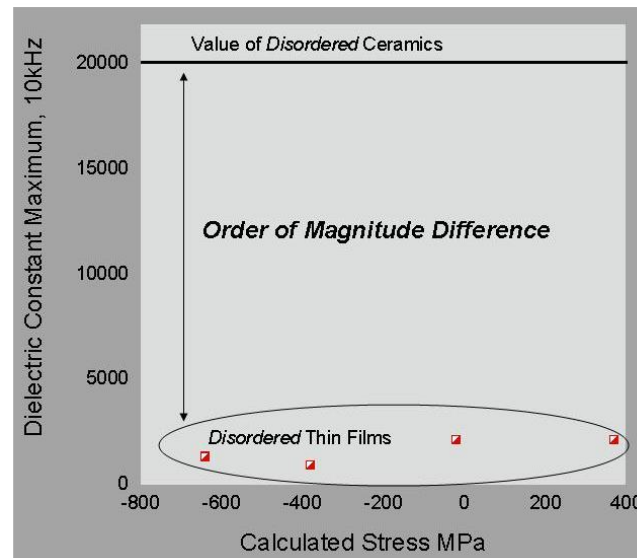
Figure 6.5: *The effect of substrate via thermal induced stress for Disordered PST thin films as compared to ceramic samples*

6.2.4 Grain Size

The SEM microstructures of disordered PST thin films fabricated on Pt/Si substrates with and without a $PbTiO_3$ seed layer are presented in figure (6.6b). From the dielectric measurements presented in (6.6a)it is seen that no detectable change in the value is observed by reducing the grain size from 325 to 140 nm. In addition, even epitaxial films fabricated on STO and MgO substrates displayed a reduced dielectric response. It is therefore concluded, that in this study the effects of grain size is not a primary factor for the reduced dielectric response of TFR.

6.2.5 Built In Field/Self Polarization

The presence of a fixed layer of polarization, or an equivalent internal bias field which could produce such a polarization response is clearly detrimental to the dielectric properties of thin films. However, the quantitative impact of self-polarization on the dielectric response was estimated to be a 10% reduction in the dielectric constant at temperatures close to
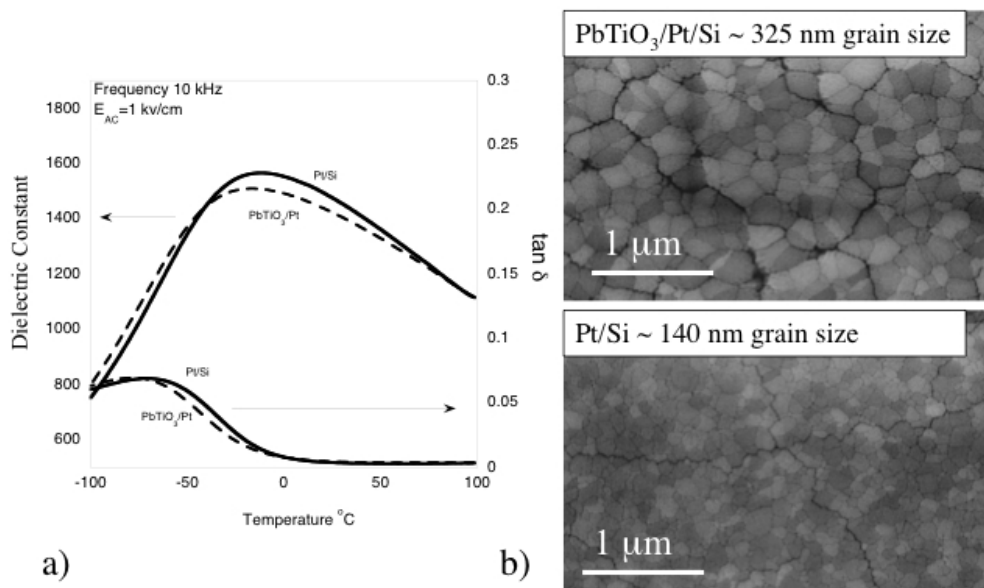
Figure 6.6: *a) Dielectric constant and loss tangent versus temperature for 300nm PST films on Pt/Si (grain size 140 nm) and PbTiO₃ (grain size ~ 325 nm) seeded substrates and b)SEM images of Pt/Si and PbTiO₃ seeded films*

the dielectric maximum. Therefore, in the case of the present study, it cannot account for the drastically reduced permittivity of thin films as compared to bulk relaxors (section 5.5, page 193).

Summary: The examined extrinsic contributions not enough to account for order of magnitude drop in dielectric constant observed between disordered ceramics and disordered thin films. Furthermore, these extrinsic effects should also impact the ordered films in a similar fashion, however the dielectric behavior was observed to be similar in ordered thin films and ordered ceramic samples.

6.3   Hypothesis: Different State of "Disorder" in Bulk and Thin Films Due to Processing

Since there are polar regions with similar dynamics in thin films as compared to bulk materials, and the investigated external factors can not account for the observed reduction in permittivity, we propose that the *quantitative* contribution of polar regions is different in thin films as compares to ceramics and single crystal specimens. Specifically the reduced processing temperatures required to produce PST (700°C as compared to 1500°C for ceramics) may induce a so called *Low Temperature Disordered* state characterized by a lack of superlattice reflections as a result of a disordered arrangement of "B" site ions. This *Low Temperature Disordered* state is distinguished from the *relaxor* state by a dilution of the polar regions. In other words, the temperature is enough to disorder the lattice, but not in a way to produce a homogenous relaxor state. This state can be pictured as an incomplete transformation due to the low processing temperatures, and the dilution of the formed polar regions may account for the observed reduction in permittivity. As depicted in figure 6.7 both the *High and Low Temperature* disordered states *both* evolve to the same long range ferroelectric ordered state with post annealing at temperatures near 900°C for extended times (in excess of 24 hours).

This hypothesis may explain the salient feature of how TFR differ from bulk relaxor materials including

- The reduced values of dielectric constant for TFR as compared to bulk relaxors.

- The *absence* of a field induced phase transition (section 3.9, page 158).
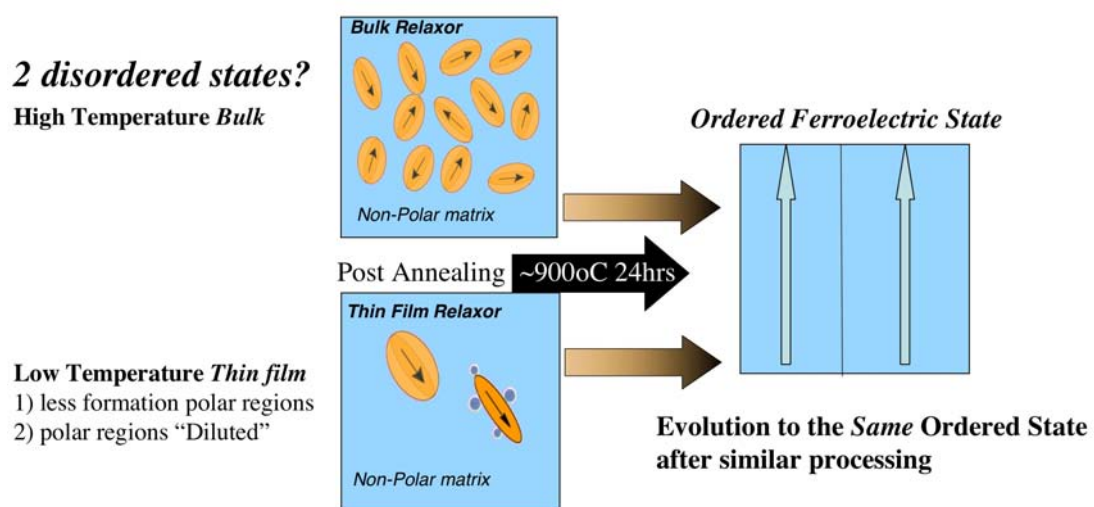
Figure 6.7: *Schematic showing 2 hypothesized disordered states arising from differences in processing temperature which converge to a final ordered state after similar post annealing conditions*

Chapter 7

Summary and Conclusions

The objective of this thesis was to use the phenomenon of positional order in PST as a tool to examine the nature of relaxor ferroelectric behavior in thin films form. The motivation was to achieve a convenient "basis" of comparison by producing highly ordered PST films which exhibit a long range polar state and behave essentially as conventional ferroelectrics. By the comparison of ordered (*conventional* ferroelectrics), with disordered (*relaxor* ferroelectrics), both in the thin films state it was possible to comment on the nature of the relaxor state, and specifically to answer the question posed in the introduction, *"Is the intrinsic nature of relaxor behavior the same in thin films form as in ceramics/single crystals?"*

The PST films were made by a sol-gel technique, using dehydration and subsequent scandium precursor modification in order to form a stable stoichiometric solution. The optimization of processing conditions were achieved for ordered and disordered thin films. It was found that excess lead was required in amounts greater than 20% to compensate for lead loss during annealing, and that a *"Thicklayer"* annealing procedure could be used to fabricate films up to 2 microns in thickness. Disordered films with measurable properties were only achieved at low annealing temperatures near 700°C as higher temperatures up to 1000°C , resulted in "B" site ordering. Temperatures in excess of 1000°C resulted in significant film degradation. The ordering of PST thin films was limited to low degrees of

order up to S=0.22 on Pt/Si substrates after annealing at 800°C for 20 minutes. Longer times and higher temperatures resulted in the destruction of the bottom electrode and unmeasurable properties. Higher degrees of order were achieved on single crystal substrates, without a bottom electrode, which necessitated special techniques for the measurement of the "In-Plane" dielectric response. By long time annealing with a controlled atmosphere, ordering degrees up to S=0.91 were achieved on sapphire substrates. In addition, it was possible to tailor the stress level and grain size in the films by choice of substrate and seed layer, with the fabrication of epitaxial films evidenced on single crystal substrates.

An examination of the dielectric response of ordered and disordered PST thin films indicated that the dielectric constant maximum was significantly impacted by the level of "B" site order. In contrast to ceramic and single crystal samples which display a *decrease* in the value of the dielectric constant with an increase in "B" site order, thin film samples on a variety of substrate systems showed an *increase* in the dielectric constant with an increase in order. Highly ordered films also showed the development of a ferroelectric state comparable to their bulk counterparts.

The position of the dielectric maximum in ordered films was similar to that of ceramics and single crystals, *even* with low degrees of order and small ordered region size on a variety of substrates. However, the position of the dielectric maximum in disordered films was shown to be impacted by processing induced lead deficiency, as well as by stress in the films induced by thermal expansion mismatch between the film and substrate. Disordered films fabricated on sapphire substrates with the least amount of thermal induced stress showed a dielectric maximum temperature near that observed for ceramics with lead vacancies. The temperature of the dielectric maximum for disordered films was shifted down for film under *both* tensile and compressive stress.

Analysis of the non-linear dielectric response in disordered thin films revealed a similar "crossover" in the field dependance of the dielectric constant as a function of temperature which was previously reported in PMN single crystals. In addition, the AC and DC

field dependance of the dielectric constant was consistent with that observed in relaxors. However, unlike in ceramics and single crystals, a phase transition to a long range polar state could *not* be induced by the application of DC bias. Also, the position of the dielectric maximum as a function of measurement frequency did not follow the VF law as has been well documented for ceramic and single crystal relaxors.

The values of the dielectric constant at very low temperature (20 K) were the *same* for ordered and disordered thin films at 1MHz. However, disordered films exhibited a reduction in the value upon moving into the GHz region. Overall, highly ordered films showed dielectric behavior similar to their ceramic or single crystal counterparts. Their differences, such as a change in the order of the phase transition, could be explained in terms of mechanical effects due to the thin film state, or by differences in domain wall patterning. Therefore, disordered PST films displayed the essential features of relaxor behavior including the frequency dependance of the dielectric maximum and AC and DC field dependance, however their relaxor nature was "underdeveloped" as compared to ceramics, at least in the low frequency region.

High frequency studies in the THz range using Fourier Transform Infrared Spectroscopy (FTIR) spectroscopy showed that in the model PMN relaxor system, thin films have the same response as single crystal relaxors including the formation of nano polar regions (NPR) at the Burns temperature. In terms of lattice dynamics, both ordered and disordered PST thin films showed rather unexpectedly the same features including the transverse optic (TO1) mode softening to the Burns temperature, with the simultaneous appearance of a central mode (CM) attributed to the appearance of NPR in the paraelectric phase. Higher processing temperatures were seen to increase the dielectric strength of the CM. Ordered and disordered samples displayed drastically different behavior, at low frequencies (below 1MHz), while possessing the *same* lattice dynamics.

Commonly cited extrinsic factors for the reduction of the dielectric constant in thin film relaxors were examined and quantified. It was the direct comparison of ordered thin

films which have defects, and *still* display an enhanced response as compared to disordered samples which allowed the conclusion that the films were of sufficiently high quality. It was shown by comparing the *"In-Plane"* and *"Out-of-Plane"* dielectric response that the commonly observed low values of dielectric constant in relaxor thin films cannot be explained by a passive layer, at least in nominally thick films near 1 micron in thickness. The changes in the dielectric constant introduced as a result of thermal induced stress were small and relatively insignificant as compared to the order of magnitude reduction in the dielectric constant of thin films as compared to ceramics. A study on the effects of grain size from dielectric measurements showed no detectable change in the value of the dielectric constant by reducing the grain size from 325 to 140 nm. In addition, even epitaxial films fabricated on STO and MgO substrates displayed a reduced dielectric response. Self-polarization was observed in PST thin films and the quantitative impact on the dielectric response was estimated at about a 10% reduction in the dielectric constant at temperatures near the dielectric maximum. Therefore, in the case of the present study, none of the commonly cited extrinsic factors can account for the drastically reduced dielectric constant values of thin films as compared to bulk relaxors. Furthermore, these extrinsic effects should also impact the ordered films in a similar fashion, however the dielectric behavior was observed to be similar in ordered thin films and ordered ceramic samples.

Since there are polar regions with similar dynamics in thin films as compared to bulk materials, and the investigated external factors can not account for the observed reduction in permittivity, a new hypothesis was proposed emphasizing that the *quantitative* contribution of polar regions is different in thin films as compared to ceramics and single crystal specimens. Specifically the reduced processing temperatures required to produce PST ($700°$C as compared to $1500°$C for ceramics) may induce a so called *Low Temperature Disordered* state characterized by a lack of superlattice reflections as a result of lattice disorder. This *Low Temperature Disordered* state is distinguished from the *relaxor* state

by a dilution of the polar regions.

Finally, the response to the question, *"is the intrinsic nature of relaxor behavior the same in thin films form as in ceramics/single crystals?"* Yes, thin films show the formation of NPR and their motion has been qualitatively compared with single crystal/ceramics showing their similarity, so the essential features of relaxor behavior of a shift in the dielectric constant maximum with measuring frequency has been confirmed. The difference between the thin film and the ceramic/single crystal relaxor state seems to be in the *quantitative* response of the NPR, specifically they seem to be "diluted" in the thin film state, probably due to the reduced temperatures of processing. It is therefore suggested that further studies on thin film relaxors focus on processing methods of inducing a *High Temperature Disordered* state, preferable on single crystal substrates without bottom electrodes using the "In-Plane" dielectric measurement techniques utilized in this report. It is also believed possible that this state may be achieved by high energy deposition processes, and/or a higher level of chemical homogeneity arising from improved solution processing techniques.

Bibliography

[1] V. Bovtun, S. Kamba, A. Pashkin, and M. Savinov. Central peak components and polar soft mode in relaxor pmn crystals. *Ferroelectrics*, 298:29–38, 2004.

[2] F. Chu. *The Ferroelectric Phase Transition in complex Perovskite Relaxors*. PhD thesis, Swiss Federal Institute of Technology (EPFL), 1994.

[3] R. Schwartz, J. Voigt, B. Tuttle, D. Payne, T. Reichert, and R. DaSalla. Comments on the effects of solution precursor characteristics and thermal processing conditions on the crystallization behavior of sol-gel derived lead zirconate titanate thin films. *Journal of Materials Research*, 12(2):444–456, 1997.

[4] Zian Kighelman. Films minces relaxeur-ferroélectriques à base de pmn: élaboration, propriétés diélectriques et électromécaniques. *Ph. D. Dissertation, Swiss Federal Institute of Technology Lausanne*, 2001.

[5] Alexandre Glazounov. Non-linear dielectric response of pmn relaxor ferroelectric. *Ph. D. Dissertation, Swiss Federal Institute of Technology Lausanne*, 1997.

[6] Fan Chu. The ferroelectric phase transition in complex perovskite relaxors. *Ph. D. Dissertation, Swiss Federal Institute of Technology Lausanne*, 1994.

[7] O. Vendik, S. Zubko, and M. Nikolski. Modeling and calculation of the capacitance of a planar capacitor containing a ferroelectric thin film. *Technical Physics*, 44(4):349–355, 1999.

[8] G. Smolenskii and A. Agranovskaya. *Soviet Phys. Tech. Phys.*, 3:1380, 1958.

[9] V. Bobnar, J. Bernard, and M. Kosec. Relaxorlike dielectric properties and history-dependent effects in the lead-free knn-sto ceramic system. *Appl. Phys. Lett.*, 85(6):994–996, 2004.

[10] L. Eric Cross. Relaxor ferroelectrics. *Ferroelectrics*, 76:241–267, 1987. relaxor model structural.

[11] B. Rolov V. Fritsberg. Some factors affecting the character of ferroelectric phase transitions. *Bull. of the Acad. of Science of the USSR Phys. Series*, 38:556–559, 1964. relaxor model structural.

[12] B. Rolov V. Fritsberg. Some regularities of smeared-out transitions in ferroelectric solid solutions. *Bull. of the Acad. of Science of the USSR Phys. Series*, 29:1018–1020, 1965. relaxor model structural.

[13] G. Burns and F. Dacol. Glassy polarization behavior in ferroelectric compounds pmn and pzn. *Solid state communications*, 48(10):853–856, 1983.

[14] M. Lines and A. Glass. *Principles and Applications of Ferroelectrics and related Materials.* Clarendon Press, Oxford, 1977.

[15] S. Jang L. E. Cross M. Wuttig D. Viehland, J. Li. Dipolar-glass model for lead magnesium niobate. *Physical Review B*, 43(10):8316–8320, 1991. relaxor model structural.

[16] F. Chu, I. Reaney, and N. Setter. Spontaneous (zero-field) relaxor-to-ferroelectric phase transition in disordered psn. *J. Appl. Phys.*, 77(4):1671–1678, 1994.

[17] F. Chu, N. Setter, and A. K. Tagantsev. The spontaneous relaxor-ferroelectric transition of pb(sc0.5ta0.5)o3. *Journal of Applied Physics*, 74(8):5129–5134, 1993. MC030 J APPL PHYS.

[18] Y. Bing, A. Bokov, and Z. Ye. Structural phase transition and dielectric relaxation in pzn single crystals. *cond-mat/0405042*, 2004.

[19] G. Samara. Pressure-induced crossover from long to short range order in compositionally disordered soft mode ferroelectrics. *Physical review letters*, 77(2):314–317, 1996.

[20] G. Samara, e. Venturini, and V. Schmidt. Pressure induced crossover from long to short range order in pzn-pt single crystals. *Appl. Phys. Lett.*, 76(10):1327–1329, 2000.

[21] Z. Kighelman, D. Damjanovic, and N. Setter. Electromechanical properties and self-polarization in relaxor pmn thin films. *Journal of Applied Physics*, 89(2):1393–1401, 2001. Thin Film Relaxors.

[22] D. Liu and D. Payne. Lower temperature crystallization and ordering in sol-gel derived pb(sc.5ta.5)o3 powdes and thin layers. *Journal of Applied Physics*, 77(7):3361–3364, 1995. PST.

[23] P. Papet, J. P. Dougherty, and T. R. Shrout. Particle and grain-size effects on the dielectric behavior of the relaxor ferroelectric pb(mg1/3nb2/3)o3. *Journal of Materials Research*, 5(12):2902–2909, 1990. Article EN070 J MATER RES.

[24] G. Catalan, M. H. Corbett, R. M. Bowman, and J. M. Gregg. Effect of thermal expansion mismatch on the dielectric peak temperature of thin film relaxors. *Journal of Applied Physics*, 91(4):2295–2301, 2002. 516LB J APPL PHYS.

[25] J. H. Park and S. Trolier-McKinstry. Dependence of dielectric and piezoelectric properties on film thickness for highly 100-oriented lead magnesium niobate-lead titanate (70/30) thin films. *Journal of Materials Research*, 16(1):268–275, 2001. 390DV J MATER RES.

[26] L. Francis, Y. Oh, and D. Payne. Sol-gel processing and properties of lead magnesium niobate powders and thin layers. *Journal of Materials Science*, 25:5007–5013, 1990. Thin film relaxors.

[27] C. Parker, J. P. Maria, and A. Kingon. Temperature and thickness dependent permittivity of bst thin films. *Appl. Phys. Lett.*, 81(2):340–342, 2002.

[28] F. Xu, S. Trolier-McKinstry, W. Ren, and B. Xu. Domain wall motion and its contribution to the dielectric and piezoelectric properties of lead zirconate titanate films. *Journal of Applied Physics*, 89(2):1336–1348, 2001.

[29] J. Junquera and P. Ghosez. Critical thickness for ferroelectricity in perovskite ultrathin films. *Nature*, 422:506–509, 2003.

[30] R. Kretschmer and K. Binder. Surface effects on phase transitions in ferroelectrics and dipolar magnets. *Physical Review B*, 20(3):1065–1076, 1979.

[31] I. Batra and B. Silverman. *Solid state communications*, 11:291, 1972.

[32] A. Tagantsev, V. Sherman, K. Astafiev, J. Venkatesh, and N. Setter. Ferroelectric materials for microwave tunable applications. *Journal of Electroceramics*, 11:5–66, 2003.

[33] S. Hiboux. *Study of growth and properties of in-situ sputter deposited PZT thin films.* PhD thesis, EPFL, 2002.

[34] N. Mathan, E. Husson, G. Calvarin, J. Gavarri, A. Hewat, and A. Morell. A structural model for the relaxor pmn at 5k. *J. Phys.: condens. Matter*, 3:8159–8171, 1991. Relaxor model structural.

[35] M. Glinchuk V. Westphal, W. Kleemann. Diffuse phase transitions and random-field induced domain states of the "relaxor" ferroelectric pmn. *Physical Review Letters*, 68(6):847–850, 1992. relaxor model structural.

[36] J. Li, X. Dai, A. Chow, and D. Viehland. Polariztion switching mechanisms and elec-tromechanical properties of la-modified lead zirconate titanate ceramics. *J. Mater. Res.*, 10(4):926–938, 1995.

[37] C. Kittel. *Introduction to Solid State Physics*. John Wiley and Sons, Inc., seventh edition edition, 1996.

[38] Y-M. Chiang, D. Birnie, and D. Kingery. *Physical Ceramics: Principles for Ceramic Science and Engineering*. John Wiley and Sons, Inc., 1996.

[39] R. Cohen. Origin of ferroelectricity in perovskite oxides. *Nature*, 358:136–138, 1992.

[40] H. Krause, J. Cowley, and J. Whatley. *Acta Crystallogr.*, A35:1015, 1979.

[41] Y. Yan, S. Pennycook, Z. Xu, and D. Viehland. Determination of the ordered structures of pmn and bmn by atomic resolution z-contrast imaging. *Appl. Phys. Lett.*, 72(24):3145–3147, 1998.

[42] M. Cantoni, S. Bharadwaja, S. Gentil, and N. Setter. Direct observation of the b-site cationic order in the ferroelectric relaxor pmt. *Journal of Applied Physics*, 96(7):3870–3875, 2004.

[43] I-Wei Chen, P. Li, and Y. Wang. Structural origin of relaxor perovskites. *J. Phys. Chem. Solids*, 57(10):1525–1536, 1996.

[44] B. Burton and E. Cockayne. Why pb(b,b')o3 perovskites disorder at lower temper-atures than ba(b,b')o3 perovskites. *Physical Review B*, 60(18):R12–542–545, 1999.

[45] C. Stenger and A. Burggraaf. Order-disorder reactions in the ferroelectric per-ovskites psn and pst. part 1. kinetics of the ordering process. *Phys. stat. sol. (a)*, 61:275–285, 1980.

[46] C. Stenger and A. Burggraaf. Order-disorder reactions in the ferroelectric per-ovskites psn and pst. part 2. relation between ordering and properties. *Phys. stat. sol. (a)*, 61:653–664, 1980.

[47] N. Setter and E. Cross. The role of b-site cation disorder in diffuse phase transition behavior of perovskite ferroelectrics. *Journal of Applied Physics*, 51(8):4356–4360, 1980.

[48] R. Watton and M. Todd. Induced pyroelectricity in sputtered lead scandium tanta-late films and their merit for ir detector arrays. *Ferroelectrics*, 118:279–295, 1991.

[49] W. Dmowski, M. Akbas, P. Davies, and T. Egami. Local structure of pst and related compounds. *Journal of Physics and Chemistry of Solids*, 61:229–237, 2000.

[50] D. Viehland, M. Wuttig, and E. Cross. The glassy behavior of relaxor ferroelectrics. *Ferroelectrics*, 120:71–77, 1991.

[51] A. Glazounov and A. Tagantsev. A "breathing" model for the polarization response of relaxor ferroelectrics. *Ferroelectrics*, 221:57–66, 1999. Relaxor model structural.

[52] R. Pirc and R. Blinc. Spherical random-bond-random-field model of relaxor ferro-electrics. *Physical Review B*, 60(19):13470–13478, 1999.

[53] R. Blinc, J. Dolinek, A. Gregorovic, B. Zalar, C. Filipic, Z. Kutnjak, A. Levstik, and R. Pirc. Local polarization distribution and edwards-anderson order parameter of relaxor ferroelectrics. *Physical review letters*, 83(2):424–427, 1999. relaxor model structural.

[54] I. Reaney, D Barber, and R. Watton. Tem studies of rf magnetron-sputtered thin films. *Journal of Materials Science: Materials in electronics*, 3:51–63, 1992. PST.

[55] M. A. Todd, P. P. Donohue, M. A. C. Harper, and J. C. Jones. Sputtered lead scandium tantalate thin films for dielectric bolometer mode thermal detector arrays. *Integrated Ferroelectrics*, 35(1-4):1845–1855, 2001.

[56] Z. Huang, P. P. Donohue, M. A. Todd, J. C. Jones, and R. W. Whatmore. Sputtered lead scandium tantalate thin films: crystallization behaviour during post-deposition annealing. *Journal of Physics D-Applied Physics*, 34(21):3121–3129, 2001.

[57] Z. Huang, M. A. Todd, R. Watton, and R.W. Whatmore. Sputtered lead scandium tantalate thin films: a microstructural study. *Journal of Materials Science*, 33:363–370, 1998. PST.

[58] R. Whatmore, Z. Huang, and M. Todd. Sputtered lead scandium tantalate thin films: Pb4+ in b sites in the perovskite structure. *Journal of Applied Physics*, 82(11):5686–5694, 1997. PST.

[59] P. Muralt, S. Hiboux, C. Mueller, T. Maeder, T. Sagalowicz, T. Egami, and N. Setter. Excess lead in the perovskite lattice of pzt thin films made by in-situ reactive sputtering. *Integrated Ferroelectrics*, 36(1-4):53–62, 2001.

[60] C. Bjormander, K. Sreenivas, A. Grishin, and K. Rao. Pyroelectric pst/ybco thin-film heterostructures. *Appl. Phys. Lett.*, 67(1):58–60, 1995. PST.

[61] R. W. Whatmore, A. Patel, N. Shorrocks, and F. W. Ainger. Ferroelectric materials for thermal ir sensors state-of-the-art and perspectives. *Ferroelectrics*, 104:269–283, 1990. PST.

[62] R. Whatmore A. Patel, N. Shorrocks. Physicochemical properties of sol-gel derived lead scandium tantalate pst thin films. *Ferroelectrics*, 134:343–348, 1992. PST.

[63] D. Liu, L. Ma, D. Payne, and D. Viehland. Sol-gel synthesis of pst powders and thin layers. *Materials Letters*, 17:319–322, 1993. PST.

[64] David A. Payne Donhang Liu, Linqing Ma. Synthesis and procesing of pst thin layers by solution sol-gel method. *Proceedings of the British Ceramic Society*, ?:?, ? PST.

[65] V. Fuflyigin, E. Salley, P. Vakhutinsky, A. Osinsky, J. Zhao, I. Gergis, and K. Whiteaker. Free-standing films of pst for uncooled infrared detectors. *Applied Physics Letters*, 78(3):365–367, 2001. PST.

[66] Z. Huang, P. P. Donohue, Q. Zhang, D. Williams, C. J. Anthony, M. A. Todd, and R. W. Whatmore. Comparative studies of pst thin films as prepared by sol-gel, ldcvd and sputtering techniques. *Integrated Ferroelectrics*, 45:79–87, 2002.

[67] J. Ebelmen. *Ann.*, page 331, 1846.

[68] J. Brinker and G. Scherer. *Sol-Gel Science*. Academic Press, Inc., 1990.

[69] C. Chandler, C. Roger, and M. Hampden-Smith. Chemical aspects of solution routes to perovskite-phase mixed-metal oxides from metal-organic precursors. *Chem. Rev.*, 93:1205–1241, 1993.

[70] K. Budd, S. Dey, and D. Payne. *Brit. Ceram. Soc. Proc.*, 36:197, 1985.

[71] S. D. Ramamurthi and D. A. Payne. Structural investigations of prehydrolyzed precursors used in the sol-gel processing of lead titanate. *Journal of the American Ceramic Society*, 73(8):2547–2551, 1990. Note.

[72] Y. Tu and S. Milne. Processing and characterization of pb(zr,ti)o3 films, up to 10 micron thick, produced from a diol sol-gel route. *Journal of materials research*, 11(10):2556–2564, 1996.

[73] R. Assink and R. Schwartz. *Chem. Mater.*, 5:511–517, 1993.

[74] R. Vest and J. Xu. *Ferroelectrics*, 93:21, 1989.

[75] J. Wright and L. Francis. *Mat. Res. Soc. Symp. Proc.*, 433:357, 1996.

[76] M. Ng and M. Cima. *J. Mater. Res. Soc. Symp. Proc.*, 341:145, 1994.

[77] M. Pechini, 1967.

[78] T. Boyle, D. Dimos, R. Schwartz, T. Alam, M. Sinclair, and C. Bucheit. Aging characteristics of a hybrid sol-gel pb(zr,ti)o3 precursor solution. *Journal of Materials Research*, 12(4):1022–1030, 1997.

[79] C. D. E. Lakeman and D. A. Payne. Processing effects in the sol-gel preparation of pzt dried gels, powders, and ferroelectric thin-layers. *Journal of the American Ceramic Society*, 75(11):3091–3096, 1992. Article.

[80] B. Malic, M Kosec, K. Smolej, and S. Stavber. Effect of precursor type on the microstructure of pbtio3 thin films. *Journal of the European Ceramic Society*, Volume 19:1345–1348, 1999.

[81] B. Malic, I. Arcon, M. Kosec, and A. Kodre. A structural study of amorphous alkoxide derived lead titanium complexes. *Journal of Materials Research*, 12(10):2602–2611, 1997.

[82] I. Arcon, B. Malic, M. Kosec, A. Kodre, and R. Frahm. *Journal Physique IV France*, C2:1193, 1997.

[83] B. Malic, I. Arcon, A. Kodre, and M Kosec. Exafs study of amorphous precursors for pb(zr,ti)o3 ceramics. *Journal of Sol-Gel Science and Technology*, 16:135–141, 1999.

[84] F. Babonneau, S. Doeuff, A. Leaustic, C. Sanchez, C. Cartier, and M. Verdaguer. *Inorganic Chemistry*, 27:3166, 1988.

[85] O. Glatter and O. Kraty. *Small Angle X-ray Scattering*. Academic Press, London, 1982.

[86] Q. Zhang, M. Vickers, A. Patel, and R. Whatmore. Determination of particle size and shape during the hydrolysis of pb(zr0.3ti0.7(o3 precursor solutions. *Journal of Sol-Gel Science and Technology*, 11:141–152, 1998.

[87] M. Huggins. *Journal of American Ceramic Society*, 64:2716, 1942.

[88] Q. Zhang and R. Whatmore. A comparison of the nanostructure of lead zirconate, lead titanate and lead zirconate titanate sols. *Journal of Sol-Gel Science and Technology*, 15:12–22, 1999.

[89] T. Tani and D. A. Payne. Lead-oxide coatings on sol gel-derived lead lanthanum zirconium titanate thin-layers for enhanced crystallization into the perovskite structure. *Journal of the American Ceramic Society*, 77(5):1242–1248, 1994. Article.

[90] A. Seifert, N. Ledermann, S. Hiboux, J. Baborowski, P. Muralt, and N. Setter. Processing optimization of solution derived pzt thin films for piezoelectric applications. *Integrated Ferroelectrics*, 35:159–166, 2001.

[91] M. Lefevre, J. Speck, R. Schwartz, D. Dimos, and S. Lockwood. Microstructural development in sol-gel derived lead zirconate titanate thin films: The role of precursor stoichiometry and processing environment. *Journal of Materials Research*, 11(8):2076–2084, 1996.

[92] R. Schwartz, J. Voigt, T. Boyle, T. Christenson, and C. Bucheit. Control of thin film processing behavior through precursor structural modifications. *Ceram. Eng. Sci. Proc.*, 16:1045, 1995.

[93] C. D. E. Lakeman, Z. Xu, and D. Payne. *Journal of Materials Research*, 10(8):2042–2051, 1995.

[94] J. Chang and S. Desu. *Journal of materials research*, 9(4):955–969, 1994.

[95] B. Tuttle, R. Schwartz, D. Doughty, and J. Voigt. *Ferroelectric Thin Films*, Mater. Res. Soc. Symp. Proc.(200):159, 1990.

[96] J. Revesz, J. Li, N. Szabo, J. Mayer, D. Caudillo, and E. Myers. *Mater. Res. Soc. Symp. Proc.*, 243:101, 1991.

[97] P. Muralt, T. Maeder, L. Sagalowicz, and S. Hiboux. Texture control of pbtio3 and pb(zr,ti)o3 thin films with tio2 seeding. *Journal of Applied Physics*, 83(7):3835–3841, 1998.

[98] S. Y. Chen and I. W. Chen. Temperature-time texture transition of pb(zr1-xtix)o-3 thin-films .1. role of pb-rich intermediate phases. *Journal of the American Ceramic Society*, 77(9):2332–2336, 1994. Article.

[99] S. Y. Chen and I. W. Chen. Temperature-time texture transition of pb(zr1-xtix)o-3 thin-films .2. heat-treatment and compositional effects. *Journal of the American Ceramic Society*, 77(9):2337–2344, 1994. Article.

[100] S. Y. Chen and I. W. Chen. Texture development, microstructure evolution, and crystallization of chemically derived pzt thin films. *Journal of the American Ceramic Society*, 81(1):97–105, 1998. Article.

[101] K. Brooks, I. Reaney, R. Klissurska, Y. Huang, L. Bursill, and N. Setter. *Journal of materials research*, 9(10):2540–2553, 1994.

[102] L. Fe, G. Norga, D. Wouters, and H. Maes. Chemical structure evolution and orientation selection in sol-gel prepared ferroelectric pb(zr,ti)o3 thin films. *Journal of Materials Research*, 16(9):2499–2504, 2001.

[103] D. Taylor. *Dielectric and Piezoelectric properties of sol-gel derived PZT thin films.* PhD thesis, EPFL, 1999.

[104] A. Seifert, F. Lange, and J. Speck. Epitaxial growth of pbtio3 thin films on (001) srtio3 from solution precursors. *Journal of Materials Research*, 10(3):680–691, 1995.

[105] C. J. Anthony, M. A. Todd, P. P. Donohue, M. A. C. Harper, Z. Huang, and J. C. Jones. High performance pst thin films on polysilicon sacrificial layers for uncooled ir detectors. *Integrated Ferroelectrics*, 49:233–243, 2002.

[106] D. Liu and H. Chen. Low-temperature preparation of perovskite pst thin films using mocvd. *Materials Letters*, 28:17–20, 1996. PST.

[107] C. Lin, S. Lee, H. Chen, and T. Wu. Dielectric properties of metal-organic chemical vapor deposited highly textured pst-pt relaxor ferroelectric thin films on lanio3 electrode buffered si. *Applied Physics Letters*, 75(16):2485–2487, 1999. PST.

[108] G. Scherer. Sintering of sol-gel films. *Journal of Sol-Gel Science and Technology*, 8:353–363, 1997.

[109] J. Van Der Merwe, J. Woltersdorf, and W. Jesser. Low energy dislocation structures in epitaxy. *Materials Science and Engineering*, 81:1–33, 1986.

[110] B. Tuttle, J. Voigt, T. Garino, D. Goodnow, R. Schwartz, D. Lamppa, J. Headley, and M. Eatough. Chemically prepared pzt thin films: the effects of orientation and stress. *Proceedings of the eighth Enternational symposium on Applications of Ferroelectrics*, pages 344–348, 1992.

[111] N. A. Pertsev, A.G. Zembilgotov, and A. K. Tagantsev. Effect of mechanical boundary conditions on phase diagrams of epitaxial ferroelectric thin films. *Physical Review Letters*, 80(9):1988–1991, 1998.

[112] N. Pertsev, A.G. Zembilgotov, S. Hoffman, R. Waser, and A. Tagantsev. Ferroelectric thin films grown on tensile substrates: Renormalization of the curie=weiss law and apparent absence of ferroelectricity. *Journal of Applied Physics*, 85(3):1698, 1999.

[113] J. P. Maria, W. Hackenberger, and S. Trolier-McKinstry. Phase development and electrical property analysis of pulsed laser deposited pmn-pt (70/30) epitaxial thin films. *Journal of Applied Physics*, 84(9):5147–5154, 1998. Thin Film Relaxor.

[114] V. Nagarajan, S. Alpay, C. Ganpule, B. Nagaraj, S. Aggarwal, E. Williams, A. Roytburd, and R. Ramesh. Role of substrate on the dielectric and piezoelectric behavior of epitaxial lead magnesium niobate-lead titanate relaxor thin films. *Appl. Phys. Lett.*, 77(3):438–440, 2000. Thin Film Relaxors.

[115] Nava Setter. The role of positional disorder in ferroelectric relaxors. *Ph. D. Dissertation, The Pennsylvania State University*, 1980.

[116] D. Damjanovic. Ferroelectric, dielectric and piezoelectric properties of ferroelectric thin films and ceramics. *Reports on progress in physics*, 61:1267–1324, 1998.

[117] S. Kasap. *Principles of electronic materials and devices.* McGraw-Hill, New York, NY, second edition, 2002.

[118] K. Cole and R. Cole. *J. Chem. Phys.*, 9:341, 1941.

[119] A. Jonscher. *Universal Relaxation Law.* Chelsea Dielectrics Press, London, 1996.

[120] E. Courtens. *Physical Review B*, 33:2975, 1986.

[121] A. Tagantsev. Volgel-fulcher relationship for the dielectric permittivity of relaxor ferroelectrics. *Physical review letters*, 72(7):1100–1103, 1994.

[122] A. Tagantsev and A. Glazounov. Dielectric non-linearity and the nature of polarization response of pmn relaxor ferroelectric. *Journal of the Korean Physical society*, 32:S951–S954, 1998.

[123] A. Tagantsev and A. Glazounov. Mechanism of polarization response in the ergodic phase of a relaxor ferroelectric. *Physical Review B*, 57(1):18–21, 1998. Relaxor model structural.

[124] C. Filipic, A. Levstik, and Z. Kutnjak. Analytical behavior of dielectric non-linearity in pmn relaxor ferroelectric. *Ferroelectrics*, 257:63–68, 2001.

[125] D. Taylor and D. Damjanovic. Domain wall pinning contribution to the nonlinear dielectric permittivity in pzt thin films. *Appl. Phys. Lett.*, 73(14):2045–2047, 1998.

[126] A. Glazounov A. Tagantsev. Mechanism of polarization response and dielectric non-linearity of pmn relaxor ferroelectric. *Phase Transtions*, 65:117–139, 1998. Relaxor model structural.

[127] M. Tyunina and J. Levoska. Coexistence of ferroelectric and relaxor properties in epitaxial films of bst. *Physical Review B*, 70:1–4, 2004.

[128] L. S. Kamzina and N. N. Krainik. Behavior of a lead scandium tantalate ferroelectric in an ac electric field. *Physics of the Solid State*, 43(10):1958–1961, 2001.

[129] F. Chu, G. Fox, and N. Setter. Dielectric properties of comples perovskite lead scandium tantalade under dc bias. *Journal of American Ceramic Society*, 81(6):1577–1582, 1998.

[130] A. Naberezhnov, S. Vakhrushev, B. Dorner, D. Strauch, and H. Moudden. *Eur. Phys. J.*, B 11:13, 1999.

[131] P. Gehring, S. Wakimoto, Z. Ye, and G. Shirane. Soft mode dynamics above and below the burns temperature in the relaxor pmn. *Physical review letters*, 87(27):277601–1, 2001.

[132] P. Gehring, S. Park, and G. Shirane. Soft phonon anomalies in the relaxor ferroelectric pzn-pt. *Physical review letters*, 84(22):5216–5219, 2000.

[133] S. Wakimoto, C. Stock, Z. Ye, W. Chen, P. Gehring, and G. Shirane. Mode coupling and polar nanoregions in the relaxor ferroelectric pmn. *Physical Review B*, 66:224102, 2002.

[134] S. Wakimoto, C. Stock, R. Birgeneau, Z. Ye, W. Chen, W. buyers, P. Gehring, and G. Shirane. Ferroelectric ordering in the relaxor pmn as evidenced by low temperature phonon anomalies. *Physical Review B*, 65:172105, 2002.

[135] J. Hlinka, S Kamba, and J. Petzelt. Origin of the waterfall effect in phonon-dispersion of relaxor perovskites. *Physical review letters*, 91(10):107602, 2003.

[136] J. Petzelt, E. Buixaderas, and A. Pronin. Infrared dielectric response of ordered and disordered ferroelectric pst ceramics. *Materials Science and Engineering B*, B55:86–94, 1998.

[137] J. Petzelt, T. Ostapchuk, and S. Kamba. Ferroelectric soft-mode spectroscopy in disordered bulk and thin-film perovskites. In G. Borstel et al., editor, *Defects and Surface induced effects in advanced perovskites*, pages 233–248. Kluwer Academic Publishers, Netherlands, 2000.

[138] S. Kamba, V. Bovtun, J. Petzelt, I. Rychetsky, R. Mizaras, and A. Brilingas. Dielectric dispersion of the relaxor plzt ceramics in the frequency range 20 hz-100 thz. *J. Phys. Condens. Matter*, 12:497–519, 2000.

[139] O. Heavens. *Reports on progress in physics*, 22:1, 1960.

[140] P. Muralt. Micromachined infrared detectors based on pyroelectric thin films. *Reports on progress in physics*, 64(10):1339–1388, 2001.

[141] R. W. Whatmore S. Dunn, A. P. De Kroon. An examination of thin film lead scandium tantalum oxide (pst) using piezoafm. *Journal of Materials Science Letters*, 20:179–181, 2001. PST.

[142] R. W. Whatmore A. P. De Kroon, S. C. Dunn. Piezo- and pyroelectric properties of lead scandium tantalate thin films. *Integrated Ferroelectrics*, 35:209–218, 2001. PST.

[143] V. Shvartsman, A. Emelyanov, A. Kholkin, and A. Safari. Local hysteresis and grain size effect in pmn-pt thin films. *Appl. Phys. Lett.*, 81(1):117, 2002.

[144] A. Bell, Y. Huang, O. Paul, Y. Nemirovsky, and N. Setter. A thin film pyroelectric detector. *Integrated Ferroelectrics*, 6:231–240, 1995.

[145] M. Kohli, Y. Huang, T. Maeder, C. Wuthrich, A. Bell, P. Muralt, N. Setter, P. Ryser, and M. Forster. Processing and properties of thin film pyroelectric devices. *Microelectronic Engineering*, 29:93–96, 1995.

[146] N. Shorrocks, A. Patel, M. Walker, and A. Parsons. Integrated thin iflm pzt pyroelectric detector arrays. *Microelectronic Engineering*, 29:59–66, 1995.

[147] A. Kholkin, C. Wuthrich, D. Taylor, and N. Setter. Interferometric measurements of electrid field-induced displacements in piezoelectric thin films. *Review of Scientific Instruments*, 67(5):1935–1941, 1996.

[148] B. J. Kuh, W. K. Choo, K. Brinkman, D. Damjanovic, and N. Setter. Dielectric and piezoelectric properties of relaxor pb(sc1/2nb1/2)o-3 thin films. *Applied Physics Letters*, 83(8):1614–1616, 2003.

[149] N. Donnelly, G. Catalan, C. Morros, R. Bowman, and J. Gregg. Dielectric and electromechanical properties of pmn-pt thin films grown by pulsed laser deposition. *Journal of Applied Physics*, 93(12):9924–9929, 2003.

[150] K. Abe, N. Yanase, T. Yasumoto, and T. Kawakubo. Voltage shift phenomena in heteroepitaxial batio3 thin film capacitor. *Journal of Applied Physics*, 91(1):323–330, 2002.

[151] T. Ostapchuk, J. Petzelt, V. Zelezny, A. Pashkin, J. Pokorny, I. Drbohlav, R. Kuzel, D. Rafaja, B. Gorshunov, M. Dressel, C. Ohly, S. Hoffman-Eifert, and R. Waser. Origin of soft-mode stiffening and reduced dielectric response in sto thin films. *Physical Review B*, 66:235406–1, 2002.

Acknowledgments

I would like to thank the following for helping me on my way: Prof. Nava Setter who convinced me that coming to Switzerland was a better choice than life in a factory. Her knowledge and intense curiosity about my thesis subject of *relaxors* and her own example of hard work often prompted me to stop *relaxing* and keep at it; even when the light at the end of the tunnel was nowhere in sight. I would also like to thank my Masters thesis advisor Prof. R. Schwartz for encouraging and aiding me to pursue academic work abroad. I was fortunate enough to be exposed to a team of scientists including Dr. A. Tagantsev, Dr. P. Muralt, Dr. D. Damjanovic, and Dr. E. Colla, who were always willing to share their knowledge and to help guide me along.

Discussions with Dr. R. Houriet, and Dr. P. Bowen are also gratefully acknowledged. Their insight into processing was a great help, especially at the initial stages of my work. A fruitful collaboration with the Institute of Physics in Prague was an enriching experience both professionally and personally. I would like to thank my hosts Dr. Stanislav Kamba and Prof. Jan Petzelt for their hospitality and great working atmosphere during my stay in Prague. An important part of this thesis was the TEM imaging of ordered regions, and for these studies i am deeply indebted to two colleagues who spent numerous hours in sample preparation and microscope time: Dr. Marco Cantoni, and Dr. Dong Su, thanks a lot! I would also like to thank my other thesis committee members, Prof. H. Hoffman (EPFL), Prof. M. Kosec (Ljubljana), Prof. J. Petzelt (Institute of Physics, Prague), and Prof. H. Mathieu (EPFL- Jury President) for their interest and input on my work.

I wish to thank members of the LC past and present for a great 4 years, both for their help with technical issues (Zian-Sol-gel Kighelman, Simon-electrode Buhlmann, Vladimir-help my computer doesn't work-Cherman) as well as for a great lab ambiance.

Finally I would like to thank my parents for always supporting to the fullest no matter what path i decided to follow, and Mylene for her patience and big smile which greeted me at the end of the day, *Merci Cherie!*

Publications

K. Brinkman, M. Cantoni, A. Tagantsev, P. Muralt and N. Setter, *Dielectric Response and Structural Features of PST Sol-Gel Derived Thin Films*, Journal of Electroceramics **13** 105-110 (2004)

B. Kuh, W. Choo, K. Brinkman, D. Damjanovic, and N. Setter, *Dielectric and Piezoelectric Properties of Relaxor PSN Thin Films*, Applied Physics Letters **83** (8) 1614-1616 (2003)

B. Kuh, W. Choo, K. Brinkman, J. Kim, D. Damjanovic, and N. Setter, *Sol-Gel Derived PSN Thin Films: Processing and Dielectric Properties*, Japanese Journal of Applied Physics, part1 **41** (11B) 6765-6767 (2002)

B. Kuh, K. Brinkman, D. Damjanovic, N. Setter, and W. Choo, *Preparation and Dielectric Properties of PST-PT Thin Films Near MPB Compositions* Ferroelectrics **271** 1665-1670 (2002)

K. Brinkman, and R. Schwartz, *UV Radiation Effects in Sol-Gel Processing of Ferroelectric PZT Thin Films* Materials Science of Novel Oxide Based Electronics, MRS Symposium Proceedings (2000)

K. Brinkman, R. Schwartz, K. Markus, and A. Angone, *Depth Profiling of Solution Deposited Lead Zirconate Titanate Thin Films by Radio Frequency Glow Discharge Atomic Emission Spectroscopy (rf-GDAES)* Ferroelectric Thin Films VIII, MRS Symposium Proceedings (2000)

Curriculum Vitae

Name:	Kyle
Family name:	Brinkman
Date of birth:	August 3,1975
Place of birth:	USA
Nationality:	American

EDUCATION

October 2000 – December 2004:   Ph.D. student in the Ceramics Laboratory, Swiss Federal Institute of Technology, Lausanne, Switzerland.

September 1998 – June 2000:   Graduate student in the Department of Materials Science and Engineering, Clemson University, Clemson SC, USA. Master's degree in Ceramic and Materials Engineering was obtained.

September 1993 – June 1998:   Student in the Department of Chemical Engineering, Clemson University, Clemson SC, USA. Bachelor's degree in Chemical Engineering was obtained.

WORK EXPERIENCE

October 2000 – December 2004:   Research Assistant. Ceramics Laboratory, Swiss Federal Institute of Technology, Lausanne, Switzerland.

September 1998 – June 2000:   Research Assistant. Center for Advanced Engineering Fibers and Films (CAEFF), Clemson University, Clemson SC, USA .